



International Agreement Report

Experimental Study of Narrow Pulse Effects on the Behavior of High Burnup Fuel Rods with Zr-1%Nb Cladding and UO₂ Fuel (VVER Type) under Reactivity-Initiated Accident Conditions:
Program Approach and Analysis of Results

Prepared by

L. Yegorova, K. Lioutov, N. Jouravkova
Nuclear Safety Institute of Russian Research Centre “Kurchatov Institute”
Kurchatov Square 1, Moscow 123182, Russian Federation

O. Nechaeva, A. Salatov
A.A. Bochvar All-Russian Research Institute of Inorganic Materials
Rogov Street 5, Moscow 123182, Russian Federation

V. Smirnov, A. Goryachev
State Research Centre “Research Institute of Atomic Reactors”
Dimitrovgrad 433510, Russian Federation

V. Ustinenko, I. Smirnov
Russian Federal Nuclear Centre “All-Russian Research Institute of Experimental Physics”
Sarov 607200, Russian Federation

**Office of Nuclear Regulatory Research
U.S. Nuclear Regulatory Commission
Washington, DC 20555-0001**

May 2006

Prepared for

U.S. Nuclear Regulatory Commission (United States),
Institute for Radiological Protection and Nuclear Safety (France),
and Joint Stock Company “TVEL” (Russian Federation)

Published by

U.S. Nuclear Regulatory Commission

AVAILABILITY OF REFERENCE MATERIALS IN NRC PUBLICATIONS

NRC Reference Material

As of November 1999, you may electronically access NUREG-series publications and other NRC records at NRC's Public Electronic Reading Room at <http://www.nrc.gov/reading-rm.html>. Publicly released records include, to name a few, NUREG-series publications; *Federal Register* notices; applicant, licensee, and vendor documents and correspondence; NRC correspondence and internal memoranda; bulletins and information notices; inspection and investigative reports; licensee event reports; and Commission papers and their attachments.

NRC publications in the NUREG series, NRC regulations, and *Title 10, Energy*, in the Code of *Federal Regulations* may also be purchased from one of these two sources.

1. The Superintendent of Documents
U.S. Government Printing Office
Mail Stop SSOP
Washington, DC 20402-0001
Internet: bookstore.gpo.gov
Telephone: 202-512-1800
Fax: 202-512-2250
2. The National Technical Information Service
Springfield, VA 22161-0002
www.ntis.gov
1-800-553-6847 or, locally, 703-605-6000

A single copy of each NRC draft report for comment is available free, to the extent of supply, upon written request as follows:

Address: Office of the Chief Information Officer,
Reproduction and Distribution
Services Section
U.S. Nuclear Regulatory Commission
Washington, DC 20555-0001

E-mail: DISTRIBUTION@nrc.gov
Facsimile: 301-415-2289

Some publications in the NUREG series that are posted at NRC's Web site address <http://www.nrc.gov/reading-rm/doc-collections/nuregs> are updated periodically and may differ from the last printed version. Although references to material found on a Web site bear the date the material was accessed, the material available on the date cited may subsequently be removed from the site.

Non-NRC Reference Material

Documents available from public and special technical libraries include all open literature items, such as books, journal articles, and transactions, *Federal Register* notices, Federal and State legislation, and congressional reports. Such documents as theses, dissertations, foreign reports and translations, and non-NRC conference proceedings may be purchased from their sponsoring organization.

Copies of industry codes and standards used in a substantive manner in the NRC regulatory process are maintained at—

The NRC Technical Library
Two White Flint North
11545 Rockville Pike
Rockville, MD 20852-2738

These standards are available in the library for reference use by the public. Codes and standards are usually copyrighted and may be purchased from the originating organization or, if they are American National Standards, from—

American National Standards Institute
11 West 42nd Street
New York, NY 10036-8002
www.ansi.org
212-642-4900

Legally binding regulatory requirements are stated only in laws; NRC regulations; licenses, including technical specifications; or orders, not in NUREG-series publications. The views expressed in contractor-prepared publications in this series are not necessarily those of the NRC.

The NUREG series comprises (1) technical and administrative reports and books prepared by the staff (NUREG-XXXX) or agency contractors (NUREG/CR-XXXX), (2) proceedings of conferences (NUREG/CP-XXXX), (3) reports resulting from international agreements (NUREG/IA-XXXX), (4) brochures (NUREG/BR-XXXX), and (5) compilations of legal decisions and orders of the Commission and Atomic and Safety Licensing Boards and of Directors' decisions under Section 2.206 of NRC's regulations (NUREG-0750).

DISCLAIMER: This report was prepared under an international cooperative agreement for the exchange of technical information. Neither the U.S. Government nor any agency thereof, nor any employee, makes any warranty, expressed or implied, or assumes any legal liability or responsibility for any third party's use, or the results of such use, of any information, apparatus, product or process disclosed in this publication, or represents that its use by such third party would not infringe privately owned rights.



NUREG/IA-0213, Vol. 1
IRSN/DPAM 2005-275
NSI RRC KI 3230

International Agreement Report

Experimental Study of Narrow Pulse Effects on the Behavior of High Burnup Fuel Rods with Zr-1%Nb Cladding and UO₂ Fuel (VVER Type) under Reactivity-Initiated Accident Conditions:
Program Approach and Analysis of Results

Prepared by

L. Yegorova, K. Lioutov, N. Jouravkova
Nuclear Safety Institute of Russian Research Centre "Kurchatov Institute"
Kurchatov Square 1, Moscow 123182, Russian Federation

O. Nechaeva, A. Salatov
A.A. Bochvar All-Russian Research Institute of Inorganic Materials
Rogov Street 5, Moscow 123182, Russian Federation

V. Smirnov, A. Goryachev
State Research Centre "Research Institute of Atomic Reactors"
Dimitrovgrad 433510, Russian Federation

V. Ustinenko, I. Smirnov
Russian Federal Nuclear Centre "All-Russian Research Institute of Experimental Physics"
Sarov 607200, Russian Federation

**Office of Nuclear Regulatory Research
U.S. Nuclear Regulatory Commission
Washington, DC 20555-0001**

May 2006

Prepared for

U.S. Nuclear Regulatory Commission (United States),
Institute for Radiological Protection and Nuclear Safety (France),
and Joint Stock Company "TVEL" (Russian Federation)

Published by

U.S. Nuclear Regulatory Commission

ABSTRACT

Twelve pulse tests of fuel rods with UO_2 high burnup fuel and Zr-1%Nb cladding were performed in the Russian research reactor, BIGR. Fuel rods were refabricated from Russian VVER pressurized water reactor commercial fuel elements with burnups of 47–49 MWd/kg U and 60 MWd/kg U. The reactor pulse tests were carried out to validate the behavior of high burnup fuel rods under reactivity-initiated-accident conditions. This experimental program, compared to previous investigations, was focused on the determining the sensitivity of the failure mechanisms and the failure thresholds of high burnup fuel to such effects as the narrow pulse (2.5–3.1 ms), ductile Zr-1%Nb cladding, fuel burnup with relatively small rim layer effects (47–49 MWd/kg U) and with relatively significant ones (60 MWd/kg U).

FOREWORD

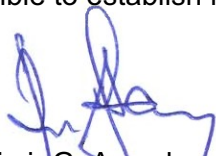
This two-volume report provides results of a cooperative research program involving the Russian Research Center–Kurchatov Institute, the French Institute for Radiological Protection and Nuclear Safety (IRSN), and the United States Nuclear Regulatory Commission (NRC). The research addresses the behavior of high-burnup nuclear fuel under postulated reactivity-initiated accident (RIA) conditions, based on experimental results from the Russian fast-pulse graphite reactor, known as BGR.

The Kurchatov Institute initiated its RIA test program in 1983, several years before the accident at Chernobyl. That accident, which resulted from a rapid increase in reactivity, demonstrated that severe fuel damage may occur too quickly to be easily mitigated. However, the consequences of such an event can be reduced by thorough understanding and design.

Information concerning Russian reactivity insertion experiments in the Impulse Graphite Reactor (IGR) was first revealed to western observers in 1992. Differences between IGR and other fuel behavior tests were initially attributed to differences in Russian fuel designs and the larger pulse width of the IGR test reactor. However, the test rods used in the IGR were taken from zirconium-niobium clad uranium dioxide (UO₂) fuel rods that were commercially irradiated in pressurized, light-water-reactors. This type of cladding material is used throughout the world, and generated great interest. The IRSN and NRC recognized the value of this test program and, in 1995, joined with the Kurchatov Institute in assessing and interpreting the IGR data. Then, in July 1999, the agencies jointly published the results in a three-volume compendium, identified as NUREG/IA-0156, “Data Base on the Behavior of High Burnup Fuel Rods with Zr-1%Nb Cladding and UO₂ Fuel (VVER Type) Under Reactivity Accident Conditions.”

More recently, the Kurchatov Institute addressed the issue of the broad pulse width effects in the IGR with a series of narrow pulse width experiments in the BGR fast-pulse graphite reactor. The work was performed in cooperation with other Russian institutes and support of the Russian fuel vendor (Joint Stock Company “TVEL”). Pulses produced by the two test reactors span an extraordinary range, from 3 milliseconds in BGR to over 700 milliseconds in IGR, and bound the expected pulse widths for postulated RIA events in commercial light-water reactors. Taken together, these test results show that cladding with very light corrosion is remarkably resistant to failure — even under high-burnup conditions.


Results of the BGR program, as documented in this report, demonstrate the continued value of the cooperative efforts of the Kurchatov Institute, the IRSN, and the NRC. This collaborative program further allows a comparison of conclusions from other data sources (e.g., France, Japan, and the U.S.). By comparing these results, studying the employed techniques, and creating a common language necessary for the mutual understanding these events, it will be possible to establish more appropriate regulatory limits for reactivity-initiated accidents.



Vladimir G. Asmolov, Director
Research and Development
Russian Research Centre -
“Kurchatov Institute”



Michel Schwarz, Director
Major Accident
Prevention Division
Institut de Radioprotection
et de Sûreté Nucléaire



Carl J. Paperiello, Director
Office of Nuclear
Regulatory Research
U.S. Nuclear Regulatory
Commission

TABLE OF CONTENTS

	Page
1. INTRODUCTION	1.1
2. THE BIGR/RIA TEST PROGRAM: MAJOR PROVISIONS	2.1
3. THE CHARACTERIZATION OF THE VVER HIGH BURNUP FUEL RODS AND OF THE BIGR REACTOR	3.1
3.1. The VVER fuel and refabricated test rods.....	3.1
3.2. The BIGR reactor and capsule device	3.4
3.3. Scoping tests used to determine energy deposition in BIGR	3.7
4. MAJOR PROVISIONS FOR THE PROCEDURES USED TO DETERMINE THE SPATIAL AND TIME DEPENDENT DISTRIBUTIONS OF ENERGY DEPOSITION AND FUEL ENTHALPY IN THE VVER HIGH BURNUP FUEL RODS UNDER THE BIGR TEST CONDITIONS	4.1
4.1. Energy deposition in the VVER high burnup fuel rods	4.1
4.2. Fuel enthalpy and thermal mechanical parameters of fuel rods	4.5
4.2.1. <i>Background</i>	4.5
4.3. Description of computer codes used and results of calculations	4.6
5. BIGR TEST RESULTS AND DISCUSSION	5.1
5.1. Thermal mechanical behavior of high burnup fuel rods under BIGR narrow pulse conditions	5.1
5.2. The general overview of the BIGR test results.....	5.9
5.3. The behavior of high burnup fuel and fission gas release in the BIGR pulse tests	5.11
5.4. Cladding mechanical behavior under the BIGR test conditions.....	5.23
5.5. The interpretation of mechanisms and thresholds for the high burnup fuel failure under the BIGR test conditions	5.34
6. THE COMPARATIVE ANALYSIS OF THE RIA TESTS WITH THE VVER AND PWR HIGH BURNUP FUEL RODS	6.1
7. SUMMARY	7.1
Appendix A The characterization of test procedures used to determine parameters of high burnup fuel rods	A-1
Appendix B The major provisions for the procedure developed to determine the ratio between fission numbers in the VVER high burnup fuel and the BIGR energy deposition	B-1
Appendix C Description of some models in the RAPTA-5 computer code	C-1

LIST OF FIGURES

	Page
Fig. 1.1. Demonstration of different types of the cladding failure under the RIA conditions.....	1.2
Fig. 2.1. The correlation between the peak average fuel enthalpy in the VVER fuel with 47–49 and 60 MW d/kg U burnup and energy deposition in the BGR reactor	2.4
Fig. 2.2. Demonstration of experimental uncertainties between the designated test mode of the BGR reactor (285 MJ in this case) and fuel enthalpy in the VVER high burnup fuel	2.4
Fig. 2.3. Cooperative efforts of research institutes involved in the BGR test program	2.5
Fig. 3.1. The refabrication procedure for the BGR/RIA tests	3.1
Fig. 3.2. The VVER-440 commercial fuel element (FA #228, FE #081) after the base irradiation up to burnup of 60 MWd/kg U (a) The cross-section view, (b) The cladding microstructure.....	3.3
Fig. 3.3. Design of refabricated fuel rods.....	3.3
Fig. 3.4. Axial section of the BGR reactor.....	3.4
Fig. 3.5. Axial section of the BGR side channel with capsule and VVER fuel rod.....	3.6
Fig. 3.6. Configuration for the BGR reactor, side channel and capsule device (cross-section view)	3.7
Fig. 3.7. The comparison of calculated (by TRIFOB code) and measured data characterizing the fuel isotopic composition in the VVER refabricated fuel rods #RT1–6).....	3.8
Fig. 3.8. The data characterizing the axial distribution of fission numbers in VVER fuel rods during the BGR tests	3.9
Fig. 3.9. Results of the BGR scoping tests.....	3.10
Fig. 3.10. The sensitivity of the VVER fuel enthalpy to methods of the BGR power history measurement....	3.11
Fig. 3.11. The BGR power history.....	3.11
Fig. 3.12. The power history interpretation at the supercritical state of the BGR reactor	3.12
Fig. 3.13. The comparison of the test and calculated BGR power histories in 0.1–1000 second range from the pulse beginning	3.13
Fig. 3.14. Major provisions of the procedure used for the determination of the BGR power history	3.13
Fig. 3.15. Comparative data characterizing the RRC KI and VNIIEF procedures developed for the determination of fission numbers in the VVER high burnup fuel rods (#RT1–6) as a function of energy deposition in the BGR reactor with the graphite side channel.....	3.15
Fig. 4.1. The arrangement of the procedure to determine the spatial and time dependent distributions of energy deposition in the VVER high burnup fuel rod under the BGR test conditions.....	4.1
Fig. 4.2. The structural scheme of the RRC KI and VNIIEF procedures developed for the energy deposition determination	4.3
Fig. 4.3. The RRC KI and VNIIEF comparative data characterizing the energy deposition as a function of the number of fissions in the VVER fuel	4.3
Fig. 4.4. The RRC KI and VNIIEF comparative data characterizing the total energy deposition in the VVER fuel rods under the BGR conditions	4.5
Fig. 4.5. The radial distribution of energy deposition in four fuel radial layers (averaged over the layer thickness) in the refabricated fuel rods with burnup of 47 and 60.3 MWd/kg U.....	4.6
Fig. 4.6. The comparison of the FRAP-T6/VVER calculations with the NSRR test data.....	4.10
Fig. 4.7. The comparison of the NSRR data characterizing the thermal and mechanical behavior of the pressurized unirradiated fuel rod with the RAPTA-5 calculations before (original) and after (modified) the heat transfer module modification.....	4.11
Fig. 4.8. The surface heat flux as a function of the surface temperature: correlations used in the VVER version of the FRAP-T6 code and in the original version of the RAPTA-5 code	4.11
Fig. 4.9. The comparison of the RAPTA-5 calculations and NSRR test data characterizing the sensitivity of the cladding temperature to the initial pellet/cladding gap	4.12

Fig. 4.10. The comparative data characterizing the calculated (by the FRAP-T6/VVER version of the code) and measured cladding residual hoop strain under the NSRR test conditions	4.13
Fig. 4.11. The comparison of calculated and measured FGR using the IGR test data for the VVER high burnup fuel	4.14
Fig. 4.12. The comparison of calculated and measured effects of high burnup fuel swelling (the IGR test data).....	4.14
Fig. 4.13. Results of determination of the peak averaged fuel enthalpy in fuel rods tested under the BIGR test conditions (#RT1–12).....	4.15
Fig. 5.1. Appearance of high burnup fuel rods after the BIGR tests	5.1
Fig. 5.2. Demonstration of the rim layer structure using the metallographic sample of the VVER fuel with burnup of 50 MWd/kg U.....	5.2
Fig. 5.3. Radial distributions of ^{235}U and ^{239}Pu relative concentrations; Burnup radial distribution in the VVER fuel with average burnup of 50 MWd/kg U	5.2
Fig. 5.4. The radial distributions of the fuel enthalpy as a function of time for the fuel rod #RT6 (48 MWd/kg U).....	5.3
Fig. 5.5. Demonstration of the bonding layer on the cladding inner surface of the VVER-440 fuel element irradiated up to 60 MWd/kg U	5.4
Fig. 5.6. Experimental data characterizing the degradation of mechanical properties of Zr-1%Nb (the VVER type) cladding after the base irradiation up to 50 MWd/kg U.....	5.4
Fig. 5.7. The experimental data obtained from the results of biaxial mechanical tests: the characterization of the true stress at the cladding rupture as a function of the temperature and cladding irradiation	5.5
Fig. 5.8. Time dependent energy parameters of the fuel rod #RT6 at the BIGR test	5.5
Fig. 5.9. Thermal mechanical behavior of the high burnup fuel rod #RT6 during the BIGR test in accordance with the FRAP-T6 calculations	5.7
Fig. 5.10. Results of the BIGR tests with pressurized fuel rods of 47–49 MWd/kg U burnup	5.9
Fig. 5.11. Results of the BIGR test with the unpressurized fuel rod of 47.4 MWd/kg U burnup	5.10
Fig. 5.12. Results of the BIGR tests of pressurized and unpressurized fuel rods with 60 MWd/kg U burnup ..	5.11
Fig. 5.13. The design of the VVER fuel pellets used in the BIGR tests.....	5.12
Fig. 5.14. The cross-sections of two VVER-1000 and VVER-440 high burnup fuel elements after the base irradiation	5.12
Fig. 5.15. Demonstration of typical macroscopic tendencies characterizing the fuel state of fuel rods with 47–49 and 60 MWd/kg U burnup tested under the BIGR narrow pulse conditions	5.13
Fig. 5.16. Transformation of the fuel microstructure as a function of the peak fuel enthalpy in unfailed fuel rods with 47–49 MWd/kg U burnup	5.14
Fig. 5.17. The cross-section and fuel microstructure of the unpressurized fuel rod with burnup of 47.4 MWd/kg U tested at 155 cal/g and remained unfailed	5.15
Fig. 5.18. Transformation of the fuel microstructure in the fuel rod with 60 MWd/kg U burnup tested at 125 cal/g of the peak fuel enthalpy in comparison with the state before the BIGR test	5.16
Fig. 5.19. Rim layer mechanical behavior in unfailed fuel rods with burnup of 47–49 MWd/kg U.....	5.17
Fig. 5.20. Rim layer mechanical behavior in unfailed fuel rods with burnup of 60 MWd/kg U.....	5.19
Fig. 5.21. Results of FGR measurements in unfailed fuel rods after the BIGR tests	5.20
Fig. 5.22. Cross-sections and fuel microstructure of failed fuel rods with burnup of 47–49 MWd/kg U	5.20
Fig. 5.23. Cross-sections and fuel microstructure of pressurized and unpressurized failed fuel rods with burnup of 60 MWd/kg U in unfailed region	5.21
Fig. 5.24. Cross-sections and the fuel microstructure of pressurized and unpressurized failed fuel rods with burnup of 60 MWd/kg U in the cladding rupture area	5.23
Fig. 5.25. The microstructure of Zr-1%Nb (E110) cladding after the base irradiation up to ≈ 50 and 60 MWd/kg U	5.24

Fig. 5.26. Demonstration of the relationship between the local decrease of fuel mass in the pellet interface areas and the local decrease of the cladding hoop strain in these areas in comparison with the cladding strain corresponding to the pellet middle height areas	5.25
Fig. 5.27. The sensitivity of γ -scanning results obtained before the BGR tests to different fuel pellet shapes: with chamfers (Type B) and without chamfers (Type A)	5.26
Fig. 5.28. Some data illustrating the significant correlation between axial distributions of fuel mass and the cladding hoop strain under the BGR narrow pulse conditions (#RT3)	5.27
Fig. 5.29. General tendencies characterizing the cladding hoop strain in pressurized fuel rods with burnup of 47–49 MWd/kg U under the BGR narrow pulse conditions.....	5.28
Fig. 5.30. The comparison of axial distributions of the cladding average outer diameter in pressurized and unpressurized unfailed fuel rods (47–49 MWd/kg U) tested at the same peak fuel enthalpy	5.29
Fig. 5.31. The sensitivity of the cladding hoop strain to the initial pressurization of unfailed fuel rods with burnup of 47–49 MWd/kg U.....	5.29
Fig. 5.32. The cladding deformation sensitivity to fuel burnup: for pressurized unfailed fuel rods under consideration	5.30
Fig. 5.33. The comparison of the cladding hoop strain in pressurized unfailed fuel rods at burnup of 47–49 and 60 MWd/kg U.....	5.31
Fig. 5.34. Characterization of the cladding mechanical behavior at the failure threshold of pressurized fuel rods with burnup of 47–49 MWd/kg U.....	5.32
Fig. 5.35. The comparative appearances of pressurized and unpressurized fuel rods with burnup of 60 MWd/kg U after the BGR narrow pulses	5.32
Fig. 5.36. Spatial effects of the cladding deformation in pressurized and unpressurized fuel rods with burnup of 60 MWd/kg U after the BGR tests at the peak fuel enthalpy of 164–165 cal/g	5.33
Fig. 5.37. Comparative data characterizing the thermal and mechanical behavior of unfailed fuel rods with burnup of 48 and 60 MWd/kg U in accordance with results of the FRAP-T6/VVER calculations.....	5.36
Fig. 5.38. The margin to the cladding rupture at the PCMI stage for fuel rods with burnup of 48 MWd/kg U (RT6) and 60 MWd/kg U (RT4) in accordance with the conservative failure criterion based on the uniform elongation.....	5.37
Fig. 5.39. The low temperature CSED for the Zr-1%Nb irradiated commercial cladding.....	5.39
Fig. 5.40. The low temperature CSED for the Zry-4 irradiated cladding at the low oxidation.....	5.39
Fig. 5.41. The FRAPTRAN calculations of the fuel rod #RT10 parameters at the PCMI stage of the BGR test.....	5.40
Fig. 5.42. The comparison of the SED of twelve fuel rods tested in the BGR reactor with the CSED determined in accordance with results of ring tensile tests	5.40
Fig. 5.43. 16 azimuthal measurements of cladding outer diameter of fuel rod #RT6 after the BGR test	5.40
Fig. 5.44. The clarification of the contribution of the hot PCMI and gas loading stages into the cladding strain.....	5.41
Fig. 5.45. The comparison of the cladding strains in the pressurized and unpressurized failed fuel rods with burnup of 60 MWd/kg U.....	5.42
Fig. 5.46. Metallographic samples illustrating the effects of fuel and cladding deformation and failure	5.43
Fig. 5.47. Types of azimuthal distributions of residual cladding thickness as a functions of the BGR test conditions	5.45
Fig. 5.48. The organized test data characterizing the Zr-1%Nb (E110) cladding mechanical behavior	5.48
Fig. 5.49. Data characterizing failure thresholds for fuel rods with burnup of 47–49 MWd/kg U	5.49
Fig. 5.50. Data characterizing failure thresholds for fuel rods with burnup of 60 MWd/kg U	5.49
Fig. 6.1. The sensitivity of the thermal mechanical behavior of the VVER high burnup fuel rod (49.2 MWd/kg U) to the pulse width under the RIA test conditions	6.3
Fig. 6.2. The reference data and interpretation of the BGR tests performed with the low oxidized VVER high burnup fuel rods: (a) fuel rods with burnup of 47–49 MWd/kg U, (b) fuel rods with burnup of 60 MWd/kg U	6.4

Fig. 6.3. Reference data and the RRC KI interpretation of the IGR tests performed with the low oxidized VVER high burnup fuel rods	6.5
Fig. 6.4. The sensitivity of the VVER high burnup fuel behavior to the RIA pulse width	6.6
Fig. 6.5. Reference data and the RRC KI interpretation of the NSRR tests performed with the JMTR irradiated fuel rods	6.8
Fig. 6.6. The sensitivity of the mechanical behavior of the VVER and PWR low oxidized irradiated cladding to the RIA pulse width and cladding pressurization at the wide gas gap condition	6.8
Fig. 6.7. Reference data and the RRC KI interpretation of the NSRR tests performed with the low oxidized PWR high burnup fuel rods.....	6.10
Fig. 6.8. The comparison of the VVER and PWR high burnup fuel rods behavior (fuel rods with the low oxidized cladding) under BIGR and NSRR narrow pulse conditions	6.11
Fig. 6.9. Reference data and the RRC KI interpretation of the FGR in the VVER and PWR high burnup fuel rods tested under the IGR, BIGR, NSRR pulse conditions.....	6.12
Fig. 6.10. Comparative data characterizing the cladding mechanical response at the BIGR and NSRR tests of the VVER and PWR high burnup fuel rods (≈ 50 MWd/kg U)	6.12
Fig. 6.11. The sensitivity of the cladding hoop strain to the fission gas release in accordance with the data of different pulse tests.....	6.14
Fig. 6.12. The sensitivity of the mechanical behavior of the VVER low oxidized irradiated cladding to the fuel burnup under the BIGR narrow pulse conditions	6.17

LIST OF TABLES

	Page
Table 1.1. Some comparative data characterizing the RIA tests with the VVER and PWR high burnup fuel	1.2
Table 2.1. Research tasks	2.1
Table 2.2. The parameters for the BGR tests	2.5
Table 3.1. General neutronic parameters of the BGR reactor	3.5
Table 3.2. The characterization of the approach used to determine the number of fissions in the VVER high burnup fuel rods at the BGR pulse tests	3.14
Table 4.1. The specific number of fissions determined with the use of the RRC KI and VNIIEF procedures for the VVER fuel rods tested at the second stage of the BGR program.....	4.2
Table 4.2. Components of energy per one fission in accordance with the RRC KI and VNIIEF procedures.....	4.4
Table 4.3. The list of modifications made in the FRAP-T6 code to determine parameters of the VVER high burnup fuel rods under the RIA conditions.....	4.7
Table 4.4. The brief characterization of the RAPTA-5 code major models.....	4.8
Table 5.1. The schematic analysis of the major physical phenomena accompanying high burnup fuel behavior under the BGR pulse conditions	5.6
Table 5.2. The comparison of calculated and measured maximum residual hoop strains of claddings	5.35
Table 6.1. The general characterization of the BGR, IGR, NSRR, CABRI ^b test programs performed with the VVER and PWR (UO ₂ fuel) high burnup fuel rods	6.1
Table 6.2. Some comparative data characterizing the design of the VVER and PWR high burnup fuel rods tested under the BGR, IGR and NSRR pulse conditions.....	6.14

ACKNOWLEDGEMENTS

The practical implementation of the BGR research program outlined in this report was not an ordinary procedure because the challenges faced at the end of the century in the context of the experimental validation of high burnup fuel effects under reactivity initiated accident conditions were quite unpredictable. Therefore, the authors of the report would like to emphasize specially that the consolidated efforts of the following key persons made possible the resolution of the complex of managerial and organization problems brought up in this program:

- P. Lavrenyuk (Joint Stock Company “TVEL”)
- V. Asmolov (Russian Research Center “Kurchatov Institute”)
- Yu. Bibilashvili (All-Russian Research Institute of Inorganic Materials)
- Yu. Trutnev (Russian Federal Nuclear Center “All-Russian Research Institute of Experimental Physics”)

The second volume of the report contains special thanks to the researchers who provided for the scientific and technical basis of the BGR test program. The authors would like to express our gratitude to J. Papin (Institute for Radiological Protection and Nuclear Safety, France) and R. Meyer (U.S. Nuclear Regulatory Commission, United States) who supported the idea concerning the preparation of the International Report devoted to the presentation of the BGR test program results.

Finally, we would like to appreciate specially:

- J. Papin (Institute for Radiological Protection and Nuclear Safety, France) and J. Voglewede (U.S. Nuclear Regulatory Commission, United States) who made numerous important scientific comments and editorial remarks to this report
- O. Dobudoglo (Russian Research Center “Kurchatov Institute”) who assisted in the improvement of the English version of this report.

LIST OF ACRONYMS

BIGR	Bystry Impulsny Graphitovy Reaktor (Russian Fast Pulse Graphite Reactor)
CABRI	French research reactor
DNB	departure from nucleate boiling
EPRI	Electric Power Research Institute (U.S.)
FGR	fission gas release
FRAP-T6	fuel rod analysis program, transient version 6 (U.S.)
FRAPTRAN	fuel rod analysis program transient (U.S.)
GIDRA	Russian IIN-3M research reactor (Russian spelling of “Hydra”)
IGR	Impulsny Graphitovy Reaktor (Pulsed Graphite Reactor, Kazakhstan)
IRSN	Institute for Radiological Protection and Nuclear Safety (France)
JMTR	Japan Material Testing Reactor (Japan)
JSC “TVEL”	Joint Stock Company “TVEL” (Russia)
LWR	light water reactor
NRC	Nuclear Regulatory Commission (U.S.)
NSRR	Nuclear Safety Research Reactor (Japan)
OD	outer diameter
PBF	Power Burst Facility (U.S.)
PCMI	pellet-cladding mechanical interaction
PNNL	Pacific Northwest National Laboratory
PWR	pressurized-water reactor
RAPTA-5	code for calculating the fuel behavior under accident transients (Russia)
RIA	reactivity- initiated accident
RIAR	Research Institute of Atomic Reactors (Russia)
RRC KI	Russian Research Center “Kurchatov Institute” (Russia)
SED	strain energy density
SPERT	Special Power Excursion Reactor Test (U.S.)
VNIIEF	All-Russian Research Institute of Experimental Physics (Russia)
VNIINM	All-Russian Research Institute of Inorganic Materials (Russia)
VVER	Vodo-Vodyanoy Energetichesky Reaktor (Russian pressurized-water reactor)

1. INTRODUCTION

During 1980s and at the beginning of 1990s, experimental investigations were performed in the IGR and GIDRA research reactors to validate safety criteria for the unirradiated and irradiated Russian VVER pressurized water reactor (PWR) fuel under reactivity-initiated accident (RIA) conditions [1, 2]. Results of these investigations revealed the following:

1. The fuel fragmentation threshold of unirradiated VVER fuel rods (Zr-1%Nb cladding and UO₂ pellets with the central hole) occurred when the peak averaged fuel enthalpy^a reached 300 cal/g. The fragmentation threshold of the VVER fuel irradiated up to burnup of 50 MWd/kg U was higher than 250 cal/g (the maximum value achieved in the IGR tests). The fragmentation threshold of the unirradiated fuel was insensitive to the coolant pressure in the range of 0.1–16 MPa.
2. As for the failure threshold^b, three different mechanisms appear to define this threshold as a function of the initial pressure drop across the cladding:
 - A high temperature cladding burst for the case when the fuel rod internal gas pressure exceeded the coolant pressure significantly^c.
 - The cladding melting for the case when the pressure drop across the cladding was close to zero.
 - A high temperature cladding collapse and the cladding melting for the case when the coolant pressure exceeded the fuel rod internal gas pressure significantly.
3. These three cases were characterized by the following failure thresholds (the peak averaged fuel enthalpies at failure):
 - 160 cal/g for unirradiated and irradiated pressurized fuel rods (2–2.5 MPa).
 - 270 cal/g for unirradiated, unpressurized fuel rods.
 - 250 cal/g for unirradiated pressurized fuel rods (2–2.5 MPa) tested under high-pressure coolant conditions (16 MPa).

The consideration of these results suggested that the high enthalpy failure thresholds are typical for a range of fill gas pressure level in VVER fuel under RIA conditions. In addition, results from the IGR reactor with high burnup fuel rods refabricated from the VVER-1000 commercial fuel elements further suggested that unirradiated and irradiated (50 MWd/kg U) VVER fuel rods had the same failure mechanism and the same failure threshold.

Comparative analysis of the VVER RIA test data developed for unirradiated fuel and the similar data obtained for the PWR unirradiated fuel rods (Zircaloy-4 cladding and UO₂ solid pellets) [3, 4] showed that the RIA behavior of both fuel types had no significant differences. But the comparison of the VVER and PWR^d high burnup fuel behavior indicated that as distinct from the VVER fuel, some PWR fuel rods with the burnup of 50–60 MW d/kg U failed at a very low fuel enthalpy (30–80 cal/g) [5, 6]. Further analyses showed that the low enthalpy failure of the PWR fuel was caused by the mechanical interaction between fuel and the highly corroded

^a The procedure of the peak averaged fuel enthalpy determination consists of two steps:

- The average enthalpy along the fuel radius is calculated for each time step and each axial elevation.
- The maximum (peak) value is selected from the obtained time dependent and axial distributions

^b In contrast to the fragmentation threshold, which is associated with the core coolability limit, the failure threshold characterizes the cladding failure conditions, i.e. the failure of the first safety barrier and the beginning of the fuel/coolant contact. In general, the failure threshold is lower than the fragmentation threshold. The consideration of these two thresholds separately may be of importance for the analysis of high burnup fuel phenomena

^c This case was studied taking into account the results of the previous calculations characterizing the maximum FGR and internal fuel pressure at the end of the VVER-1000 fuel base irradiation. These calculations were performed with the use of more than conservative assumptions

^d The PWR experimental data base characterizing the high burnup fuel behavior was obtained due to RIA tests in the CABRI and NSRR research reactors

cladding at the early stage of power pulse (low temperature pellet-cladding mechanical interaction or PCMI failure) [5, 6, 7, 8].

Thus, the experimental results obtained for the VVER high burnup fuel did not agree with the experimental results obtained for the PWR high burnup fuel. Clues to these differences can be seen in Fig. 1.1.

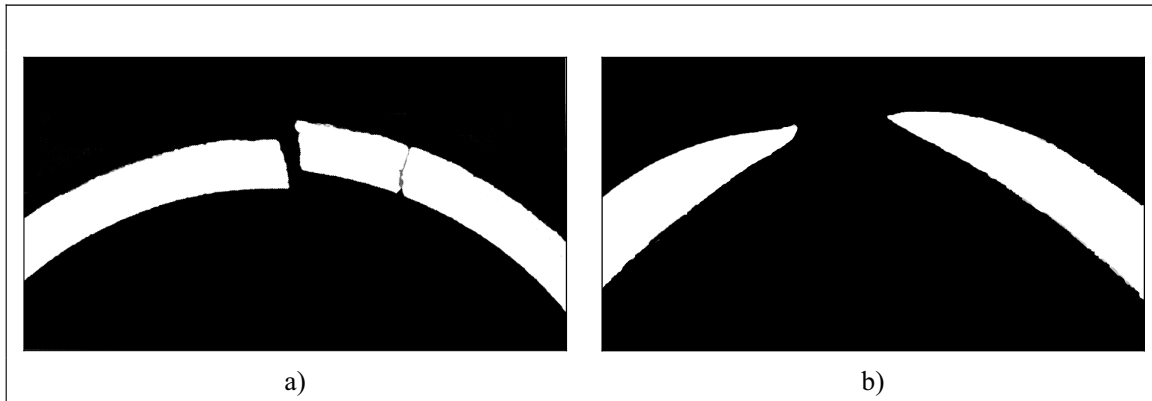


Fig. 1.1. Demonstration of different types of the cladding failure under the RIA conditions
(a) The brittle fracture of the PWR irradiated cladding caused by the PCMI loading at the low cladding temperature [9]^a and (b) the ductile rupture of the VVER irradiated cladding at the high temperature [2]^b

Possible reasons for these differences are further illustrated by the data in Table 1.1.

Table 1.1. Some comparative data characterizing the RIA tests with the VVER and PWR high burnup fuel [2, 5, 6]

Parameter	Unit	Value	
		VVER	PWR
1. Burnup	MW d/kg U	48	44–64
2. Cladding oxidation (ZrO ₂ thickness) after the base irradiation ^c	μm	3–5	40–80 with the spalling effect
3. Hydrogen content in the irradiated cladding after the base irradiation ^c	ppm	30–60	Tendency towards the local hydride accumulation with the concentration up to 2600 ^d
4. Pulse width under RIA test conditions	ms	700–900	4–10 ^e

These data show that two key factors may be responsible for the different behavior of high burnup fuel rods with Zr-1%Nb and Zry-4 claddings under RIA conditions:

- ductility margin of the irradiated cladding;
- pulse width in RIA tests.

It should be noted that a sharp increase in power leads to a sharp increase of the fuel temperature that subsequently results in fuel radial thermal expansion and swelling. Due to the thermal lag effect, the cladding

^a The CABRI test (REP-Na 1)

^b The IGR test (fuel rod #H7T)

^c Presented data characterize the cladding samples used for the RIA tests

^d Result of evaluations are presented in [6]

^e The first CABRI tests (REP-Na 1–3, 5) are presented in this Table

temperature is kept low at the beginning of this process. At that moment when the radial fuel strain becomes larger than the radial pellet/cladding gap, the PCMI type of the cladding loading is observed. The stress caused by the contact pressure of the fuel expanding on the “cold” cladding is a reason for the cladding premature failure under RIA conditions (the failure at the low fuel enthalpy). Moreover, it is obvious that these phenomena are more pronounced for high burnup fuel because the pellet/cladding gap disappears at high burnup. In addition, effects of the radiation damage and cladding oxidation during the base irradiations lead to a decrease in cladding ductility. These considerations have shown that a reasonable margin of the cladding residual ductility provides the prevention of the PCMI failure at the low fuel enthalpy provided that no local hydride accumulation exists.

The comparative studies of the IGR and NSRR/CABRI tests suggested that the VVER irradiated claddings had a significant ductility margin in contrast to the tested PWR irradiated cladding. This assumption was in agreement with the data presented in Table 1.1. Specifically:

- The Zr-1%Nb cladding had a very low oxidation and hydriding.
- The Zry-4 cladding had more significant oxidation accompanied not only by the uniform cladding hydriding but also by the presence of hydride clusters or rim layers on the outer cladding surface.

These preliminary conclusions concerning the Zr-1%Nb and Zry-4 ductility were confirmed by the first results of special mechanical tests [10, 11]. In spite of these results, a wide international discussion was initiated at that time. The focus of this discussion was concentrated on several issues:

- The IGR tests with ductile cladding were performed under the wide pulse conditions (700–900 ms).
- The NSRR and first CABRI tests (REP-Na 1–3, 5) with the oxidized claddings were performed under the very narrow pulse conditions (4–10 ms).
- Taking into account that the narrow pulse conditions led to more significant stresses at the PCMI loading, the following two questions were formulated:
 - ⇒ Is ductility of irradiated cladding sufficient to avoid PCMI failure at a specific enthalpy but arbitrary pulse width?
 - ⇒ Would tests of irradiated cladding with a significant degradation of the cladding ductility avoid PCMI failure (at low enthalpy) if these tests were performed at a wider pulse width than NSRR and some CABRI tests?

The development of appropriate questions had a practical purpose because IGR pulses were wider than the commercial reactor case, and NSRR and some CABRI pulses were shorter than the commercial reactor case.

To answer these questions, numerous calculations were performed with the use of different computer codes but it was understood that results of these calculations had quite a speculative character. This was a result of:

- the limited data base on the mechanical and thermal physical properties of high burnup fuel and the irradiated cladding;
- simplified modeling of high burnup fuel behavior;
- the absence of the cladding failure criteria for specific PCMI loading.

Therefore, results of the international discussion led to the following conclusion: only direct experiments could provide convincing answers to the above formulated questions. In accordance with this conclusion, the decision to test the VVER high burnup fuel (50–60 MW d/kg U) under the narrow pulse conditions was made by the Russian vendor of the VVER fuel (Joint Stock Company “TVEL”)^a. To develop and perform this new test program, the following Russian Institutes were involved:

- A.A. Bochvar All-Russian Research Institute of Inorganic Materials (VNIINM);
- Russian Research Centre “Kurchatov Institute” (RRC KI);

^a The similar decision concerning new tests with the PWR high burnup fuel at wider pulses of the CABRI reactor was made in France

- Russian Federal Nuclear Centre “All-Russian Research Institute of Experimental Physics” (VNIIEF);
- State Research Centre “Research Institute of Atomic Reactors” (RIAR).

The preliminary analysis of this program showed that the BGR reactor, located in the VNIIEF, could be used to produce narrow pulses needed for high burnup fuel tests. However, more detailed studies of this task revealed a serious technical problem: installation of the VVER fuel rod surrounded with the water coolant in the central channel of the BGR reactor would result in dangerous thermal stresses in the BGR core. To solve this problem, it was decided to develop a new side channel for the BGR reactor. Implementation of this approach allowed the program of tests for the VVER high burnup fuel in the BGR reactor.

This program was carried out during 1997–2001. Twelve fuel rods refabricated from the VVER-1000 and VVER-440 commercial fuel elements with burnups of 47–49 and 60 MW d/kg U, respectively, were tested under narrow pulse conditions with radial average fuel enthalpy in the 115–188 cal/g range [12, 13, 14, 15]. Taking into account the importance of the test results, preparation of this BGR report was arranged with the support of the following organizations:

- Joint Stock Company “TVEL” (Russian Federation);
- U.S. Nuclear Regulatory Commission (United States);
- Institute for Radiological Protection and Nuclear Safety (France).

The report concept and structure are characterized by the following provisions:

- The report consists of two volumes.
- The first volume is devoted to the test program presentation, the description of test procedures, computer codes, analytical approaches, and to the analysis of test results. The Volume 1 structure was optimized on the basis of the following general principles:
 - ⇒ The main part of Volume 1 contains the information concerning the interpretation and analysis of multiparametric test results.
 - ⇒ All technical aspects of these investigations, including the methods used to obtain test and calculation results, are described in appendices attached to this volume.
- The second volume contains the BGR test data organized in Appendices A, B, C, D, E in accordance with the following logical approach:
 - ⇒ Reference characteristics of the VVER-440 and VVER-1000 fuel elements before the base irradiation (Appendix A).
 - ⇒ Fuel cycle parameters and post-irradiation characteristics of commercial fuel rods (Appendix B).
 - ⇒ Characteristics of refabricated fuel rods before the BGR tests (Appendix C).
 - ⇒ Characteristics of the BGR power pulses (Appendix D).
 - ⇒ Characteristics of refabricated fuel rods after the BGR tests (Appendix E).

It should be noted that the individual characteristics for each of twelve refabricated fuel rods before and after the BGR tests are presented in this volume. These characteristics include the test and calculation data needed both for the interpretation of the major physical phenomena and for the use of these data for the verification of computer codes.

References

- 1 V. Asmolov, L. Yegorova “The Russian RIA Research Program: Motivation, Definition, Execution, and Results”, *Nuclear Safety*, Vol.37, No.4, 1996.
- 2 L. Yegorova, V. Asmolov, G. Abyshov, V. Malofeev, A. Avvakumov, E. Kaplar, K. Lioutov, A. Shestopalov, A. Bortash, L. Maiorov, K. Mikitiouk, V. Polvanov, V. Smirnov, A. Goryachev, V. Prokhorov, and A. Vurim

- “Data Base on the Behavior of High Burnup Fuel Rods with Zr-1%Nb Cladding and UO₂ Fuel (VVER Type) under Reactivity Accident Conditions”, *NUREG/IA-0156 (IPSN99/08-02, NSI/RRC KI 2179)*, Vol.1, 2, 1999.
- 3 P. MacDonald, S. Seiffert, Z. Martinson, R. McCardell, D. Owen and S. Fukuda “Assessment of Light-Water-Reactor Fuel Damage During a Reactivity-Initiated Accident”, *Nuclear Safety*, Vol.21, No.5, 1980.
 - 4 M. Ishikawa, S. Shiozawa “A Study of Fuel Behavior under Reactivity Initiated Accident Conditions – Review”, *Journal of Nuclear Materials* 95, 1980.
 - 5 J. Papin, M. Balourdet, F. Lemoine, F. Lamare, J. Frizonett, and F. Schmitz “French Studies on High Burnup Fuel Transient Behavior under RIA Conditions”, *Nuclear Safety*, Vol.37, No.4, 1996.
 - 6 T. Fuketa, F. Nagase, K. Ishijima, and T. Fujishiro “NSRR/RIA Experiments with High Burnup PWR Fuels”, *Nuclear Safety*, Vol.37, No.4, 1996.
 - 7 R. Meyer, R. McCardell, H. Chung, D. Diamond, and H. Scott “A Regulatory Assessment of Test Data for Reactivity-Initiated Accidents”, *Nuclear Safety*, Vol.37, No.4, 1996.
 - 8 R. Montgomery, Y. Rashid, O. Ozer, and R. Yang “Assessment of RIA-Simulation Experiments on Intermediate- and High-Burnup Test Rods”, *Nuclear Safety*, Vol.37, No.4, 1996.
 - 9 F. Schmitz, J. Papin, M. Haessler, J. Nervi, P. Permezer, “Investigation of the behavior of high burnup PWR fuel under RIA conditions in the CABRI test reactor”, *Proc. of the 22nd WRSM*, Bethesda, USA, October 23-26, 1994 (NUREG/CP-0140, Vol.2).
 - 10 L. Yegorova, F. Schmitz, J. Papin “Mechanical Behavior of Fuel Element during RIA Transients”, *Proceedings of Forum for Nuclear Safety (EUROSAFE)*, Paris, 1999.
 - 11 M. Balourdet, C. Bernaudat, V. Basini, N. Hourdequin “The PROMETRA Programme: Assessment of Mechanical Properties of Zircaloy 4 Cladding during an RIA”, *SMIRT 15th*, Seoul, August 1999.
 - 12 Yu. Bibilashvili, L. Yegorova “Some Results of the New In-Pile Tests on the VVER High Burnup Fuel Behavior at a Narrow Pulse”, *Proceedings of the 2nd CABRI Technical Review Meeting*, Cadarache, France, 1999.
 - 13 Yu. Bibilashvili, N. Sokolov, O. Nechaeva, A. Salatov, F. Sokolov, V. Asmolov, L. Yegorova, E. Kaplar, Yu. Trutnev, I. Smirnov, V. Ustinenko, V. Sazhnov, V. Smirnov, A. Goryachev “Experimental Study of VVER High Burnup Fuel Rods at the BGR Reactor Under Narrow Pulse Conditions”, *Proceedings of International Topical Meeting on Light Water Reactor Fuel Performance*, Park City, USA, 2000.
 - 14 V. Asmolov, L. Yegorova, Yu. Bibilashvili, and O. Nechaeva “Summary of Results on the Behavior of VVER High Burnup Fuel Rods Tested under Wide and Narrow Pulse RIA Conditions”, *Proceedings of the Twenty-Seventh Water Reactor Safety Information Meeting*, Washington DC, USA, 1999 (NUREG/CP-0169).
 - 15 Yu. Bibilashvili, A. Goryachev, O. Nechaeva, A. Salatov, V. Sazhnov, I. Smirnov, N. Sokolov, Yu. Trutnev, V. Ustinenko, L. Yegorova “Study of High Burnup VVER Fuel Rod Behavior at the BGR Reactor Under RIA Conditions: Experimental Results”, *Proceedings of the OECD Topical Meeting on RIA Fuel Safety Criteria*, Aix-en-Provence, France, 2002 (NEA/CSNI/R(2003)8/Vol.2).

2. THE BGR/RIA TEST PROGRAM: MAJOR PROVISIONS

The goal of this program was to study the VVER high burnup fuel behavior in the maximum wide range of the peak averaged fuel enthalpy generated by the narrow power pulse (2.5–3.1 ms) of the BGR reactor. The practical achievement of this goal was accompanied by the development of the combined investigations listed in Table 2.1.

Table 2.1. Research tasks

Task	List of actions
1. Manufacturing of high burnup fuel rods and capsule devices	<ul style="list-style-type: none"> To refabricate test fuel rods from commercial high burnup fuel elements
	<ul style="list-style-type: none"> To provide the close connection between the design of the BGR and IGR fuel rods
	<ul style="list-style-type: none"> To manufacture 12 capsule devices for the test fuel rods surrounded with the water coolant. To provide for free axial displacement of fuel rods during the heating phase
2. The preliminary determination of neutronic parameters for the BGR side channel and the optimization of the channel design ^a	<ul style="list-style-type: none"> To perform neutronic calculations of the BGR reactor with the side channel and to optimize the design and material scheme of the side channel taking into account the following general requirement: to increase the fission numbers in the VVER high burnup fuel as much as possible
3. Development of experimental data characterizing neutronic parameters of the BGR/RIA tests	<ul style="list-style-type: none"> To perform the scoping tests with the VVER unirradiated fuel rods and to determine the correlation between energy deposition in the VVER fuel rod and in the BGR reactor
	<ul style="list-style-type: none"> To obtain the test data characterizing the spatial and time dependent distributions of energy deposition in the VVER fuel rod
4. BGR tests of the first six VVER high burnup fuel rods (The first stage of the BGR tests)	<ul style="list-style-type: none"> To perform the BGR tests of five VVER pressurized fuel rods with 47–49 MW d/kg U burnup in the 100–160 cal/g range of the peak average fuel enthalpy^b at the test-to-test successive increase of fuel enthalpy and to determine the failure threshold of these fuel rods
	<ul style="list-style-type: none"> To perform the first test of the fuel rod with 60 MW d/kg U burnup at the maximum possible peak fuel enthalpy^c
	<ul style="list-style-type: none"> To perform the preliminary post-test examinations of these fuel rods and to develop the program for the next six VVER high burnup fuel rods

^a The capsule with the VVER high burnup fuel rod was placed in this channel before the BGR test

^b The motivation of this approach was connected with the following considerations:

– the use of pressurized fuel rods was to perform a direct comparison of the IGR (wide pulse) and BGR (narrow pulse) test results. Taking into account that the IGR tests were performed with pressurized fuel rods, it was decided to keep this approach for the BGR fuel rods;

– the failure threshold of the VVER high burnup fuel was estimated as 160 cal/g under the IGR test conditions. Therefore, this value was used as the absolute maximum for the BGR tests;

– the analysis of the first NSRR and CABRI tests with PWR high burnup fuel rods showed that the failure threshold of fuel rods with the relatively ductile cladding was higher than 100 cal/g

^c It was assumed that the character and scale of the fuel damage after this test would allow adjustment in testing other fuel rods with 60 MW d/kg U burnup

Task	List of actions
5. BGR tests of the next six VVER high burnup fuel rods (The second stage of the BGR tests)	<ul style="list-style-type: none"> • To modify the material of the BGR side channel: to change the graphite (C) moderator for the beryllium (Be) moderator^a • To perform the BGR tests of six VVER high burnup fuel rods (three with burnup of 47 MW d/kg U and three with burnup of 60–61 MW d/kg U) and: <ul style="list-style-type: none"> ⇒ to determine the failure threshold of pressurized fuel rods with burnup of 60 MW d/kg U; ⇒ to compare the failure thresholds and mechanisms of pressurized and unpressurized fuel rods with burnup of 47 and 60–61 MW d/kg U; ⇒ to obtain the additional experimental data confirming the lack of fragmentation of the VVER high burnup fuel rods in the maximum wide range of the peak fuel enthalpy
6. Pre-test and post-test examinations of the VVER commercial fuel elements used for the refabrication and the VVER high burnup fuel rods used for the BGR tests	<ul style="list-style-type: none"> • To perform the examination of the VVER fuel elements used for the refabrication of the BGR test fuel rods emphasising the following parameters: axial burnup distribution, radial geometrical sizes (including the rim layer thickness), parameters of the cladding oxidation (ZrO₂ thickness and hydrogen content), fuel grain size and fuel density, radial pellet/cladding gap, etc. • To develop the reference data characterizing the VVER high burnup fuel rods before the BGR tests • To obtain the individual data for each refabricated fuel rod including: axial sizes, burnup, fuel mass, free gas volume, pellet/cladding gap, cladding outer diameter • To measure the individual characteristics of each fuel rod after the BGR tests (results of γ-scanning, axial distribution of the cladding outer diameter, fuel outer diameter, ZrO₂ thickness, the cladding residual hoop strain, FGR parameters for the unfailed fuel rods) • To prepare photographs of macro- and microstructure of fuel elements and fuel rods
7. Determination of energy deposition in refabricated fuel rods during the BGR tests	<ul style="list-style-type: none"> • To measure the BGR power as a function of time and to determine the number of fissions in the fuel of refabricated fuel rods for each BGR test • To develop and to validate (using results of special tests) the procedure for the determination of neutronic parameters of the VVER high burnup fuel rods during the BGR tests • To determine the radial axial and time-dependent distributions of energy deposition for each tested fuel rod

^a This action was performed in accordance with results of the first stage of the BGR tests. These results showed that the use of the graphite moderator did not achieve failure in VVER fuel rods with 60 MW d/kg U burnup. Appropriate calculations demonstrated that the Be moderator would allow a significant increase in the fuel enthalpy. It was assumed that the character and scale of the fuel damage after this test would allow adjustment in the testing of other fuel rods with 60 MW d/kg U burnup

Task	List of actions
8. Determination of fuel enthalpy in tested fuel rods	<ul style="list-style-type: none"> • To select thermal mechanical computer codes which will be used for this goal and to perform the verification of these codes
	<ul style="list-style-type: none"> • To prepare the initial data for each fuel rod
	<ul style="list-style-type: none"> • To perform the calculations and to determine the spatial and time dependent distributions of fuel enthalpy for each fuel rod using two independent computer codes
	<ul style="list-style-type: none"> • To compare obtained results and to use the average value from codes as the best estimation of fuel enthalpy

The detailed considerations of these tasks revealed several general program problems:

- It was impossible to obtain the information characterizing the mechanical response of the fuel rod (failed, unfailed) at a given enthalpy just after the test because the BIGH reactor had no hot cells intended for examinations of high burnup fuel.
- The scoping tests performed with the unirradiated fuel rods showed that the BIGH side channel with the graphite moderator would achieve 150 and 125 cal/g maximum enthalpy for fuel rods with burnup of ≈ 50 and 60 MW d/kg U, respectively.
- The accurate determination of the coefficient characterizing the ratio between the energy deposition in the BIGH reactor and energy deposition in the tested high burnup fuel rod was not performed earlier because special radiochemical measurements of fission numbers in the tested high burnup fuel were not completed.

The program approach developed to take into account these and other problems resulted in the following provisions:

- Each of two stages of the BIGH test program (six and six VVER fuel rods) was divided into two substages: each substage included tests of three fuel rods. After each substage, the capsules with tested fuel rods were transported to hot cells of the RIAR. The information obtained during the visual examinations of tested fuel rods was used to adjust the program of the next substage of tests.
- In this connection, it should be noted that the analysis of post-test examination results obtained after the first program stage showed that neutronic characteristics of the BIGH side channel (manufactured with the use of graphite as the moderator) did not achieve maximum enthalpy for both types of the VVER fuel rods (fuel rods with burnup of 47–49 and 60 MW d/kg U). To solve this problem, it was decided to manufacture a new side channel with the Be moderator. Thus, the second stage of the BIGH program was performed with the modified side channel. The comparative data characterizing the capabilities of these types of side channels are presented in Fig. 2.1.

In spite of above listed actions, the development of technical requirements for each test was combination of technical judgement and expert opinion (based on the research intuition). This fact was caused by the following reasons:

- the significant uncertainty in the experimental correlation between the given parameters of the BIGH reactor (the control rod set position) and the fuel enthalpy in the VVER high burnup fuel rod (see Fig. 2.2);
- the disparity between the number of varied test parameters and the number of available test rods.

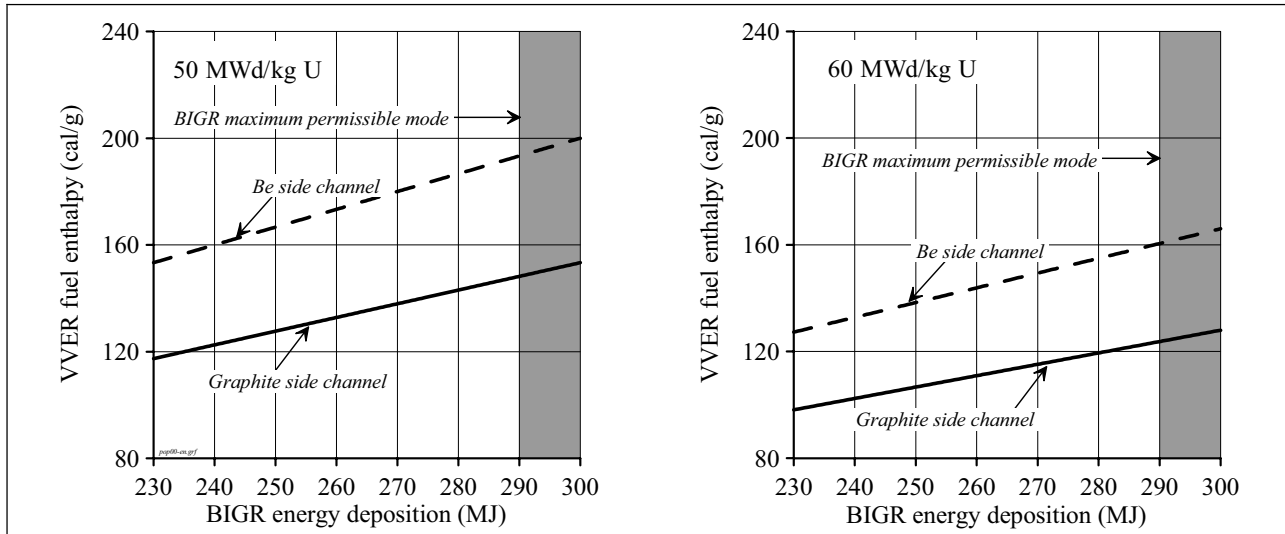


Fig. 2.1. The correlation between the peak average fuel enthalpy in the VVER fuel with 47–49 and 60 MW d/kg U burnup and energy deposition in the BGR reactor

As for the varied test parameters, the compromise was found on the basis of the following list:

- fuel burnup: 47–49, 60 MW d/kg U;
- fill gas pressure inside fuel rods: 2, 0.1 MPa^a;
- fuel enthalpy: the adjustment of designated values after each substage of the program taking into account:
 - ⇒ the first task connected with the determination of failure thresholds as a function of burnup and may be as a function of fill gas pressure;
 - ⇒ the second task connected with the estimation of the maximum fuel enthalpy not causing the fuel rod fragmentation.

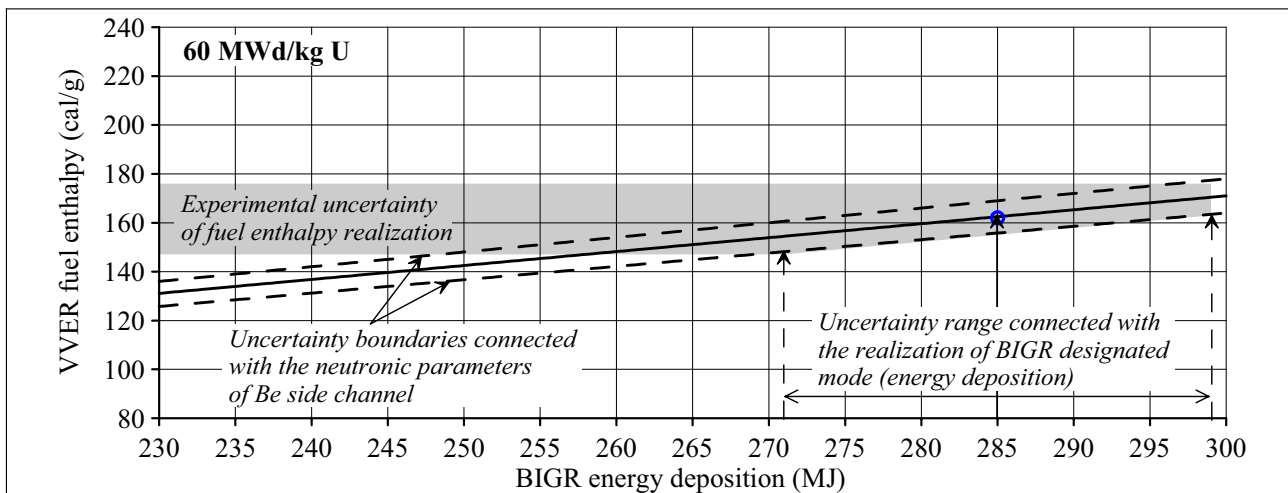


Fig. 2.2. Demonstration of experimental uncertainties between the designated test mode of the BGR reactor (285 MJ in this case) and fuel enthalpy in the VVER high burnup fuel

^a Helium at the room temperature

In accordance with these considerations, twelve VVER high burnup fuel rods were manufactured. Parameters of these fuel rods and the program scheme for the BGR tests are presented in Table 2.2.

Table 2.2. The parameters for the BGR tests

Parameter	First program stage						Second program stage					
	First substage			Second substage			Third substage			Forth substage		
Fuel rod number	RT1	RT2	RT3	RT4	RT5	RT6	RT7	RT8	RT9	RT10	RT11	RT12
Fuel burnup (MW d/kg U)	48.3	48.0	47.5	60.1	48.6	47.8	60.5	60.0	59.8	46.9	47.2	47.3
Fill gas pressure (He at room temperature) (MPa)	2.1	2.1	2.1	2.1	2.1	2.1	2.0	2.0	0.1	2.0	2.0	0.1

The BGR test program was performed in cooperation with several Russian institutes in accordance with the scheme illustrated in Fig. 2.3. The use of this cooperation was the basis to combine efforts of different specialists and to carry out tests of twelve high burnup fuel rods, pre-test and post-tests examinations of these fuel rods, organization and analysis of obtained data within a very short period of time.

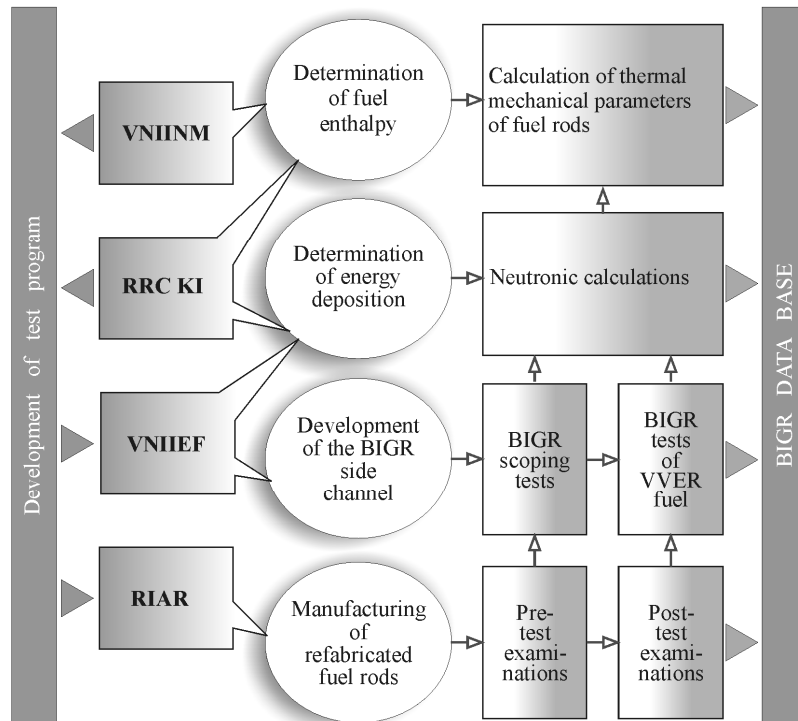


Fig. 2.3. Cooperative efforts of research institutes involved in the BGR test program

3. THE CHARACTERIZATION OF THE VVER HIGH BURNUP FUEL RODS AND OF THE BIGR REACTOR

3.1. The VVER fuel and refabricated test rods

12 VVER high burnup fuel rods (#RT1–12) were refabricated from six commercial fuel elements irradiated in three fuel assemblies (FA) #222, 228, 108^a in the Unit 3 of the Kola^b nuclear power plant (the Kola NPP, #222), in the Unit 4 of the NovoVoronezh^c nuclear power plant (NV NPP, #228), in the Unit 5 of the NovoVoronezh nuclear power plant (NV NPP, #108).

In accordance with the pattern presented in Fig. 3.1, FAs #222 and 228 were irradiated in the VVER-440 reactor and FA #108 was of the VVER-1000 type.

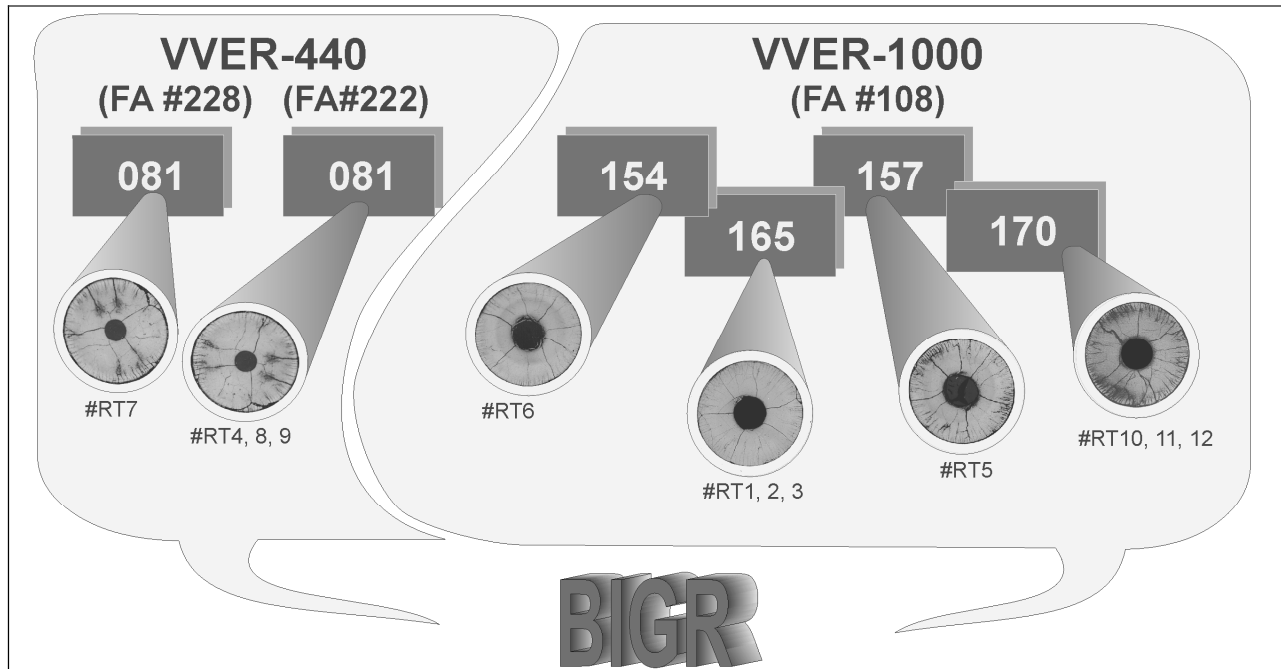


Fig. 3.1. The refabrication procedure for the BIGR/RIA tests^d

The detailed data characterizing the design and material scheme of the VVER fuel assemblies and VVER commercial fuel elements before and after the base irradiation are organized in Appendices A and B of Volume 2. Appendix B contains characteristics of the appropriate fuel cycles. The procedures used to obtain the experimental values of fuel parameters are described in Appendix A of this volume of the report.

The analysis of the whole scope of obtained data provided several important comments needed to understand and to interpret results of the BIGR tests:

^a These reference numbers correspond to the following commercial numbers:

228. 23635228

222. 14422222

108. ED4108

^b Abbreviation of the word “Kolskaya”

^c Abbreviation of the word “NovoVoronezhskaya”

^d Numbers of the VVER commercial fuel elements (081, 154, 157, 165, 170) correspond to those presented in Figs. B.2, B.4, B.6 in Appendix B of Volume 2

1. The VVER fuel elements are characterized by the following design features:
 - the VVER cladding is manufactured from the Zr-1%Nb alloy (the E110 alloy);
 - the VVER fuel pellets (UO_2) have a central hole. The diameter of the central hole is 1.2–1.7 mm and 2.4 mm for the VVER-440 and VVER-1000 fuel pellets, respectively^a (see Fig. 3.2);
 - the fill gas pressure is 0.5–0.7 MPa for the VVER-440 fuel elements and 1.9–2.4 MPa for the VVER-1000 fuel elements^b;
 - reference radial geometrical sizes (for both types of fuel elements) are as follows^c:
 - ⇒ the cladding outer diameter: 9.1–9.13 mm;
 - ⇒ the cladding inner diameter: 7.72 mm;
 - ⇒ the pellet outer diameter: 7.54–7.60 mm.
2. The VVER-1000 fuel elements were used to refabricate VVER/BIGR fuel rods with 47–49 MWd/kg U burnup. The VVER/BIGR fuel rods with 60 MWd/kg U burnup were refabricated from the VVER-440 fuel elements.
3. Those parts of the VVER-440 and VVER-1000 mother fuel elements used for the refabrication had the following parameters of the cladding oxidation (see Fig. 3.2):
 - ZrO_2 outer layer: 3–5 μm ;
 - ZrO_2 inner layer^d: 0 μm for the VVER-1000 fuel elements with burnup of 47–49 MWd/kg U, 8–10 μm for the VVER-440 fuel elements with burnup of 60 MWd/kg U.
 - hydrogen content in the irradiated cladding: 50–80 ppm weight.

The refabricated fuel rods for the BIGR/RIA tests were manufactured in accordance with the nomenclature presented in Table 2.2 (Chapter 2). These fuel rods had the following reference characteristics:

- the cladding outer diameter: 9.06–9.09 mm;
- the cladding thickness: 0.69–0.73 mm;
- fuel outer diameter: 7.57–7.69 mm;
- fuel/cladding radial gap: 0.012–0.032 mm for fuel rods with 47–49 MWd/kg U burnup, 0.000–0.003 mm for fuel rods with 60 MWd/kg U burnup;
- fill gas pressure (helium) at the room temperature:
 - ⇒ 10 fuel rods: 2.0–2.1 MPa;
 - ⇒ 2 fuel rods: 0.1 MPa.
- fuel burnup:
 - ⇒ 8 fuel rods: 47–49 MWd/kg U;
 - ⇒ 4 fuel rods: 60 MWd/kg U.
- fissile length: 149–155 mm.

Fig. 3.3 illustrates the design of fuel rods.

^a For fuel elements used on the refabrication of the BIGR fuel rods

^b The initial values (before the irradiation) at the room temperature

^c Before the irradiation

^d The chemical composition of these layers was not analyzed during the BIGR test program. This structure is the layer of pellet/cladding chemical interaction and, based on the expert view of the authors, the chemical composition of this layer is close to ZrO_2

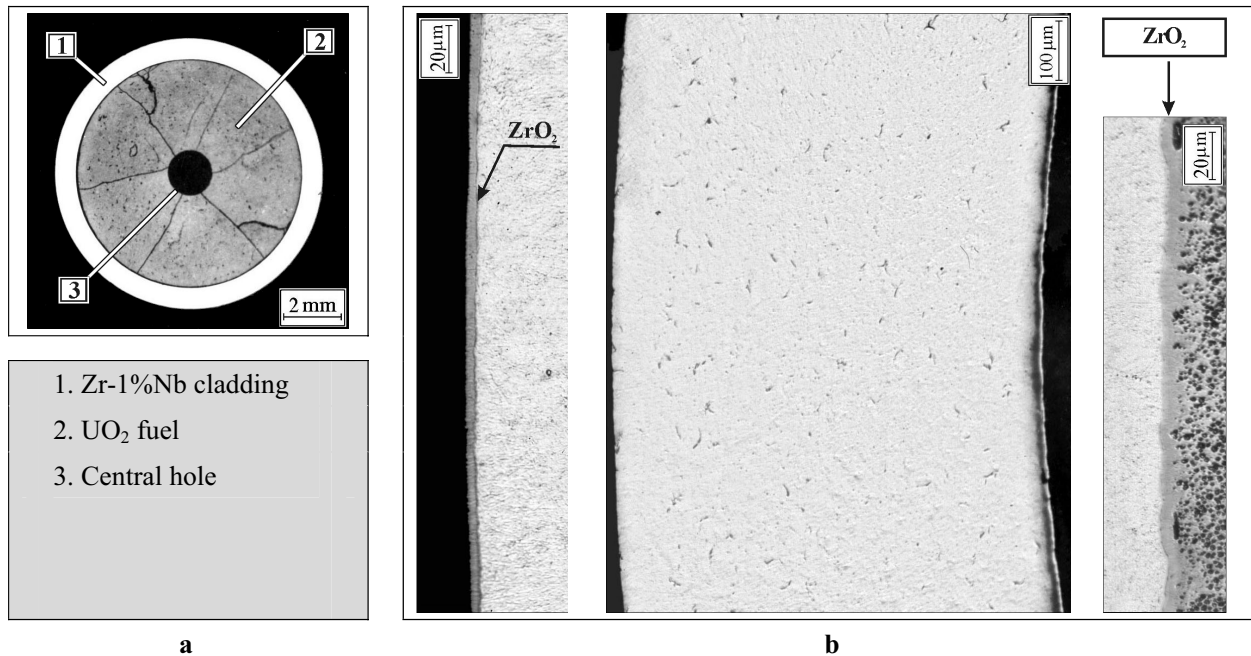


Fig. 3.2. The VVER-440 commercial fuel element (FA #228, FE^a #081) after the base irradiation up to burnup of 60 MWd/kg U (a) The cross-section view, (b) The cladding microstructure

To provide the most complete comparative analysis of the BIGH test results, careful pre-test examinations and neutronic calculations of refabricated fuel rods were performed including the individual determination of such parameters as:

- axial and radial geometrical sizes;
- the radial distribution of isotope nuclear concentrations and burnup;
- axial distributions of the cladding outer diameter (in 16 azimuthal positions), fuel mass, burnup, free gas volume.

The γ -scanning, eddy-current examinations were also performed.

The whole scope of the obtained pre-test data is presented in Appendix C of Volume 2 of the report. The procedures used for the determination of these parameters are described in Appendix A of this volume of the report.

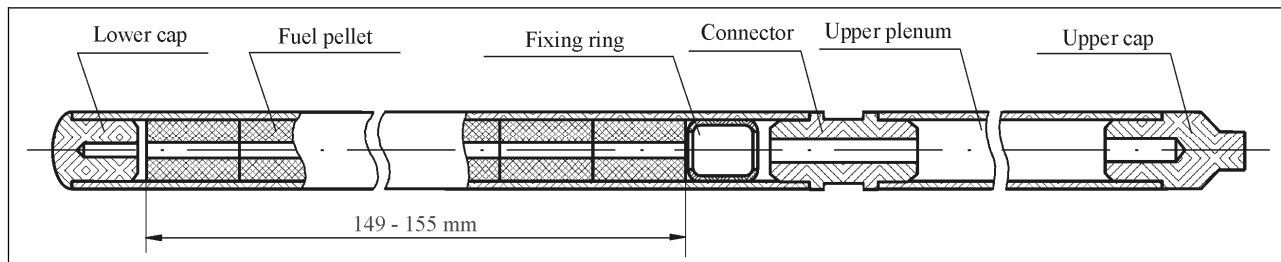


Fig. 3.3. Design of refabricated fuel rods

^a FE – fuel element

3.2. The BGR reactor and capsule device

The BGR reactor is a fast pulse research reactor with a homogeneous uranium-graphite core. The reactor core is arranged (along the height and radius) from the ring-type sections. Each ring is manufactured from the mixture of UO_2 and graphite by pressing. The reactor height is 670 mm and the outer diameter is 760 mm (see Fig. 3.4).

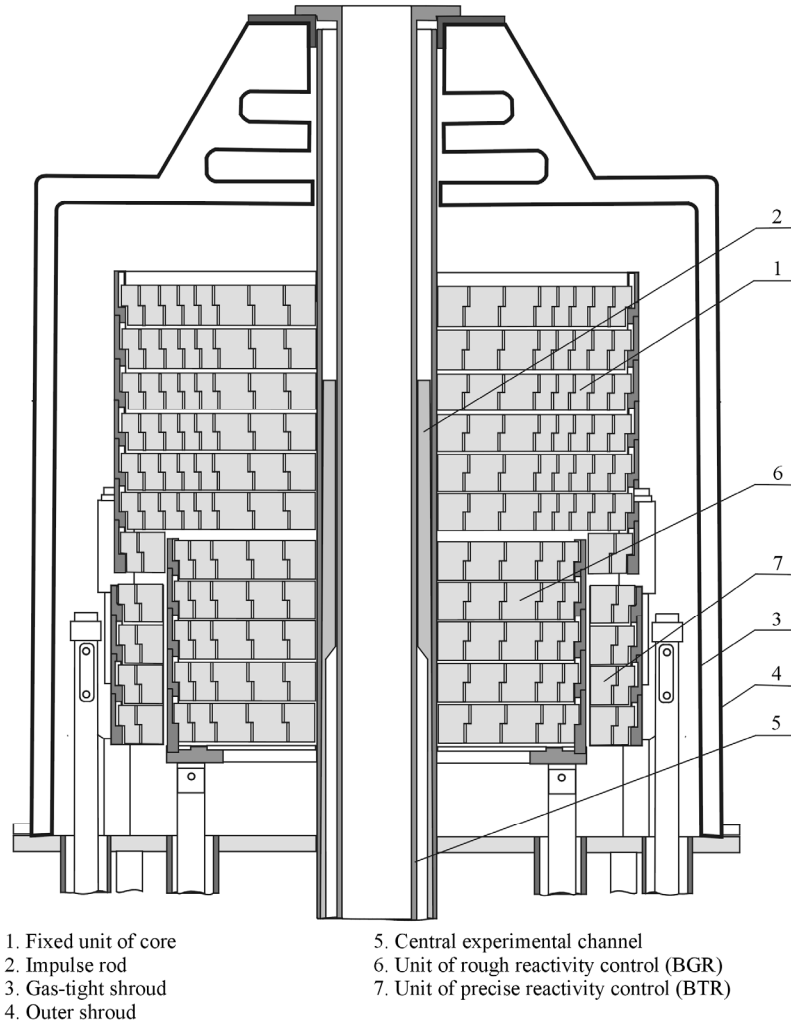


Fig. 3.4. Axial section of the BGR reactor

The central experimental channel of 100 mm diameter is located inside the reactor core. The reactor core consists of three parts:

- the unmovable part (fixed unit);
- the movable (in the axial direction) part intended for the rough reactivity control (BGR)^a.
- the movable part intended for the precise reactivity control (BTR)^b.

The power pulse is generated in the BGR reactor due to the following actions and physical phenomena:

- the relocation of BGR and BTR into a definite position provides the pre-set positive reactivity;

^a BGR is an abbreviation of the Russian term “Block Gruboy Regulirovki”

^b BTR is an abbreviation of the Russian term “Block Tochnoy Regulirovki”

- a fast insertion of a special impulse rod into the reactor core brings the reactor into super prompt critical condition and causes the power rise due to fission on fast neutrons;
- taking into account that the BGR reactor has the negative temperature coefficient of reactivity, the increase of the reactor core temperature leads to the decrease of the reactor power;
- the fast relocation of BGR and BTR into the lowest position provides for the reactor shutdown. The basic characteristics of the BGR reactor are listed in Table 3.1.

Table 3.1. General neutronic parameters of the BGR reactor

Fuel	homogeneous mixture of UO ₂ with graphite
C/ ²³⁵ U ratio	~16
Enrichment	90%
UO ₂ -C fuel mass	833 kg
²³⁵ U mass	400 kg
Effective neutron lifetime	3.6×10^{-7} s
Effective delayed neutron fraction	0.78×10^{-2}
Quasi-static thermal coefficient of reactivity	$-0.089 \times 10^{-2} \beta_{\text{eff}}/\text{MJ}$
Total energy release in core during the maximum pulse	~300 MJ (~ 1×10^{19} fissions)
Maximum fuel temperature	~900°C
Pulse half width	~2.0 ms
Maximum pulse power	70 GW
Maximum steady-state power	500 kW
Maximum neutron fluence per pulse:	
• in central hole	1.2×10^{16} 1/cm ²
• at side surface of core	1.1×10^{15} 1/cm ²
Maximum γ -dose per pulse	3.3×10^6 rad

To provide tests of the VVER high burnup fuel, the BGR reactor was modified. The reason for the modification was as follows: when the capsule device with water and the VVER fuel is located in the reactor central channel the reactor power pulse will result in the local increase of a thermal neutron flux. This fact will cause a significant spatial nonuniformity of the core temperature and, as a consequence, dangerous thermal stresses in the reactor core material. Therefore, the decision was made to locate the capsule with the VVER fuel rods on the outer side of the BGR reactor. However, neutronic calculations showed that in this case, the neutron fluence would be approximately one order of magnitude reduced. In addition, a significant azimuthal nonuniformity of fissions would occur in the VVER fuel. The additional analytical studies revealed the fact that both problems might be solved if the capsule with the VVER fuel rod was surrounded by a graphite layer. The graphite layer in this case will play a part of the reflector and moderator, and this effect will provide the additional thermal neutron flux and reduce the azimuthal nonuniformity of fissions. This design modification was implemented by a special side channel illustrated in Fig. 3.5.

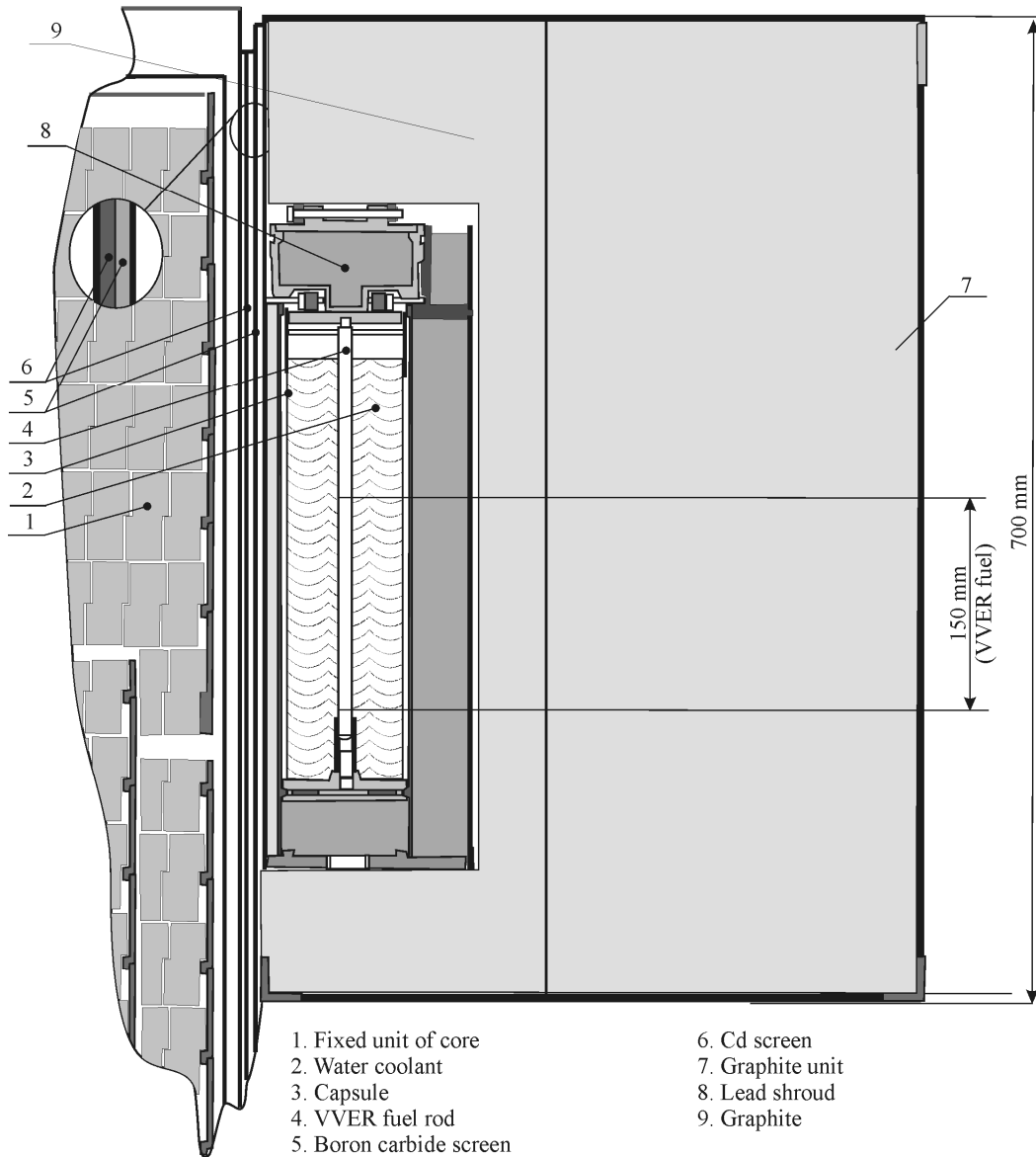


Fig. 3.5. Axial section of the BGR side channel with capsule and VVER fuel rod

The BGR side channel used at the first stage of the program represented the graphite unit with a cavity (see Fig. 3.6). The shape of the graphite unit was the rectangular parallelepiped with the cross-section dimensions 500×700 mm. The capsule device surrounded by the lead shroud^a was installed into the cavity of the graphite unit before the BGR test. After that, the side channel was transported right up to the BGR reactor. To decrease the local overheating of the BGR reactor core and to increase the thermal neutron flux in the capsule device, the boron carbide screen was located between the BGR reactor and side channel. This design scheme of the side channel was used for the BGR test of the refabricated fuel rods #RT1–6. As it was mentioned in Chapter 2, the analysis of obtained results showed that the failure threshold for both types of the VVER high burnup fuel rods (47–49 and 60 MWd/kg U) was not achieved in spite of the maximum test mode of the BGR reactor (290 MJ). A new cycle of neutronic calculations demonstrated that the beryllium substitution for graphite would allow the increase of the maximum fission numbers in the VVER fuel by 30–35%. Taking into account these calculations,

^a The purpose of the lead shroud was to provide the protection of the BGR operating personnel (performing technological manipulations) from γ -radiation caused by the VVER high burnup fuel placed inside the capsule device

the beryllium unit instead of the graphite one was manufactured. The design of the side channel remained approximately the same. The new side channel was used to perform the BGR tests of the VVER high burnup fuel rods #RT7–12 (the second stage of the program).

Fig. 3.5 demonstrates the design scheme of the capsule device designed for the BGR tests. Each of 12 refabricated fuel rods was placed into the central position of the stainless steel capsule. To provide the axial thermal expansion of the fuel rod during the BGR test, a special spring was supplied in the capsule device. The internal volume of the capsule device was filled with water at the room temperature and atmospheric pressure. After that, the capsule device was sealed by welding. No instrumentations of the VVER fuel rods were stipulated for these tests. Therefore, the detailed scoping tests and verification procedures were performed to validate the procedures to determine the energy deposition and fuel enthalpy.

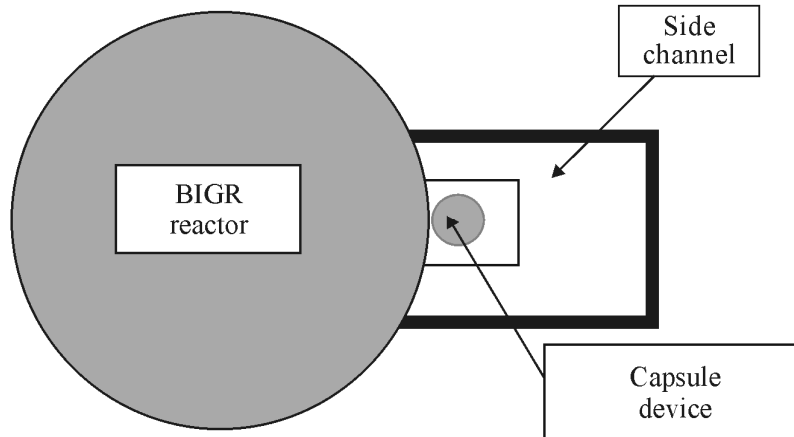


Fig. 3.6. Configuration for the BGR reactor, side channel and capsule device (cross-section view)

3.3. Scoping tests used to determine energy deposition in BGR

The preliminary analysis showed that several different types of special post-test examinations and scoping tests should be performed to determine and to verify the following neutronic parameters of the VVER high burnup fuel during the BGR tests:

- isotopic composition of the VVER fuel;
- axial distribution of the number of fissions in the refabricated fuel rod;
- power history of the BGR refabricated fuel rod;
- the relationship between the BGR energy deposition and the number of fissions in the VVER fuel.

The major provisions of the appropriate experimental procedures and the characterization of obtained results are described in the paragraphs of this section.

Development of test data to verify the computer codes used to determine the isotopic composition of the VVER high burnup fuel

The fuel isotopic composition is the important component of the initial data needed for the energy deposition determination in the VVER refabricated fuel rod during the BGR test. In accordance with the appropriate procedure (see Chapter 4), the isotopic composition was calculated using the TRIFOB computer code [1]. This computer code as applied for the determination of radial and burnup dependent distributions of the VVER high burnup fuel isotopic composition was verified in detail on developing the IGR/RIA test results [2]. But taking into account the limited number of 50 MWd/kg U samples used for the previous verification and the absence of test data characterizing this parameter at the 60 MWd/kg U burnup, it was decided to perform the radio chemical measurements of nuclear concentrations in fuel of six VVER refabricated fuel rods tested at the first stage of the BGR program (#RT1–RT6, burnup of ≈ 50 and 60 MWd/kg U). The description of these special measurements is

presented in Appendix A of this volume. The comparison of calculated and measured nuclear concentrations (see Fig. 3.7) confirmed that a good agreement is observed between these data for all examined samples.

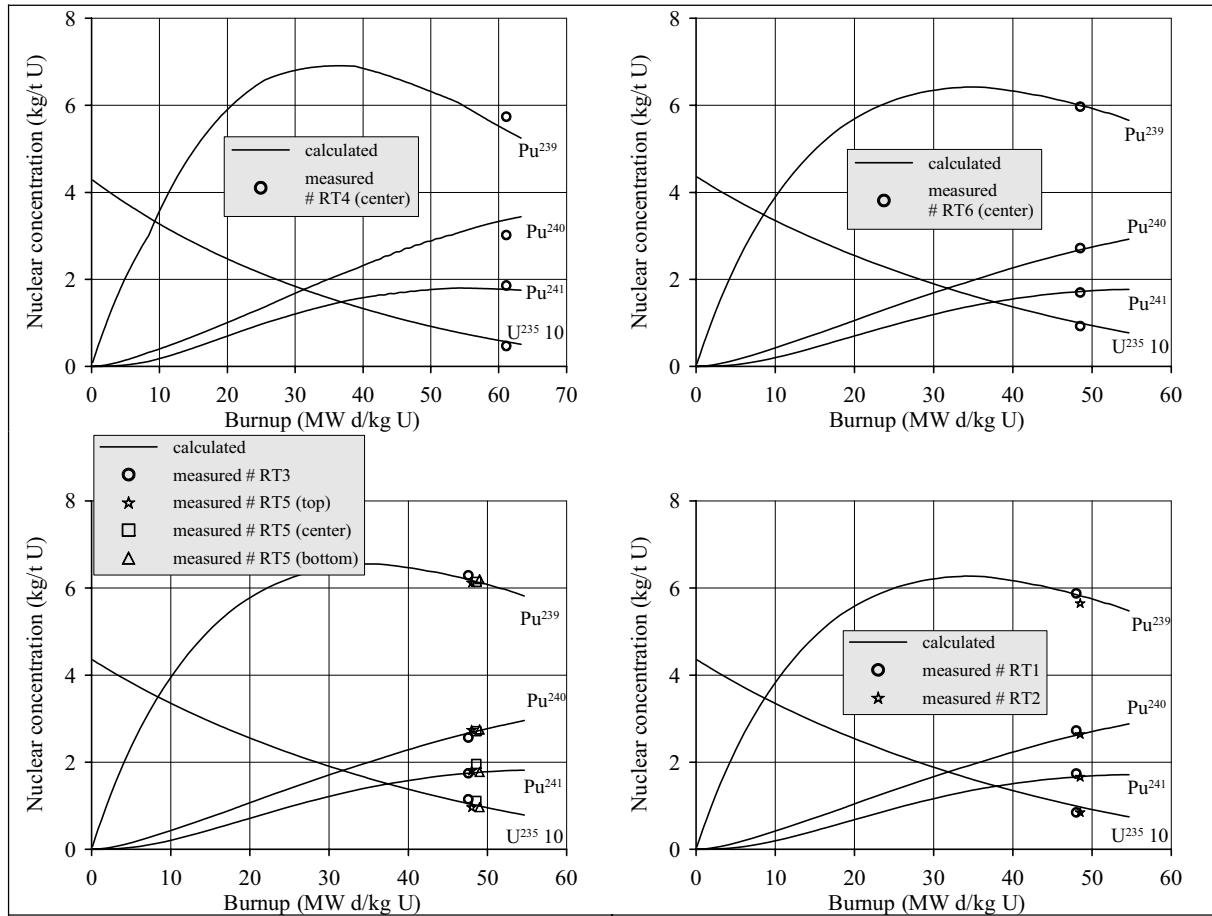


Fig. 3.7. The comparison of calculated (by TRIFOB code^a) and measured data characterizing the fuel isotopic composition in the VVER refabricated fuel rods #RT1–6)

Development of the test data characterizing the axial and azimuthal distributions of the number of fissions in the refabricated fuel rods

To obtain the appropriate data, the following test approaches were used for the first and second stages of the BGR program (graphite and beryllium side channels, respectively):

1. The first stage:

The BGR test of special VVER fuel rods containing unirradiated pellets and two types of activation detectors:

- 1.1. The copper wire installed in the central hole of the fuel column was used as the activation detector of the first type.
- 1.2. Small copper foils placed on the fuel outer surface in several azimuthal directions were applied as the activation detector of the second type.

^a TRIFOB calculations were performed by A. Avvakumov (RRC KI)

2. The second stage:

The BGR tests of special VVER fuel rods containing the activation detector of the first type (copper wire installed in the central hole of the fuel column) and three UO₂ disks (of 7.57 mm diameter, 1 mm thickness) placed between the VVER fuel pellets in three axial positions (top, middle, bottom).

The spectrometric measurements with the use of irradiated activation detectors (performed before the first program stage) revealed the following:

- As for the axial distribution of the number of fissions in the VVER fuel rods Fig. 3.8): it can be assumed with a good accuracy that the most of the fuel column is characterized by the uniform (from the practical point of view) axial distribution of fission numbers. Some increase of fission numbers is observed in two end pellets.
- As for the azimuthal distribution of fission numbers: the analysis of test results obtained with the use of copper foils has shown that the neutron flux is practically uniform in all azimuthal directions.

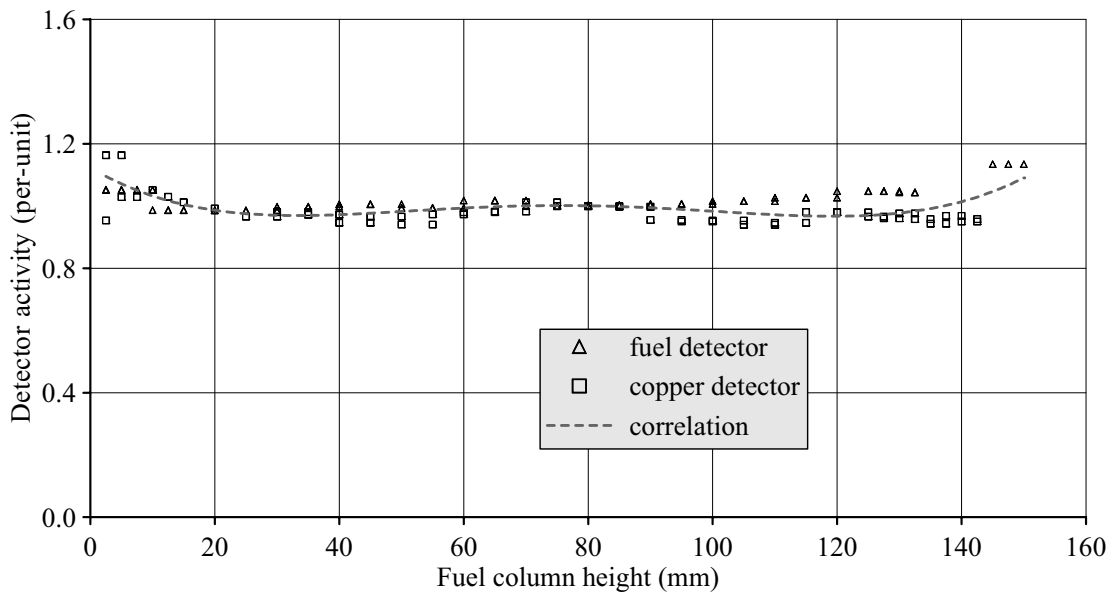


Fig. 3.8. The data characterizing the axial distribution of fission numbers in VVER fuel rods during the BGR tests

The data obtained on preparing the program second stage confirmed previous results and, besides, these additional investigations made it possible:

- to verify the calculations of fission numbers as a function of the fuel height performed with the use of the WIMS-6 code (see Fig. 3.9a and Chapter 4);
- to confirm that the axial distribution of fission numbers is insensitive to the BGR test mode (pulse or steady-state, see Fig. 3.9b); it was important because some scoping tests with activation detectors were performed at the steady-state mode of the BGR reactor.

Development of test data for the determination of the power history of the VVER refabricated fuel rods under the BGR pulse conditions

The problem of the accurate determination of the fuel rod power history is difficult for the pulse reactor tests as a whole and for the BGR tests in particular. The BGR aspects of this problem were connected with the following reasons:

- it was impossible to measure the power history of each VVER fuel rod directly;
- the BGR power history measured with the standard neutron detector was used as the input data for the determination of the fuel rod power;
- the BGR standard neutron detector was placed outside of the BGR reactor and, besides, this detector measured fast neutrons but 98% of fissions and more occur in the VVER fuel due to thermal neutrons;

- the standard neutron detector did not provided for the accurate measurement of low power generated by delayed neutrons.

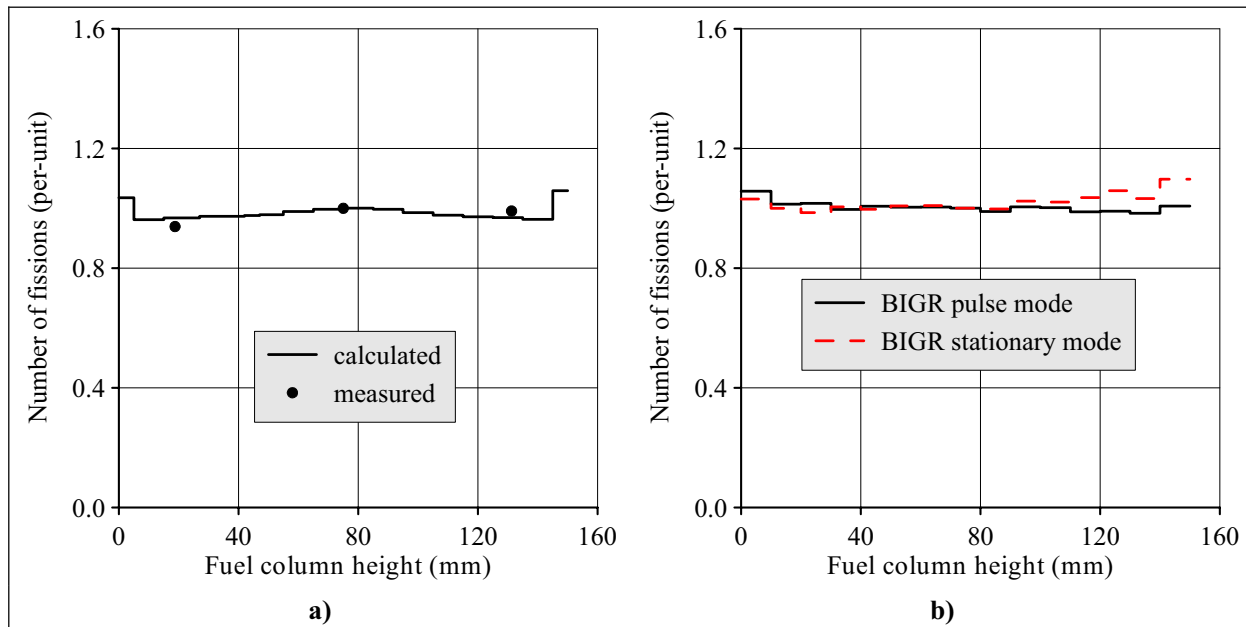


Fig. 3.9. Results of the BGR scoping tests
(a) The comparison of the calculated and measured (using three UO₂ disks) axial distributions of fission numbers, (b) The comparison of data characterizing the axial distributions of fission numbers for the pulse and steady-state BGR test modes

To clarify different aspects of the above-formulated problem, several types of reactor tests were performed. These tests were necessary:

- to determine the difference between the power pulse in the position of the standard neutron detector of the BGR reactor and the power pulse in the position of the VVER refabricated fuel rod, the fission chamber was installed (instead of the VVER fuel rod) in the capsule device of the BGR side channel. This fission chamber recorded the relative rate of U²³⁵ fissions. Due to this fact, the experimental data were obtained characterizing the change of power shape caused by processes of neutron transport and neutron slowing down;
- to take into account the effect of the side channel material, the appropriate BGR tests were performed for the graphite and beryllium side channels separately;
- to determine the sensitivity of thermal response of the VVER fuel to the power shape effects, the calculations of fuel enthalpy in the VVER fuel were performed for each measured power history. The comparison of obtained results is presented in Fig. 3.10.

The comparative analysis of these data has shown that:

- time dependent effects of graphite and beryllium side channels are the same;
- the significant sensitivity of the VVER fuel enthalpy to the power histories measured by the standard neutron detector and by the fission chamber was revealed for the initial phase of the BGR pulse (time is less than 0.09 s);
- the peak fuel enthalpy and enthalpies characterizing the BGR test results at the time longer than 0.09 s are insensitive to different variants of power history measurements. The maximum difference in peak fuel enthalpies is 2–3 cal/g.

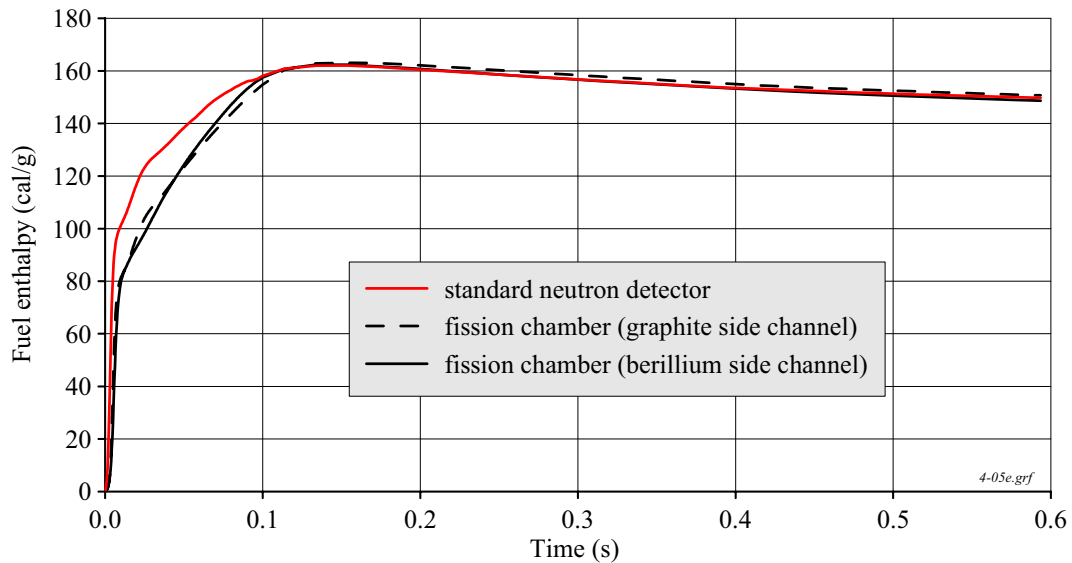


Fig. 3.10. The sensitivity of the VVER fuel enthalpy to methods of the BGR power history measurement

Taking into account these results, it was decided to use the BGR standard neutron detector for the development of input data characterizing the BGR power history for each pulse test of the VVER refabricated fuel rod. Obtained input data are presented in Appendix D of Volume 2 of this report. The demonstration of the BGR typical power history in the as-measured standard is shown in Fig. 3.11.

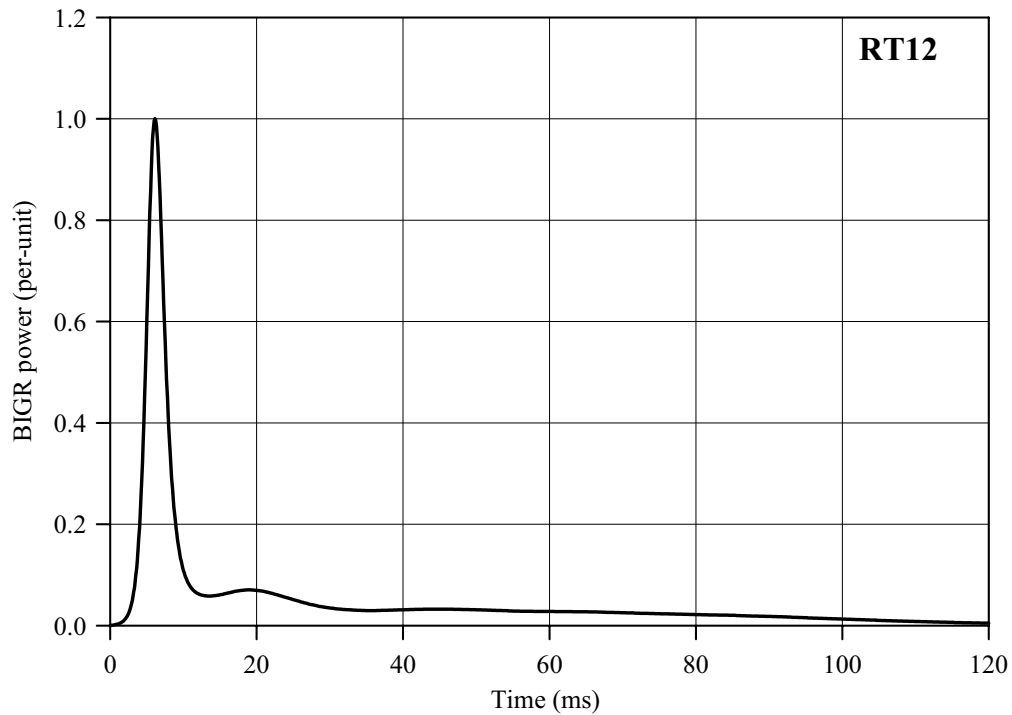


Fig. 3.11. The BGR power history

The second type of the BGR scoping tests was devoted to the adjustment of power measurements in the vicinity of the sensitivity limit for the standard neutron detector (at the time longer than 60 ms in accordance with the data of Fig. 3.11). This problem may be illustrated in detail with the use of data presented in Fig. 3.12. These data characterize the BGR power history measured by the standard neutron detector. The special analysis has shown that the neutron detector low sensitivity begins to be exhibited in the 2–1% range of the maximum power (the

area of instable indications). Measured results become apocryphal at power less than 0.2% (the unreliable indications).

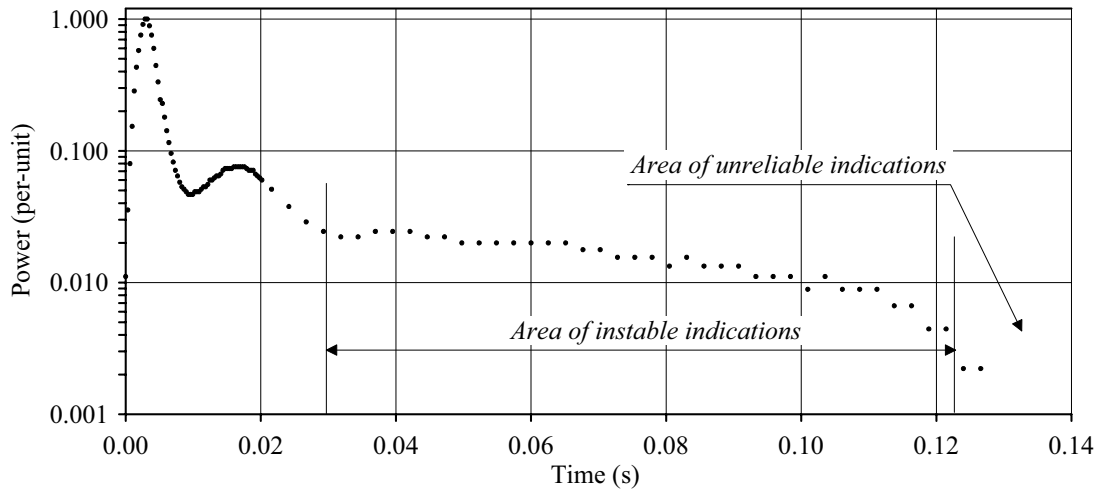


Fig. 3.12. The power history interpretation at the supercritical state of the BGR reactor

To clarify this problem, the BGR scoping tests were performed with the use of a more sensitive fission chamber, which was placed in the side channel of the BGR reactor. The neutronic calculations directed to the accurate modeling of the delayed neutron history were also performed. The obtained results (see Fig. 3.13) shown that:

- the fission chambers provided for the tolerant recording of the power history in the range of 0–30 s;
- a good agreement between the fission chamber data and calculated data was observed for nine scoping tests;
- the whole set of the test and calculated data and the additional data obtained with the use of copper activation detectors (a part of them was withdrawn from the BGR reactor at the time of 1 second from the beginning of the BGR pulse) indicated that:
 - ⇒ the energy deposition generated by the delayed neutrons in the range of 1–1000 seconds was approximately the 5% fraction of the total energy deposition;
 - ⇒ the fraction of the total energy deposition generated at the time longer than 30 s was approximately 0.7%.

The following procedure^a for the determination of the power history of each VVER refabricated fuel rod was developed on the basis of all obtained test and calculated results (see Fig. 3.14):

- in the time range from the beginning of the BGR pulse to the time of 30 ms (2.2% of the maximum power): the data of the BGR standard neutron transducer records were used;
- in the time range from ≈30 ms (2.2% of the maximum power) up to 120–170 ms (1% of the maximum power): the measured data of the standard neutron transducer were flattened by the spline interpolation method;
- in the time range from 120–170 ms (1% of the maximum power) up to 30 s (6×10^{-7} of the maximum power): the data obtained by the fission chamber were used;
- in the time range from 30 s (6×10^{-7} of the maximum power) up to 1000 s (0% of the maximum power): the calculated data were used.

The file of data characterizing the BGR power history for each tested VVER fuel rods is presented in Appendix E (relative reactor power) of Volume 2 of the report.

^a This procedure was developed by A. Bortash (RRC KI)

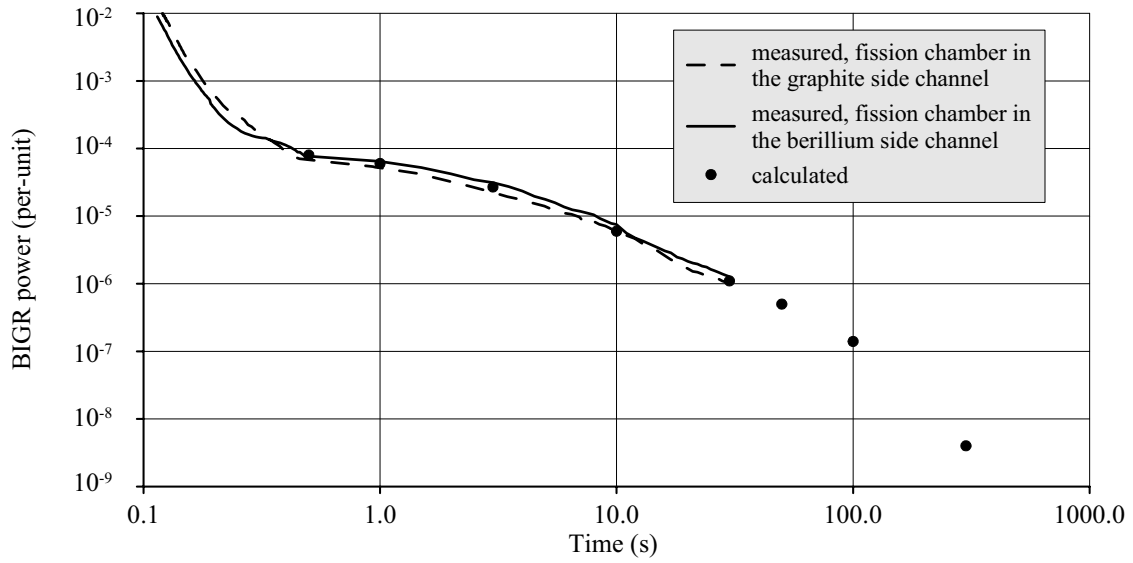


Fig. 3.13. The comparison of the test and calculated BIGR power histories in 0.1–1000 second range from the pulse beginning

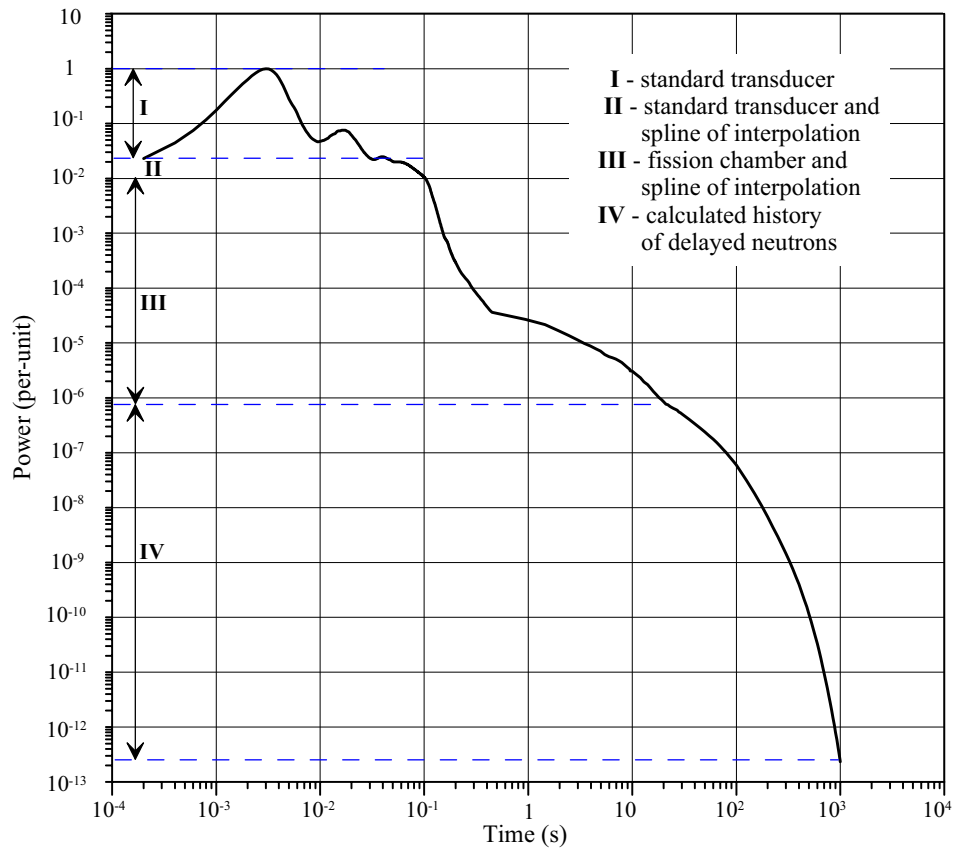


Fig. 3.14. Major provisions of the procedure used for the determination of the BIGR power history

Development of test data for the determination of the relationship between the BGR energy deposition and the number of fissions in the VVER fuel rods

The numerous scoping tests, special measurements and neutronic calculations were performed to determine and to validate the procedure for the calculation of the number of fissions in the VVER high burnup fuel under the BGR test conditions. The major provisions for the developed procedure and the set of special experimental investigations performed for this goal are listed in Table 3.2. The detailed description of the procedure is presented in Appendix B of this volume of the report.

Table 3.2. The characterization of the approach used to determine the number of fissions in the VVER high burnup fuel rods at the BGR pulse tests

Tasks	Research method	Results
1. To determine the type of correlation between the BGR test mode (the value of the BGR energy deposition) and fission numbers in test sample	1. To perform the irradiation of copper samples at the BGR different energy depositions and to measure the sample activities	1. It was confirmed that the ratio between fission numbers in the VVER fuel and BGR energy deposition ^a is a constant
2. To measure the coefficient characterizing the ratio between the fission number in the VVER unirradiated fuel ^b and the BGR energy deposition	2. To perform the BGR pulse tests with the VVER unirradiated fuel rods and to perform spectrometrical measurements of fission numbers	2. Two appropriate coefficients (for graphite and beryllium side channels) were determined on the basis of these tests
3. To determine the coefficient characterizing the ratio between fission numbers in the VVER unirradiated ^b and high burnup fuel, respectively	3. To perform independent neutronic calculations in the RRC KI and VNIIEF using different computer codes	3. The average discrepancy between the RRC KI and VNIIEF data was less than 1%
4. To verify the procedure in Item 3	4. To perform radiochemical measurements of Ba ¹⁴⁰ activity in fuel of several VVER high burnup fuel rods tested in the BGR reactor and to use obtained data for the determination of fission numbers in these rods	see Fig. 3.15

The practical implementation of this approach provided results, which are presented in Fig. 3.15 for the BGR design with the graphite side channel (other results are presented in Appendix B of this volume of the report). The analysis of these data led to the following conclusions:

- the maximum relative discrepancy of obtained results is not higher than 4%;
- systematical errors are not observed;
- the use of averaged results of different approaches reduced significantly the final procedure error.

^a The BGR energy deposition was measured with a high accuracy for each test

^b This term “unirradiated” is used here and after in the context of fuel state before BGR tests

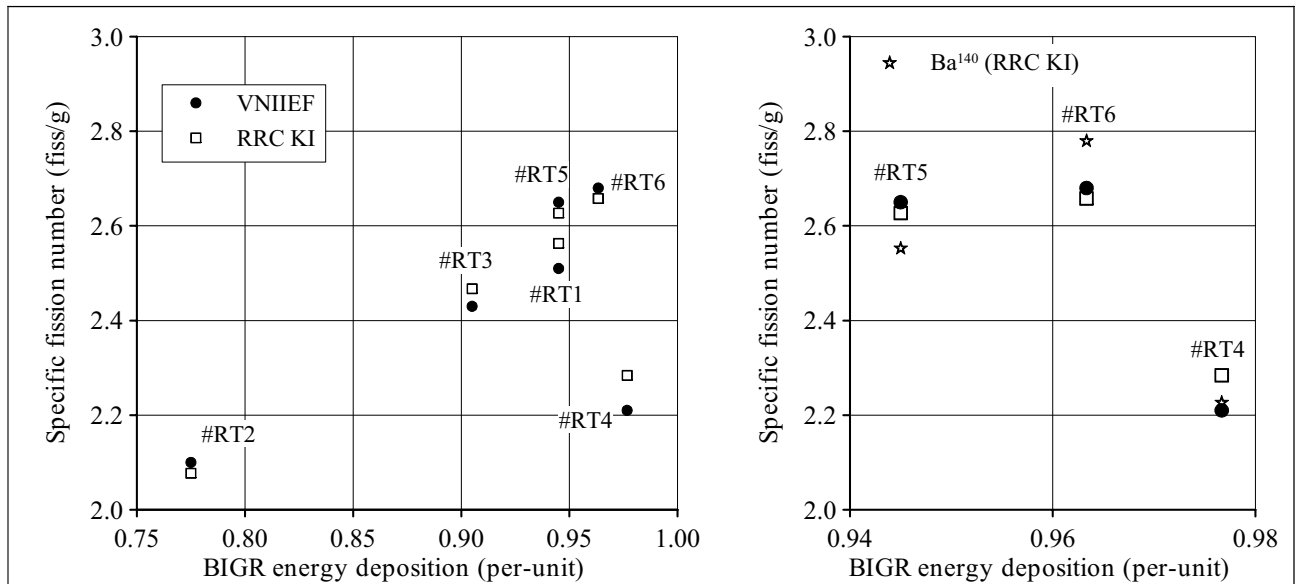


Fig. 3.15. Comparative data characterizing the RRC KI and VNIIEF procedures developed for the determination of fission numbers in the VVER high burnup fuel rods (#RT1–6) as a function of energy deposition in the BGR reactor with the graphite side channel. The data were obtained on the basis of (a) Test correlation between fission numbers in the VVER unirradiated fuel and BGR energy deposition; (b) Results of radiochemical measurements of Ba^{140} activity in the VVER high burnup fuel after the BGR tests

References

- 1 M. Vostrikov, B. Kochurov “TRIFOB – the Code for Calculation of Isotopic Composition in a Cylindrical Reactor Cell Taking Into Account Neutron Spatial-Energy Distribution”, Rus., Report ITEP-106, Moscow, 1981.
- 2 L. Yegorova, V. Asmolov, G. Abyshov, V. Malofeev, E. Kaplar, K. Lioutov, A. Shestopalov, A. bortash, L. maiorov, K. Mikitiouk, V. Polvanov, V. Smirnov, A. Goryachev, V. Prokhorov, and A. Vurim “Data Base on the Behavior of High Burnup Fuel Rods with Zr-1%Nb Cladding and UO_2 Fuel (VVER Type) under Reactivity Accident Conditions”, *NUREG/IA-0156 (IPSN99/08-02, NSI/RRC KI 2179)*, Vol.1, 2, 1999.

4. MAJOR PROVISIONS FOR THE PROCEDURES USED TO DETERMINE THE SPATIAL AND TIME DEPENDENT DISTRIBUTIONS OF ENERGY DEPOSITION AND FUEL ENTHALPY IN THE VVER HIGH BURNUP FUEL RODS UNDER THE BIGR TEST CONDITIONS

4.1. Energy deposition in the VVER high burnup fuel rods

The procedure of the energy deposition^a determination consists of three major stages^b:

1. Determination of the spatial distribution of fission numbers for all fissile nuclides.
2. Determination of the total energy deposition for the time interval of 0–1000 s.
3. Determination of time dependent distributions of power and energy deposition in the VVER high burnup fuel rods.

The detailed development and validation of the procedure for the energy deposition determination in the reactor pulse tests was performed earlier for the IGR/RIA tests [1, 2]. Some improvements and modifications of this procedure were made for the BIGR/RIA tests. The most important modification was connected with the decision to minimize the procedure uncertainties due to the agreed use of two relatively independent methods of neutronic calculations performed by the RRC KI and VNIIEF. The organization of both approaches in the form of the unified algorithm is presented in Fig. 4.1.

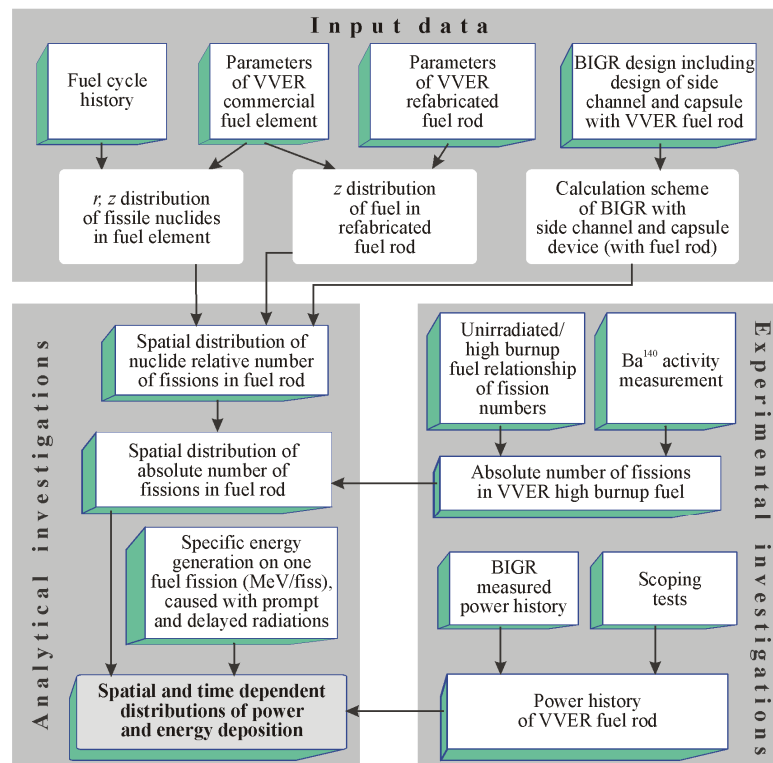


Fig. 4.1. The arrangement of the procedure to determine the spatial and time dependent distributions of energy deposition in the VVER high burnup fuel rod under the BIGR test conditions

^a Energy deposition is the ratio of energy accumulated by the VVER fuel during the fission process to the fuel mass. In accordance with the historical tradition, this parameter is presented in the units: cal/g(fuel)

^b Great effort was taken by A. Bortash and E. Kaplar (RRC KI) to develop and implement this procedure

The practical implementation of this algorithm in the RRC KI and VNIIEF procedures is illustrated in Fig. 4.2. In this connection, the following additional comments should be made for two approaches:

The RRC KI procedure

- the nuclide spatial distributions in each VVER high burnup fuel rod before the BGR test were calculated by the TRIFOB code [3]^a. The obtained data were used as the input data for both procedures (RRC KI and VNIIEF);
- the spatial distribution of the relative number of fissions in twelve VVER fuel rods and the unirradiated/high burnup fuel ratio were calculated by the WIMS6 computer code [4]^b;
- the spatial distribution of the absolute number of fissions was performed by the ENDEP computer code [5]^c. The WIMS6 calculated results and the ratio characterizing the unirradiated and high burnup fuel (see Section 3.3) were used as the input data for these calculations;
- the spatial and time dependent distributions of power and energy deposition in the VVER fuel was determined by the ENDEP code on the basis of following input data:
 - ⇒ the rod relative power history (see Section 3.3);
 - ⇒ the data characterizing the energy component caused by the prompt neutronic and gamma radiation, delayed beta and gamma radiation. These data were calculated by the ANISN code [6].

The VNIIEF procedure

- the C-95 neutronic code of the Monte Carlo type was used for this research [7];
- due to potentialities of this code, the spatial and time dependent tasks were not separated in this case;
- nevertheless, the experimental data characterizing the relationship between the number of fissions in the unirradiated fuel and the BGR energy deposition (see Section 3.3) were introduced into the appropriate procedure;
- the final data characterizing the spatial (r,z) and time dependent distributions of energy depositions were obtained with the use of the test power history for the VVER fuel rods (see Section 3.3).

The first comparison of the BGR test results obtained in accordance with these two procedures was performed for the specific number of fissions in the VVER high burnup fuel. The appropriate comparative data are presented in Fig. 3.15 (the first stage of the BGR program, RT #1–6) and in Table 4.1 (the second stage of the BGR program, RT #7–12). The analysis of these results has shown that the average relative discrepancy in the RRC KI and VNIIEF data is 3%.

Table 4.1. The specific number of fissions determined with the use of the RRC KI and VNIIEF procedures for the VVER fuel rods tested at the second stage of the BGR program

Fuel rod number	BGR energy deposition (MJ)	Number of fissions in the VVER high burnup fuel (10 ¹³ fiss/g)	
		RRC KI procedure	VNIIEF procedure
#RT7	261	2.38	2.42
#RT8	288	2.84	3.02
#RT9	288	2.84	2.94
#RT10	254	3.11	2.91
#RT11	291	3.41	3.35
#RT12	240	2.93	2.88

^a The variant calculations of nuclide spatial distributions were performed by A. Avvakumov (RRC KI)

^b The variant calculations of these parameters were performed by O. Feinberg (RRC KI)

^c The calculations were performed by V. Polvanov (RRC KI)

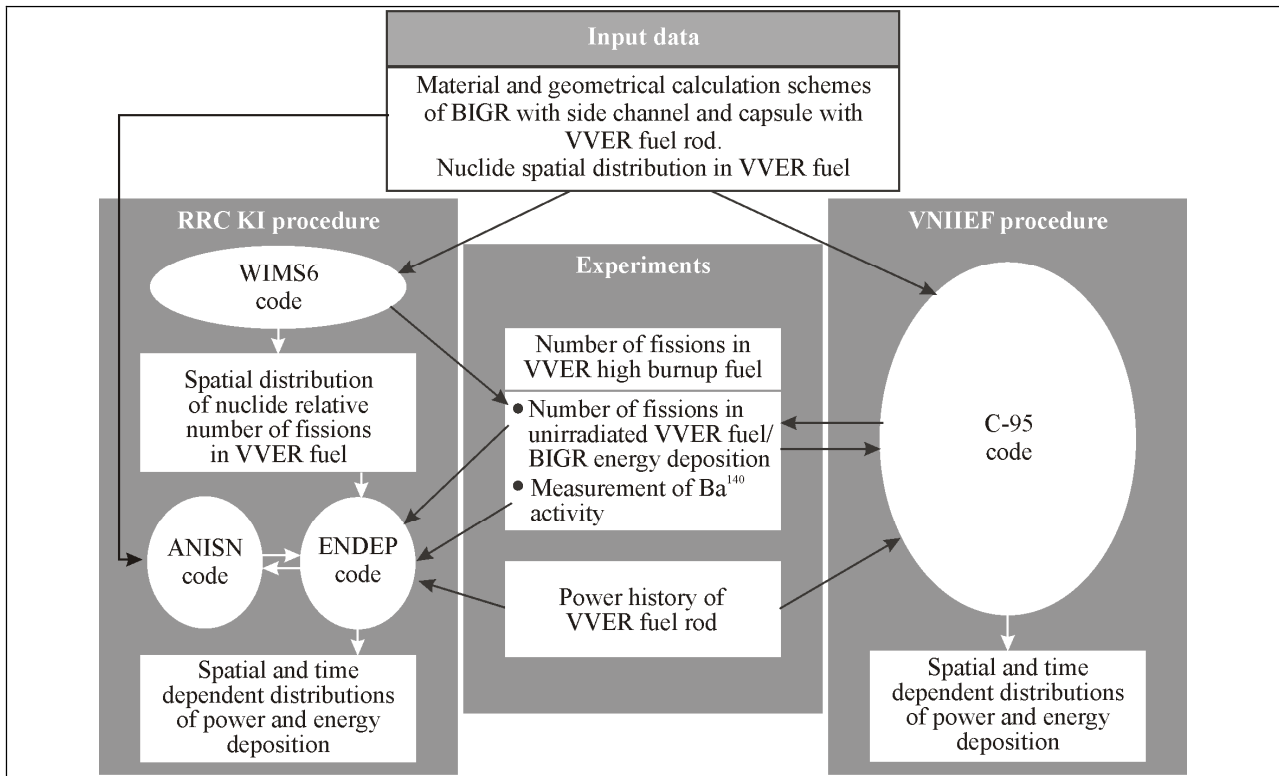


Fig. 4.2. The structural scheme of the RRC KI and VNIIEF procedures developed for the energy deposition determination

The next comparative study was devoted to the correlation between the energy deposition and specific number of fissions in the VVER fuel. The results of this study for the fuel rods #1–6 are demonstrated in Fig. 4.3.

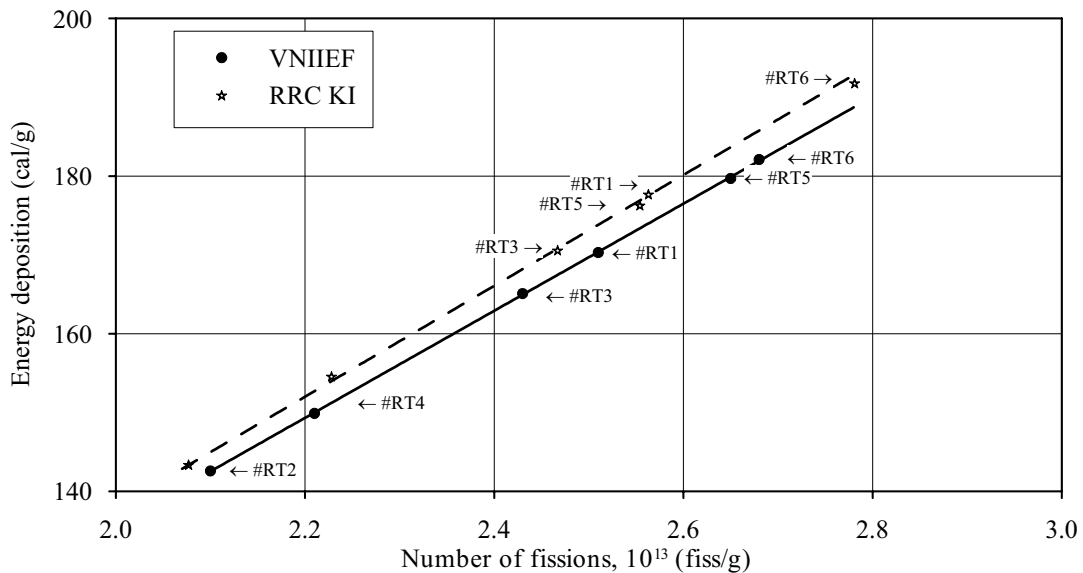


Fig. 4.3. The RRC KI and VNIIEF comparative data characterizing the energy deposition as a function of the number of fissions in the VVER fuel

It is known that all these data must be approximated by the straight line passing through the origin with the angle coefficient, which is proportional to energy generated at one fission. The analysis of obtained results shown that:

- the RRC KI and VNIIEF data are approximated by a straight line with a good accuracy;
- the RRC KI and VNIIEF straight lines had the following angle coefficients (the energy per one fission):
 - ⇒ RRC KI: 180.9 MeV/fiss;
 - ⇒ VNIIEF: 177.8 MeV/fiss.

The observed difference does not exceed 2%. This difference is connected with approaches to the determination of energy components. This effect is illustrated by the data presented in Table 4.2.

Table 4.2. Components of energy per one fission in accordance with the RRC KI and VNIIEF procedures

Component	RRC KI		VNIIEF
	#RT4	#RT6	#RT1–12
Kinetic energy of fragments (MeV/fiss)	173.6	173.3	169
Energy of prompt radiation (MeV/fiss)	2.4	2.1	2.6
Energy of delay radiation (MeV/fiss)	5.2	5.2	6.2
Total energy (MeV/fiss)	181.6	180.6	177.8

It should be noted that the RRC KI procedure provides for the individual calculation of energy components for each tested fuel rod. Moreover, the RRC KI procedure takes into account the difference between the kinetic energy of fragments for uranium and plutonium. The VNIIEF procedure uses the constant values of energy components in accordance with the data presented in Table 4.2. Following this procedure, the kinetic energy of fragments is not the function of the nuclide type.

The final conclusions concerning the use of the data obtained due to the RRC KI and VNIIEF procedures were as follows (see Fig. 4.4):

- to take into account that energy characteristics estimated on the basis of two procedures have the reasonable dispersion;
- to take into account that it is impossible to select the best procedure from these two procedures;
- to determine the final data characterizing the spatial and time dependent distributions of power and energy deposition as the average value of the RRC KI and VNIIEF results.

Spatial and time dependent distributions of energy parameters were calculated in accordance with this decision. These results are presented individually for each fuel rod in Appendix E of Volume 2 of the report.

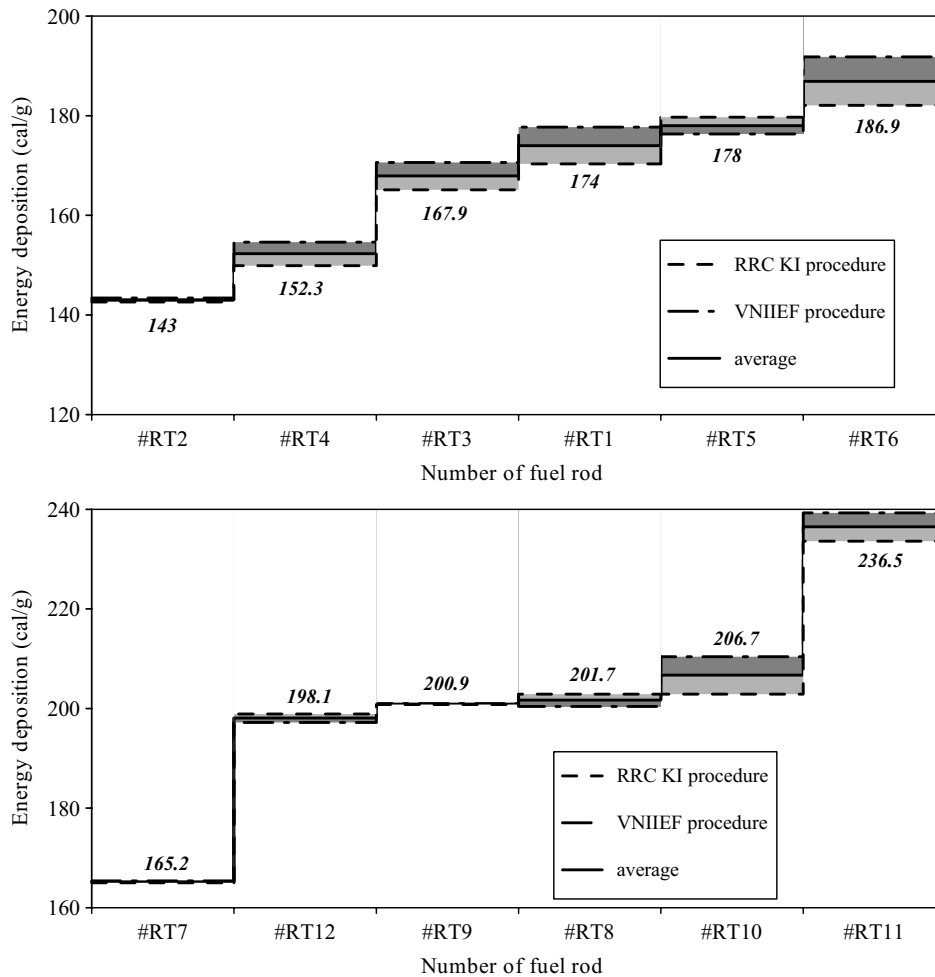


Fig. 4.4. The RRC KI and VNIIEF comparative data characterizing the total energy deposition in the VVER fuel rods under the BGR conditions
(a) The first program stage, (b) The second program stage

4.2. Fuel enthalpy and thermal mechanical parameters of fuel rods

4.2.1. Background

The accurate determination of fuel enthalpy at the fast transient processes characterizing the BGR tests was one of the major tasks of these investigations. This was associated with the fact that the peak fuel enthalpy is used as the failure criterion under the RIA conditions. Generally, the spatial and time dependent distributions of fuel enthalpy should be calculated for this goal. To the first approximation of these distributions, appropriate distributions of energy deposition in the tested fuel can be analyzed. The results of this analysis carried out on the basis of the data presented in Chapter 3 and Section 4.1 of this volume showed that:

- the axial distribution of energy deposition along the fuel height was uniform;
- the radial distribution of energy deposition in the VVER high burnup fuel had the exponential form (see Fig. 4.5).

This effect was connected with the initial nonuniformity of the radial distribution of fissile isotopes in high burnup fuel (high concentration of Pu isotopes in the fuel outer layer). Thus, the radial distribution of fuel

enthalpy as a function of time should be calculated for the computer codes adapted to fast pulse processes. Moreover, these codes must be adapted to the high burnup fuel.

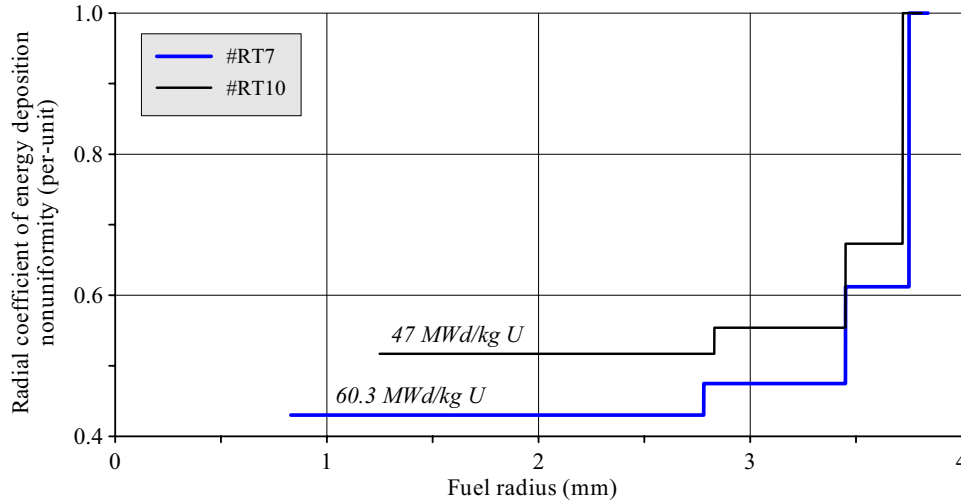


Fig. 4.5. The radial distribution of energy deposition in four fuel radial layers (averaged over the layer thickness) in the refabricated fuel rods with burnup of 47 and 60.3 MWd/kg U

The preliminary analysis of the BIGN program showed that the following specific phenomena should be taken into account on selecting computer codes for the fuel enthalpy calculations:

- the unsteady-state character of thermal and mechanical processes in the VVER fuel rods during the BIGN tests;
- the specific heat transfer to the stagnant water in the capsule device;
- the fuel burnup effects.

It should be noted that the following specific effects accompany these phenomena:

- the formation of the local temperature maximum in the rim layer of fuel at the beginning of power transient;
- the mechanical interaction between the fuel and cladding caused by the fuel high heating rate;
- the fuel swelling and fission gas release;
- the unsteady-state heat flux from the fuel rod to the coolant on the change of heat transfer modes: convection, nucleate boiling, transient and film boiling, cladding rewetting during the cooling phase, etc.).

The previous experience in the solution of similar problems on the development of the IGR/RIA program [2] shown that the modified version of the U.S. NRC FRAP-T6 code (FRAP-T6/VVER) could be used for the calculation of thermal and mechanical processes in the VVER high burnup fuel rods under the BIGN test conditions [8]. To widen the analysis area and to estimate the sensitivity of results to the calculation models, it was decided to use the second code for this goal. This second computer code was the RAPTA-5 code developed in the VNIINM for the computer modeling of the design basis accidents in the VVER fuel [9].

4.3. Description of computer codes used and results of calculations

To organize the appropriate cycle of investigations, the following additional works were performed:

- the reassessment of selected computer codes;
- the code verification on the basis of the IGR and NSRR test results;
- the additional modification of computer codes taking into account the verification results;

- the calculation of the thermal and mechanical behavior of twelve VVER high burnup fuel rods under the BGR test conditions.

The following paragraphs of this section of the report contain the consideration of appropriate works.

Description of the modified version of the FRAP-T6 computer code [8]

The original version of the FRAP-T6 code was developed for the thermal and mechanical calculations of the LWR fuel elements under transient and accident conditions [10]. Although the code developers recommended to use this code for the analysis of such reactor modes as transients at normal operation, loss-of-coolant accidents, reactivity initiated accidents and severe accidents, two last items of this list were not described in the code models in detail. The same conclusion can be made in relation to the high burnup fuel behavior. The original version of the FRAP-T6 code provides the calculation of the following parameters of fuel elements:

- the temperature distributions in the fuel, cladding and gas plenum;
- deformation of fuel and the cladding including such fuel effects as thermal expansion and swelling;
- high temperature oxidation of the cladding;
- fission gas release;
- the cladding rupture caused by the internal gas pressure.

To calculate the heat transfer coefficient characterizing the fuel rod/coolant heat transfer under RIA conditions, the following modes are used:

- convection;
- film boiling;
- nucleate boiling;
- free convection and convective heat transfer at the low flow rate transient boiling.

The appropriate modes were taken from the RELAP4 code [10]. The material and mechanical properties of fuel rods were calculated with the use of the MATPRO-VII library [11]. The FRAP-T6 code modified in the RRC KI for the interpretation of the IGR test results was used to solve three major tasks:

1. To take into account the specific geometry and material properties of the VVER fuel elements.
2. To improve some FRAP-T6 models for the specific test conditions (stagnant coolant under normal conditions).
3. To develop the approach to the calculation of the parameters of high burnup fuel at the end of the base operation.

A brief description of the major modifications in the FRAP-T6 code is presented in Table 4.3.

Table 4.3. The list of modifications made in the FRAP-T6 code to determine parameters of the VVER high burnup fuel rods under the RIA conditions

Phenomenon	Key modifications
1. Material and mechanical properties of Zr-1%Nb cladding, thermal conductivity of high burnup fuel	<ul style="list-style-type: none"> • The introduction of specific thermal physical properties of zirconium niobium cladding • The introduction of mechanical properties of the unirradiated and irradiated Zr-1%Nb cladding as a function of the temperature and strain rate. These properties were obtained due to a special experimental program • The organization of experimental data characterizing the fuel thermal conductivity degradation as a function of burnup
2. The parameters of fuel at the end of the base operation	<ul style="list-style-type: none"> • The introduction of special models to calculate the fission gas distribution in the VVER fuel at the end of the base operation

Phenomenon	Key modifications
3. Specific correlations for the fuel rod and coolant heat transfer	<ul style="list-style-type: none"> The change of the original FRAP-T6 model for film boiling on the Labuntzov correlation developed for stagnant water conditions [12]. The use of the original FRAP-T6 model leads to the significant overestimation of the cladding temperature Development of a special rewetting model [13]. The original FRAP-T6 model overestimates the film boiling duration
4. Thermal conductivity of the pellet/cladding gap	<ul style="list-style-type: none"> The change of some coefficients for the appropriate model of high burnup fuel
5. Models of the cladding mechanical behavior	<ul style="list-style-type: none"> The adaptation of the BALON2 module with the introduction of the criterion for the high temperature rupture of Zr-1%Nb cladding Development of the conservative criterion for the PCMI failure of Zr-1%Nb cladding using results of special tests [14, 15]

The description of the RAPTA-5 computer code [9, 16, 17]

The RAPTA-5 computer code^a was developed in the VNIINM for the calculation of the thermal, mechanical and oxidation behavior of the VVER fuel elements under design basis accident conditions (LOCA and RIA). This fifth version of the code provides the consideration of the thermal and mechanical processes in the fuel element taking into account:

- the unsteady-state energy generation in fuel and energy generation due to high temperature effects of the cladding oxidation;
- the unsteady-state boundary conditions on the cladding surface;
- the temperature and burnup dependent material properties of the fuel element;
- the change of radial geometrical sizes of the fuel element caused by:
 - ⇒ the fuel thermal expansion and the elastic strain of the cladding;
 - ⇒ the high temperature cladding creep due to the unsteady-state pressure drop;
 - ⇒ the development of oxide layers on the cladding outer and inner surfaces.

It should be noted that the specific effects of fuel burnup (swelling, the specific FGR etc.) were not included in this version of the RAPTA code. The additional information characterizing the most important models of the RAPTA-5 code is presented in Table 4.4 and Appendix C of this volume of the report.

Table 4.4. The brief characterization of the RAPTA-5 code major models

Effect	General approach to the modeling
1. The spatial and time dependent distributions of temperature	The introduction of specific thermal physical properties of zirconium niobium cladding
2. Fuel rod and coolant boundary conditions for the reactor capsule tests	<p>A special set of correlations to calculate the heat transfer coefficient for the capsule test conditions (stagnant water at room temperature and atmospheric pressure (see Appendix C)). This set includes the following heat transfer modes:</p> <ul style="list-style-type: none"> convection

^a Russian spelling is Raschertny Analiz Povedeniya Tvela pri Avarii, which means “Calculation analysis of the fuel element behavior under accident conditions”

Effect	General approach to the modeling
	<ul style="list-style-type: none"> • nucleate boiling • transient boiling • film boiling • critical heat flux
3. Thermal conductivity of the fuel/cladding gap	The RAPTA-5 model (see Appendix C) is similar to the FRAP-T6 model. Both codes used the Ross and Stoute modified model as the basis. The RAPTA-5 code has specific numerical values of the appropriate coefficients
4. The cladding mechanical response	The cladding stress/strain state is determined with the use of the creep flow theory and at the assumption of the additivity of elastic and creep strains. The stress/strain calculations at the cladding ballooning are accompanied by the cladding rupture criterion. This deformation criterion is based on the file of experimental data (see Appendix C)

Special verification procedures applied before the BGR calculations and additional modifications of computer codes

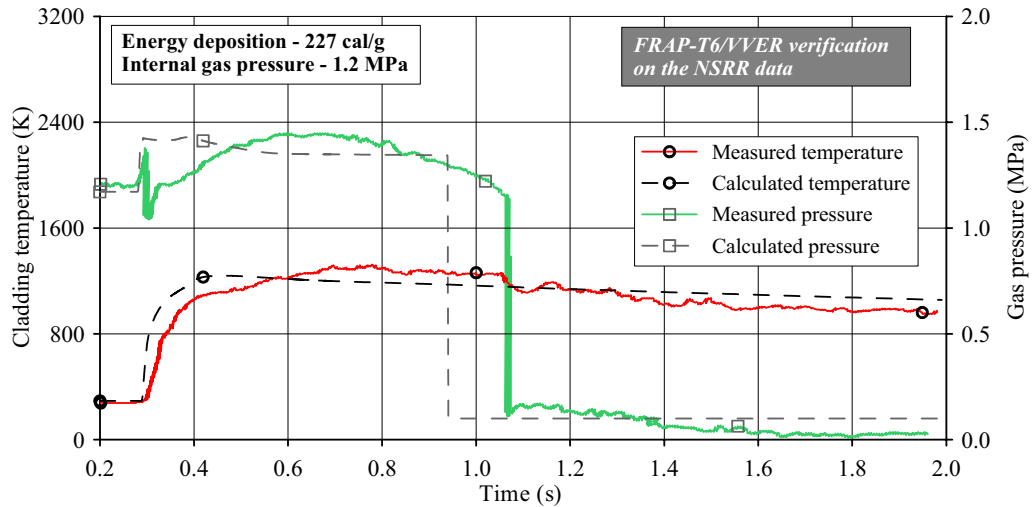
The following general principles were used at the development of verification procedures:

- the major goal for the comparison of the test and calculated parameters was the confirmation of the fact that the peak fuel enthalpy was determined with the acceptable accuracy under the BGR test conditions;
- the focus of investigations was directed to the verification of models determining the heat balance in the fuel rods, therefore, the cladding temperature history was selected as the representative parameter characterizing the adequacy of the calculation modeling of thermal processes in the high burnup fuel rods;
- special attention was paid to the thermal conductivity of the pellet/cladding gap and heat removal from the fuel rod to the coolant (especially for the time interval from the process beginning up to the peak fuel enthalpy);
- the models used for the cladding rupture prediction were verified.

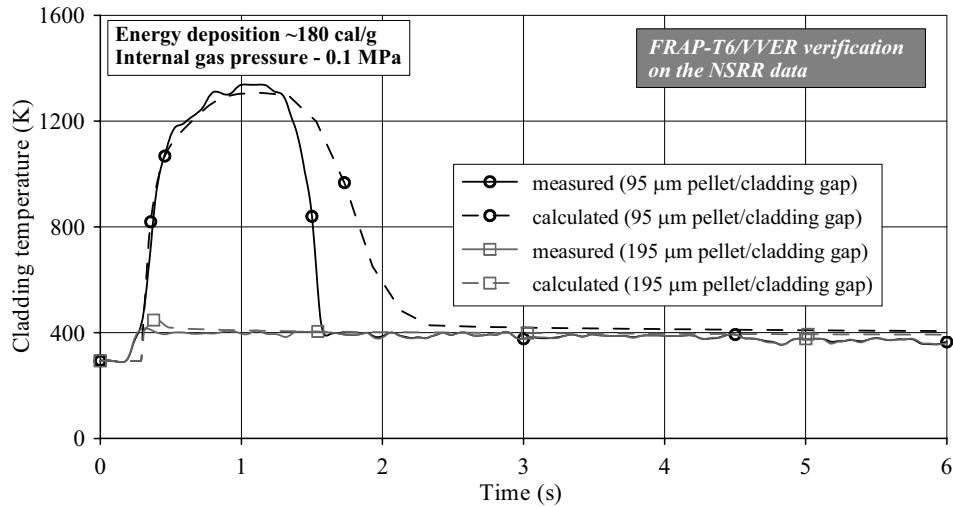
It should be noted that the FRAP-T6/VVER modified version was verified in detail on the basis of the IGR tests with the VVER high burnup fuel [2]. Numerous verifications were also made for the RAPTA-5 code. But taking into account specific difficulties associated with the narrow pulse conditions in the BGR tests, it was decided to perform additional verifications of both codes on the basis of the published test results obtained in the NSRR tests of the PWR unirradiated fuel rods. This choice is motivated by the fact that the BGR and NSRR tests are characterized by the similar pulse width and similar coolant parameters (stagnant water under normal conditions). Results of the verification procedures are presented for the FRAP-T6 and RAPTA-5 codes in Fig. 4.6 and Fig. 4.7, respectively^a.

The analysis of results obtained for the FRAP-T6/VVER version of the code confirmed the conclusion made earlier on the analysis of the IGR tests: this version of the FRAP-T6 code provides for a good prediction of thermal parameters for fuel rods under the RIA test conditions including such important phenomena as the thermal conductivity of the pellet/cladding gap and the critical heat flux at the departure from the nucleate boiling (DNB) and at the initiation of the rewetting process. It should be noted that the problem of the thermal conductivity of the pellet/cladding gap is very important for the modeling of high burnup fuel behavior because the decrease of pellet/cladding gap leads to the decrease of thermal resistance of the gas gap. This effect provides for the increase of heat flux from fuel to the cladding and, consequently, to the coolant. The appropriate process is accompanied by the decrease of the fuel temperature and enthalpy and by the increase of the cladding temperature.

^a The NSRR data presented in these figures were numbered by the RRC KI specialists



a)



b)

Fig. 4.6. The comparison of the FRAP-T6/VVER calculations with the NSRR test data [18, 19]
(a) The temperature and gas pressure histories of the pressurized fuel rod failed under the narrow pulse conditions; (b) The sensitivity of the cladding temperature to the thermal conductivity of the pellet/cladding gap

The results of precise NSRR tests (#200-3, 232-1) performed at the same energy deposition with two unirradiated fuel rods manufactured with two different gas gaps (standard (95 μm) and wide (195 μm)) were used for this verification stage. A special choice of energy deposition revealed a very important effect: the presence or absence of DNB conditions as a function of the pellet/cladding gap.

The obtained verification data showed that the heat flux from the fuel rod with the gap of 95 μm achieved the critical value, after that the fuel rod was cooled at the film boiling of subcooling water. The cladding maximum temperature was about 1350 K. The second fuel rod with the wide gas gap was cooled at the nucleate boiling mode only. The DNB condition was not achieved in this test and the cladding maximum temperature was 410–420 K. The analysis of the FRAP-T6/VVER calculations of these two tests showed that these difficult transient processes were described with a good accuracy. The obtained results also showed that the FRAP-T6/VVER version of the code produced the reasonable results for the prediction of the cladding rupture under pressurization conditions.

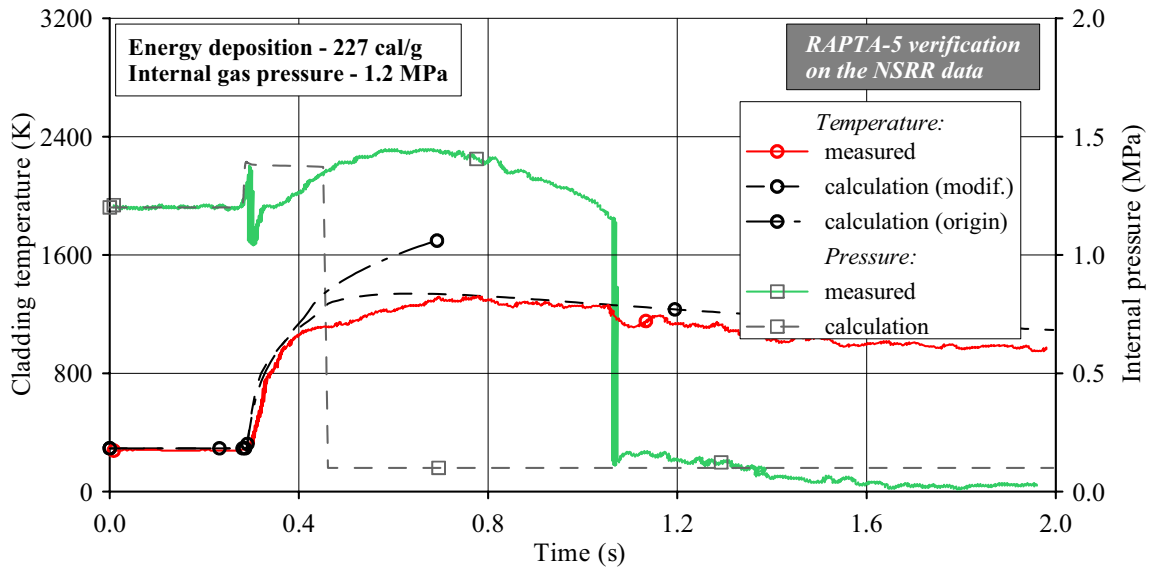


Fig. 4.7. The comparison of the NSRR data characterizing the thermal and mechanical behavior of the pressurized unirradiated fuel rod [18, 19] with the RAPTA-5 calculations before (original) and after (modified) the heat transfer module modification

As for the RAPTA-5 code, the first results of the verification performed with the use of the NSRR test data [18, 19] showed that the original version of RAPTA-5 code overestimated the cladding temperature at the film boiling mode (see Fig. 4.7, the original version of the RAPTA-5 code). A careful consideration of possible reasons for these results established that the heat transfer coefficient for this mode in the RAPTA-5 code was significantly lower than that in the modified version of the FRAP-T6 code^a (see Fig. 4.8).

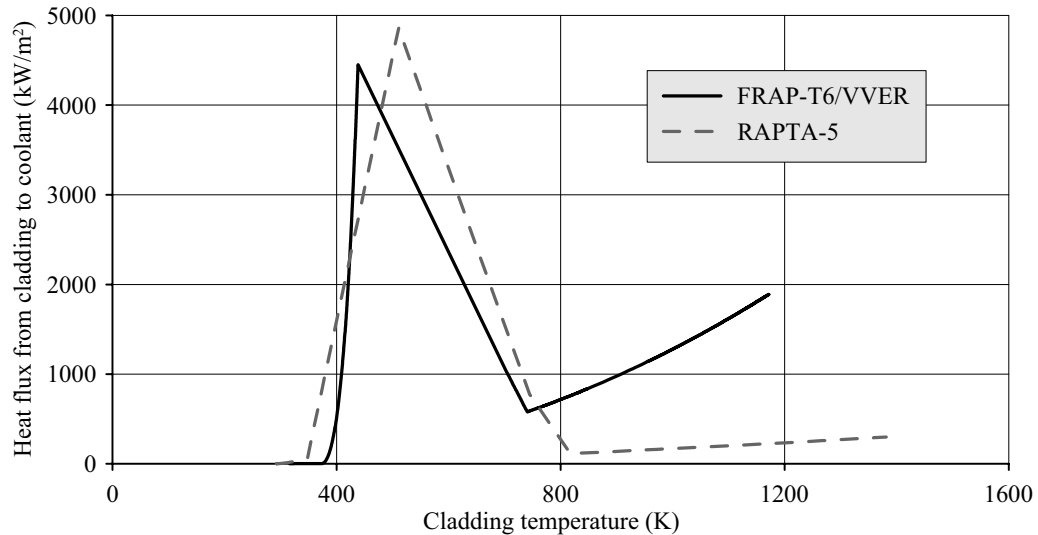


Fig. 4.8. The surface heat flux as a function of the surface temperature: correlations used in the VVER version of the FRAP-T6 code and in the original version of the RAPTA-5 code

^a It should be noted that the original version of the RAPTA-5 code is used for the design calculations on the VVER safety analysis. This is the major reason for the use of conservative correlations in the code. It is interesting that the original version of the FRAP-T6 code has the similar correlation for the film boiling mode. Therefore, the appropriate model was improved on developing the FRAP-T6/VVER version

Taking into account this analysis results, it was decided to introduce the film boiling correlation of the heat flux developed for the FRAP-T6/VVER version of the code into the RAPTA-5 code. As it can be observed from the data presented in Fig. 4.7, this modification resulted in the reasonable agreement between the measured and calculated cladding temperature.

As for the time of the cladding rupture, the RAPTA-5 data presented in Fig. 4.7 characterize a low (conservative) boundary of the deformation criterion used for these calculations. The comparison of measured and calculated pressure histories showed that the realistic rupture models should be applied for the estimation of the mechanical behavior of fuel rods under the RIA test conditions.

The next stage of the RAPTA-5 code verification was devoted to the thermal conductivity of the pellet/cladding gap. The same NSRR tests (#200-3, 232-1) were used for this task (see Fig. 4.9).

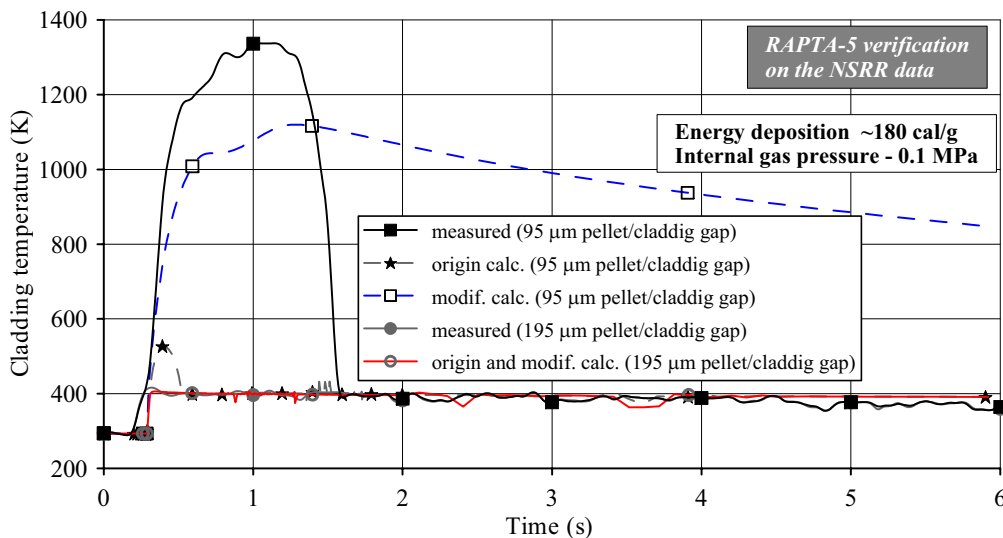


Fig. 4.9. The comparison of the RAPTA-5 calculations and NSRR test data [18, 19] characterizing the sensitivity of the cladding temperature to the initial pellet/cladding gap

The analysis of calculated results in comparison with the measured data led to some observations and the following additional modifications of the RAPTA-5 code:

- the original version of the RAPTA-5 code predicted the presence of the DNB condition in the fuel rod with the 95 μm gap and the absence of the DNB condition in the fuel rod with the 195 μm gap; this result was in the complete agreement with the test data;
- the maximum cladding temperature in the test of the fuel rod with the 95 μm gap was significantly underestimated on using the original version of the RAPTA-5 code. The detailed analysis showed that this effect was caused by the overestimation of the temperature drop in the gas gap. This overestimation could be explained by the similar reason as that in the previous case: the conservative approach was used in this version for the prediction of the fuel enthalpy. After some modifications, the significant improvement in the calculated cladding temperature history was obtained for the NSRR fuel rod with the 95 μm gap;
- the overestimation for film boiling duration obtained by the RAPTA-5 code in comparison with the test data was explained by the rewetting effect mentioned earlier at the consideration of the FRAP-T6 code. The original version of the FRAP-T6 code overestimated also the film boiling duration. The FRAP-T6/VVER version of the code contained a special rewetting model developed for these test conditions. This model was not installed into the RAPTA-5 code because the comparative calculations of the BGR tests performed by the FRAP-T6/VVER and modified version of the RAPTA-5 code showed that the peak fuel enthalpy was insensitive to the rewetting effects.

Taking into account the verification results, it was decided to use both codes to determine the peak fuel enthalpy in the VVER fuel rods under the BGR test conditions. As for the representativity of other calculated thermal mechanical parameters of fuel rods, the additional verification cycle was run for the FRAP-T6 code. This cycle included the verification of several important parameters:

- the cladding residual hoop strain;
- fission gas release;
- fuel residual hoop strain.

The NSRR test data obtained in the narrow pulse tests of unirradiated and unpressurized fuel rods were used for the verification first direction [18]. The choice of unirradiated claddings was connected with the fact that the VVER irradiated cladding tested in the BGR reactor was ductile. The comparative analysis of calculated and measured results characterizing the cladding residual hoop strain of unpressurized fuel rods clarified the specific PCMI effects. Results of this verification procedure are presented in Fig. 4.10.

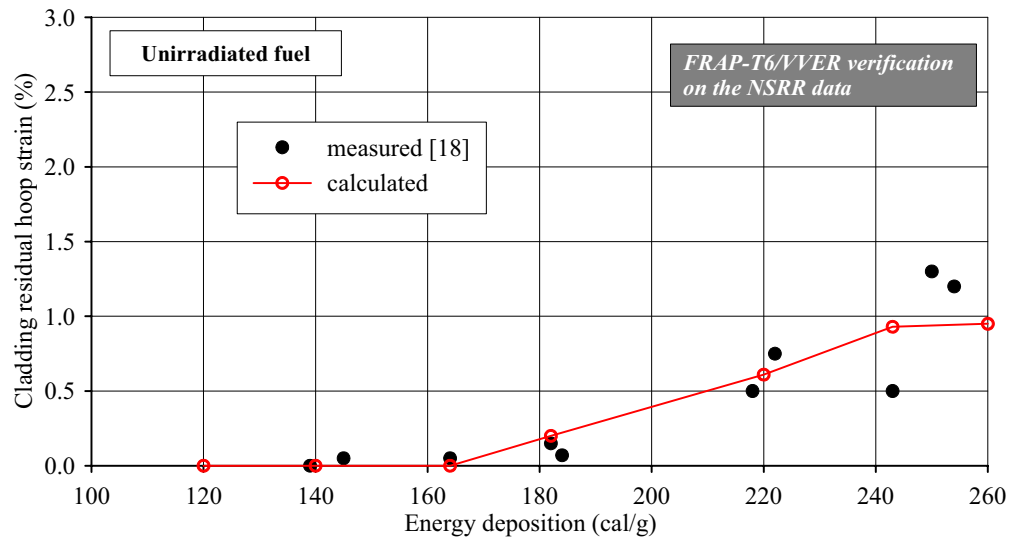


Fig. 4.10. The comparative data characterizing the calculated (by the FRAP-T6/VVER version of the code) and measured cladding residual hoop strain under the NSRR test conditions

The analysis of obtained results showed that the modified version of the FRAP-T6 code^a determined the mechanical response of the ductile cladding caused by the PCMI loading with a good accuracy. The next verification stages were devoted to the following important effects characterizing the high burnup fuel behavior: the fission gas release and fuel swelling. The IGR test data were used to fulfill these tasks [2]. The comparison of calculated and measured Xe, Kr release is presented in Fig. 4.11.

The preliminary considerations of appropriate FRAP-T6 models suggested that gas contained along the grain boundaries and in the intergranular space provided for the main contribution into the FGR value. Gas release out of the grain is very small due to the mechanism of thermal activation diffusion. The analysis of obtained comparative data showed that the FRAP-T6 code underestimated the FGR at low enthalpies (low fuel temperatures and low gas release).

To estimate the accuracy of fuel swelling calculations, the IGR test results characterizing the residual fuel strain were used (Fig. 4.12). The comparison of calculated and measured data showed that the FRAP-T6 calculations overestimated the fuel swelling. But the absolute value of this overestimation was not so bad.

^a The original mechanical properties of Zircaloy cladding were used for the verification procedures on the basis of the NSRR test data

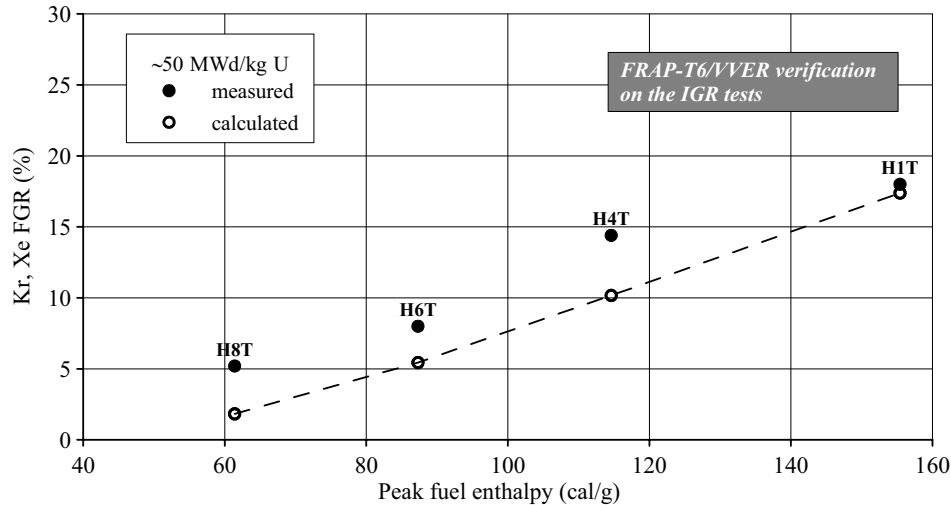


Fig. 4.11. The comparison of calculated and measured FGR using the IGR test data for the VVER high burnup fuel [2]

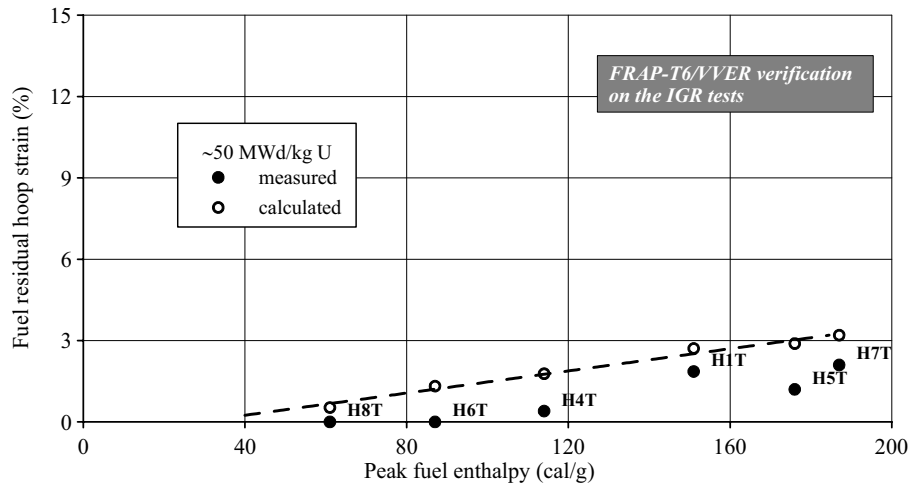


Fig. 4.12. The comparison of calculated and measured effects of high burnup fuel swelling (the IGR test data [2])

Results of the FRAP-T6 and RAPTA-5 calculations

These versions of the FRAP-T6 and RAPTA-5 codes were used to determine the spatial and time dependent distributions of thermal mechanical parameters for twelve fuel rods tested under the BIGHR pulse conditions. The graphical data characterizing obtained results are presented in Appendix E of Volume 2 of the report. Each tested fuel rod was described by the following set of parameters:

- heat balance (power, enthalpy, energy leakage, heat transfer coefficient);
- temperature (fuel, cladding);
- cladding mechanics (gas pressure, fuel/cladding gap, cladding stress and strain);
- fuel mechanics and FGR (swelling, total strain, FGR).

It should be noted in this connection that the following general differences were observed in the FRAP-T6 and RAPTA-5 data:

- Due to the special rewetting model implemented in the FRAP-T6/VVER version, this code predicted the cladding rewetting and sharp decrease of the cladding temperature much earlier than the RAPTA-5 code.

- This version of the RAPTA-5 code had no fuel swelling model. Therefore, significant differences were observed in the FRAP-T6 and RAPTA-5 comparative mechanical behavior of fuel rods.

In addition to the graphical data, the tabular data characterizing the time-dependent distribution of radial averaged fuel enthalpy for each fuel separately based on the FRAP-T6 and RAPTA-5 calculations are presented in Appendix E. The appendix contains also 12 Tables with the organized experimental and calculated test data characterizing the following important parameters of each tested fuel rod: fuel burnup, initial fill gas pressure, total energy deposition, peak averaged fuel enthalpy, fuel maximum temperature, the cladding outer maximum temperature, the cladding residual hoop strain, FGR (Xe, Kr), the cladding failure characteristics.

As for the peak averaged fuel enthalpy, it was decided that the average value of the FRAP-T6 and RAPTA-5 calculations must be used as the best estimation of this parameter (see Fig. 4.13).

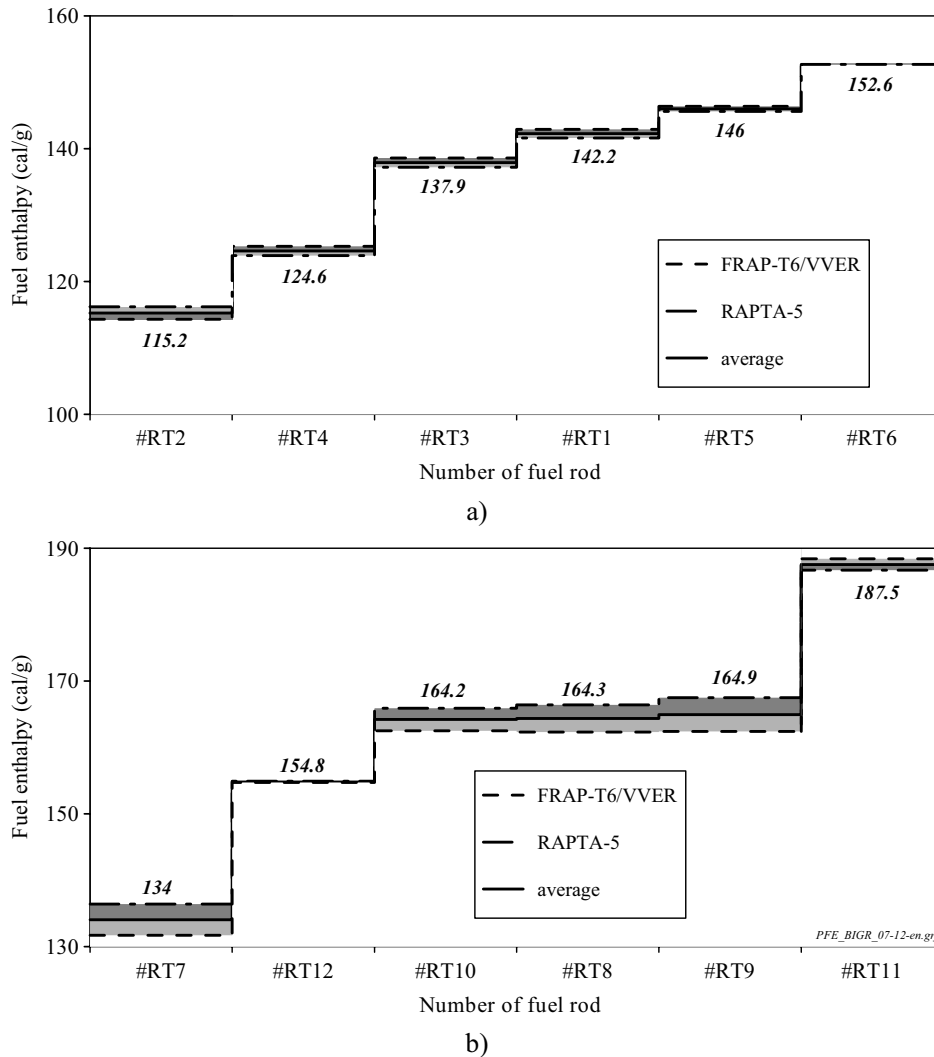


Fig. 4.13. Results of determination of the peak averaged fuel enthalpy in fuel rods tested under the BGR test conditions (#RT1–12) (a) the first program stage, (b) the second program stage

References

- 1 A. Bortash, L. Yegorova, A. Zvyageen, V. Polvanov “The Determination of the r, z, t-Distributions of the Energy Deposition in the VVER Fuel Rods under RIA Test Conditions in the IGR and GIDRA Reactors”, RRC KI report (Report IAE-6088/3), rus., 1998.

- 2 L. Yegorova, V. Asmolov, G. Abyshov, V. Malofeev, A. Avvakumov, E. Kaplar, K. Lioutov, A. Shestopalov, A. Bortash, L. Maiorov, K. Mikitiouk, V. Polvanov, V. Smirnov, A. Goryachev, V. Prokhorov, and A. Vurim "Data Base on the Behavior of High Burnup Fuel Rods with Zr-1%Nb Cladding and UO₂ Fuel (VVER Type) under Reactivity Accident Conditions", *NUREG/IA-0156 (IPSN99/08-02, NSI/RRC KI 2179)*, Vol.1, 2, 1999.
- 3 M. Vostrikov, B. Kochurov "The Annotation of TRIFOB Code", Rus., VANT, Ser. Nuclear Reactor Physics and Engineering, Vol.4, 1985.
- 4 AEA Technology. The ANSWERS Software Package WIMS. (A WIMS Modular Scheme for Neutronics Calculations). User Guide. ANSWERS/WIMS(95)4, Issue 3. Atomic Energy Agency Technology (AEA), Winfrith, United Kingdom, 1997. AEEW-R-2442
- 5 A. Bortash, A. Zvyageen, V. Polvanov "ENDEP Code for the Calculation of Energy Deposition in Fuel Rods at Reactor Capsule Tests", RRC KI report, 1998.
- 6 W.Engle "A User Manual for ANISN". Union Carbide Corporation, K-1693, 1967.
- 7 E. Danskoy, V. Yeltsov, A. Zhitnik, et al. "The Monte Carlo Method in the VNIIEF", Rus., VANT, Ser. Mathematical Modeling of Physical Process, Vol.2, 1993.
- 8 A. Shestopalov, K. Lioutov, L. Yegorova, G. Abyshov, K. Mikitiouk "Modification of USNRC's FRAP-T6 Fuel Rod Transient Code for High Burnup VVER Fuel", NUREG/IA-0164, RRC KI 2180, IPSN 99/10 May 1999.
- 9 Yu. Bibilashvily, N. Sokolov, A. Salatov, O. Nechaeva, L. Andreeva-Andrievskaya, F. Vlasov "Modeling of VVER Fuel Rod Behavior in Accident Conditions Using RAPTA-5 code", Second International Seminar on VVER Fuel Performance, Modeling and Experimental Support, Sandanski, Bulgaria, 21-25 April 1997.
- 10 L. Siefkin, Ch. Allison, M. Bohn, S. Peck "FRAP-T6: Computer code for the transient analysis of oxide fuel rods", NUREG/CR-2148 EGG-2104, May 1981.
- 11 D. Hagrman, G. Reymann, R. Mason "MATPRO-Version 11 (revision 1): A Handbook of Material Properties for Use in the Analysis of Light Water Reactor Fuel Rod Behavior", NUREG/CR-0497 TREE-1280, Rev 1, February 1980.
- 12 A. Labuntzov, *Teploenergetika*, Vol.12, Rus, 1959.
- 13 G. Poletaev "Approximation of Analytical Equations for Cladding Rewetting under RIA conditions", RRC KI (IAE-6090/5), Rus, 1998.
- 14 K. Lioutov, L. Yegorova, E. Kaplar, A. Konobeyev, V. Smirnov, A. Goryachev, V. Prokhorov, and S. Yeremin "Mechanical properties of unirradiated and irradiated Zr-1%Nb cladding under accident conditions". Proceedings of the 27th Water Reactor Safety Information Meeting, NUREG/CP-0169, 1999.
- 15 E. Kaplar, L. Yegorova, K. Lioutov, A. Konobeyev, N. Jouravkova, A. Goryachev, V. Prokhorov, S. Yeremin, A. Svyatkin "Mechanical Properties of Unirradiated and Irradiated Zr-1%Nb Cladding", RRC "Kurchatov Institute" report NSI RRC 2241, 2001 (also USNRC report NUREG/IA-0199 and IPSN report IPSN 01-16).
- 16 Yu. Bibilashvili, N. Sokolov, A. Salatov, L. Andreeva-Andrievskaya, O. Nechaeva, F. Vlasov "RAPTA-5 Code: Modelling of Behavior of Fuel Elements of VVER Type in Design Accidents. Verification Calculations", *Proc. of IAEA Technical Committee Meeting on "Behavior of LWR Core Materials under Accident Conditions"*, Dimitrovgrad, Russia, on 9-13 October 1995. IAEA-TECDOC-921, Vienna, 1996.
- 17 Yu. Bibilashvili, N. Sokolov, A. Salatov, L. Andreeva-Andrievskaya, O. Nechaeva, V. Nalivaev, V. Semishkin, V. Smirnov at al. "Experimental Researches and Modeling of WWER Fuel Rods Behavior in LOCA Conditions using RAPTA-5 Code", Third International Seminar on WWER Fuel Performance, Modeling and Experimental Support, Pamporovo, Bulgaria, 4-8 October 1999.
- 18 M. Ishikawa, S. Shiozawa "A Study of Fuel Behavior under Reactivity Initiated Accident Conditions-Review" *Journal of Nuclear Materials* v.95 (1980), p. 1-30.
- 19 M. Ishikawa, T. Inabe "The nuclear safety research reactor (NSRR) in Japan", *Advance in nuclear science and technology*. New-York/London, 1979.

5. BIGR TEST RESULTS AND DISCUSSION

Twelve VVER high burnup fuel rods were tested at narrow pulses of the BIGR reactor (see Fig. 5.1). Results of reactor tests were amplified by results of post-test examinations^a and results of neutronic and thermal physical calculations performed for each fuel rod. The obtained data were organized and presented in twelve subappendices of Appendix E of Volume 2 of the report. The consideration of all aggregate of developed data is carried out in sections of this chapter of the report.

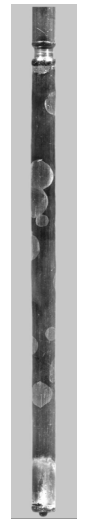


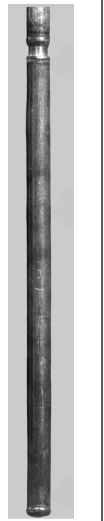
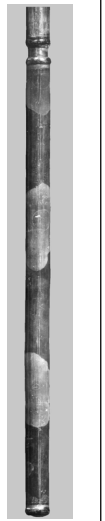
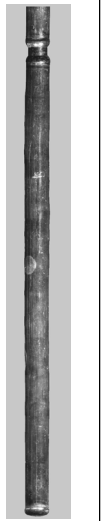
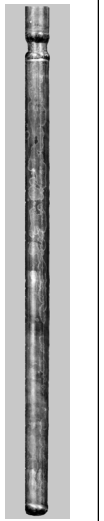
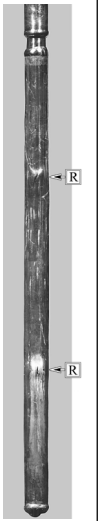
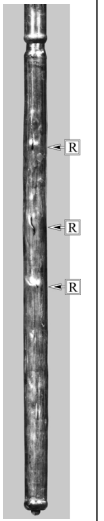


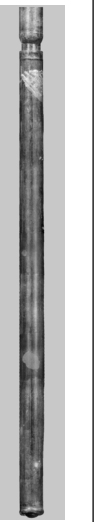

#RT1	#RT2	#RT3	#RT4	#RT5	#RT6	#RT7	#RT8	#RT9	#RT10	#RT11	#RT12
48.3 MWd/ kg U	48.0 MWd/ kg U	47.5 MWd/ kg U	60.1 MWd/ kg U	48.6 MWd/ kg U	47.8 MWd/ kg U	60.5 MWd/ kg U	60.0 MWd/ kg U	59.8 MWd/ kg U	46.9 MWd/ kg U	47.2 MWd/ kg U	47.3 MWd/ kg U
2.1 MPa	2.1 MPa	2.1 MPa	2.1 MPa	2.1 MPa	2.1 MPa	2.0 MPa	2.0 MPa	0.1 MPa	2.0 MPa	2.0 MPa	0.1 MPa
142 cal/g	115 cal/g	138 cal/g	125 cal/g	146 cal/g	153 cal/g	134 cal/g	164 cal/g	165 cal/g	164 cal/g	188 cal/g	155 cal/g
											
 = Cladding rupture. 0.1, 2.0, 2.1 MPa correspond to the initial fill gas pressure in fuel rods											

Fig. 5.1. Appearance of high burnup fuel rods after the BIGR tests

5.1. Thermal mechanical behavior of high burnup fuel rods under BIGR narrow pulse conditions

It should be taken into account that the following features define the high burnup fuel behavior under the RIA conditions:

- the disappearance of the gas gap;
- the formation of specific fuel structure which is characterized by such effects as:
 - ⇒ the presence of new fissile nuclides (^{239}Pu , ^{240}Pu , ^{237}Np , ^{241}Am) in fuel;
 - ⇒ the nonuniform radial distribution of fuel porosity, concentration of fissile nuclides and fission gases, UO_2 grain size and development of the rim layer with the high porosity in the form of overpressurized pores with high gas content and small grain size on the fuel pellet edge (see Fig. 5.2);
 - ⇒ the decrease of fuel thermal conductivity caused by the increase of porosity;

^a The reference information characterizing the appropriate experimental procedures is presented in Appendix A of this volume of the report

- the degradation of the cladding mechanical properties as a result of radiation damages, oxidation and hydriding of the cladding material during the base irradiation.

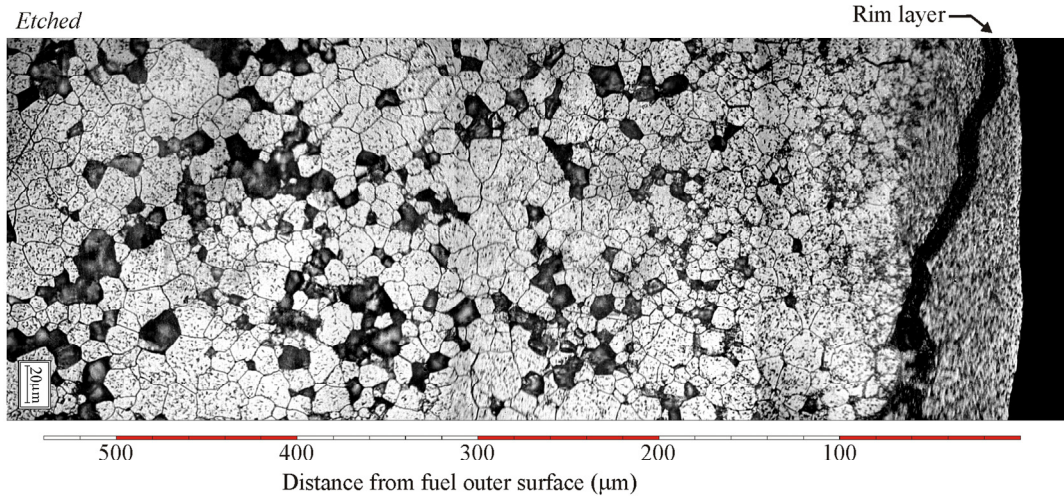


Fig. 5.2. Demonstration of the rim layer structure using the metallographic sample of the VVER fuel with burnup of 50 MWd/kg U

Effects connected with the transformation of fuel structure lead to the change of the spatial picture of fission processes in this fuel. Thus, in the case with high burnup fuel, the sharp increase of concentration of plutonium fissile isotopes is observed as the pellet edge is approached (see Fig. 5.3a). Moreover, fuel burnup in this area of the pellet is doubled at the average burnup of 50 MWd/kg U in comparison with the fuel middle area (see Fig. 5.3b). So, the rim layer demonstrates the fuel structure at overburnup (≈ 80 MWd/kg U).

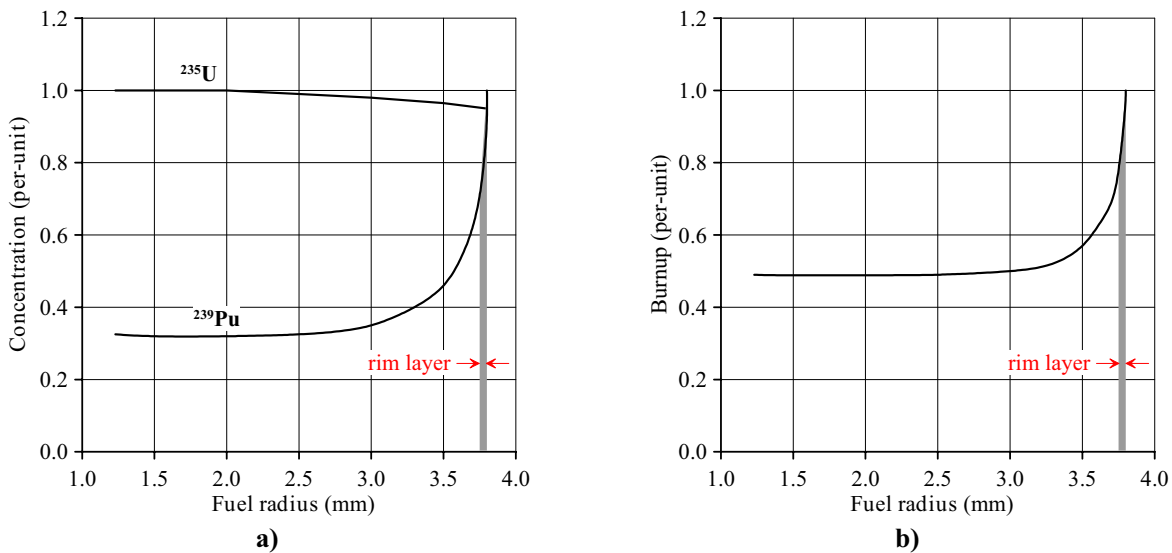


Fig. 5.3. a) Radial distributions of ^{235}U and ^{239}Pu relative concentrations; b) Burnup radial distribution in the VVER fuel with average burnup of 50 MWd/kg U

Taking into account that fissions on plutonium isotopes (^{239}Pu , ^{241}Pu) consist of a significant part of the total number of fissions, the radial profile of energy deposition in high burnup fuel is similar to the plutonium radial distribution at the BGR tests. This fact leads to the very important phenomenon accompanying the narrow pulse tests of the RIA type. The phenomenon illustrated in Fig. 5.4 for the VVER fuel rod tested in the BGR reactor can be characterized in the following way:

- a sharp increase of the fuel enthalpy (temperature) was observed on the fuel edge at the beginning of the RIA process (0.01 s). The fuel enthalpy achieved 145 cal/g in this area at this time but the fuel enthalpy in the fuel central part was only 85 cal/g;
- this tendency was kept during the next 90 ms;
- the typical parabolic radial temperature profile was formed in the fuel pellet within 500 ms after the beginning of power pulse.

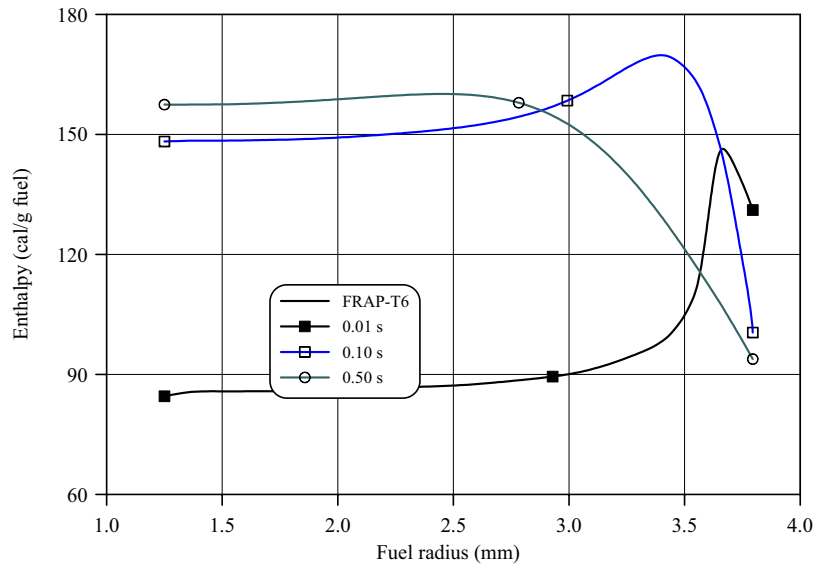


Fig. 5.4. The radial distributions of the fuel enthalpy as a function of time for the fuel rod #RT6 (48 MWd/kg U)

To interpret thermal mechanical behavior of high burnup fuel rods at the BGR tests, the list of fuel specific effects must be supplemented with the cladding material effects. As it was noted in the first chapter of the report, the VVER zirconium niobium cladding was characterized by the high resistance to the degradation of the cladding mechanical properties caused by the oxidation and hydriding during the base irradiation. As for the irradiated claddings used for the BGR tests, the appropriate consolidated parameters were as follows (see Table C.1 of Appendix C of Volume 2 of the report):

- ZrO₂ outer thickness: 3–5 μm for fuel rods with 47–49 and 60 MWd/kg U burnup;
- ZrO₂ inner thickness: 0 μm for fuel rods with 47–49 MWd/kg U burnup, 8–10 μm for fuel rods with 60 MWd/kg U burnup;
- Hydrogen content: 50 ppm by weight for fuel rods with 47–49 MWd/kg U burnup and 60–80 ppm by weight for fuel rods with 60 MWd/kg U burnup.

Thus, one new effect corresponding to the cladding oxidation behavior during the base irradiation was revealed only for these fuel rods. This effect was associated with the formation of ZrO₂ layer on the irradiated cladding inner surface of the fuel rods with 60 MWd/kg U burnup (see Fig. 5.5). Moreover, in the strict sense, this layer was the bonding layer, which is characterized by the compound chemical composition^a.

Nevertheless, the analysis of above listed parameters for the base irradiation oxidation showed that the reduction of the cladding ductility caused by these factors was small. The major factor determining the decrease of the cladding ductility as a function of burnup was the radiation damage in the cladding material.

^a This issue will be considered later in this chapter

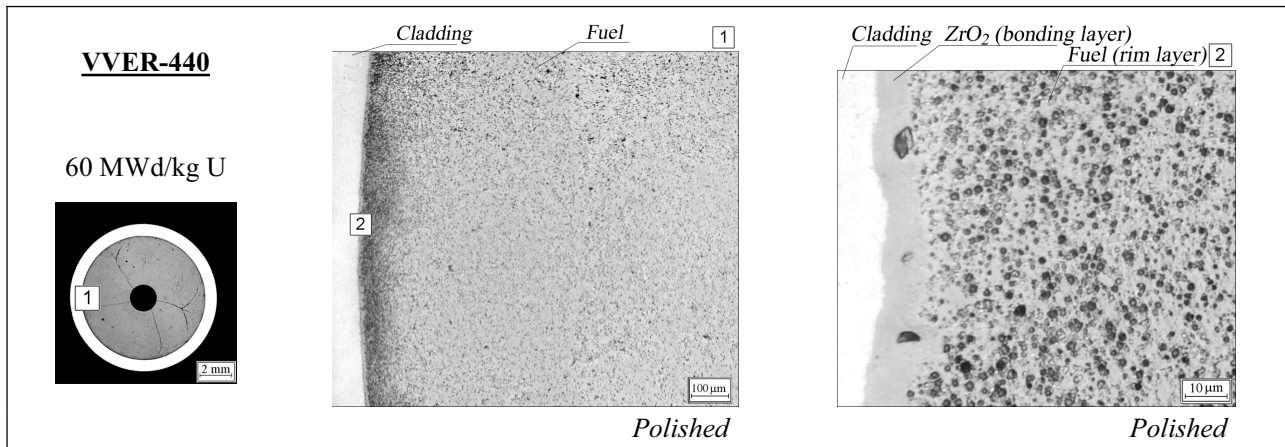


Fig. 5.5. Demonstration of the bonding layer on the cladding inner surface of the VVER-440 fuel element irradiated up to 60 MWd/kg U

Special cycles of investigations performed to determine mechanical properties of Zr-1%Nb (VVER type)^a cladding and the burst characteristics of this cladding (including RIA conditions) resulted in the data characterizing the total effects of the cladding ductility degradation [1, 2]. Some results of these investigations are presented in Fig. 5.6.

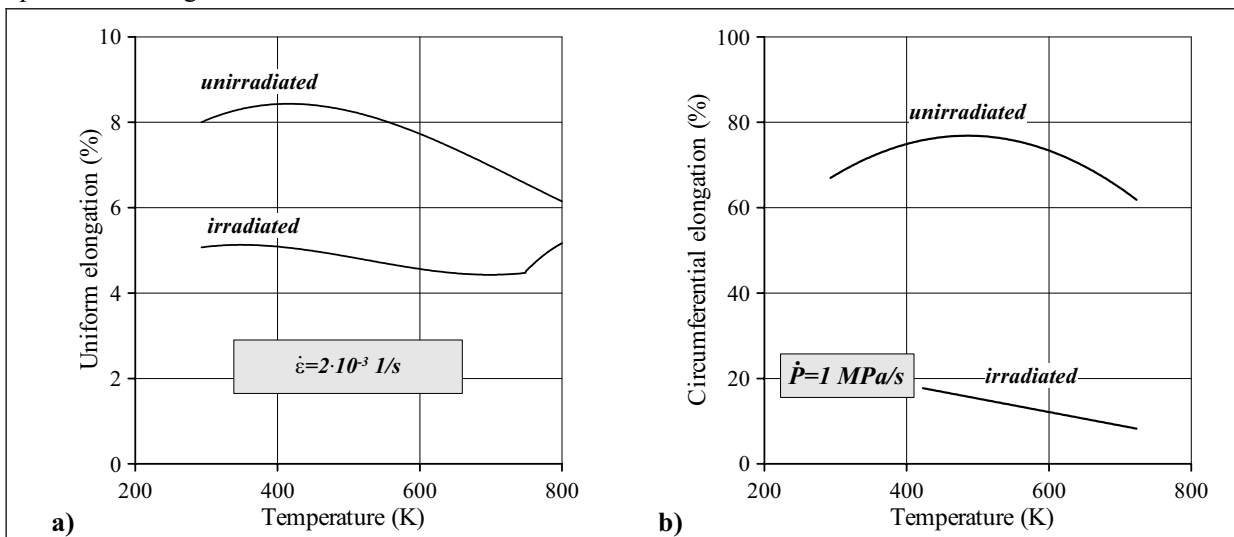


Fig. 5.6. Experimental data characterizing the degradation of mechanical properties of Zr-1%Nb (the VVER type) cladding after the base irradiation up to 50 MWd/kg U
a) uniaxial mechanical tests [1, 2], b) biaxial low temperature tests [2]

The analysis of the whole scope of these results led to the following observations:

- in spite of the fact that the irradiated cladding ductility decreases significantly in comparison with the unirradiated cladding, sufficient ductility margin remains in the VVER irradiated cladding even at the room temperature;
- due to annealing of radiation damages, the difference between the ductility of unirradiated and irradiated claddings disappears at the temperature higher than 600 C [1];

^a The E110 alloy was used to manufacture these claddings

- the low temperature biaxial tests have shown the significant increase in strength properties of Zr-1%Nb irradiated claddings [2] (see Fig. 5.7); this effect can lead to the compensation of the ductility decrease effect.

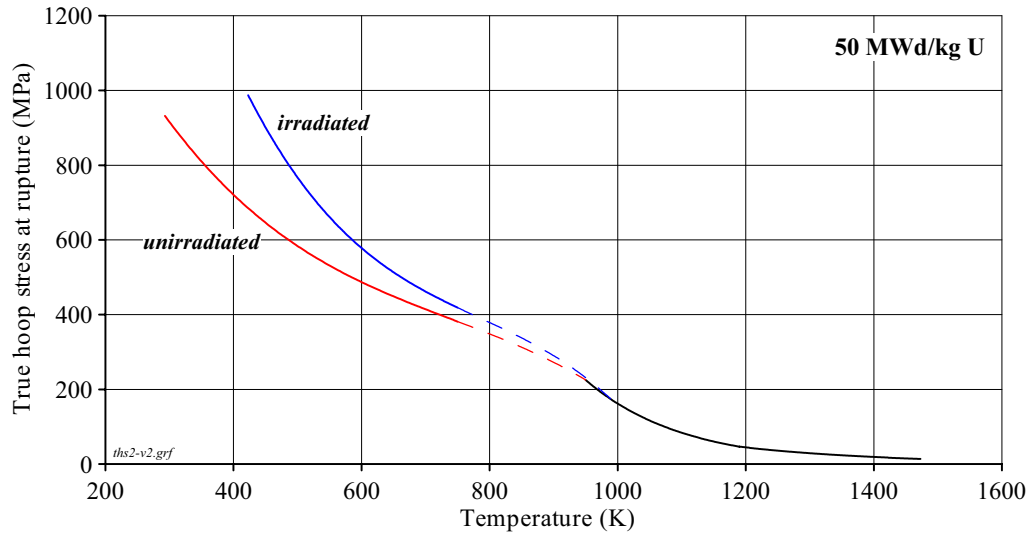


Fig. 5.7. The experimental data obtained from the results of biaxial mechanical tests: the characterization of the true stress at the cladding rupture as a function of the temperature and cladding irradiation

Considered separate aspects of the high burnup fuel behavior under the RIA conditions can be used as the background for the analysis of the fuel rod behavior phenomenology under the BGR test conditions. Specific features of these BGR conditions for one of twelve tested fuel rods (#RT6) are generally illustrated in Fig. 5.8.

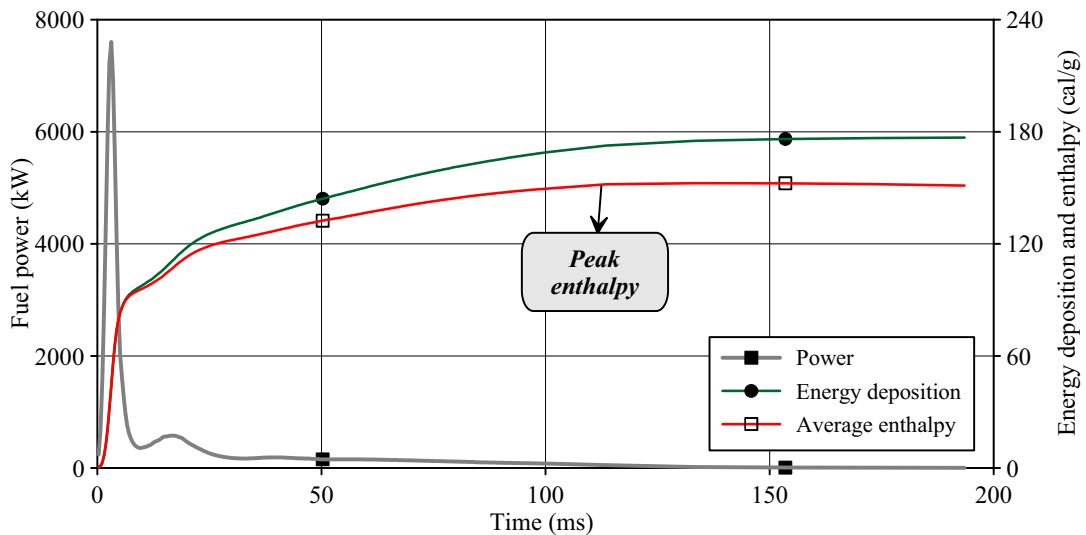


Fig. 5.8. Time dependent energy parameters of the fuel rod #RT6 at the BGR test

The time history of the fuel rod loading at the fast pulse change of power can be analyzed subdividing all processes into three stages. Each stage of the process is characterized by the specific set of physical phenomena listed in Table 5.1.

Table 5.1. The schematic analysis of the major physical phenomena accompanying high burnup fuel behavior under the BGR pulse conditions

Thermal and mechanical mode	List of physical phenomena at separate stages of the test		
	1 st stage: “Cold” PCMI ^a	2 nd stage: “Hot” PCMI ^b	3 rd stage: Pre-cooling and cooling phases
Fuel rod temperature	The sharp increase of fuel temperature and the formation of specific radial distribution with the maximum in the rim layer. Insignificant change of the cladding temperature	The significant increase of the cladding temperature. The following changes in the fuel temperature: <ul style="list-style-type: none"> the displacement of temperature maximum from the edge to the pellet center; the formation of the parabolic type temperature radial profile the achievement of the maximum temperature in the fuel center 	The possible insignificant increase in the cladding temperature at the stage beginning. The decrease in the fuel temperature. The cladding rewetting accompanied by the fast decrease in the cladding temperature
Fuel rod/coolant heat exchange conditions	Free convection of subcooling water	The consecutive change of the following heat exchange types: <ul style="list-style-type: none"> convection nucleate boiling DNB film boiling 	The transition from the film boiling to the nucleate boiling during the rewetting phase
Cladding stress-strain state	The elastic strain with possible transition to the plastic strain or the cladding failure	The plastic strain caused by the PCMI loading and possible cladding rupture	Before the cladding rewetting the plastic strain of the ballooning type with the possible rupture during the cladding rewetting. The possible brittle failure of the oxidized cladding
Cladding mechanical loading mechanism	The gap closure loading initiated by the “hot” fuel. Insignificant gas loading (for pressurized fuel rods)	The loading caused by the contact pressure of expanding fuel (thermal and swelling effects). Local gas loading caused by the initial pressurization and the FGR effect	Development of gas loading (due to the FGR and gas gap opening) before the cladding cooling. The possible axial tensile loading caused by the fuel /cladding constraint during the cladding rewetting

Of course, the interplay of physical processes is more complex than that in the approach presented in Table 5.1. The basic physical phenomena as a function of the peak fuel enthalpy, fuel burnup and cladding initial pressurization can be considered in detail using the results of the FRAP-T6/VVER^c and RAPTA-5^c calculations of twelve high burnup fuel rods tested under the BGR test conditions (see Appendix E of Volume 2 of the report). One of the variants of these calculations was selected to widen and to adjust the data presented in Table 5.1. This variant was developed for the fuel rod #RT6:

- burnup of 48 MWd/kg U;
- initial pressurization of 2.1 MPa;
- peak fuel enthalpy of 152.5 cal/g.

^a The “cold” PCMI is characterized by the fuel high temperature and cladding low temperature

^b The “hot” PCMI is characterized by the high temperature of fuel and the cladding

^c The VVER version of the FRAP-T6 code and the BGR version of the RAPTA-5 code are described in Chapter 4 of this volume of the report

The organized results of FRAP-T6 calculations are presented in Fig. 5.9.

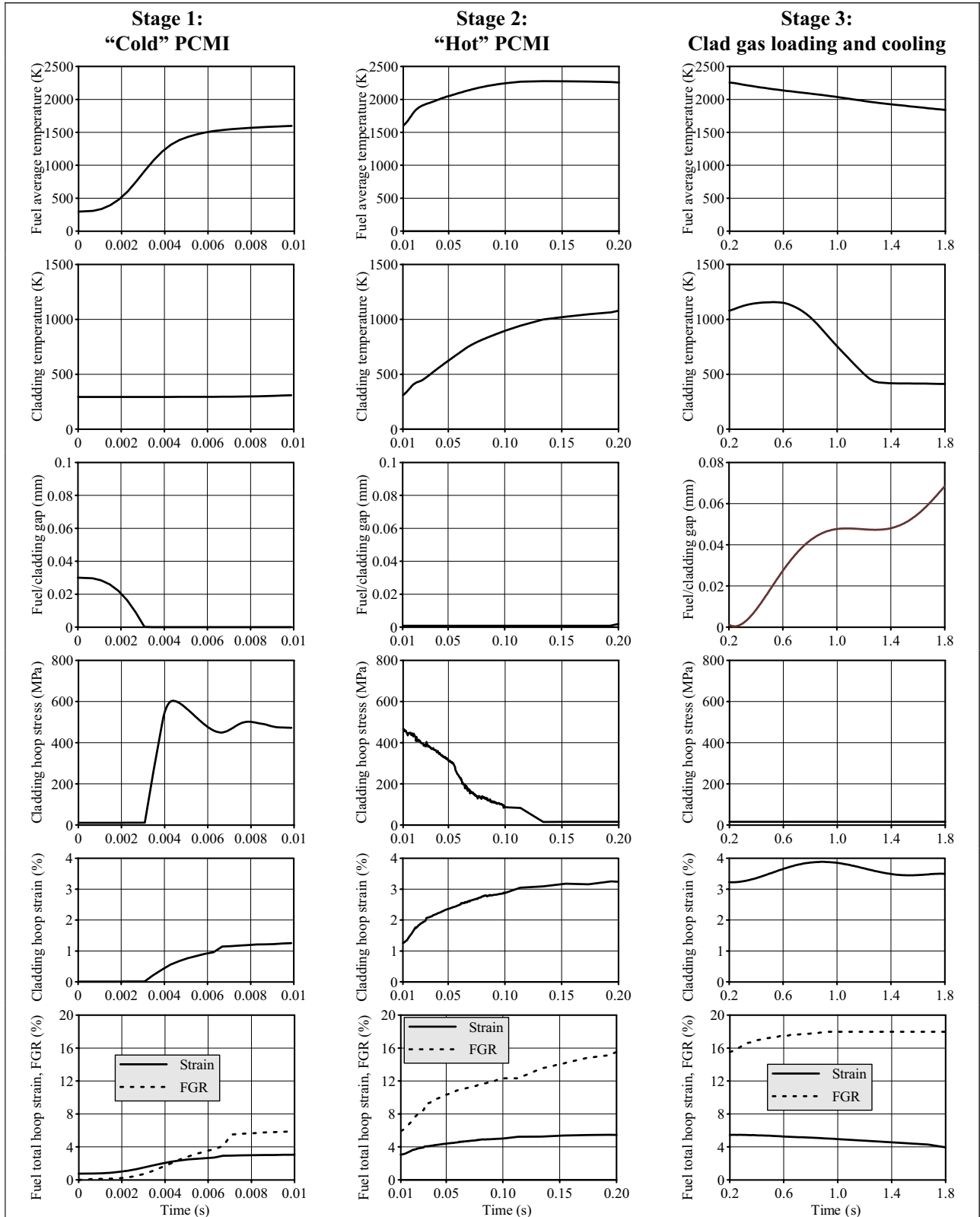


Fig. 5.9. Thermal mechanical behavior of the high burnup fuel rod #RT6 during the BGR test in accordance with the FRAP-T6 calculations

During the first stage of the BGR test, the energy generation occurred so that the adiabatic increase of the fuel temperature and enthalpy can be observed. The fuel temperature increase led to the increase of the fuel pellet diameter caused by the thermal expansion and swelling effects. The gain of these effects took place due to the local temperature burst in the fuel rim layer (see Fig. 5.4). This temperature burst provoked the fast pressure increase in gas pores containing fission gases, the fast increase of stresses in fuel and, as a consequence, the possible fuel cracking (grain boundary cracking)^a.

The fuel expansion resulted in the decrease of the pellet/cladding gap and in the appearance of mechanical contact between fuel and the cladding^b. This early phase of the fuel/cladding mechanical interaction corresponded to the sharp increase of tensile stresses in the “cold” cladding caused by the fuel expansion. Taking into account that the cladding temperature did not increase but the stress in the cladding achieved the yield stress threshold, the plastic deformation of the cladding was initiated. It should be noted that the cladding failure would be observed in this case at the peak fuel enthalpy of 60 cal/g, if a highly oxidized and embrittled cladding was tested. The described set of physical phenomena characterizes the “cold” PCMI stage.

The next stage, which can be named as the “hot” PCMI, was initiated when the cladding temperature began to increase. This increase of the cladding temperature was caused by the increase of heat flux from fuel to the cladding. The cladding temperature increase and, consequently, the increase of heat flux from the cladding to the coolant led to the nucleate boiling on the cladding outer surface. But, taking account that heat flux from fuel continued to increase, the nucleate boiling time was very short and DNB conditions were achieved. After that, the cladding was cooled under the film boiling conditions. The poor heat exchange conditions led to the fast increase of the cladding temperature up to 700 C and higher. Of course, this process was accompanied by the deterioration of the cladding strength properties. Therefore, the cladding plastic deformation under the widening fuel was continued in the presence of the stress relief effect. During the whole this time interval, the fuel temperature and enthalpy were increasing. This process was accompanied by the transformation of the fuel temperature radial profile with the tendency towards the typical parabolic form. Simultaneously with the fuel temperature increase, the increase of fuel thermal expansion, swelling and the FGR were observed. Moreover, the stress-strain state of fuel was characterized by a very high compression stress in the central part of fuel and high tensile stress in the fuel edge. This effect had the following sequences:

- the radial transportation of fill gas and fission gases along the macroscopic channels (between the neighboring pellets) and radial cracks were impossible in the central area of fuel, because all these paths were healed by the compressed fuel;
- additional paths for the fission gas migration in the radial direction were developed in the fuel outer area.

These sequences made possible the assumption that the hot cladding with low strength properties was subjected not only to the tension from the expanding fuel but also to the local pressurization by gas concentrated in the local gas holes inside separate fuel cracks. All these phenomena may be responsible for the cladding rupture at the “hot” PCMI stage of the RIA process. But in our case, the appropriate loads were lower than the failure threshold and the fuel rod #RT6 was not failed.

The initiation of the BGR test third stage was caused by the decrease of the fuel temperature and the reopening of the pellet/cladding gap. In the case with the pressurized fuel rod, the gap reopening process was additionally stimulated by gas (fill gas and grain boundary gas, which were realized after the grain boundary cracking of the first stage) as well as by some increase of the cladding temperature. The important aspect of this gas loading was connected with the fact that very low strength properties of the cladding at that temperature may be the cause for the potential cladding failure (ballooning and burst) in spite of the insignificant increase of the cladding temperature and low stresses in the cladding material. The last phase in the consideration of the thermal mechanical behavior of high burnup fuel under the BGR conditions was devoted to the cooling phenomena. In general case, the cladding cooling can be accompanied by such sufficient effects as:

^a It should be noted that the description of physical phenomena corresponding to the BGR test of the fuel rod #RT6 is some wider than the real modeling of these processes in the FRAP-T6 code

^b In case of fuel rods with 60 MWd/kg U burnup, this effect is more pronounced because these fuel rods were characterized by the disappearance of the fuel/cladding gap before the BGR tests

- thermal stresses during the rewetting process. These stresses are not the factor of importance for the ductile cladding. But, if the cladding has the significant oxidation and high hydrogen content, the cladding fracture may occur;
- the additional axial tensile stresses caused by the cladding rewetting at the retention of the fuel/cladding mechanical contact^a.

As for the considered case, these effects did not determine the mechanical response of the fuel rod #RT6 during the cooling stage. In addition to the cladding effects, the fuel effects should be formulated also for this stage of the RIA analysis. The major fuel effect is connected with the formation of the bonding layer between fuel and the cladding at high burnup. The cooling phase of such fuel rod leads to the separation of the cladding with some fuel peripheral layer from the fuel pellet and to the formation of the pseudo-gap. This effect will be considered more carefully in the next sections of this chapter.

5.2. The general overview of the BIGR test results

The major results characterizing the behavior of seven pressurized fuel rods with burnup of 47–49 MWd/kg U are presented in Fig. 5.10 (see Appendix E of Volume 2 of the report for the more detailed results).

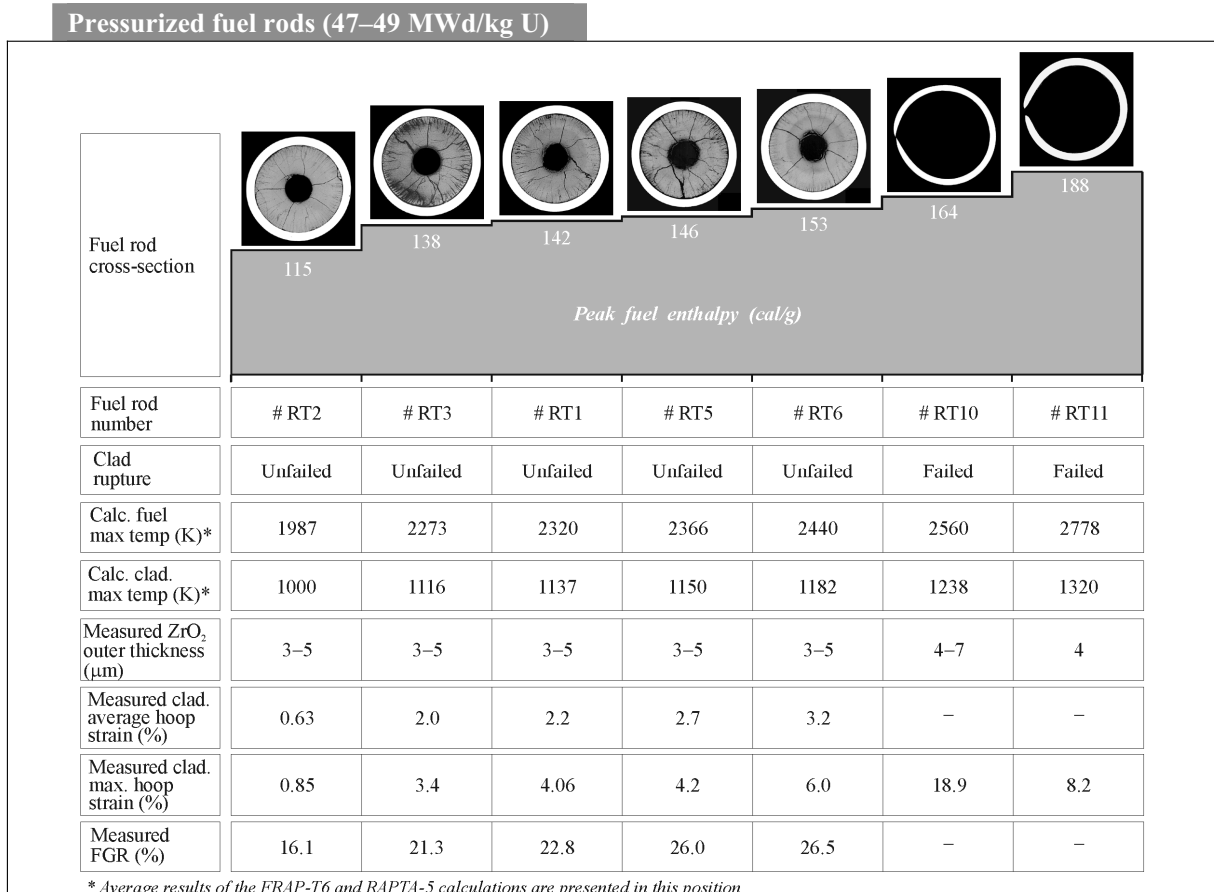


Fig. 5.10. Results of the BIGR tests with pressurized fuel rods of 47–49 MWd/kg U burnup

The preliminary analysis of these results led to the following general conclusions:

^a This variant of the fuel rod behavior can be observed for the fuel burnup higher than 60 MWd/kg U

1. The reasonable margin of residual ductility in Zr-1%Nb (E110) irradiated cladding (due to the low oxidation and hydriding) provided a high resistance to the low temperature (“cold”) PCMI failure under the narrow pulse conditions. This failure type was not observed in any tested fuel rods.
2. The failure threshold of pressurized fuel rods tested at narrow BGR pulses correlated with that at the wide IGR pulse. The BGR threshold was located between 153 and 164 cal/g of the peak fuel enthalpy. The appropriate IGR threshold was 160 cal/g.
3. The plastic cladding rupture (caused by the combination of the high temperature and cladding pressurization) was the leading mechanism for the fuel rod failure at the failure threshold.

To develop the test data for the comparison of pressurized and unpressurized fuel rods, one unpressurized fuel rod #RT12 with burnup of 47.4 MWd/kg U was tested in the BGR reactor. Results of this test are presented in Fig. 5.11. The obtained data shown that the value 155 cal/g of the peak fuel enthalpy was low for the failure of the fuel rod with 47.4 MWd/kg U burnup with the ductile cladding in accordance with the standard (for this type of unpressurized fuel rods) “hot” PCMI mechanism.

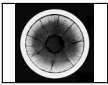
Unpressurized fuel rod #RT12 (47.4 MWd/kg U)								
Fuel rod cross-section	Peak fuel enthalpy (cal/g)	Clad. rupture	Calc. fuel max temp. (K)	Calc. clad max temp. (K)	Measured ZrO ₂ outer thickness (μm)	Measured clad aver hoop strain (%)	Measured clad max hoop strain (%)	Measured FGR (%)
	154.8	Unfailed	2469	1215	3–5	4.35	5.78	22.7

Fig. 5.11. Results of the BGR test with the unpressurized fuel rod of 47.4 MWd/kg U burnup

The effects characterizing the behavior of fuel rods of 60 MWd/kg U burnup could be revealed using the BGR results of four tests presented in Fig. 5.12.

The first conclusions concerning the sensitivity of high burnup fuel rod RIA behavior to the increase of fuel burnup up to 60 MWd/kg U can be formulated as follows:

- all tested fuel rods retained the high resistance to the low-enthalpy PCMI failure (“cold” PCMI). This failure type was not observed at the BGR tests in the fuel enthalpy range of 125–165 cal/g;
- the failure threshold for fuel rods of 60 MWd/kg U burnup was located in the peak fuel enthalpy range of 134–164 cal/g;
- the change of the failure mechanism was observed as compared to fuel rods with 47–49 MWd/kg U burnup. In contrast to the cladding failure of fuel rods with 47–49 MWd/kg U burnup induced by fill gas (with the accompaniment of the fission gas), the cladding failure induced by high temperature PCMI was observed for the fuel rods^a of 60 MWd/kg U burnup. It can be assumed that the differences in the initial gas gaps, rim layer thicknesses, FGR processes are the best candidates for the explanation of the failure mechanism change;
- the pressurized and unpressurized fuel rods of 60 MWd/kg U burnup demonstrated practically the same thermal mechanical behavior at the BGR tests. This fact confirms the high temperature PCMI version of the failure mechanism for fuel rods of 60 MWd/kg U burnup.

^a The presence of several cladding ruptures in each failed fuel rod was the indicator for this conclusion

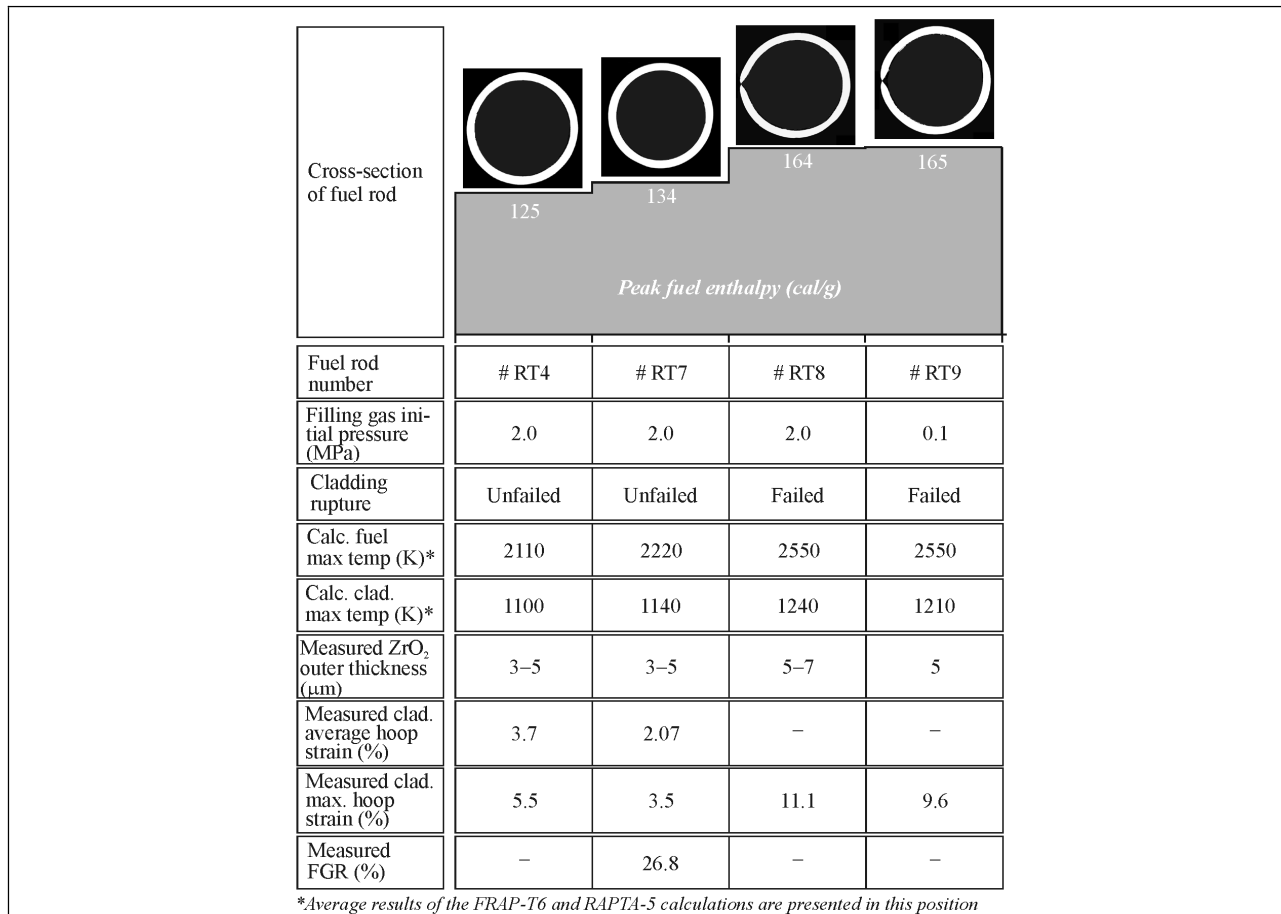


Fig. 5.12. Results of the BIGH tests of pressurized and unpressurized fuel rods with 60 MWd/kg U burnup

The analysis of the BIGH results will be continued in next sections of this chapter. The analysis is devoted to the consideration of such important aspects of these tests as:

- fuel behavior and FGR phenomena;
- cladding behavior;
- failure mechanisms and failure criteria.

5.3. The behavior of high burnup fuel and fission gas release in the BIGH pulse tests

Design and state of the VVER fuel before the BIGH tests

As-fabricated VVER fuel pellets have several modifications in design. The VVER fuel elements used for the refabrication of twelve high burnup fuel rods tested in the BIGH reactor had two types of fuel pellets (A and B types) presented in Fig. 5.13 (see Appendix A of Volume 2 of the report).

The majority of refabricated fuel rods contained the A type of fuel pellets. As-fabricated pellets of this type were of the strong cylindrical form with the central hole. The diameter of the central hole varied from 1.6–1.7 mm in the VVER-440 pellets up to 2.4 mm in the VVER-1000 pellets. One fuel rod #RT7 was refabricated from the VVER-440 fuel element which contained the fuel pellets of the B type. The major difference in these fuel pellets was the presence of chamfers of 0.4-0.4 mm on the pellet ends. These fuel pellets had the minimum diameter of the central hole (1.2 mm).

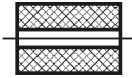
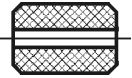
Parameter	Characterization of fuel rods with the fuel pellets of A and B design	
	Type A	Type B
Fuel pellet design		
Fuel rod number	#RT1–6 #RT8–12	#RT7
Pellet height (mm) ^a	8–14	11
Pellet OD (mm) ^a	7.54–7.57	7.6
Central hole diameter (mm) ^a	#RT4,8,9: 1.6–1.7 #RT1–3,5,6,10–12: 2.4	1.2

Fig. 5.13. The design of the VVER fuel pellets used in the BGR tests

The examinations of fuel in the mother fuel elements used for the refabrication revealed the following fuel features after the base irradiation up to 47–49 and 60 MWd/kg U burnup (see Appendices B and C of Volume 2 of the report):

- several radial cracks were observed in the cross-sections of the mother fuel elements of 48 and 60 MWd/kg U burnup (see Fig. 5.14);
- in accordance with the optical microscopy data, three types of the fuel microstructure were observed for three radial layers of high burnup fuel:
 - ⇒ the first outer layer (the rim layer (see Fig. 5.2)) was 50 μm and 150 μm thick for fuel elements with 48 and 60 MWd/kg U burnup, respectively. This layer had a high porosity (10–25%) and very small grain size;
 - ⇒ the second layer (the transient zone) was located just next to the rim layer; this layer was considerably thicker than the rim layer (approximately 550 μm for fuel of 60 MWd/kg U burnup). This layer was characterized by the mixture of the original UO_2 microstructure and the sub-grain UO_2 microstructure and by the tendency towards changing in porosity from 6–10% on the edge down to 3% closer to the center;
 - ⇒ the third layer (the basic zone) was located in the inner part of fuel pellets. This layer had the same grain size as that of as-fabricated fuel. The porosity of this layer was varied in the range of 2.7–4% as a function of burnup.



Fig. 5.14. The cross-sections of two VVER-1000 and VVER-440 high burnup fuel elements after the base irradiation

The fuel examinations performed after the BGR tests (see Appendix E of Volume 2 of the report) provided several general observations (see Fig. 5.15).

^a as-fabricated

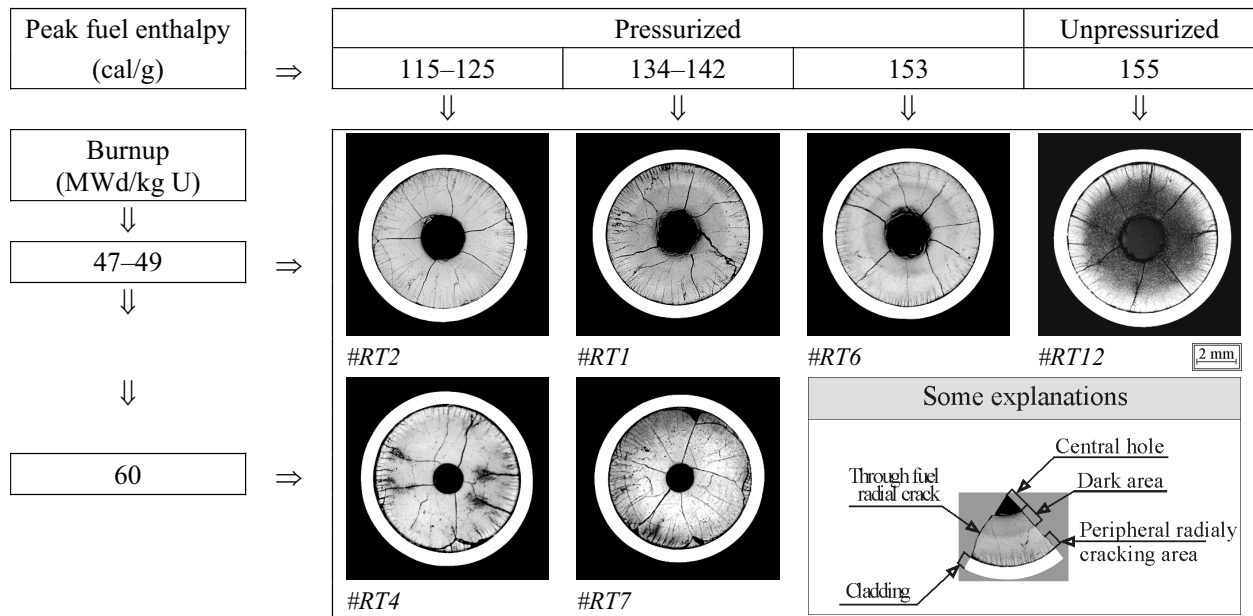


Fig. 5.15. Demonstration of typical macroscopic tendencies characterizing the fuel state of fuel rods with 47–49 and 60 MWd/kg U burnup tested under the BGR narrow pulse conditions

These observations based on the organized data characterizing the fuel macroscopic state in unfailed fuel rods after the BGR tests can be listed as follows:

- All tested pellets had 4–9 radial cracks penetrating along the whole fuel radius (from the periphery to the central hole). Despite the fact that similar cracks were observed on the fuel cross-sections before the BGR tests, it can be assumed that these cracks are different. The initial cracks could disappear due to the high fuel temperature and high compression stresses during the heating mode of the BGR test. The formation of new global radial cracks occurred during the cooling down phase of the BGR test.
- The dark area appeared in the central part of many fuel pellets. The effects of dark zone were observed and examined earlier in connection with the studies of high burnup fuel under steady-state and transient conditions (see, for example, [3, 4]). In accordance with the results of these investigations, the dark zone was characterized as fuel with a high concentration of fission gas bubbles within the fuel grain (intragranular bubbles).
- Fine radial cracks appeared in the fuel peripheral zone in all types of tested fuel rods.

As for this cracking in the outer layer, the similar phenomenon was observed at pulse tests of the VVER and PWR high burnup fuel in the IGR [5], CABRI [6], and NSRR [7] reactors. Moreover, this layer was developed with the strong function of fuel burnup because this effect was not observed at tests of the unirradiated VVER and PWR fuel. The nature of these fine radial cracks can be connected with the stresses initiated at the following stages of the RIA tests:

- heating up phase;
- cooling down phase.

It is obvious that the cooling down phase can provoke the creation of peripheral cracks due to the large temperature gradient between the fuel center and peripheral area of the fuel pellet. To estimate the fuel mechanical response to the cooling down stresses, the VVER fuel (≈ 50 MWd/kg U burnup) and PWR fuel (≈ 50 MWd/kg U burnup) tested in the IGR [5] and NSRR [7] reactors, respectively, were compared. The choice of these data for the comparison was motivated by the following considerations:

- these tests had different heating up rates because of the significant difference between the NSRR narrow pulse width (several milliseconds) and the IGR wide pulse width (several hundreds milliseconds);

- these tests had the same cooling down rate because of the same coolant conditions (stagnant water at the room temperature and atmospheric pressure) in these tests.

Results of these comparisons revealed that:

- the occurrence of fine peripheral cracks in high burnup fuel after the NSRR tests was noted at very low peak fuel enthalpies: the lowest value was 157 J/g (37.5 cal/g);
- high burnup fuel tested in the IGR reactor had no peripheral cracks at enthalpy of 60 cal/g. The first indications of the beginning of this process were noted at 85 cal/g. At higher enthalpies, fuel tested in the IGR reactor had the similar peripheral cracking zone.

Thus, the heating up phase plays the key role in the formation of this specific layer. This conclusion is confirmed by the results obtained in the computer analysis of fuel behavior during these stages of the RIA tests. As it was noted earlier, the heating up phase was accompanied by the sharp temperature burst in the fuel peripheral area (see Fig. 5.4). This specific phenomenon leads to the generation of very high tensile stresses in this circumferential fuel layer. Moreover, the additional stresses were produced by the overpressurization of fission gas bubbles inside the fuel. The more detailed analysis of these effects can be performed using the data presented in Fig. 5.16.

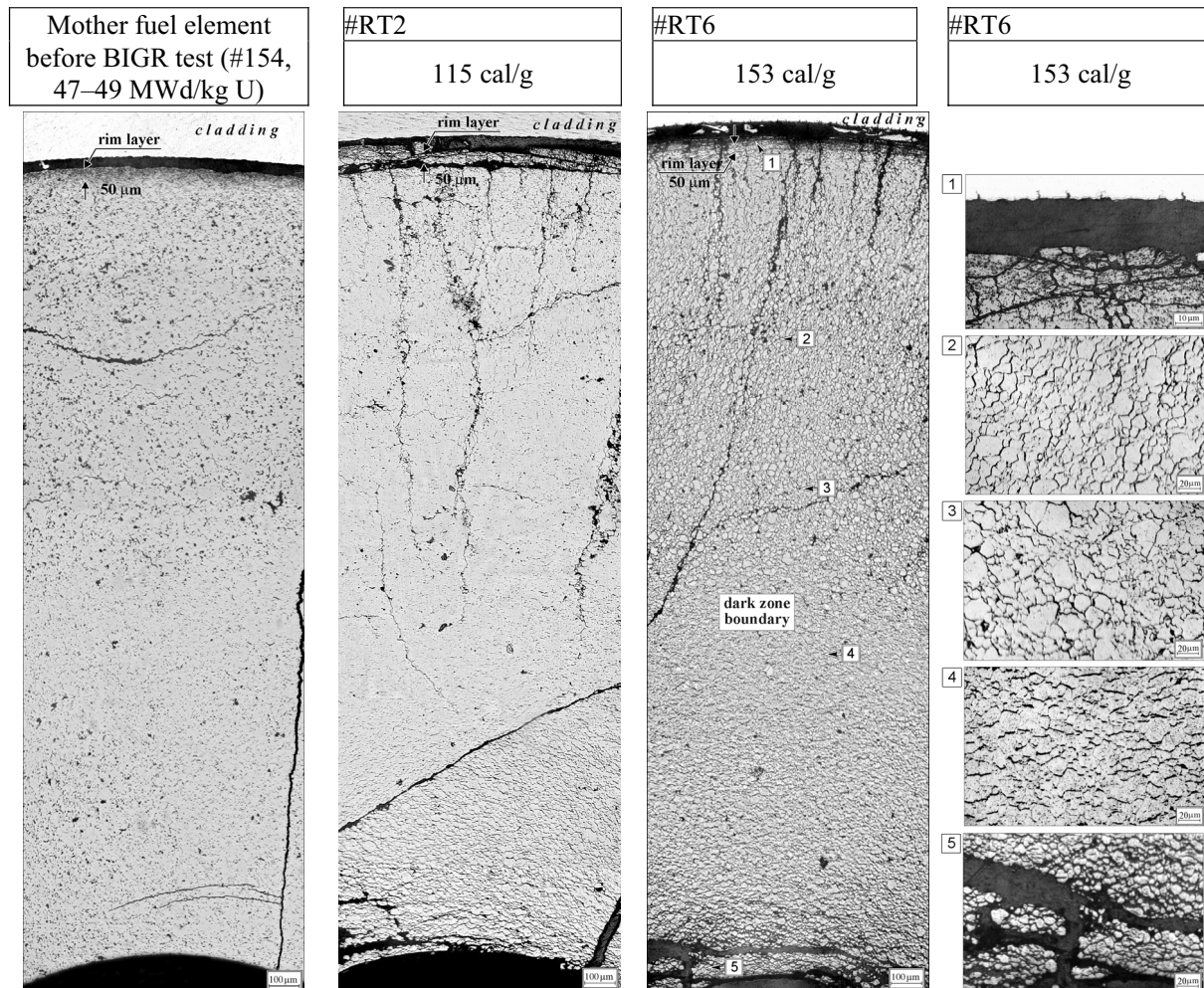


Fig. 5.16. Transformation of the fuel microstructure as a function of the peak fuel enthalpy in unfailed fuel rods with 47–49 MWd/kg U burnup

The figure contains the comparative data characterizing the microstructure of the VVER fuel with burnup of 47–49 MWd/kg U before and after the BGR tests. The comparative studies of all data obtained for six unfailed fuel rods^a of this type revealed the following specific effects:

- the inner fuel layer located close to the central hole has the tendency towards the tangential cracking and separation from the fuel matrix at the fuel enthalpy increase in the range of 115–155 cal/g;
- the inner part of the fuel matrix, which is identified as the dark zone on the macroscopic views of pressurized fuel rods, has the tangential type of the fuel grain separation (the grain boundary opening) and local tangential cracking on microscopic views. These effects become more pronounced at the fuel enthalpy increase. The increase of the intragranular porosity is observed at the increase of the fuel enthalpy in the range of 115–153 cal/g. It seems that tangential effects of the grain separation result from the fuel brittle failure caused by the temperature overpressurization of fission gas intragranular bubbles in the presence of high compression stresses in this fuel region;
- the next fuel layer marked as pos.3 of #RT6 in Fig. 5.16 is the intermediate layer between the inner region with the compression stresses and the outer region with the tensile stresses. This intermediate layer is characterized by the uniform grain size and by the grain boundary separation at the fuel enthalpy increase;
- the following fuel layer on moving to the pellet periphery (marked as pos.2 of #RT6 in Fig. 5.16) is characterized by the tendency towards the formation of the radially-pronounced grain separation and radial gas tunnels at the fuel enthalpy increase. These effects are in the agreement with the tensile stresses, which are preferential in this fuel region;
- the fuel visual (from the macroscopic view) peripheral layer containing fine radial cracks is in the correlation with the transient zone described earlier in the context of the radial distribution of fuel grain size, fission gas content, burnup and plutonium concentration. This fuel layer located in the range of the fractional fuel radius of 0.9–1 is characterized by the decrease in the fuel grain size from the standard grain down to the fine subgrain and by the increase of gas porosity;
- the last peripheral rim layer demonstrated the tendency towards the separation from the fuel matrix and towards the fragmentation at the fuel enthalpy increase.

All above listed indicators of the fuel behavior at narrow pulse conditions were related to the pressurized fuel rods with burnup of 47–49 MWd/kg U. As for the comparative behavior of unpressurized fuel rods with the same burnup, the microstructure of the fuel rod #RT12 can be analyzed (see Fig. 5.17).

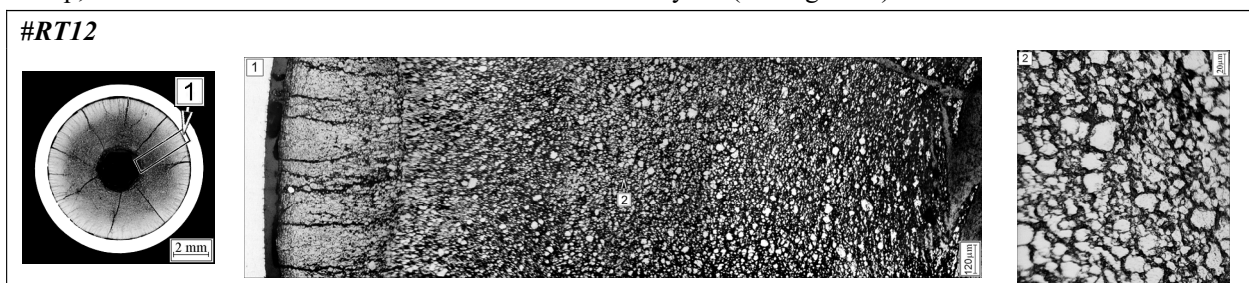


Fig. 5.17. The cross-section and fuel microstructure of the unpressurized fuel rod with burnup of 47.4 MWd/kg U tested at 155 cal/g and remained unfailed

The analysis of the macro– and microscopic structure of fuel in this fuel rod showed that:

- the most tendencies revealed on the consideration of pressurized fuel rods were also confirmed for this fuel;

^a The whole set of the appropriate PIE data containing the fuel microstructure of fuel rods with 47–49 MWd/kg U burnup after the BGR tests is presented in Appendix E of Volume 2 of the report

- the grain separation effect was slightly higher in the fuel matrix of the unpressurized fuel rod. This process was reflected in the macroscopic cross-section with the high intensity of the dark color in the appropriate fuel region.

As for the grain separation the effect of mechanical constraint of fuel radial displacement at the heating up stage should be taken into account. The mechanical constraint inhibits the run-off of fission gases in radial direction and, consequently, leads to the more pronounced grain separation. In this connection the factor of the rod internal gas pressure may be the less important, than the factor of the gap size, which was smallest in the fuel rod #RT12 of all fuel rods with 47–49 MWd/kg U burnup (suggesting a different irradiation history with also a possible impact on gas inventory). The effect of the gap size and the effect of fission gas initial content in the fuel matrix can be clarified using the test data characterizing the fuel microstructure of pressurized fuel rods^a with 60 MWd/kg U burnup after the BGR tests^b (see Fig. 5.18).

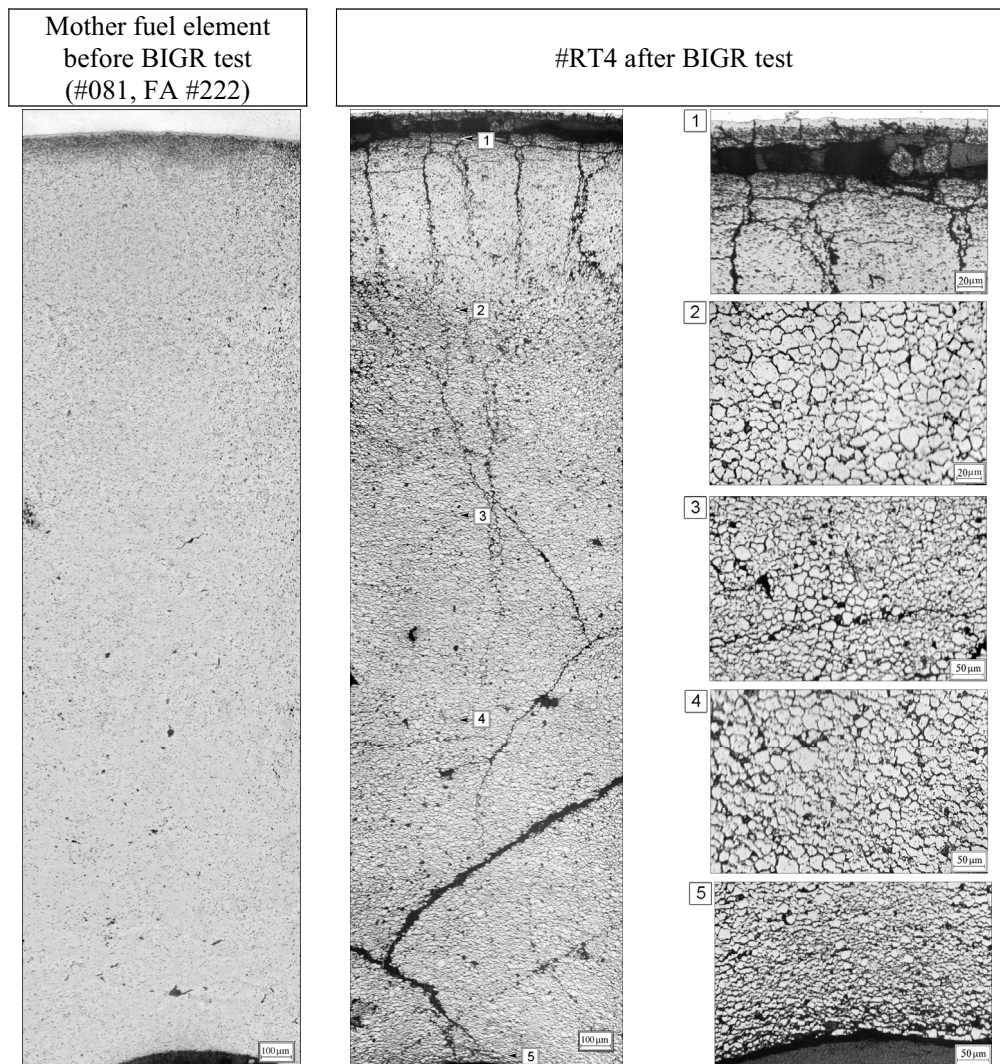


Fig. 5.18. Transformation of the fuel microstructure in the fuel rod with 60 MWd/kg U burnup tested at 125 cal/g of the peak fuel enthalpy in comparison with the state before the BGR test

^a As it was noted earlier, fuel rods with burnup of 60 MWd/kg U had no initial pellet/cladding gap

^b The whole set of the appropriate data containing the fuel microstructure of fuel rods with 60 MWd/kg U burnup after the BGR tests is presented in Appendix E of Volume 2 of the report

The presented data showed that in spite of the initial pressurization, the fuel microstructure in the middle part of the pellet with 60 MWd/kg U burnup demonstrated the tendency towards the uniform grain separation (no radial effect except for the pellet outer zone (pos.1). Therefore, the factor of the gap size makes up the dominant factor probably in the context of the analyzed problems. The effect of the initial fission gas content was observed as the more intensive separation of the fuel grain in the middle parts of fuel as a function of the peak fuel enthalpy. The formation of the specific inner layer (pos.5) adjacent to the central hole and the formation of fine radial cracks in the outer layer of these fuel rods are similar to those in the fuel rods with burnup of 47–49 MWd/kg U. In this connection, the specific effects characterizing the mechanical behavior of the outer fuel layer can be considered separately for the whole scope of tested and unfailed fuel rods.

To widen the experimental base of this consideration, the detailed pictures illustrating the fuel microstructure in this region are presented in Fig. 5.19 for the fuel rod with the initial gas gap and burnup of 47–49 MWd/kg U.

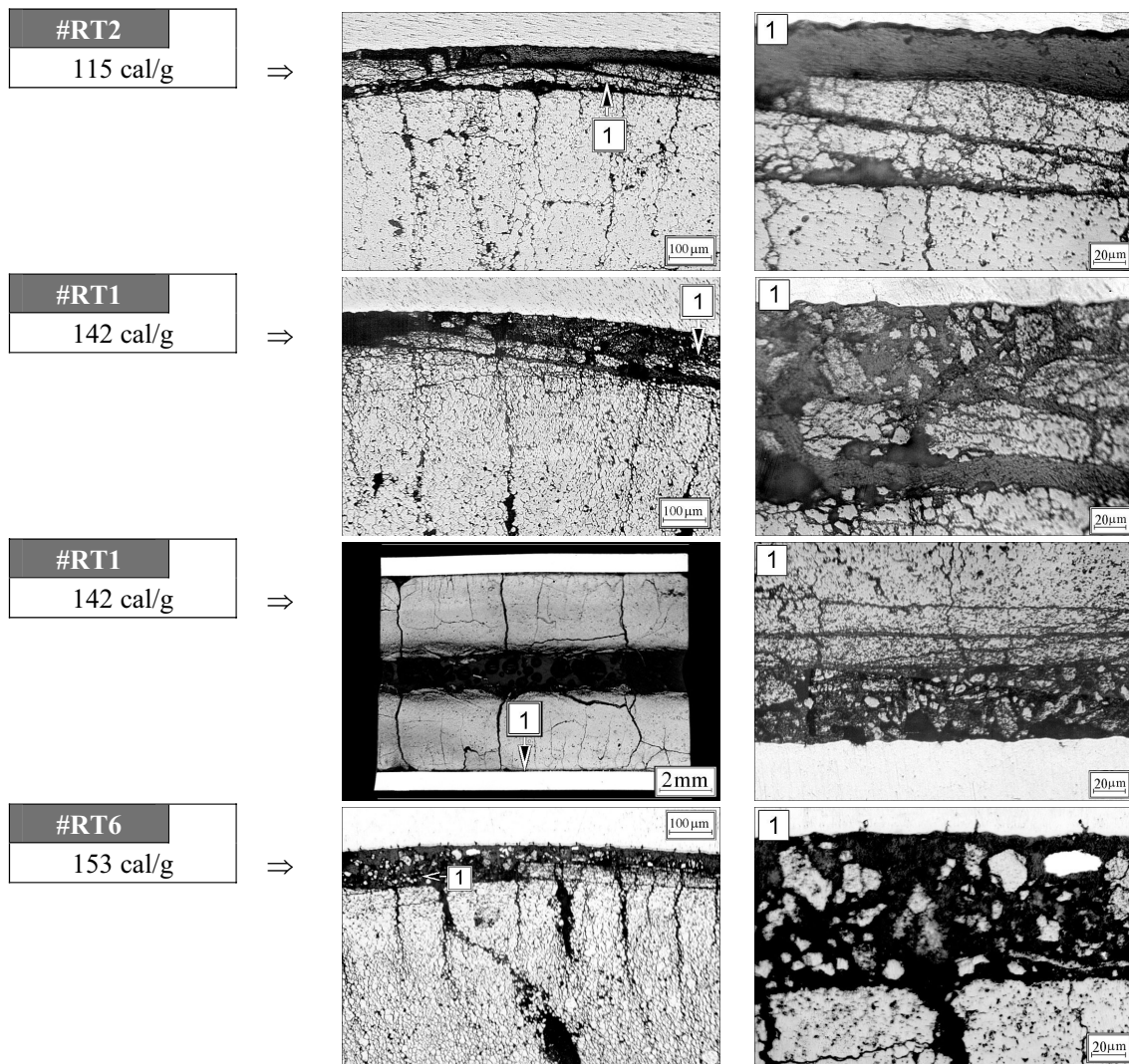


Fig. 5.19. Rim layer mechanical behavior in unfailed fuel rods with burnup of 47–49 MWd/kg U

But before the analysis of these data, some comments based on results of the previous fundamental studies devoted to the high burnup fuel microstructures [3, 4, 6, 8–14] are formulated:

- in the general case, the fuel swelling is a function of the fuel thermal expansion and of the expansion of fission gases contained in the fuel;

- the high burnup fuel is additionally characterized by the specific rim bubbles swelling;
- special investigations have shown that the rim layer consists of subdivided grains of uranium dioxide with the precipitation of large coarsened fission gas bubbles and small intragranular fission gas bubbles;
- the pressure of fission gases located in different bubbles can be very high;
- the large concentration of gas bubbles in the rim layer provides the high porosity density of this fuel region;
- during the base operation, the fission gas release is determined by recoil/ejection process and by diffusion of gas atoms and bubbles to the grain boundaries and formation of interconnected porosity on the grain boundaries;
- the most amount of fission gases (Xe, Kr)^a generated during the base irradiation remains in the fuel (in the intragranular bubbles and in the coarsened bubbles (in the rim layer).

The study of experimental data presented in Fig. 5.19 resulted in the agreement with the characterization of the rim layer as another material in comparison with the fuel matrix. Thus, the high burnup fuel consists of two different materials:

- the solid UO₂ pellet with the precipitation of fission gas components and metallic inclusions of other fission products;
- the porous U–Pu (and actinides)–O outer rim layer with the high concentration of fission gases in different bubbles at the high local pressure.

This approach to the interpretation of high burnup fuel can be confirmed on considering the rim layer mechanical behavior as a function of the peak fuel enthalpy:

- at the peak fuel enthalpy of 115 cal/g, the combination of poor mechanical properties of the rim layer and the local burst of fuel temperature generated in this layer at the beginning of the BGR test in the range of the first hundred of milliseconds led to the separation of the rim layer from the fuel matrix and to the cracking of this layer; it can be assumed that the cracking was provided by the mutual effect of stresses caused by the thermal expansion of solid components of the fuel material and by stresses caused by the overpressurization of gas bubbles;
- the increase in the peak fuel enthalpy up to values of 142, 153 cal/g led to the gain in the effect of fission gas bubbles overpressurization and, the thermal stress effect. Both these effects provided the fragmentation of the rim material up to the creation of very fine fragments (from the microscopic point of view). A special axial metallographic sample prepared from the fuel rod #RT1 demonstrated that the pellet/cladding gap along the pellet height was filled with fine fuel fragments.

The fuel rods with burnup of 60 MWd/kg U are characterized by the more specific behavior (see Fig. 5.20). This type of fuel rods had no gas gap before the BGR tests. Moreover, the specific bonding layer appeared on the cladding inner surface^b. The direct solid contact between the fuel and cladding prevented the rim layer fragmentation by the mechanism described for fuel rods with 47–49 MWd/kg U burnup. It can be assumed that high compression stresses initiated in the rim layer due to the PCMI phenomenon at the heating up stage of the BGR test led to the densification of the rim layer and to the intensification of the tight mechanical (or chemical) contact between the rim and bonding layers. This effect is illustrated by the data presented in Fig. 5.20 and in Fig. 5.23, Fig. 5.24. The initiation of tensile stresses in the rim layer (mechanically connected with the cladding)

^a It has been suggested that the behavior of cesium as an important fission product may be underestimated [15]. Following this thought, the low boiling temperature (670 C) and the same release behavior as Xe at temperatures above 1200 C suggests the cesium contribution may be a factor in the formation of grain boundary fission gas bubbles. The threshold temperature for the thermally activated release of cesium and xenon is similar and Cs radial distribution is practically the same as the radial burnup profile with the maximum in the rim layer. An unresolved issue is the pressure in the gas bubbles because, at high pressure, the critical temperature of Cs in the gaseous form will be higher than 1200 C. Below this temperature, cesium is liquid and will be present on the grain surface in the form of a film

^b The more detailed characterization of this layer is presented in the next section of this chapter of the report

during the fuel cooling down caused the tangential fracture of the rim layer material and the formation of the circumferential fracture in the rim layer material as well as the formation of the circumferential crack (pseudo gap).

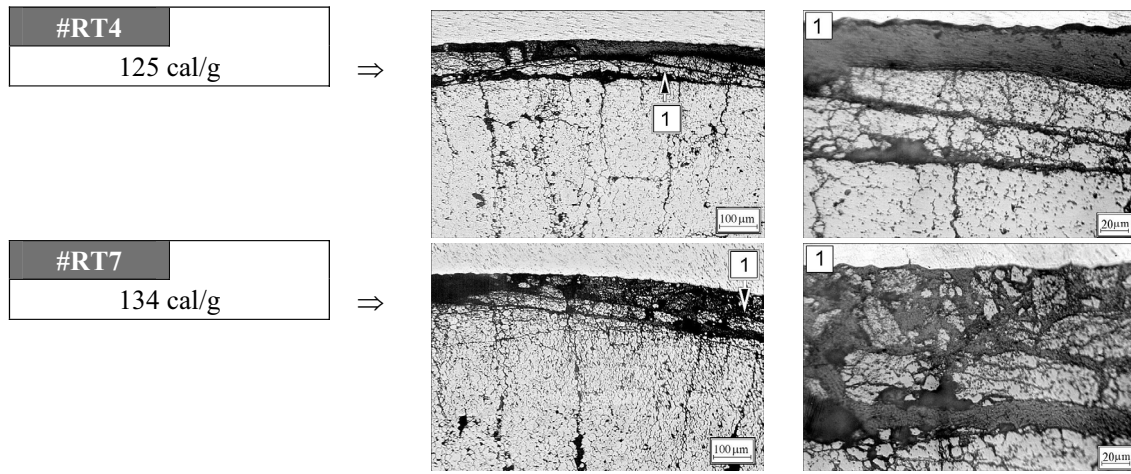


Fig. 5.20. Rim layer mechanical behavior in unfailed fuel rods with burnup of 60 MWd/kg U

The additional set of considerations continues the behavior analysis for the fuel peripheral layer, which is located directly under the rim layer in the context of fission gas release. As it was noted earlier, the thickness of this layer (or the transient zone) correlates with the thickness of the layer, which is characterized by the significant increase of plutonium content and burnup (see Fig. 5.3). This thickness correlates with the region of a sharp increase of the fuel porosity in accordance with the data presented in [16]. These facts show that the transient zone is the intermediate zone between the fuel matrix and the rim layer. If it is taken into account that the fuel strength properties are inversely proportional to the fuel porosity then it becomes clear that the high temperature gradient in this zone during the heating up stage and high tangential tensile stresses caused by this effect are the reasons for the observed radial cracking of this layer. It is obvious that total stresses are produced not only by the standard thermal expansion but also by the gas swelling. The careful consideration of effects connected with the liberation of energy stored in the fission gas bubbles, which was performed in the IRSN and presented in [17], showed that the rim layer and transient zone provided the major contribution in the FGR under narrow pulse conditions. These results are in a good agreement with the results of Japanese investigations [7].

Unfortunately, there was no opportunity to perform the detailed experimental research concerning the fission gas behavior in the frame of the BGR test program. But measurements of Xe and Kr release were made in unfailed fuel rods. Results of these measurements are presented in Fig. 5.21^a.

The obtained data led to the following preliminary conclusions:

- the monotonic increase of the FGR was noted as a function of the peak fuel enthalpy (fuel temperature) in the range of 16.1–26.5% for unfailed pressurized fuel rods with burnup of 47–49 MWd/kg U;
- the lower FGR in these tests in comparison with results of relatively slow out-of-pile tests [18] can be connected with several factors:
 - ⇒ the FGR component produced by the diffusion activated process was insignificant;
 - ⇒ the fuel cracking and grain separation in the fuel outer layers provided the major part of the measured FGR in the BGR tests;
 - ⇒ the pellet/cladding tight contact during the significant part of the temperature time history might have prevented the free migration of fission gases into the gas plenum.

^a The tabular data characterizing results of measurements are presented in Appendix E of Volume 2 of the report

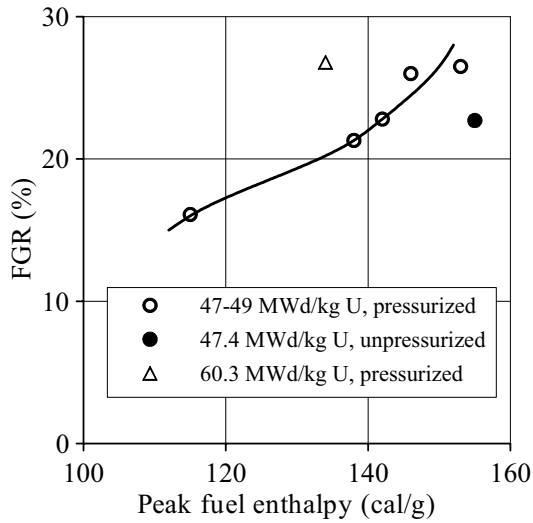


Fig. 5.21. Results of FGR measurements in unfailed fuel rods after the BGR tests

It seems that the last statement in the list of factors, which can be responsible for the FGR specific behavior under fast pulse conditions, was confirmed by the results obtained in the test of the unpressurized fuel rod (#RT12) with burnup of 47.4 MWd/kg U. So, this unfailed fuel rod had the maximum fuel enthalpy but the FGR was somewhat less than that in pressurized fuel rods. This fact can be connected with the longer duration of the pellet/cladding tight contact in the BGR test. As for the fuel rods with burnup of 60 MWd/kgU, the presented data^a showed that the increase of fuel burnup led to the reasonable increase of the FGR.

The final item of the analysis connected with the fuel behavior at the BGR tests is devoted to the consideration of phenomena revealed in failed fuel rods. In accordance with the approach used in this report, the analysis of fuel rods with burnup of 47–49 MWd/kg U (see Fig. 5.22) has been started.

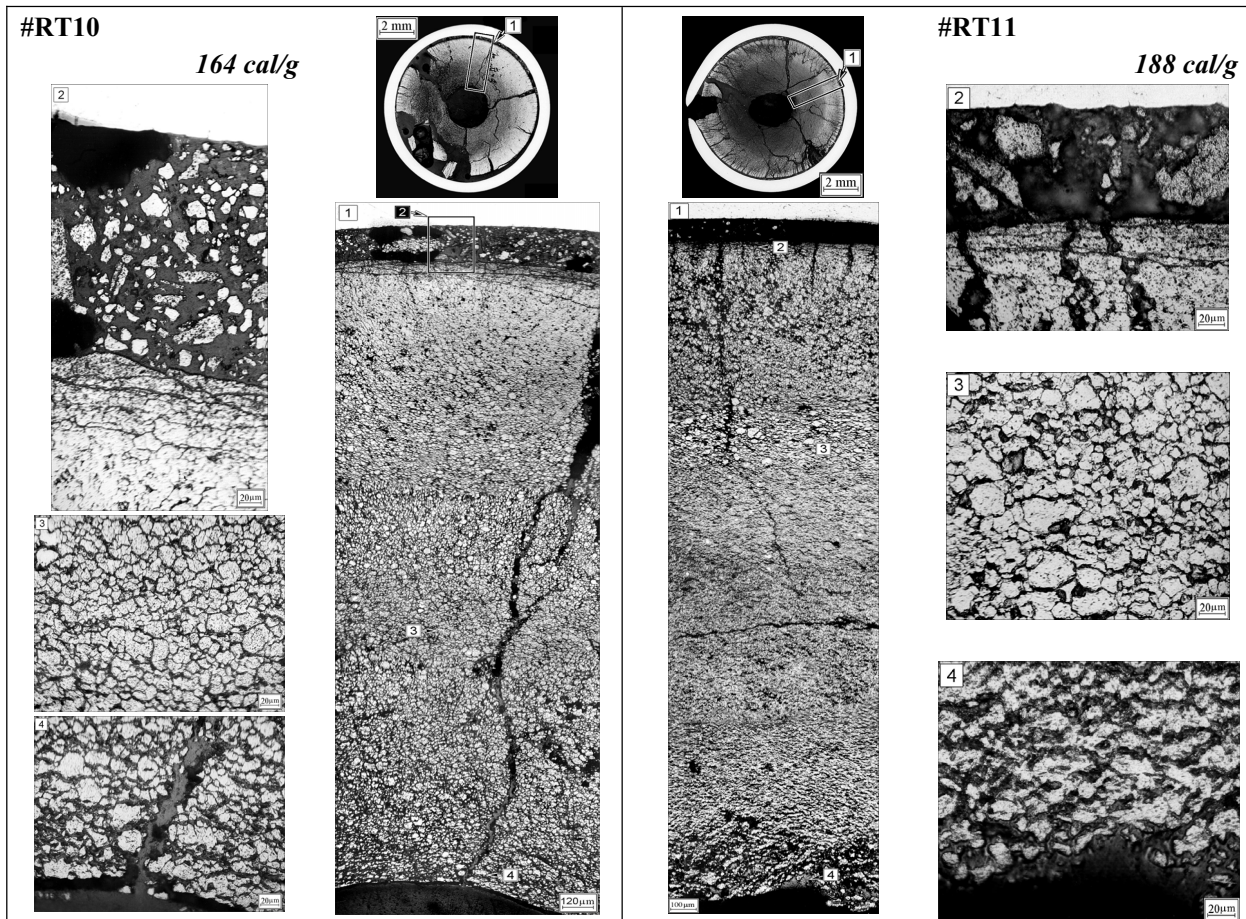


Fig. 5.22. Cross-sections and fuel microstructure of failed fuel rods with burnup of 47–49 MWd/kg U

^a Unfortunately, the FGR was not measured in the second unfailed fuel rod with burnup of 60 MWd/kg U (#RT4)

The organized test data presented in this figure provided the additional observations concerning the behavior of high burnup fuel in the peak fuel enthalpy range of 164–188 cal/g:

- the macroscopic cross-sections of appropriate fuel rods demonstrated the absence of new physical effects:
 - ⇒ the fuel rods kept the geometry of the central hole;
 - ⇒ the peripheral radial layer with fine radial cracks was formed after the tests;
 - ⇒ the significant dark zone appeared;
- the microstructure images confirmed the direct correlation between the fuel area with a severe grain separation and the dark area on the macroscopic pictures;
- the microscopic data confirmed that the significant fragmentation of the rim layer occurred in the fuel rod of this type at high enthalpies;
- no indication of fuel melting was revealed at the peak fuel enthalpy of 188 cal/g.

In other words, the major general effect connected with the increase of fuel enthalpies in the studied range is the increase of the fuel grain separation and rim layer fragmentation. The similar data characterizing the behavior of failed fuel rods with burnup of 60 MWd/kg U are presented in Fig. 5.23.

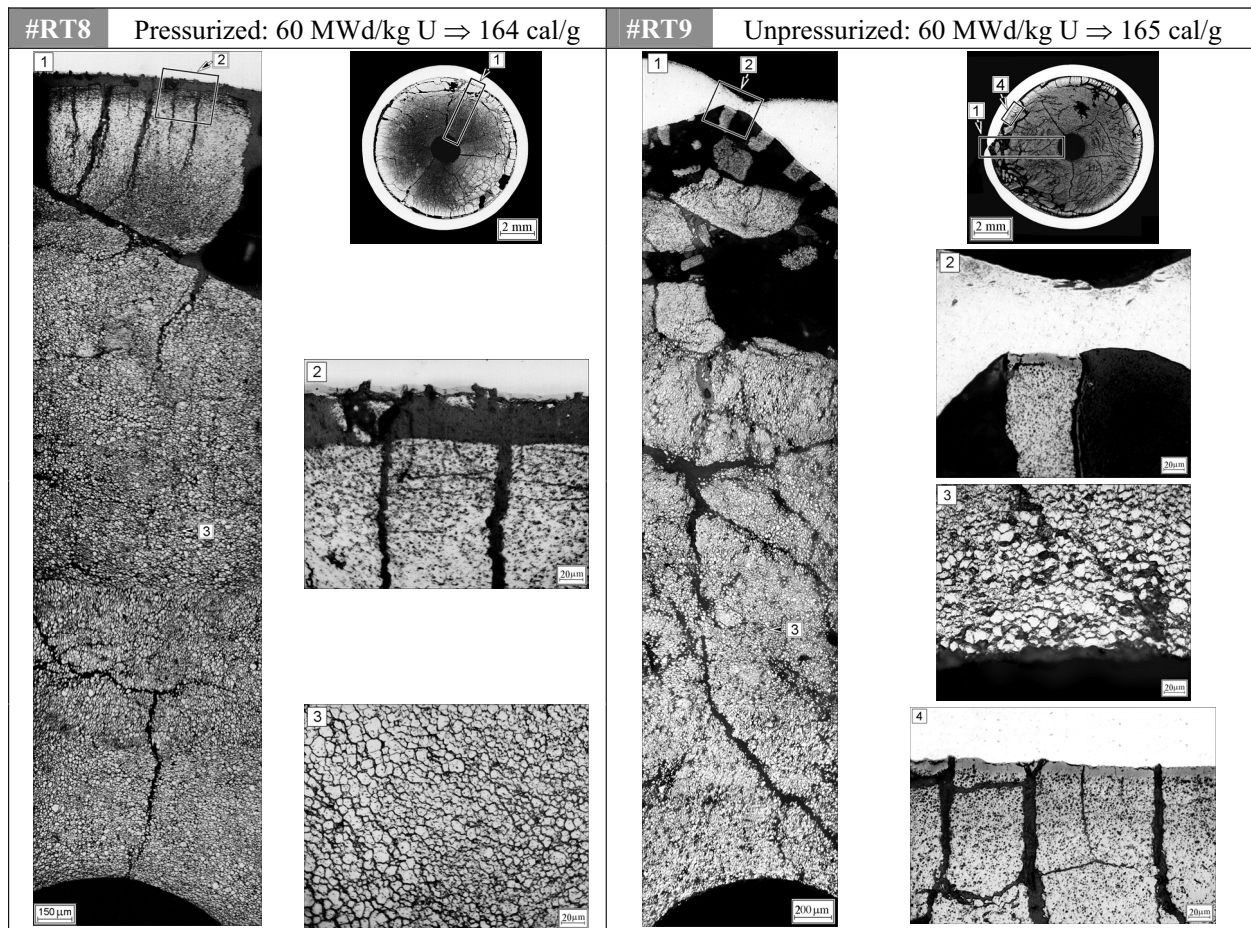


Fig. 5.23. Cross-sections and fuel microstructure of pressurized and unpressurized failed fuel rods with burnup of 60 MWd/kg U in unfailed region

The analysis of experimental data presented in this figure shows that general tendencies accepted for unfailed fuel rods with the peak fuel enthalpy of 125–134 cal/g remain at the increase of the peak fuel enthalpy up to 164–165 cal/g:

- the tight mechanical or chemical contact between the rim layer and bonding layer on the cladding inner surface at high compression stresses during the PCMI stage;
- the separation of the cladding with the outer region of the rim layer from fuel during the process of the cladding plastic strain accompanied by the diameter increase;
- the severe separation of grain boundaries in the fuel matrix.

The important features characterizing the fuel mechanical response to the test conditions at high enthalpy are noted in the context of the fuel fragmentation. The macro- and microscopic data are evidence of the significant increase in fuel fragmentation effects. The fuel pellets of these fuel rods consist of small and large fuel fragments broken down with the system of radial and tangential, long and short cracks. It is interesting also that two different fuel rods presented in Fig. 5.23 (with the initial pressurization (#RT8) and without the initial pressurization (#RT9)) demonstrated approximately the same fuel mechanical behavior. Moreover, the careful consideration of the data presented in Fig. 5.23 and additional data characterizing the behavior of these fuel rods (#RT8, RT9) in other cross-section (see Fig. 5.24) led to the following assumptions:

- the radial cracking of the fuel peripheral layer occurred at the beginning of the pulse when the fuel was brittle and tangential tensile stresses in this fuel region were very high;
- but the pellet/cladding contact pressure and appropriate contact stresses tried to block the process of the fuel radial cracking;
- studies of the cladding internal surface in areas adjacent to fuel radial cracks^a showed the presence of specific local grooves in the cladding deformation located opposite each radial crack in fuel. Possibly these grooves were initiated as a result of local microscopic cladding ruptures caused by the tangential tensile stresses at the formation of fuel radial cracks which led to the local cracking of the ZrO₂ inner layer. It should be noted that this zirconium dioxide layer retarded the cladding strain under tangential stress conditions;
- the time history of the process of the fuel thermal expansion and fuel gas swelling at the increase of the fuel enthalpy during the test was accompanied by the complex combination of radial and tangential tensile stresses in the relatively wide outer region of fuel. The appropriate region had quite a different microstructure (grain size, sizes of gas bubbles and pores) and fission gases distribution as a function of the fuel radius. These phenomena led to the cladding hoop plastic strain on the one hand and to the local relaxation of multidimensional stresses in fuel due to the local radial and circumferential cracking on the other hand;
- the direct mechanical contact between the fuel outer surface and high compression stresses in the fuel inner part produced the prerequisites for the blockage of free mass transfer in gas components inside the fuel rod. This effect provided the presence of several insulated gas volumes during the significant time of the test process: cold gas in the upper gas plenum, hot gas in the central hole of fuel gas local hot volumes produced inside the interconnected cracks surrounding the fuel separated fragments. Moreover, the pressure in the system including the upper gas plenum and gas in the central hole could be absolutely different from the gas pressures in the local gas volumes;
- due to the effects of the local cladding pressurization exceeding the uniform elongation threshold, the local cladding deformation of the ballooning type was observed in both types of pressurized and unpressurized fuel rods^b. The cladding ballooning was initiated by the high local pressure of gas contained in the fuel radial cracks located at a definite pitch along the cladding inner surface. The real mapping of this process can be observed on examining the toothed profile of the cladding inner surface (formed by remained fuel fragments) in the ballooning area (see pos.1 in Fig. 5.23, Fig. 5.24 and pos.4 in Fig. 5.24 (#RT9)).

^a See pos.4 in Fig. 5.23, pos.2 (#RT9) in Fig. 5.24 or pos.6 in Fig. E-9.5 and pos.5 in Fig. E-9.9 of Volume 2 of the report

^b The analysis of the cladding behavior at the BGR tests is continued in the next section of this chapter of the report

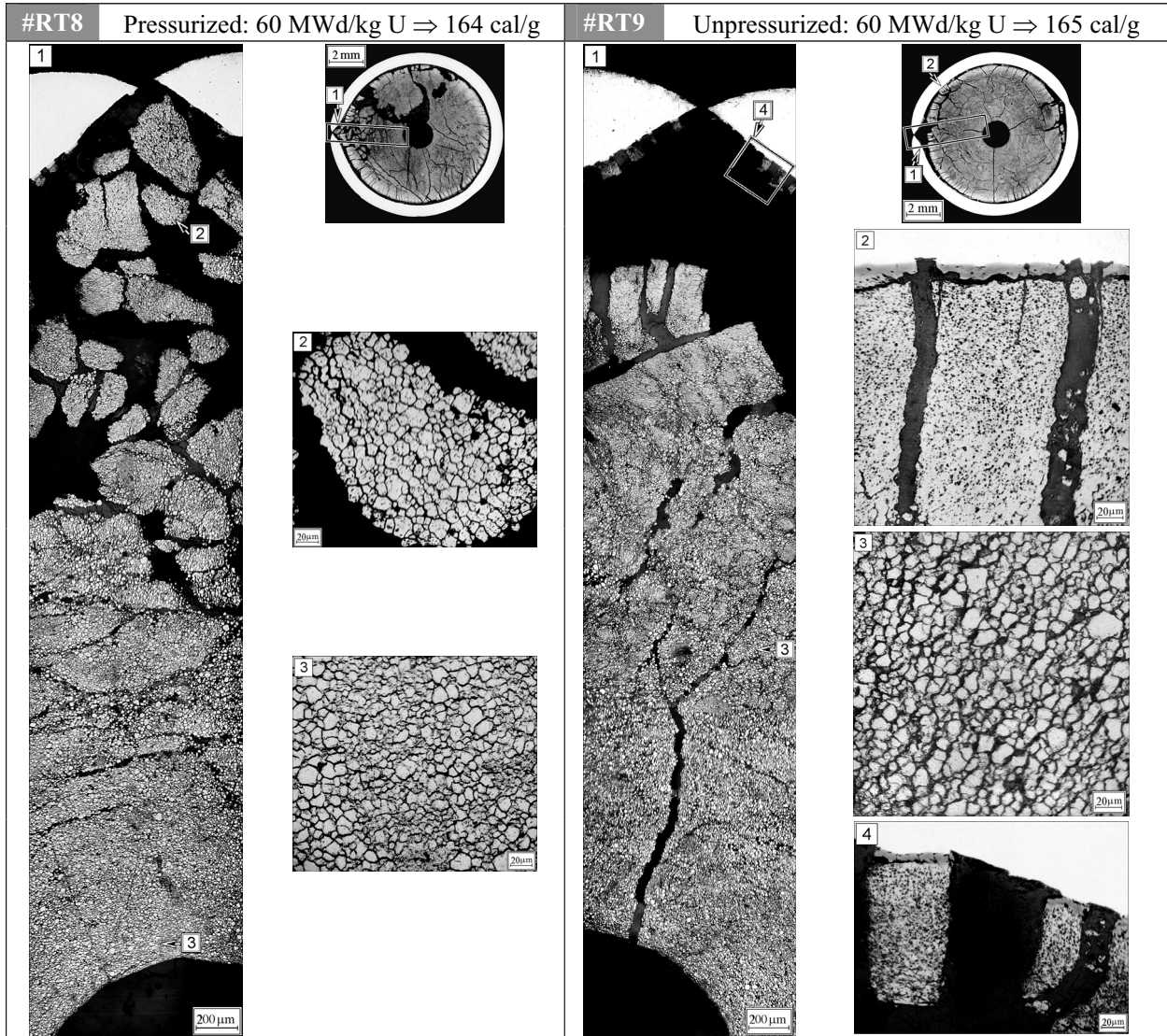


Fig. 5.24. Cross-sections and the fuel microstructure of pressurized and unpressurized failed fuel rods with burnup of 60 MWd/kg U in the cladding rupture area

5.4. Cladding mechanical behavior under the BGR test conditions

At the beginning of this section, it is important to repeat that Zr-1%Nb cladding (E110 alloy) of the VVER high burnup fuel rods tested in the BGR reactor was characterized by the following parameters^a:

- the outer diameter of 9.06–9.09 mm;
- the cladding thickness of 0.69–0.73 mm;
- ZrO₂ thickness of 3–5 μm (see Fig. 5.25);
- ZrO₂ inner thickness (see Fig. 5.25):

^a The detailed data are presented in Appendix C of Volume 2 of the report

⇒ 8–10 μm to the maximum for fuel rods with burnup of 60 MWd/kg U;

⇒ 0 μm for fuel rods with burnup of 47–49 MWd/kg U;

- hydrogen content of 50–80 ppm by weight.

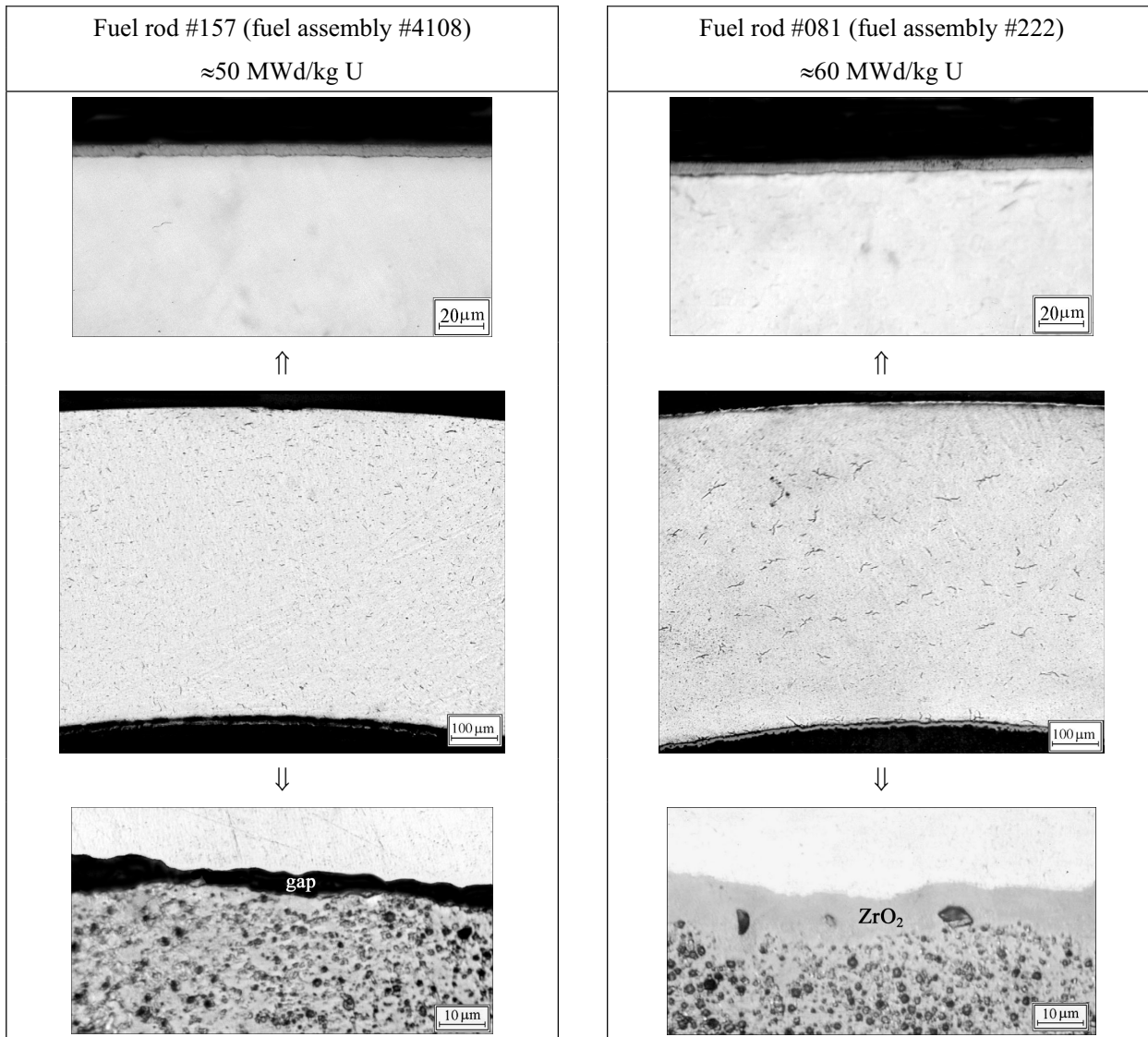


Fig. 5.25. The microstructure of Zr-1%Nb (E110) cladding after the base irradiation up to ≈ 50 and 60 MWd/kg U

As it was noted earlier, both types of the irradiated claddings (the cladding of fuel rods with 47–49 MWd/kg U burnup and cladding of fuel rods with 60 MWd/kg U burnup) had the significant margin of residual ductility. The analysis of the cladding microstructure showed that the following differences were revealed only on comparing of two cladding types:

- the content of solid hydrides in the irradiated cladding of fuel rods with 60 MWd/kg U burnup was slightly higher than that in the irradiated cladding of fuel rods with 47–48 MWd/kg U burnup but taking into account that the absolute content of hydrogen was very low in both cases, the revealed effect was insignificant;
- the irradiated cladding of fuel rods with 60 MWd/kg U burnup had the inner bonding layer.

In the frame of this work, the observed bonding layer was not examined in detail. But the results of special experimental studies performed with the PWR and BWR high burnup fuel in Japan [19] shown that:

- the bonding layer has the chemical contact with the cladding and fuel;
- the major part of the bonding layer (near the cladding inner surface) consists of ZrO_2 ;
- the other part of the bonding layer (near the outer fuel surface) consists of a solid solution of $(U,Zr)O_2$.

Several additional investigations performed on developing the BGR test program showed that the thickness of the bonding layer^a in the VVER fuel elements with the local burnup of 60 MWd/kg U varied from 0 μm up to 8–10 μm as a function of the cladding azimuthal angle.

In addition to parameters characterized above, the specific general effect was also revealed connected with the thermal and mechanical behavior of the ductile cladding under the narrow pulse conditions. This general effect was observed as the sinusoid type of the cladding outer diameter axial distribution after the BGR tests (see Fig. 5.26).

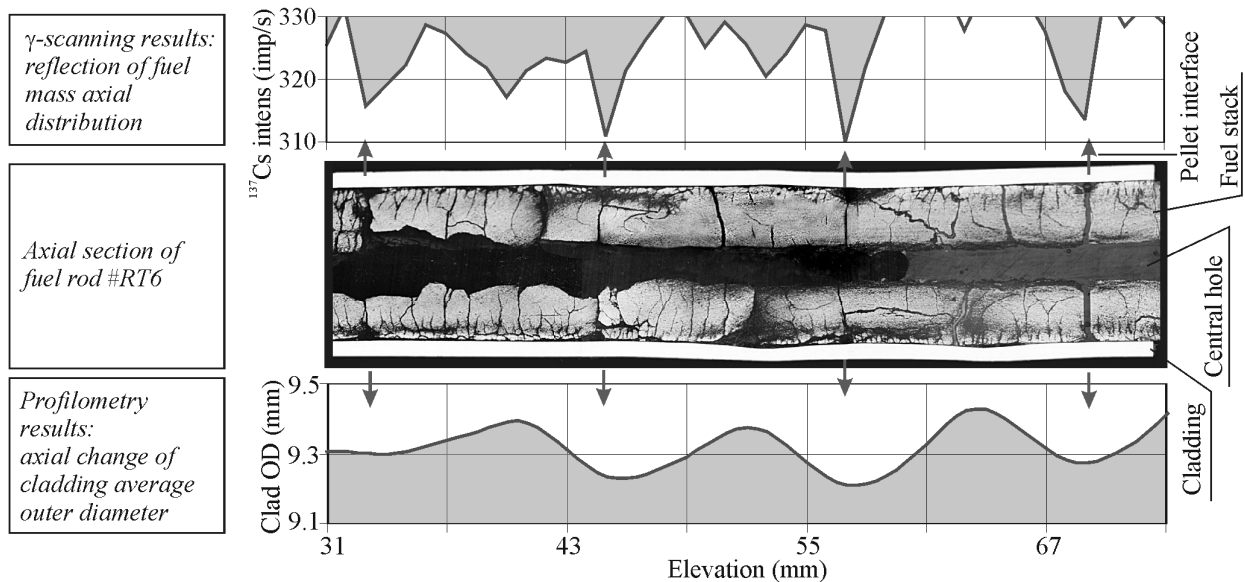


Fig. 5.26. Demonstration of the relationship between the local decrease of fuel mass in the pellet interface areas and the local decrease of the cladding hoop strain in these areas in comparison with the cladding strain corresponding to the pellet middle height areas

This figure presents three types of the test data: axial section of high burnup fuel rod #RT6 after the BGR test; axial distribution of ^{137}Cs activity measured at the γ -scanning of this fuel rod after the test; axial distribution of the cladding outer diameter in accordance with results of profilometry.

As it can be observed from these data, the axial distribution of the cladding outside diameter has a sinusoidal form. A similar effect was first observed in the CABRI tests of high burnup fuel. The explanation of obtained data was as follows [20, 21]^b:

- the radial distribution of the fuel temperature with the maximum near the outer (rim) layer is formed at the early stage of a narrow pulse and leads to the fuel deformation of the barrel shape with maximum at mid-pellet location;
- the fuel barrel shape results in a similar type of the cladding plastic strain (with the maximum in the pellet mid-plane) during the PCMI loading;

^a To simplify the text, the bonding layer is interpreted as ZrO_2 inner layer in this report

^b The similar effect observed in the NSRR tests is considered in the Chapter 6 of this volume of the report

- if significant PCMI occurs with fuel parabolic temperature profile (such as at the late phase of a narrow pulse or in case of a wide pulse), the clad plastic straining has an hourglass shape with maxima at the pellet edges.

The detailed analysis of the BGR data resulted in some additional observations. These observations showed that the cladding OD minimums corresponded to the pellet interfaces and to the minimums of ^{137}Cs activity (see Fig. 5.26). The following preliminary considerations were based on these observations:

- it was assumed that the sinusoidal profile of the cladding outer diameter is also caused by the presence of local maximums and minimums of the cladding temperature which are distributed with regular pitch along the fuel stack length;
- these temperature potential maximums and minimums can be connected with two factors:
 - ⇒ the nonuniform axial distribution of fuel mass that could provide the nonuniform distribution of the number of fissions (energy deposition) during the test;
 - ⇒ the sensitivity of cladding temperature during the film boiling phase to the axial variation in heat flux could also result in the temperature axial nonuniformity.

The data presented in Fig. 5.27 clarify the first of these factors.

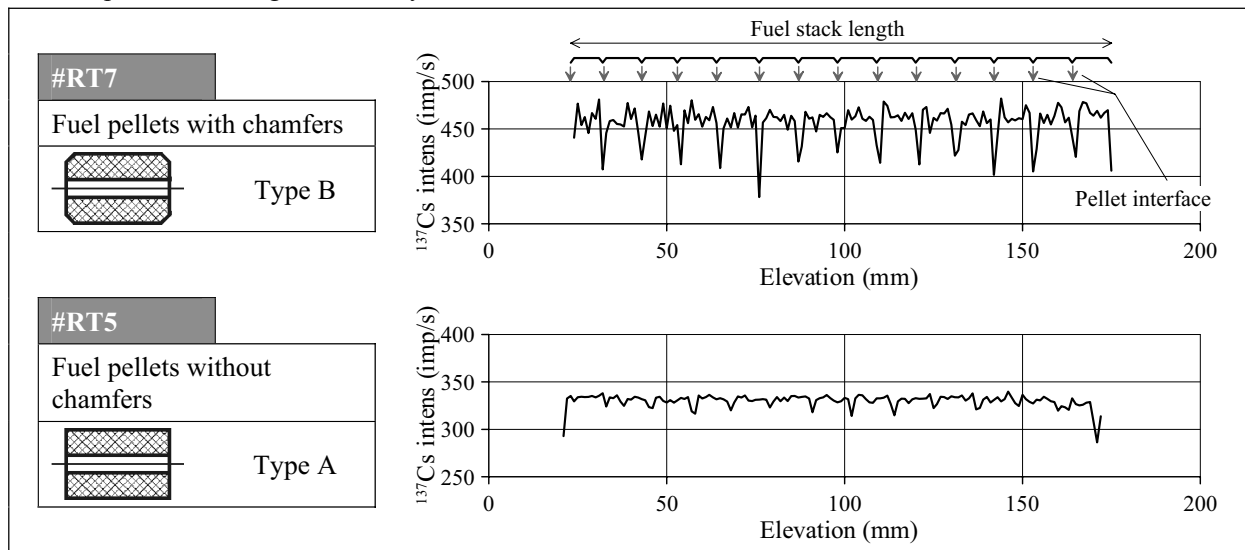


Fig. 5.27. The sensitivity of γ -scanning results obtained before the BGR tests to different fuel pellet shapes: with chamfers (Type B) and without chamfers (Type A)

These data illustrate the axial distributions of ^{137}Cs activity before the BGR tests in two fuel rods contained fuel pellets of two different types: fuel pellets with chamfers; fuel pellets without chamfers.

The analysis of presented data showed that both distributions had the tendency towards the local minimums of ^{137}Cs intensity with the pitch corresponding to the pellet height. But this tendency was more pronounced for fuel pellets with chamfers. Taking into account that the absolute value of measured ^{137}Cs intensity is a function of fuel mass, it can be assumed that revealed regular minimums in axial distributions of ^{137}Cs activity are connected with the minimums of linear fuel mass (g/cm) located at the fuel pellet interfaces. In the case with simple cylindrical pellets (Type A), this effect is lower. Moreover, in this case, the value of this effect is a function of such a factor as micro breaking off of small fuel fragments (on pellet outer ends) and of the formation of pseudo-chamfers, local microgaps between the pellets and inside pellets. The reality of these assumptions is confirmed by the data presented in Fig. 5.28.

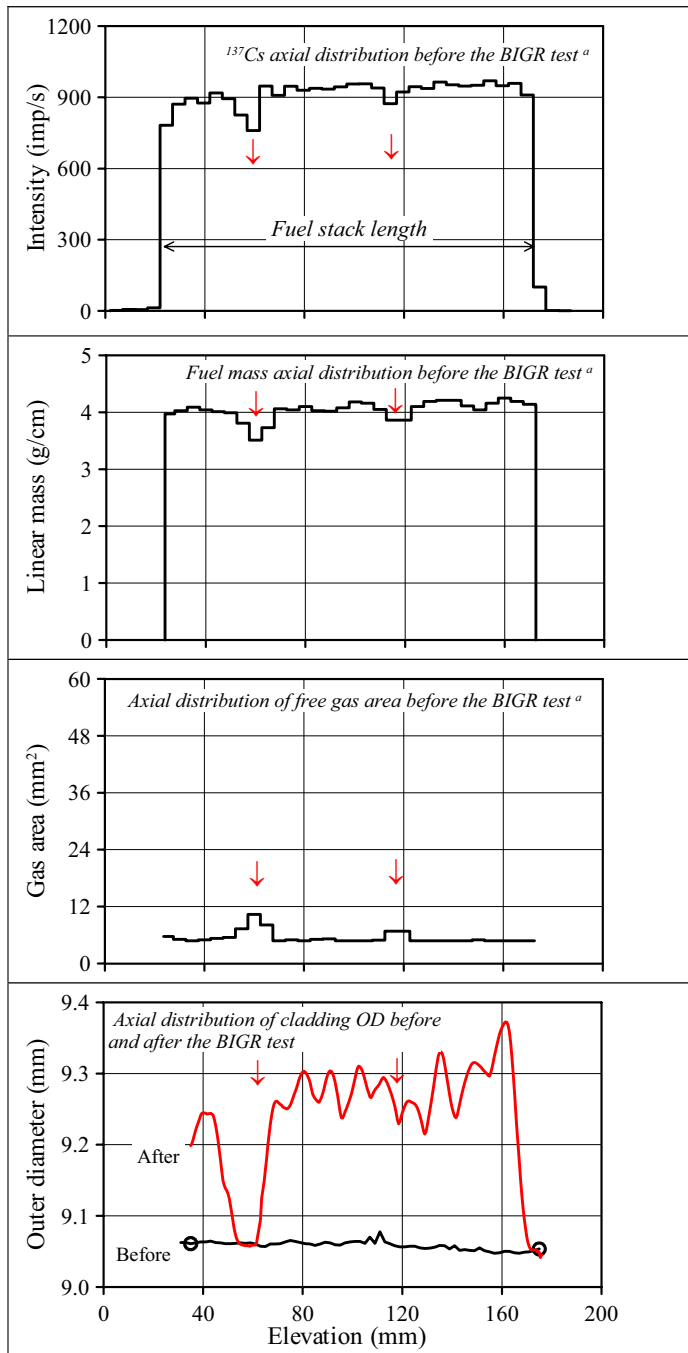


Fig. 5.28. Some data illustrating the significant correlation between axial distributions of fuel mass and the cladding hoop strain under the BGR narrow pulse conditions (#RT3)

^{137}Cs intensity distribution (after the processing manipulations connected with the transformation of as-measured data into the ordered distribution with the average value of ^{137}Cs intensity for each 5-mm length interval) was used to determine the fuel mass axial distribution^b (linear mass vs. elevation). In accordance with the obtained data, the following effects of nonuniformity in fuel mass distribution can be observed:

- local significant decrease of fuel mass^c at elevations in the range of 60–70 mm;
- local decrease of fuel mass at elevations in the range of 110–120 mm;
- local increase of fuel mass with the centers at elevations of 100, 135, 160 mm.

The analysis of axial distribution of the cladding outer diameter measured in this fuel rod after the test (see 4th picture in Fig. 5.28) showed that all effects of fuel mass redistribution along the fuel stack were reflected in the cladding outer diameter:

- the cladding OD at elevation of 60–70 mm after the test is the same as that before the test (the cladding temperature in this area was significantly lower than that in other cladding parts);
- the tendency towards the local decrease and local increase of the cladding diameter is observed at elevations of 100, 115, 135, 160 mm approximately.

The major results of the analysis performed in this paragraph can be formulated as follows:

- the cladding temperature at the film boiling stage of the test history was very sensitive to the axial distribution of fuel mass in the high burnup fuel rod during the BGR tests;
- this high sensitivity of the cladding temperature to the local fuel mass is determined by the mutual combination of such factors as the local heat flux (from fuel to the cladding), local gas gap between the cladding and fuel pellet and as the absence of

^a As-measured data after the special processing: the average value of ^{137}Cs intensity was calculated for each 5 mm interval along the fuel stack length

^b The major provisions of this procedure are presented in Appendix A of this volume of the report

^c The significant decrease of fuel mass is the result of the fuel pellet damage (fragmentation) during the procedure of the fuel rod refabrication

- the axial component of the cladding thermal conductivity due to a very fast character of thermal processes;
- local fuel mass shortage in the pellet interface may provides the local minimums of the cladding temperature in this areas;
- the sinusoidal form of the cladding hoop strain is caused by the combination of both considered effects: the barrel shape of fuel deformation and the local axial nonuniformity of fuel mass distribution.

The cladding strain effects before the failure threshold of high burnup fuel rods under the BGR test conditions

The first stage of this analysis is devoted to the consideration of the cladding deformation^a as a function of the peak fuel enthalpy in pressurized fuel rods with burnup of 47–49 MWd/kg U. (see Fig. 5.29).

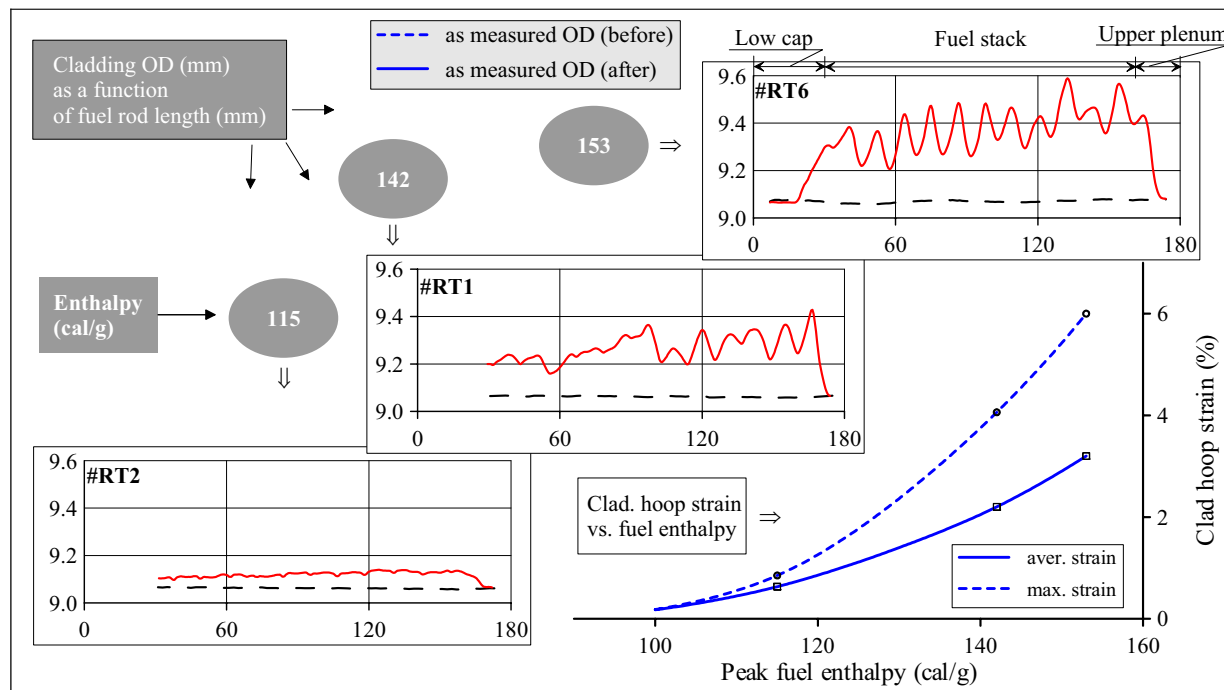


Fig. 5.29. General tendencies characterizing the cladding hoop strain in pressurized fuel rods with burnup of 47–49 MWd/kg U under the BGR narrow pulse conditions

The obtained data revealed that:

- the cladding strain is provided for by loading of the PCMI type up to 115 cal/g of the peak fuel enthalpy. This conclusion is made on the basis of RT2 test data taking into account a relatively uniform axial distribution of the cladding outer diameter after the test and the minimum difference in the cladding average and maximum hoop strains^b;
- visual effects of the cladding strain caused by gas loading are observed as the peak fuel enthalpy increases. These effects are characterized by the occurrence of the tendency towards the formation of local ballooning around each fuel pellet in pressurized fuel rods. The difference between the maximum and average cladding hoop strains is risen as a function of the peak fuel enthalpy;

^a Graphical and tabular data characterizing the cladding strain in each tested fuel rod are presented in Appendix E of Volume 2 of the report

^b The procedure of the cladding strain determination included the following manipulations:

- 16 azimuthal measurements of the cladding OD were used to determine the cladding hoop strain vs. elevation
- After that, the average cladding strain was determined and the maximum cladding strain was selected from the axial cladding hoop strain distribution

- the data have shown that the plastic irradiated cladding can be extended in diameter with no rupture up to 6% of the residual hoop strain.

To clarify the effects of the initial pressurization and pressurization due to fission gas release, the behavior of two appropriate fuel rods can be compared (see Fig. 5.30).

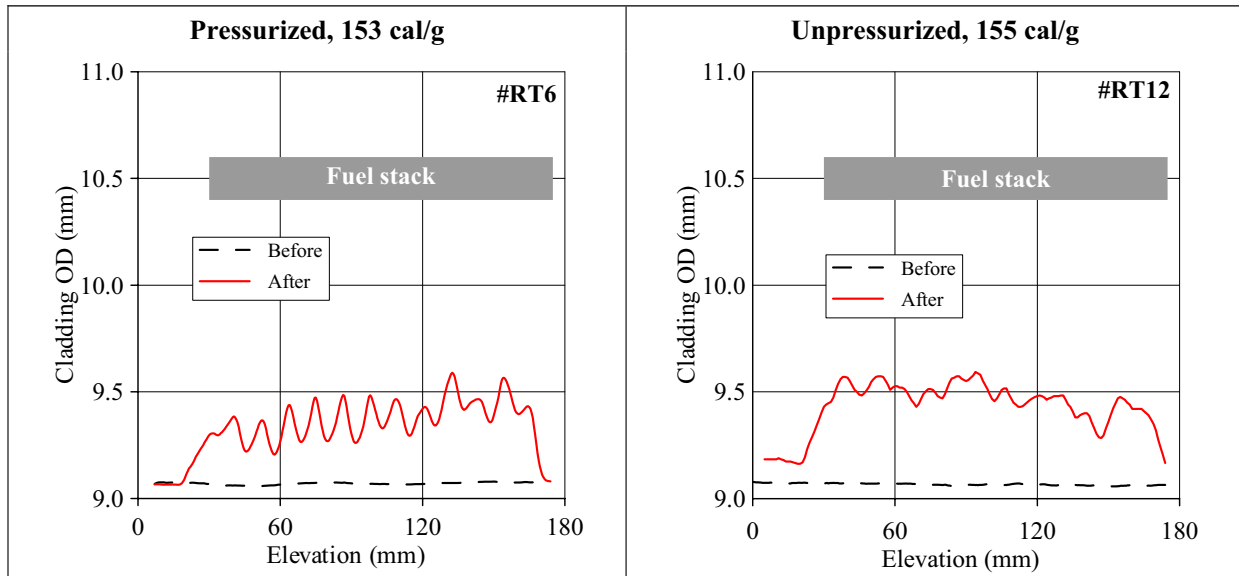


Fig. 5.30. The comparison of axial distributions of the cladding average outer diameter in pressurized and unpressurized unfailed fuel rods (47–49 MWd/kg U) tested at the same peak fuel enthalpy

These two unfailed fuel rods (RT6 and RT12) were tested at practically the same peak fuel enthalpy (153–155 cal/g). The comparison of axial distributions of the cladding diameters after tests has shown that the unpressurized fuel rod has no more smoothed axial distribution of the cladding diameter. But the tendency to the formation of local ballooning around each fuel pellet is also observed in this type of fuel rods. The revealed effects can be confirmed by the use of data characterizing the cladding residual hoop strain (as measured) for all unfailed fuel rods with burnup of 47–49 MWd/kg U (see Fig. 5.31).

The analysis of presented data shown that:

- The uniform character of the cladding hoop strain as a function of the fuel stack height is observed up to the peak fuel enthalpy of 115 cal/g.
- At the fuel enthalpy increase, the cladding strain includes two components:
 - The relatively uniform cladding strain caused by the hoop stresses at the PCMI loading of the solid contact type.
 - The cladding local ballooning with maximums associated with the middle parts of pellets, which were produced by the gas loading (the pressure of helium and of fission gas).
- The upper estimation of the first component for the cladding strain can be developed on the basis of the average cladding strain. The total effect of two components correlates with the maximum cladding hoop strain.

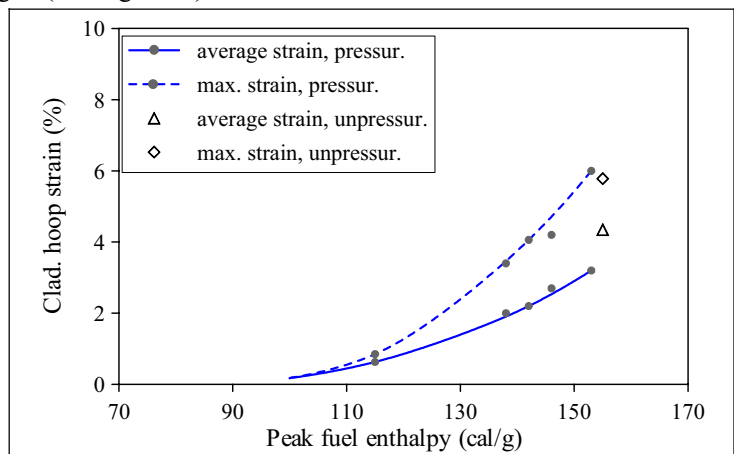


Fig. 5.31. The sensitivity of the cladding hoop strain to the initial pressurization of unfailed fuel rods with burnup of 47–49 MWd/kg U

- No principle differences between the maximum cladding hoop strain of pressurized and unpressurized fuel rods were revealed.
- The unpredictable result was connected with the average cladding hoop strain in pressurized and unpressurized fuel rods. The average cladding hoop strain in the unpressurized fuel rod was somewhat higher than that in pressurized fuel rods. The following potential explanations can be suggested for this fact:
 - ⇒ some overestimation of the peak fuel enthalpy in the unpressurized fuel rod #RT12 connected with the uncertainties in the procedure of the energy deposition determination;
 - ⇒ the physical phenomenon connected with a faster reopening of the gas gap in pressurized fuel rods at the end of the hot PCMI stage and the significant decrease of the local pressure of fission gases due to this effect.

The last topic of considerations devoted the cladding mechanical behavior in unfailed fuel rods is focused on the analysis of the cladding deformation sensitivity to fuel burnup (see Fig. 5.32)

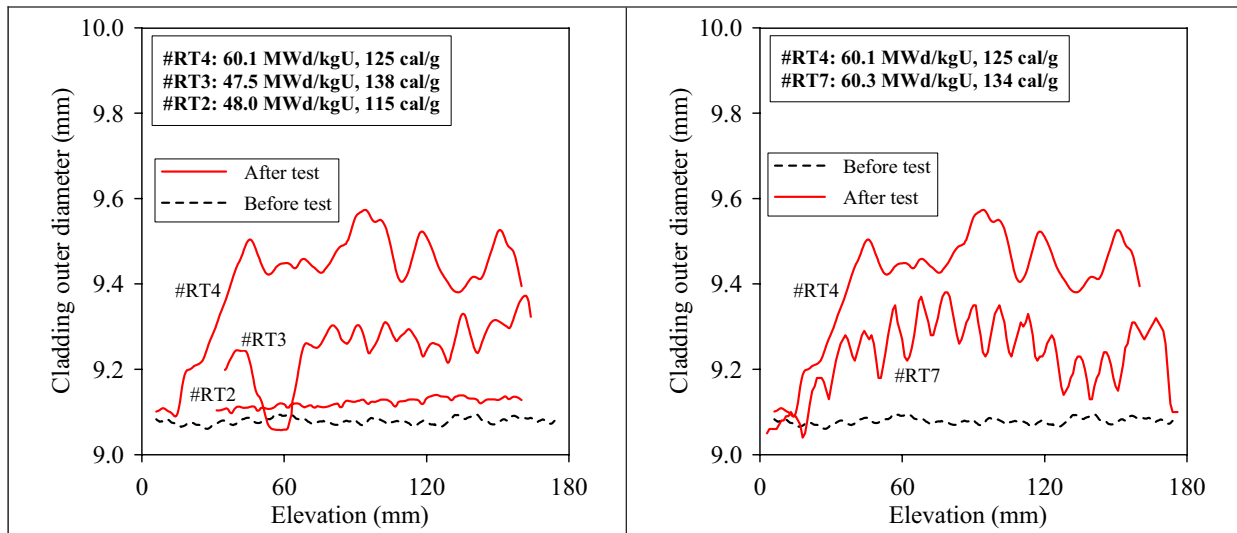


Fig. 5.32. The cladding deformation sensitivity to fuel burnup: for pressurized unfailed fuel rods under consideration

The scope of data presented in Fig. 5.32 resulted in the following:

- the increase of fuel burnup from 47–49 MWd/kg U up to 60.1–60.3 MWd/kg U leads to the increase of the cladding strain at the same peak fuel enthalpy;
- the significant difference in the behavior of two unfailed fuel rods with 60 MWd/kg U burnup was observed; the cladding strain of the fuel rod #RT4 is much higher than that of the fuel rod #RT7 in spite of the fact that the peak fuel enthalpy was higher in the fuel rod #RT7 (125 and 134 cal/g, respectively). Possible reasons for these strange results can be connected with the following facts:
 - ⇒ the fuel rod #RT7 has been refabricated from the fuel element of the called “follower fuel assembly”. These fuel assemblies are the part of the reactor control system, and the power history of these assemblies is quite different from the power history of operating assemblies (the fuel rod #RT4 was refabricated from the fuel element of the operating assembly). In this connection, it can be assumed that such effects as the rim layer, parameters and the fission gas content and distribution took place in fuel of these fuel rods. The more pronounced fuel grain separation which is observed on analyzing the RT4 microstructure in comparison with the RT7 microstructure^a confirms this assumption;

^a See Appendix E of Volume 2 of the report

⇒ but the same effects (differences in the microstructure and cladding hoop strain) can be connected with the overestimation of the peak fuel enthalpy in the fuel rod #RT7;

- nevertheless, the comparative data of the RT4 and RT7 fuel rods revealed the important tendency connected with the relationship between the geometry of the fuel pellet interfaces and the axial distribution of the cladding deformation. The presence of fuel pellets with chamfers in the fuel rod #RT7 provided the formation of local ballooning with strong regularity correlating with the number of fuel pellets. The formation of local gas volumes between fuel and the cladding in the fuel rod #RT4 was not connected directly with the fuel pellet axial pitch because of the more effective direct contact between the fuel pellet ends in this fuel rod.

The comparative data characterizing the cladding hoop strain as a function of fuel burnup are presented in Fig. 5.33 for pressurized unfailed fuel rods^a. The obtained data show that:

- the maximum and average cladding hoop strain at the fuel burnup of 60 MWd/kg U is significantly higher than that at burnup of 47–49 MWd/kg U;
- the fuel rod with 60 MWd/kg U burnup tested at 125 cal/g of the peak fuel enthalpy achieves approximately the same cladding hoop strain as the fuel rod with 47–49 MWd/kg U burnup tested at 153 cal/g of the peak fuel enthalpy.

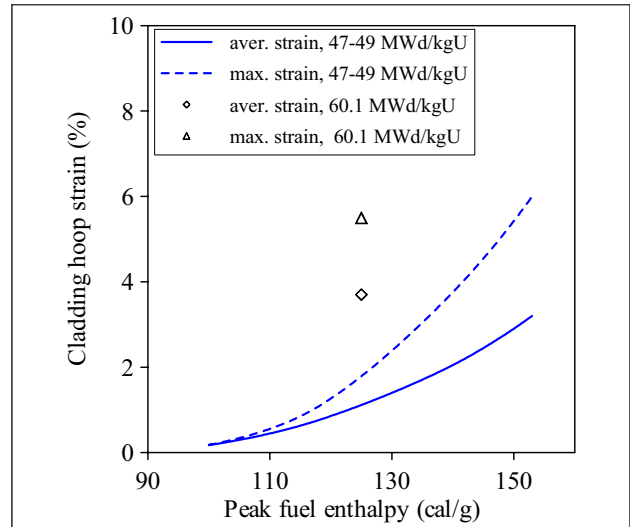


Fig. 5.33. The comparison of the cladding hoop strain in pressurized unfailed fuel rods at burnup of 47–49 and 60 MWd/kg U

The cladding rupture effects in failed high burnup fuel rods

The analysis of these effects can be started from the data presented in Fig. 5.34 for the failed fuel rod #RT10 with fuel burnup of 47.0 MWd/kg U. The obtained data led to the following observations and preliminary conclusions:

- the significant cladding radial deformation was fixed in the basic part of the fuel stack;
- the cladding deformation corresponding to the end parts of the fuel stack reflects the temperature profile with the effect of the axial thermal conductivity:
 - ⇒ the cladding deformation at the basic part of the fuel stack includes the general ballooned area with the minimum cladding hoop strain of 7.7% (at the elevation of 122 mm) and the set of local balloonings distributed along the fuel stack. The maximum hoop strain in local balloonings was 18.9%;
 - ⇒ the cladding rupture occurred in one of the local balloonings at the cladding hoop strain of 14.8%;
 - ⇒ the cladding in the rupture area had typical indicators of the plastic flow with the necking process;
 - ⇒ the cladding shape, the deformation size, the presence of the only rupture lead to consideration that the fuel rod failure was caused by the gas loading during the stage of the gas gap reopening.

^a Taking into account the set of considerations devoted to the reasons for the discrepancy between the cladding hoop strains of the RT4 and RT7 fuel rods, it was decided to select the RT4 fuel rod data as more representative ones for the goal of this report

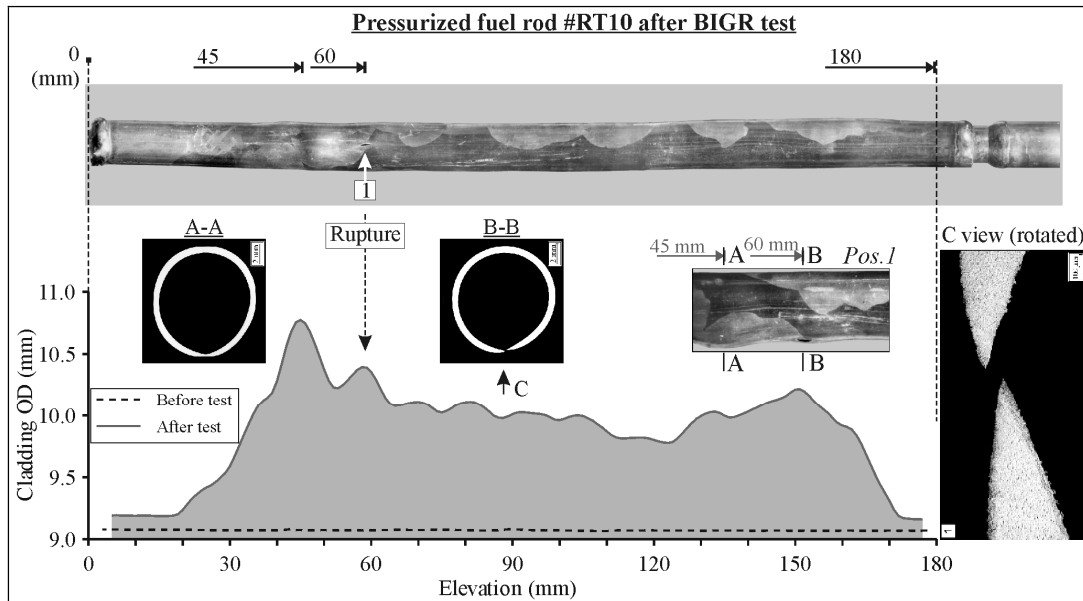


Fig. 5.34. Characterization of the cladding mechanical behavior at the failure threshold of pressurized fuel rods with burnup of 47–49 MWd/kg U

The analysis connected with the cladding behavior as a function of test parameters is continued with the use of the data characterizing the comparative behavior of pressurized and unpressurized fuel rods #RT8, RT9 with burnup of 60 MWd/kg U tested at the same peak fuel enthalpy as the pressurized fuel rod #RT10 with burnup of 47 Wd/kg U considered earlier (see Fig. 5.35).

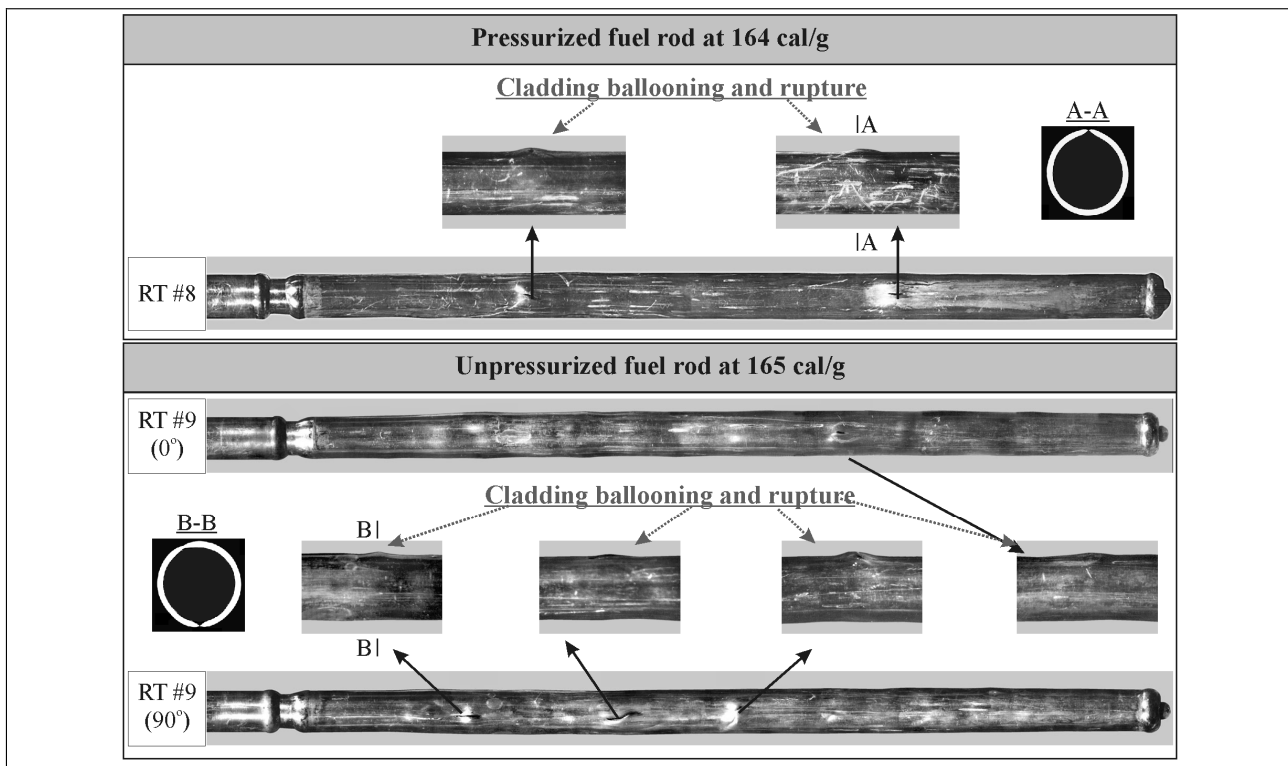


Fig. 5.35. The comparative appearances of pressurized and unpressurized fuel rods with burnup of 60 MWd/kg U after the BGR narrow pulses

The major phenomenon revealed due to the tests of these fuel rods with burnup of 60 MWd/kg U is the formation of several independent ruptures of the cladding. The more detailed study of presented pictures show that several local non-axis-symmetrical balloonings have appeared in different parts of the cladding. The cladding of the pressurized fuel rod #RT8 had two ruptures and the cladding of the unpressurized fuel rod #RT9 has failed in four places. The cladding cross-section made in rupture areas^a showed that the strain rates in the case with these fuel rods were higher than those at the test of the fuel rod with burnup of 47 MWd/kg U.

To clarify the mechanical behavior of claddings in two failed fuel rods with burnup of 60 MWd/kg U, the experimental data characterizing the cladding average outer diameter after the test are presented in Fig. 5.36.

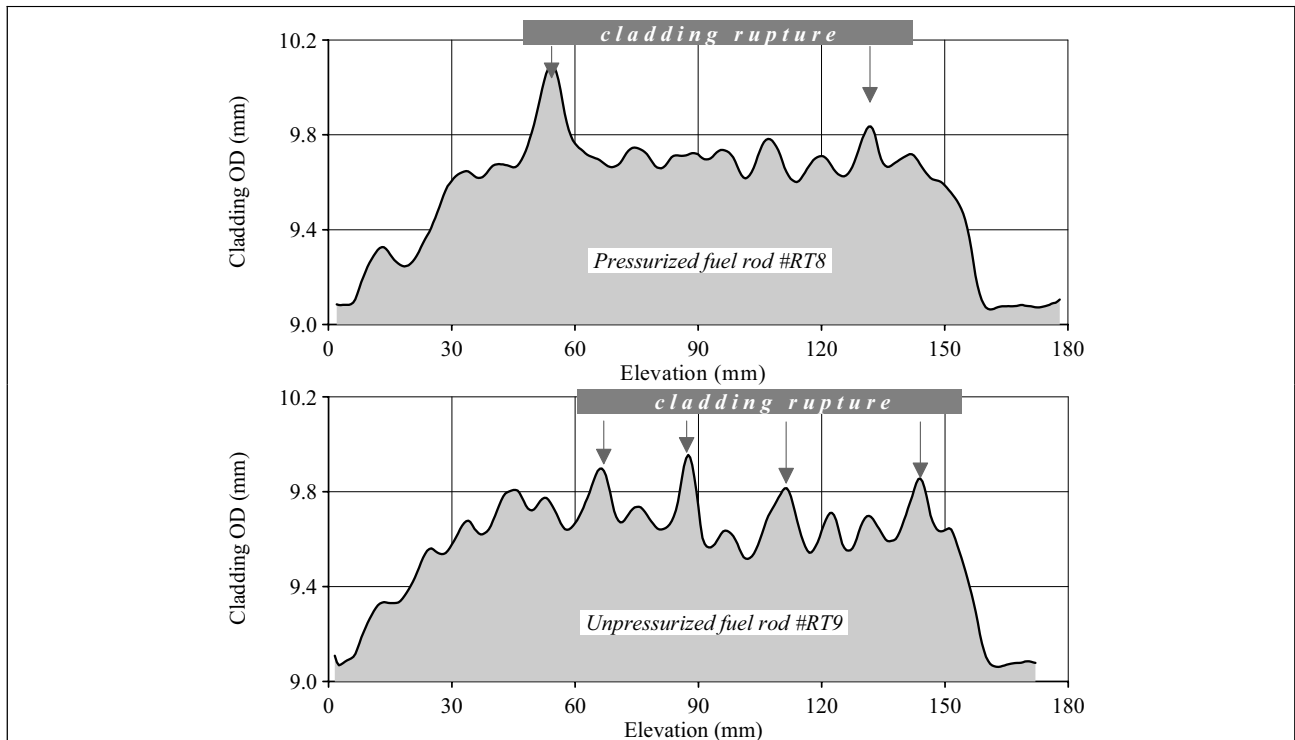


Fig. 5.36. Spatial effects of the cladding deformation in pressurized and unpressurized fuel rods with burnup of 60 MWd/kg U after the BGR tests at the peak fuel enthalpy of 164–165 cal/g

The comparative analysis of these data provided several observations and comments:

- both claddings had the similar character of deformation in spite of the fact that the first fuel rod was pressurized and the second one was unpressurized;
- this similar character can be described by the following:
 - ⇒ the cladding outer surface in both fuel rods consisted of local balloonings distributed axially with the pitch correlating with the fuel pellet height. The number of balloonings was approximately the same as the number of fuel pellets in each fuel rod;
 - ⇒ the critical hoop strain, after the achievement of which the cladding rupture becomes quite probable, was 8.1% (9.8 mm of the cladding OD).

The scope of data presented and analyzed in this and previous sections of Chapter 5 of the report made possible the consideration of the reasons for the effects connected with the failure of high burnup fuel rods under the BGR test conditions. The next section of this chapter will continue the analysis of the appropriate phenomena.

^a See additional data in Appendix E of Volume 2 of the report

5.5. The interpretation of mechanisms and thresholds for the high burnup fuel failure under the BGR test conditions

As for mechanisms for fuel rod failure, the BGR test data were analyzed taking into account the following varied parameters:

- peak fuel enthalpy (up to 188 cal/g);
- fuel burnup (47–49, 60 MWd/kg U);
- initial pressurization of fuel rods (0.1, 2.0–2.1 MPa).

The appropriate analysis can be initiated from the consideration of comparative data illustrating the time histories of two unfailed pressurized fuel rods with burnup of 48 MWd/kg U (#RT6) and 60 MWd/kg U (#RT4)^a. The choice of fuel rods for the first stage of the analysis was motivated by the fact that these fuel rods had the maximum cladding residual hoop strains in comparison with all other unfailed fuel rods.

To simplify understanding of the major physical phenomena, which accompanied the BGR tests, the following clarifying comments can be made for both fuel rods:

- the first most pronounced response to the BGR power pulse was connected with the sharp short-term increase of the fuel outer surface temperature (the combination of power and rim-layer effects);
- taking into account that the cladding temperature continued to be low (less than 400 K), the fuel temperature expansion and swelling led to closing of the fuel/cladding gas gap (for fuel rods with burnup of 48 MWd/kg U as the fuel rod with burnup of 60 MWd/kg U had the zero gap before the BGR test) and to the initiation of strong mechanical interaction with the cladding. This was the most dangerous stage of the cold PCMI loading;
- at the end of the cold PCMI stage, the fast relaxation of the cladding stresses occurred due to the cladding plastic strain. This critical event (a sharp significant reduction of cladding stresses) was classified as the transition to the hot PCMI stage in the frame of this work;
- the cladding stresses continued to decrease up to very low values during the first period of the hot PCMI stage. But the significant increase of the cladding hoop strain was observed due to the increase of the average fuel temperature, of the fuel total strain and cladding temperature accompanied by the significant decrease of the cladding strength properties at this temperature. The combination of these effects defined the potential danger in this stage of the RIA process;
- the start of the next stage in the thermal mechanical behavior of high burnup fuel rods was connected with the reopening of the gas gap in the fuel rod with burnup of 48 MWd/kg U and with the formation of the gas gap in the fuel rod with burnup of 60 MWd/kg U. This next stage named the gas loading and cooling phase was initiated by the process of the fuel temperature decrease and, as the consequence, of the fuel strain^b decrease. Thus, the gas loading stage was the regular event for all pressurized and unpressurized fuel rods, for which

^a All calculation data characterizing the behavior of these fuel rods are presented in Appendix E of Volume 2 of the report. The selection of the FRAP-T6/VVER data for the preparation of Fig. 5.37 was caused by the following considerations:
– the FRAP-T6 and RAPTA-5 data for fuel and cladding temperature histories are very similar except for the cladding cooling phase because the VVER version of the FRAP-T6 code contains a special rewetting model adapted for these specific test conditions;

– the version of the RAPTA-5 code used for the BGR calculations had no fuel swelling model. Therefore, the fuel total strain calculated by the FRAP-T6 code is more representative in this case

^b It should be noted that the decrease of fuel strain is not observed visually in presented pictures because this is quite a slow process. But from the formal mathematical point of view, the gas gap reopening begins when the fuel outer diameter becomes less than the cladding inner diameter with the accuracy to any decimal place (microscopic effect). Therefore, the accurate prediction of time for this stage initiation is an impossible task from the practical point of view. But this problem is compensated by the slow character of parametric changes. Taking into account this observation, it is clear that the results of the gas loading effect depend weakly on the absolute time of the gas gap reopening

the cladding plastic strain was observed at the foregoing PCMI stage of the test. But in the case with the unpressurized fuel rods, the gas loading was the result of the main FGR effect in respect of fuel rods with the initial pressurization by helium. Therefore, the combination of the high cladding temperature and gas pressure provided the increase of the cladding hoop strain some time before the cladding cooling. In the case with the fuel rods presented in Fig. 5.37, these strains did not exceed the critical values and the claddings did not fail. But in other cases, the gas loading could be responsible for the cladding rupture.

The cladding cooling phase was accompanied by the significant rewetting effect. This process led to a sharp decrease of the cladding temperature from the 800 K down to the temperature of nucleate boiling. It is obvious that additional stresses were caused by this phenomenon but taking into account that the cladding embrittlement did not occur due to the insignificant oxidation during these RIA tests, cooling stresses did not lead to the cladding failure.

It should be useful to amplify the above listed considerations with the analysis of the representativity of the FRAP-T6 and RAPTA-5 calculations. The appropriate analysis showed that, in general, the temperature histories of tested fuel rods were determined adequately^a. Nevertheless, it should be emphasized that important local temperature effects connected with the temperature axial nonuniformity along the fuel pellet stack (local minimums in the areas of the pellet interface and local maximums in the middle parts of fuel pellets) were not modeled in these calculations. In contrast to the conclusion made for the temperature calculations, the situation with fuel and the cladding strains was more conjectural (see Table 5.2).

Table 5.2. The comparison of calculated and measured maximum residual hoop strains of claddings

Parameter		Burnup of 47–49 MWd/kg U							Burnup of 60 MWd/kg U				
Fuel rod number		RT2	RT3	RT1	RT5	RT6	RT12	RT10	RT11	RT4	RT7	RT8	RT9
Peak fuel enthalpy (cal/g)		115	138	142	146	153	155	164	188	125	134	164	165
Max residual hoop strain (%)	Measured	0.85	3.4	4.06	4.2	6.0	5.8	18.9	8.2	5.5	3.5	11.1	9.6
	Calculated ^b	1.9	2.5	2.7	2.8	3.4	3.1	9.1	22.9	3.2	3.7	8.6	5.0

The analysis of presented data shows that the calculated maximum hoop strain is underestimated significantly for all fuel rods with the exception of fuel rods #RT2, RT11, RT7^c. Taking into account that the appropriate comparison of averaged (along the fuel stack) residual hoop strains has shown more favorable results, it can be assumed that revealed issues are as the results of following effects:

- formation of local balloonings around each pellet (this phenomenon was not modeled by the computer codes);
- underestimation of the FGR phenomena. The confirmation of this assumption can be found in the test and calculated data characterizing the gas pressure time history in the unpressurized fuel rod #RT12 (see Appendix E-12 of Volume 2 of the report).

^a Except for the previous comments concerning the absence of a special rewetting model in this version of the RAPTA-5 code

^b Results of the FRAP-T6 calculations are presented in this Table

^c As for fuel rods #RT2, RT11, RT7:

– the situation with the fuel rod #RT2 is not quite understood yet;

– the specific features of mechanical behavior of fuel rod #RT11 will be considered in next pages of this section of the report;

– the special comments concerning the specific behavior of fuel rod #RT7 were made in previous sections of this chapter of the report

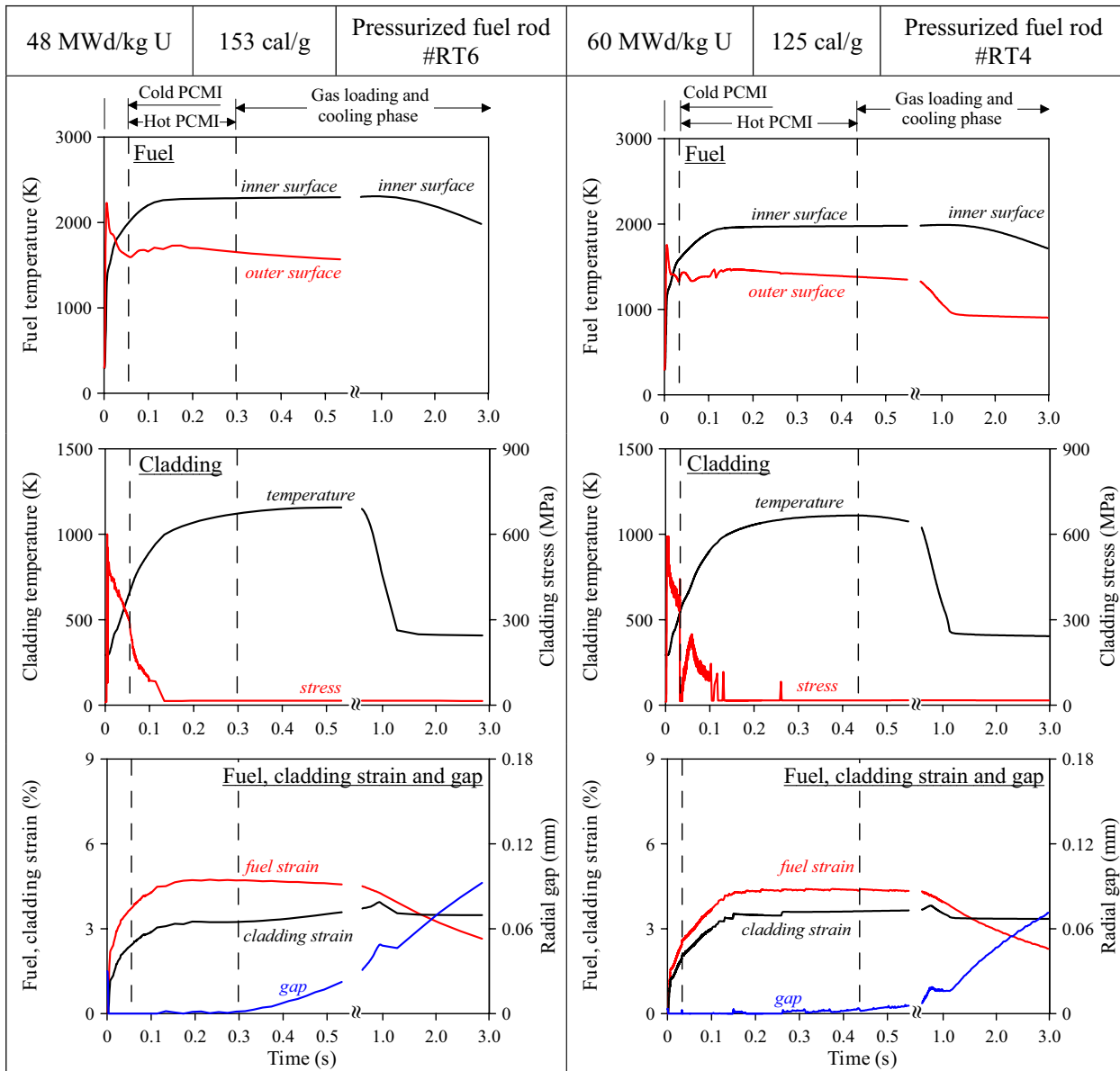


Fig. 5.37. Comparative data characterizing the thermal and mechanical behavior of unfailed fuel rods with burnup of 48 and 60 MWd/kg U in accordance with results of the FRAP-T6/VVER calculations

If we return to the comparison of the thermal and mechanical behavior of two fuel rods presented in Fig. 5.37, several important observations can be made:

- in spite of the fact that the fuel temperature in the fuel rod #RT4 was lower than that in the fuel rod #RT6 (this effect was the direct reflection of the relationship between the peak fuel enthalpies in these fuel rods), the cladding peak stresses were approximately the same at the cold PCMI stage of the BGR tests;
- this fact allowed the estimation of the gas gap effect in the context of the cladding maximum stress because presented data showed that the significant difference of the peak fuel enthalpies in these fuel rods (28 cal/g) was compensated by the difference in the initial gas gaps in fuel rods with burnup of 48 and 60 MWd/kg U.

Taking into account the importance of the criteria validation for the cladding failure at the cold PCMI stage, the additional analytical investigations were performed to clarify this issue. The background of these investigations was based on the results of mechanical tests devoted to the studies of effects of high strain rates typical for the RIA process. Special test programs confirmed that the Zr-1%Nb (E110) cladding could be considered as the

ductile material in the range of strain rates up to 10^4 1/s including the temperature of 293 K [1, 2, 22]. Taking into account this conclusion, the first attempt to develop the cladding failure criterion for the PCMI stage of the cladding loading was made. This first approach was based on the fact that during the PCMI stage, the cladding strain was determined by the fuel strain directly. It is known that the deformation failure criteria are recommended for such cases because these criteria demonstrate in an explicit form the residual strain value, which can be accommodated by the cladding before the rupture on the contact interaction between the fuel and cladding. The special analysis shows that the uniform elongation of the cladding can be used as the most conservative deformation criterion for both PCMI types (cold and hot). In accordance with this criterion the cladding rupture occurs when the cladding effective plastic strain achieves the value of the uniform elongation at this temperature and strain rate [23, 24]. This approach was applied to continue the discussion concerning the cladding mechanical behavior of fuel rods #RT4 and RT6 under the PCMI stage of the BGR tests (see Fig. 5.38).

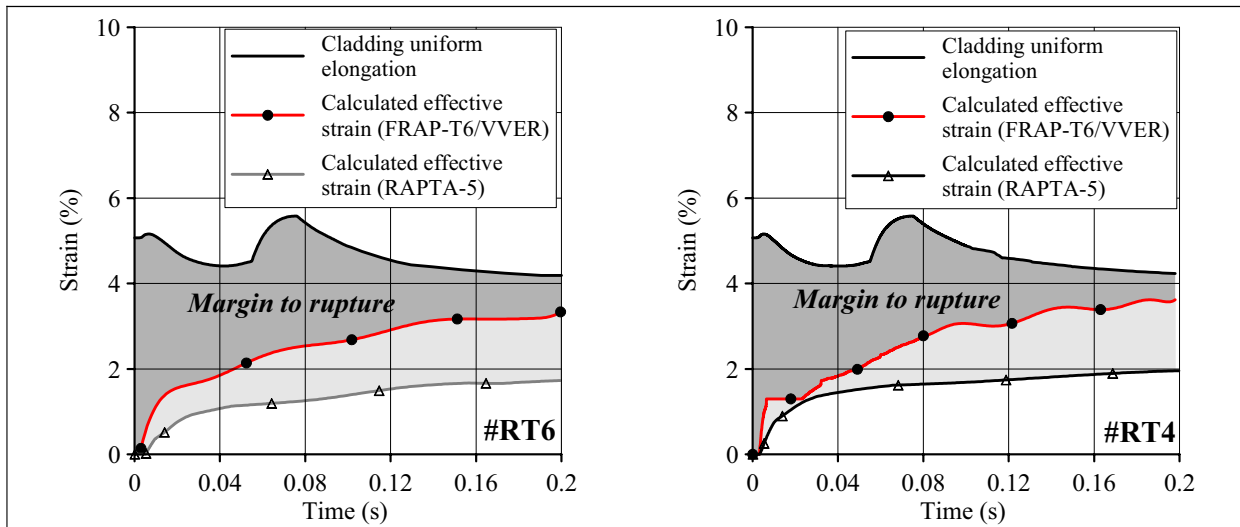


Fig. 5.38. The margin to the cladding rupture at the PCMI stage for fuel rods with burnup of 48 MWd/kg U (#RT6) and 60 MWd/kg U (#RT4) in accordance with the conservative failure criterion based on the uniform elongation

The analysis of obtained results showed that the cold PCMI stage (0–0.05 s) was not dangerous in the aspect of the cladding rupture under the BGR test conditions^a. Moreover, the margin to the cladding rupture decreased at the temperature increase. This effect was the result of the significant fuel strain caused by the thermal expansion and swelling at approximately the same cladding uniform elongation (the irradiated cladding uniform elongation was practically insensitive to the temperature in the range of 293–1223 K [2]). In accordance with the presented data, the margin to the cladding rupture became quite low in both fuel rods at the time of 0.2 s approximately. But taking into account the inadequate results of the cladding hoop strain calculations (as it was discussed earlier), another approach was used to estimate the cladding mechanical behavior at the high temperature range. However, before we consider the high temperature phenomena, it is needed to complete the analysis of the margin to the cladding rupture using another popular method based on the strain energy density (SED) determination. The major provisions for this method were formulated in [25] as the cladding integrity model for the analysis of the PCMI effect. The development of practical procedures for the implementation of this method was continued during several years (see one of the first attempts [24]). Finally, the results of most successful investigations were incorporated in the version 1.1 of the FRAPTRAN code [26] (the PNNL and EPRI approaches).

Taking into account that the SED is defined as the mechanical energy generated in the unit volume of the cladding material, this criterion seems to be the most physical because the combination of two general factors

^a As it was noted earlier, the discrepancy between the FRAP-T6 and RAPTA-5 calculations was provided by the absence of the fuel swelling model in this version of the RAPTA-5 code

(such as the stress and strain), which are considered as the reason for the cladding failure, is accounted by the Strain Energy Density (SED) formula^a as:

$$SED = \int \sigma_{eff} d\varepsilon_{eff} ,$$

where SED= strain energy density (J/m³);

σ_{eff} = true effective stress (Pa);

ε_{eff} = true effective strain (unitless).

Of course, the practical application of this criterion requires the determination of the Critical Strain Energy Density (CSED) at the cladding failure. It seems that the results of the appropriate mechanical tests can be used as the major contributor of data for the CSED. It should be noted that this task is solved quite accurately for the embrittled claddings only. The most known example of such claddings is the Zircaloy irradiated claddings of PWR fuel elements with burnup of 55–60 MWd/kg U and higher. The failure specific features for brittle materials are as follows:

- the fracture of these materials occurs before or near the yield strength limit;
- the strain of these material before the fracture includes the elastic component and, at the maximum, the plastic component correlated with the uniform elongation (not more);
- these effects are accompanied by the zero or very small changes of the cladding cross-sectional radial dimensions before the fracture;
- therefore, the processing of the load displacement diagrams obtained due to mechanical tests allows the transformation of these data into the effective stress as a function of the effective strain and to calculate the SED increase up to the CSED at the fracture.

Above listed considerations provided the choice of this criterion for the analysis of RIA tests performed with the Zircaloy embrittled irradiated claddings [6, 27, 28]. Unfortunately, the residual ductility high level in the Zr-1%Nb (E110) irradiated cladding leads to the fact that the total strain (the total elongation) at rupture of this cladding is higher significantly than the uniform elongation. Moreover, the cladding deformation in the region between the uniform and total elongation is accompanied by the significant change of the cladding cross-section with the necking at the end of this process. All these features do not allow the calculation of the effective stress (effective strain) and the determination of the SED in this region of the load-displacement diagram.

But taking into account the reference data with the CSEDs developed for the Zircaloy irradiated claddings, it was decided to process the results of mechanical tests with the E110 unirradiated claddings and to determine the CSED in the conservative assumption based on the SED at the uniform elongation. The results of these investigations are presented in Fig. 5.39 and Fig. 5.40^b.

^a This is the PNNL approach to the SED determination. The same approach was developed and validated in the RRC KI

^b It should be noted that the CSED presented in Fig. 5.40 was determined at different approach to the assessment of maximum strain included in the procedure of the CSED determination. In this case the MATPRO approach was used to calculate the parameters of cladding deformation in the region between the uniform and total elongation. Therefore this approach is less considerative than that of the RRC KI

<p>Zr-1%Nb (E110) unirradiated and irradiated (50 MWd/kg U) cladding</p>	<p>Zry-4 irradiated cladding (fast fluence: $1-1.2 \times 10^{26}$ n/m²)</p>
<p><i>Oxide/Cladding thickness ratio: 0–0.007</i></p>	<p><i>Cladding temperature ≤ 150 C</i></p>
<p>Fig. 5.39. The low temperature CSED for the Zr-1%Nb irradiated commercial cladding</p>	<p>Fig. 5.40. The low temperature CSED for the Zry-4 irradiated cladding at the low oxidation</p>

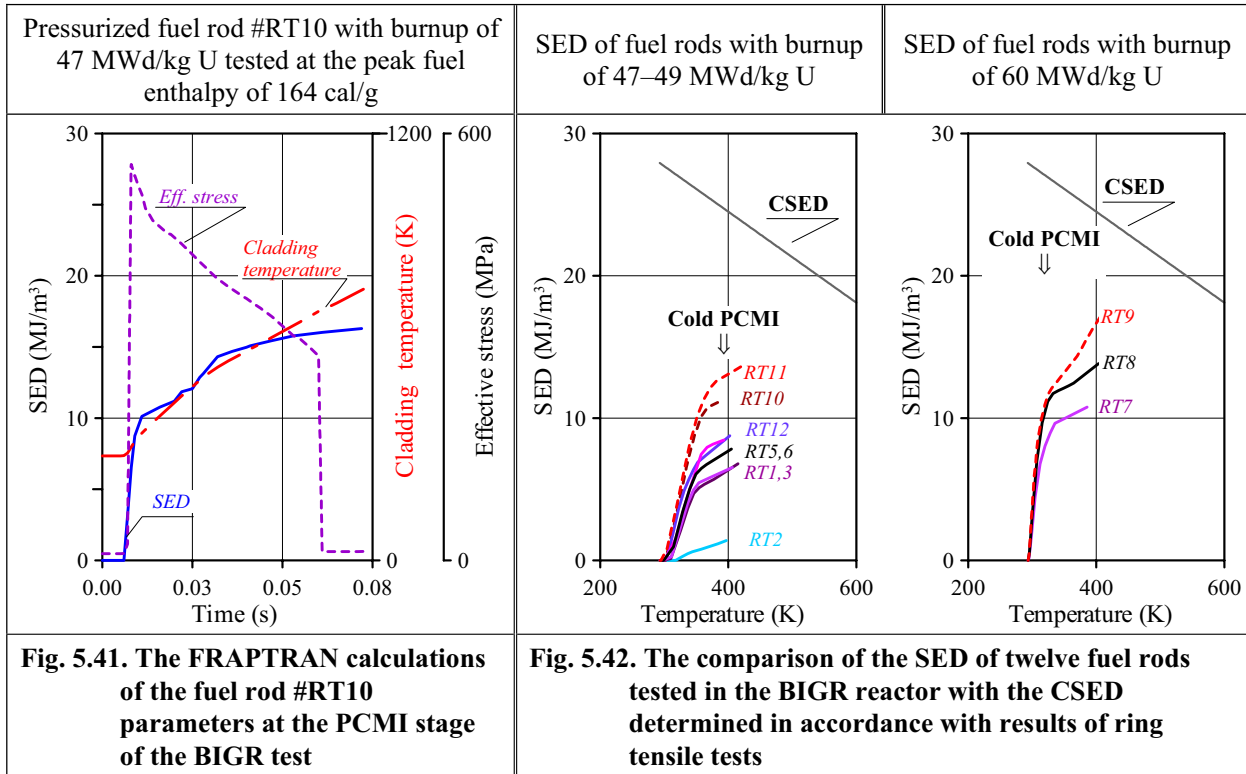
The comparison of these data revealed the following:

- the CSED of the Zr-1%Nb irradiated cladding is slightly higher than that of the unirradiated cladding. This fact is the result of the increase in the cladding strength properties at the irradiation and the conservation of high ductility properties;
- in accordance with the data presented in [27], the CSED of the Zry-4 irradiated cladding is significantly less than that of the Zr-1%Nb irradiated cladding in spite of the fact that the method of the CSED determination for the Zr-1%Nb cladding is more conservative. Certainly, the careful comparison of both procedures would be useful to be performed in future. But if we assume that these procedures do not contain the systematic errors, the most probable explanation for this difference is the following: the combination of geometrical sizes and the higher (in comparison with the Zircaloy) ductility of the unirradiated cladding led to the revealed difference in the critical strain energy densities of the Zr-1%Nb and Zry-4 irradiated claddings at the same oxidation.

The continuation of investigations connected with the determination of the SED time history at the PCMI stage of the BGR tests with the VVER high burnup fuel rods was based on the FRAPTRAN calculations of the thermal mechanical behavior of twelve tested fuel rods. After that, the FRAPTRAN 1.1 version of the code was used also for the SED calculations. The obtained data are presented in Fig. 5.41, Fig. 5.42.

The analysis of obtained data confirmed the previous conclusion concerning the fact that the Zr-1%Nb ductile cladding had the significant margin to the rupture at the cold PCMI stage of the BGR tests. It is interesting to note that the peak SED at the cold PCMI stage is very sensitive to the peak enthalpy increase. So, the increase of the peak fuel enthalpy by the factor 1.3 led to the increase of the peak SED by the factor 7.5 (in accordance with the data characterizing the behavior of unfailed fuel rods with burnup of 47–49 MWd/kg U).

^a The best fit was numbered by the RRC KI



Thus, the whole set of experimental observations and analytical investigations showed that the failure mechanism of VVER high burnup fuel rods tested in the BGR reactor was connected with the cladding mechanical behavior at the high temperature.

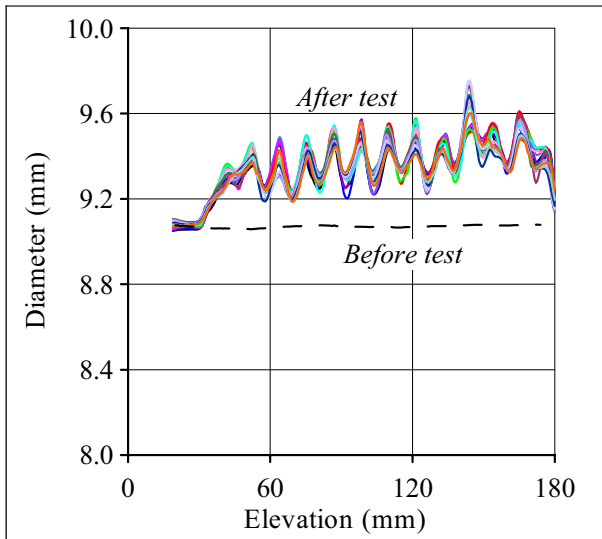


Fig. 5.43. 16 azimuthal measurements of cladding outer diameter of fuel rod #RT6 after the BGR test

The analysis performed in Section 5.4 of this chapter of the report revealed that at the fuel burnup of 47–49 MWd/kg U the cladding strain was small (<1%) and this strain was not sensitive to the rod initial pressurization up to the peak fuel enthalpy of 115 cal/g. The hot stage of the PCMI determined the cladding deformation in the region with the lower fuel enthalpies. In the range of the peak fuel enthalpies of 138–155 cal/g, the specific effect of the narrow pulse conditions began to determine the cladding temperature and mechanical behavior (see Fig. 5.43). This specific effect was caused by the extremely high sensitivity of the cladding temperature to the axial nonuniformity of the heat flux from fuel to the cladding. As it was discussed in Section 5.4, this heat flux had the local minimums corresponding to the pellet interfaces. This phenomenon provided the occurrence of the appropriate temperature minimums in the cladding during the time period when the axial component of the cladding thermal conductivity was very small. The presence of the cladding local temperature minimums distributed along the fuel stack with the pitch correlated with the pellet

height led to the formation of local balloonings.

Each of these balloonings was placed between two adjacent minimums of the cladding temperature. It is important to note that this effect of narrow pulses was of the general character because the BGR tests performed

with VVER unirradiated fuel rods demonstrated the same tendency towards the formation of the cladding deformation of the sinusoid type.

In the context of the local ballooning formation, the following important question can be formulated: with which stage of the BGR test may the process of the local ballooning initiation be connected? Is this the hot PCMI stage or the gas loading after the gas gap reopening? Moreover, the next question can be formulated also: if the hot PCMI stage is responsible for this effect, what gas produces the ballooning type deformation during the stage of the fuel/pellet mechanical contact? To answer the first of these questions, it is necessary to step aside slightly from the idealized pattern of the fuel rod behavior described earlier, which was developed on the basis of results of the FRAP-T6 and RAPTA-5 calculations. After that, it is needed to try to restore the real order of physical processes on the basis of obtained test results.

The appropriate analysis revealed that the cladding failure has occurred at the end of the hot PCMI stage. The following major observed physical effect was taken into account at the development of this statement: three of four failed fuel rods with burnup of 47–49 and 60 MWd/kg U had several cladding ruptures after the BGR tests. Moreover, the fuel rod #RT9 which had no initial pellet/cladding gap and which had no initial pressurization (both of these factors enhanced effects of the hot PCMI stage) demonstrated four separate cladding ruptures along the length of 90 mm. The more detailed revision of the sequence of the appropriate processes can be made using the data presented in Fig. 5.44.

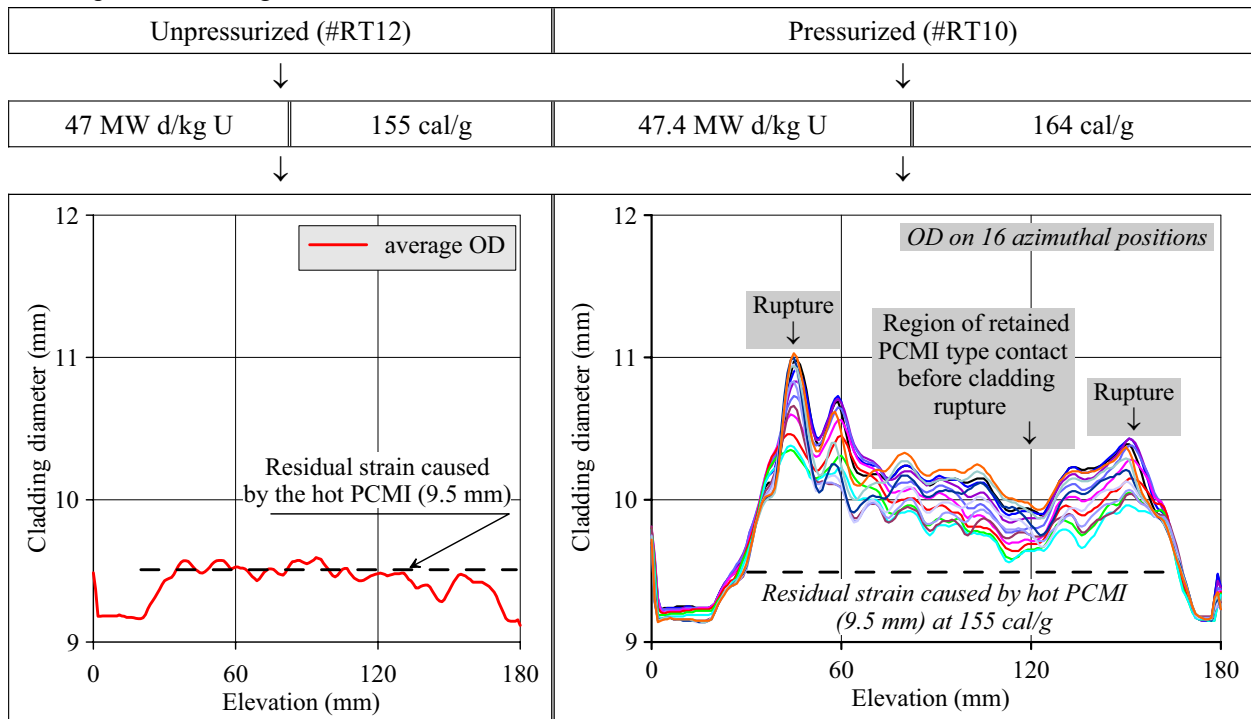


Fig. 5.44. The clarification of the contribution of the hot PCMI and gas loading stages into the cladding strain

This Figure presents the axial distributions of the cladding diameters after the BGR tests for two fuel rods:

- failed (with two ruptures) pressurized fuel rod #RT10 (47 MWd/kg U);
- unfailed unpressurized fuel rod #RT12 (47.4 MWd/kg U).

The analysis of the axial distribution of the cladding diameter for the fuel rod #RT12 provided the estimation of the average level of the cladding deformation caused by the PCMI loading at the peak fuel enthalpy of 155 cal/g. The obtained value (9.5 mm) can be used as the low evaluation of the cladding deformation at the end of the PCMI stage in the pressurized fuel rod #RT10 tested at the peak fuel enthalpy of 164 cal/g. The comparison of the final axial distribution of the cladding outer diameter in this fuel rod with the low evaluation of the cladding outer diameter at the end of the PCMI stage shown that:

- the departure from the PCMI stage to the gas loading did not occur synchronously for the whole cladding length;
- in the case with the fuel rod #RT10, two insulated gas volumes were formed between 30–115 mm and 115(120)–170 mm, respectively;
- the final state of the cladding diameter reflects the combination of gas loading which led to the cladding ruptures in both these volumes and the PCMI loading in regions of 20–30 mm, around the elevation of 115 mm and around the elevation higher than 170 mm.

Thus, the idealistic type of gas loading was not observed even for pressurized fuel rods with the initial gas gap. That is why, the specific effects of the failure at the hot PCMI stage manifested themselves still more pronouncedly in fuel rods with burnup of 60 MWd/kg U because these fuel rods had no initial gas gap before the BGR tests. The final validation of the considered process can be performed on the basis of the comparison of the cladding outer diameters for two fuel rods (#RT8 and RT9) tested at the same peak fuel enthalpy (164–165 cal/g). But it is interesting and important that the first of these fuel rods was pressurized and the second one was unpressurized (see Fig. 5.45).

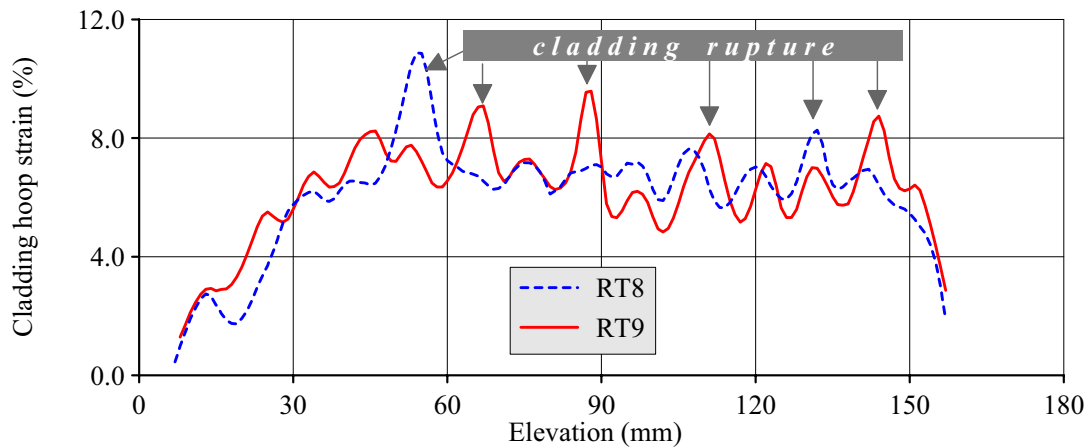


Fig. 5.45. The comparison of the cladding strains in the pressurized and unpressurized failed fuel rods with burnup of 60 MWd/kg U

The obtained data indicate quite clearly that:

- the character of the cladding deformation is similar in both fuel rods. The distinguishing feature of this deformation is the set of local ballooning distributed axially along the fuel stack;
- the average and maximum hoop strains are approximately the same in both fuel rods (7% and 9.6–11.1%, respectively);
- several ruptures were revealed in each tested fuel rod. Moreover, the unpressurized fuel rod had four ruptures but the pressurized one had two ruptures only. The critical value of the cladding hoop strain, which can be considered as the deformation threshold for the cladding failure is approximately 8%. The observation of several independent ruptures in each fuel rod denotes the presence of several gas plenums between fuel and the cladding insulated just before the ruptures.

It may seem that these data are already sufficient to prepare the following answer to the first of the questions formulated earlier: the failure of these fuel rods occurred at the hot PCMI stage of the BGR tests. But the appropriate analysis showed that if this variant of the answer is assumed as the basis, it is difficult to understand the physical mechanism for the formation of numerous gas plenums distributed axially along the fuel stack at the stage of the solid mechanical contact between the expanded fuel and cladding. To study these phenomena completely, it is useful to return to the analysis of some metallographic samples of tested fuel rods (see Fig. 5.46).

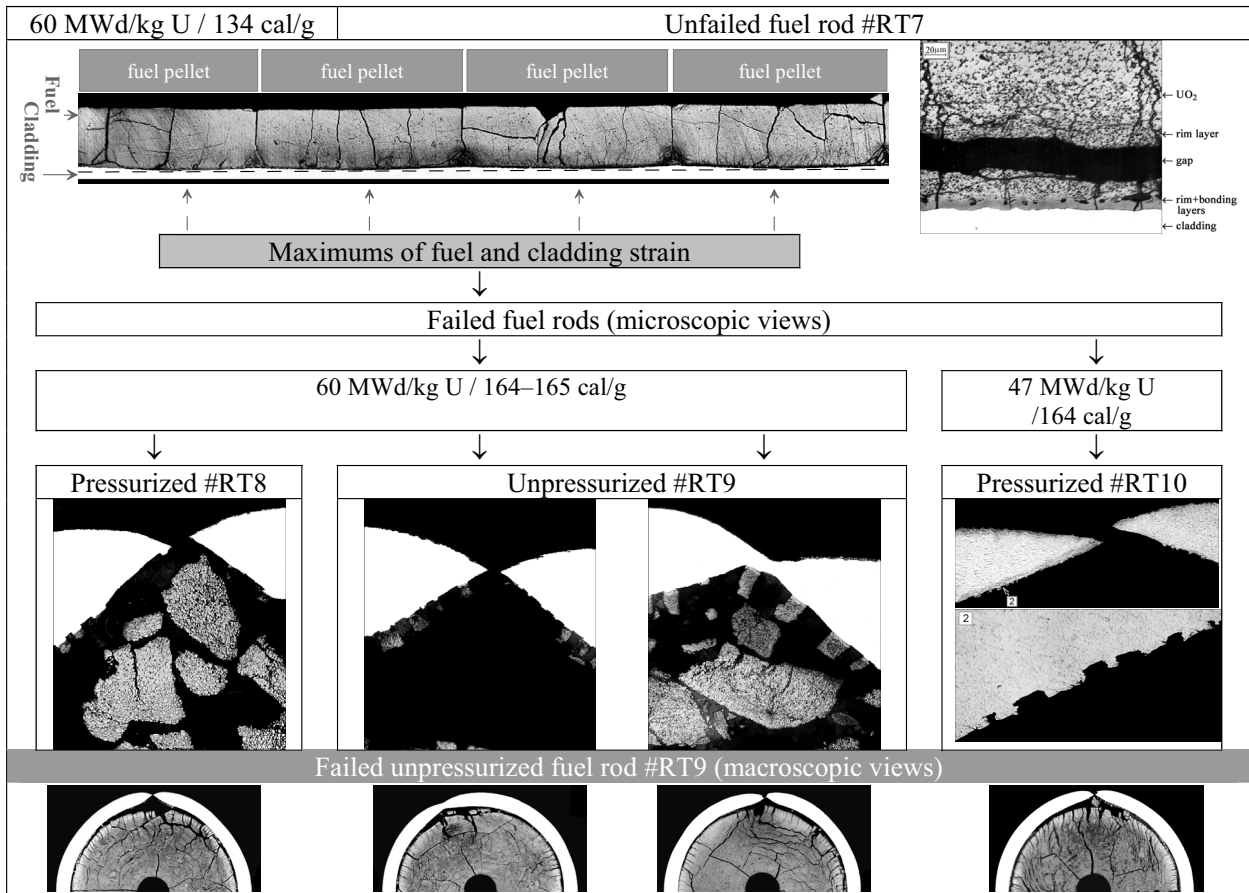


Fig. 5.46. Metallographic samples illustrating the effects of fuel and cladding deformation and failure

In accordance with the results of this analysis, the following sequence of physical phenomena accompanying the cladding loading and rupture can be suggested emphasizing the behavior of fuel rods with burnup of 60 MWd/kg U:

- at the hot PCMI stage, the radial expansion of fuel pellets was of the nonuniform character as a function of the fuel stack length. The pellet middle part had a higher temperature in comparison with the pellet end parts due to the effect described earlier (the different effective fuel linear density and, as a consequence, the different number of fissions in these fuel regions);
- the nonuniform fuel expansion of the sinusoid type provided for the similar nonuniform axial profile of the cladding plastic strain. The visual indication of these processes was noted in the axial metallographic section of the unfailed fuel rod #RT7;
- moreover, the study of cross-sections prepared from this fuel rod demonstrated that the specific gas gap appeared in the tested fuel rod after the BGR pulse. But this gap and the appropriate gas loading was not responsible for the generation of the cladding sinusoid form because the cladding was separated from fuel (during the fuel cooling stage) together with the bonding layer and peripheral part of the fuel rim layer;
- if we consider the test data characterizing the behavior of fuel rods at the higher fuel enthalpy, it can be revealed that tensile stresses in the cladding parts facing the fuel middle parts achieved values at which the formation of the cladding necks was initiated^a;

^a See the data for fuel rods #RT8, RT9 in Fig. 5.45, see Fig. 5.47, see Appendix E-13 of Volume 3 of the report, see Section 5.3 of this volume of the report

- the necking was accompanied by two important processes:
 - ⇒ the cladding separation from fuel in these regions;
 - ⇒ the formation of minor empty spaces between fuel and the cladding.
- it seems that all these processes were developed at that time when the hot PCMI stage had just been completed and the fuel diameter reduction was initiated (the transition from the hot PCMI stage to the gas loading stage);
- taking into account the presence of the bonding layer, the process of the fuel separation from the cladding was not typical because two completing effects were observed:
 - ⇒ in some cases, the bonding layer and a part of the rim layer were taken away from fuel together with the cladding;
 - ⇒ in some cases, a part of the cladding inner surface was taken away together with fuel. It is important that the second case was observed for fuel rods with burnup of 47–49 MWd/kg U also (see Fig. 5.46). The last fact may be the consequence of two possible effects: the effect of high-energy-rate-shaping of the cladding plastic surface by fuel or the effect of Zr and UO₂ chemical interaction with the appropriate eutectic formation. But the first effect is more preferential because the presence of Zr/UO₂ eutectic is not observed in the microstructural samples).
- due to all these processes, the cladding inner surface with the local sections of remained fuel acquired the specific gear shape;
- the final stage of the cladding rupture was connected with the formation of minor local empty spaces between the cladding necks and fuel. It may be assumed that these local plenums became the tanks for fission gases concentrated in these fuel regions. The pressure of fission gases in these gas plenums was the major factor for the formation of the cladding ballooning and for the subsequent cladding rupture in fuel rods #RT8, RT9.

Thus, the mechanism of the high burnup fuel rod failure is the high temperature cladding rupture caused by the following two components:

- the cladding hoop strain during the hot PCMI stage;
- the cladding local ballooning and rupture due to gas accumulated in the local gas plenums formed around the cladding necks at that time when the fuel cooling phase was initiated.

These explanations for the cladding failure mechanism answer the second question formulated earlier concerning the nature of gas generated in local balloonings just before the cladding ruptures. Moreover, these explanations also answer the following additional questions:

- Why was the number of ruptures in the unpressurized fuel rod #RT9 with burnup of 60 MWd/kg U higher than that in the pressurized fuel rod #RT8 with the same burnup?
- Why was the cladding hoop strain at rupture in the pressurized fuel rod #RT10 (14.8%) with burnup of 47 MWd/kg U
 - a) higher than the cladding hoop strain at rupture in the pressurized fuel rod #RT11 (8.2%) having the same burnup but higher peak fuel enthalpy (164 and 188 cal/g, respectively)?
 - b) higher than that in the pressurized fuel rod #RT8 (11.1% at the maximum) with burnup of 60 MWd/kg U, which was tested at the same peak fuel enthalpy?

To answer these questions, we may use the following:

- the approach suggested for the analysis of the cladding failure mechanism;
- the test data presented in Fig. 5.47.

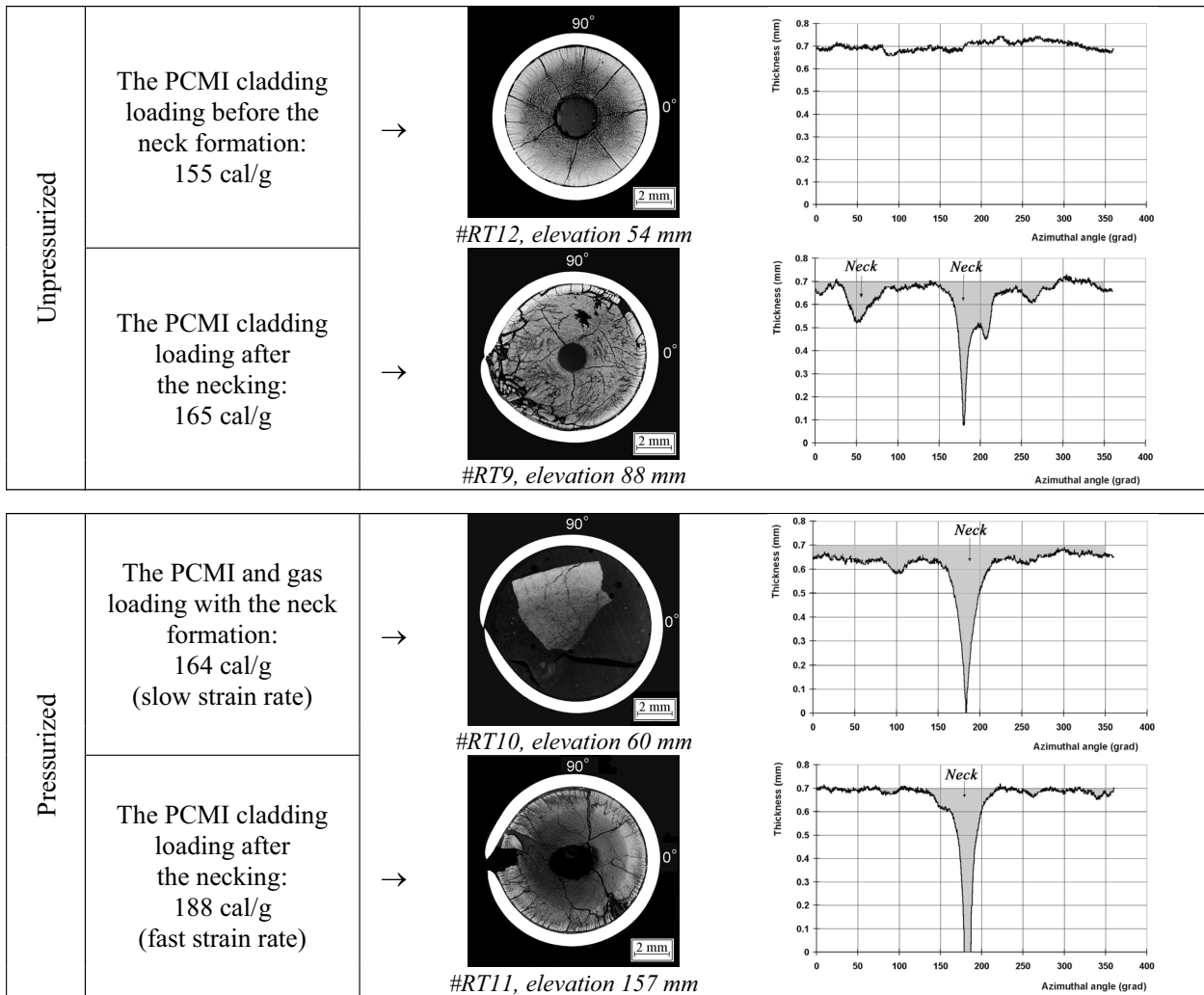


Fig. 5.47. Types of azimuthal distributions of residual cladding thickness as a functions of the BIGR test conditions

The general answer to all these questions is the following: the individual combinations of pretest parameters for fuel rods (the gas gap width and fuel burnup) and test parameters (the peak fuel enthalpy) determine the combination of individual contributions of the hot PCMI effects and gas loading effects into the cladding strain and rupture processes.

The major relationships between the above listed phenomena are as follows:

- if the cladding critical hoop tension occurred at the high strain rate and at the PCMI stage of the cladding strain, then the local neck region (or the neck regions) provided the main contribution into the total residual hoop strain; the cladding thickness in other cladding regions was not practically changed;
- if the cladding plastic flow was developed during the more significant time (the low strain rate of the gas loading stage of the test), the most part of the cladding cross-section was involved in the tension process, and the reduction of the cladding thickness was observed as a function of the significant part of the cladding perimeter.

In accordance with these observations, several conclusions can be made:

- the failure mechanism observed in fuel rods #RT11, RT8 is insensitive to the initial pressurization. The mechanism and the maximum hoop strains at failure would be approximately the same if the unpressurized fuel rods were tested. The test data concerning the fuel rod #RT9 confirm this conclusion;

- the failure in fuel rod #RT10 suggests the behavior during failure may be a strong function of the initial pressurization because gas loading may occur either during or after neck formation.

The final important item of the analysis presented in this section of the report is devoted to the consideration of the test data characterizing the failure thresholds for tested types of high burnup fuel rods. But taking into account that the test statistic of failed fuel rods is not so extensive and Zr-1%Nb cladding have specific mechanical properties at rupture (in comparison with the Zircaloy claddings), the additional test data characterizing the mechanical behavior of the Zr-1%Nb (E110) cladding are organized in Fig. 5.48.

The following brief characterization can be given for the procedures used to obtain the data presented in a),b),c) positions of Fig. 5.48^a:

- the Russian test data obtained in different biaxial rupture tests performed by different Russian organizations with the unirradiated Zr-1%Nb (E110) cladding have been used to develop Fig. 5.48b. These data characterize the pressure drop at rupture as a function of the high cladding temperature and the temperature increase rate in the range of 0.5–40 K/s^b. The analysis of these data shows that the cladding stress at rupture (the pressure drop at rupture) demonstrates the oversensitivity to the temperature in a very narrow range of the cladding temperature (1050–1190 K). The pressure drop at rupture is varied from 13.5 MPa down to 1 MPa in this temperature range. It is clear that different random and systematic errors are responsible for the high dispersion of experimental results, but taking into account the effect of the independence of separate test programs on the one hand and the presence of the general tendency characterizing the effect of the temperature increase rate on the other hand, the obtained data were outlined by two solid lines, which indicate the effects of the slow (0 K/s) and fast (40 K/s) temperature increase rates;
- the upper parts of these two solid lines were repeated in Fig. 5.48a. After that, the test data characterizing the low temperature pressure drop at rupture of the irradiated E110 cladding were presented in this Figure also for the temperature increase rate 0 K/s^c;
- the next action was connected with the introduction of the test data characterizing the α to β phase transition in the E110 cladding (the β -phase fraction in the cladding material as a function of the temperature under steady-state conditions) into Fig. 5.48a;
- the analysis of obtained data supplemented with the analysis of the knowledge data base characterizing the relationships of separate physical phenomena made possible the restoration of the pressure drop at rupture as a function of the temperature in the range of 723–973 K at the temperature increase rate of 0 K/s (dashed lines in Fig. 5.48a,b);
- the approximations of the pressure drop at rupture and the β -phase content at the temperature increase rate of 40 K/s (dash-dot lines in Fig. 5.48a) were developed using the same approaches and some additional data;
- finally, the BGR test data characterizing the cladding residual maximum hoop strain (measured) as a function of the cladding calculated maximum temperature were organized in Fig. 5.48c.

^a The goal for the preparation of these pictures was to clarify the general relationships between the different physical phenomena, which define the cladding mechanical behavior in the wide range of varied parameters. It seems that this goal warrants the implementation of quite courageous approximations used to restore those parametric dependences, which were not developed in the explicit form up to the present time

^b The minimum temperature increase rate was 0.5 K/s. To simplify the comparative analysis of these data with other data presented in Fig. 5.48, it was decided to assume that 0.5 K/s can be considered as 0 K/s from the practical point of view

^c The previous investigations performed by the RRC KI and RIAR showed that the mechanical properties of the Zr-1%Nb (E110) cladding are the function of irradiation at the low temperature. At the high temperature, the mechanical properties of irradiated and unirradiated claddings are the same due to the effect of the radiation damage annealing. Therefore, properties of unirradiated cladding were used for the low temperature range and properties of the unirradiated cladding were implemented in the high temperature range in Fig. 5.48. It is important to note that these tests were not as the creep type tests because the pressure increase rate was not as zero

The developed multifactor experimental data provided the unique opportunity for the integrated analysis of the cladding failure criteria. So, the scope of functional correlations presented in Fig. 5.48a,b allows definite conclusions:

- the sensitivity of the cladding pressure drop at rupture (the cladding stress at rupture) to the temperature increase rate is the direct consequence of the α to β -phase transition sensitivity to this factor;
- the character of the pressure drop decrease at rupture at the increase of the cladding temperature is defined by the phase composition of the cladding material:
 - ⇒ a relatively slow decrease of the cladding strength is observed in the temperature range of the α -phase existence (293–880 K for the temperature increase rate 0 K/s and 293–1050 K for the temperature increase rate 40 K/s); in other words, the cladding demonstrates the best mechanical properties when the cladding material consists of the α -phase only. The high rate of the temperature growth leads to the widening of the α -phase existence region because the process of the equilibrium phase transformation in the cladding material is less than slow;
 - ⇒ the detectable deterioration of the cladding strength is connected with the initiation of the α to β -phase transformation (880 K and 1050 K at 0 K/s and 40 K/s, respectively). In accordance with the presented data, this stage is characterized by the α – β phase composition of the cladding material;
 - ⇒ as soon as the concentration of the β -phase in the cladding material achieves approximately 10%, the sharp degradation of the cladding strength is observed (\approx 1050 K and 1190 K for 0 K/s and 40 K/s, respectively). Taking into account that the increase of the β -fraction in the cladding material from 10% up to 95% occurs in the very narrow temperature interval (less than 100 K) and, besides, taking into account the experimental uncertainties connected with the measurements of pressure and temperature at rupture, the outlined boundaries of these fragments of lines characterizing the pressure drop at rupture versus the cladding temperature in Fig. 5.48b show the immediate reduction of the rupture pressure from 12.5 MPa down to 4 MPa on achieving the temperature 1050 K or 1190 K (for 0 K/s and 40 K/s, respectively);
 - ⇒ the final part of appropriate correlations is characterized by the slower decrease of the cladding strength at the temperature increase. This part of the process is connected with the β -phase of the cladding material.

The results of these out-of-pile mechanical tests can be used as the background on considering the mechanical behavior of high burnup fuel rods tested under the BGR test conditions (see Fig. 5.48c)^a. The obtained data characterizing the mechanical behavior of claddings at different combinations of fuel rod parameters (burnup, the gas gap width, pressurization (0.1 MPa, 2.0–2.1 MPa)) and test parameters (energy deposition → the peak fuel enthalpy (115–188 cal/g) → the cladding temperature (1000–1320 K)) revealed the following:

- the cladding ruptures were not observed at any combinations of test factors if the cladding residual hoop strain was less than or equal to 8% (the cladding OD was approximately 9.8 mm);
- the cladding ruptures (fuel rod failures) were not observed at any combinations of test factors if the cladding maximum temperature did not exceed 1210 K.

These test results can be considered as the temperature failure criterion (1210 K) and the deformation failure criterion (8%) for the BGR test conditions. The comparison of the obtained temperature failure criterion with the data of out-of-pile tests shows that quite a reasonable agreement is observed between the results of the reactor and out-of-pile tests. This agreement includes two important aspects of the problem:

1. The relationship between the pressure drop at rupture, the cladding temperature, and the temperature increase rate.
2. The phase state of the failed cladding after the BGR tests.

^a Taking into account that the failed fuel rods #RT8–10 had several ruptures, the whole set of these individual measurements is presented in the picture

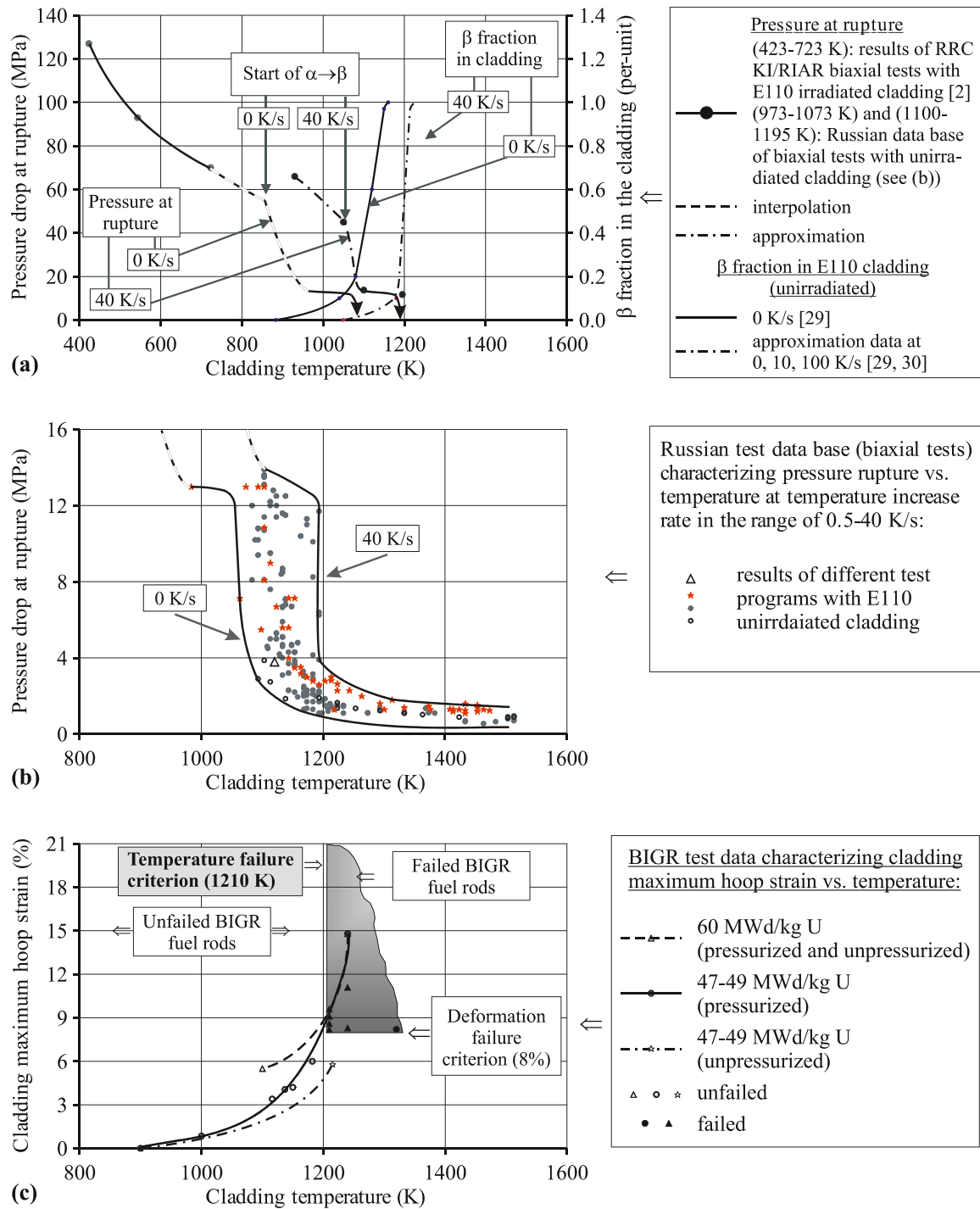
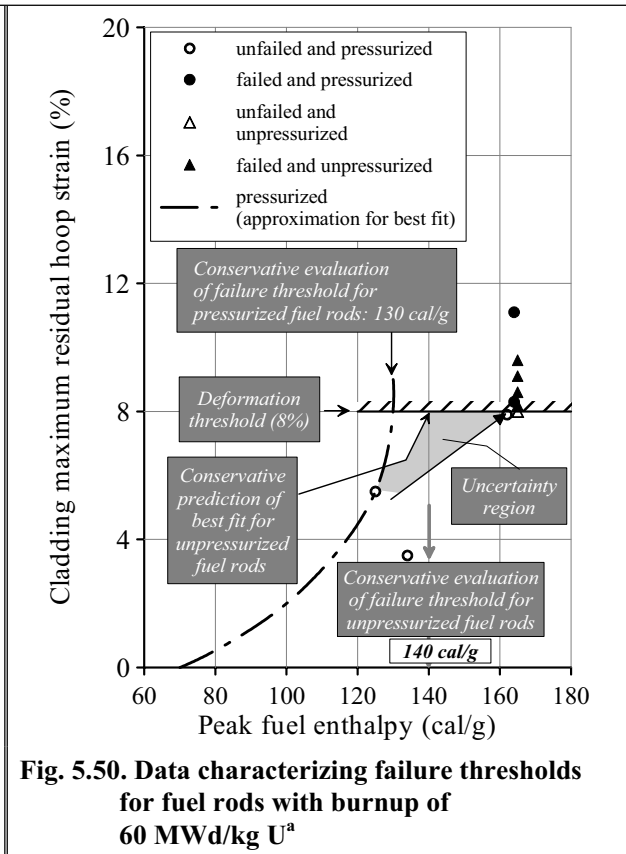
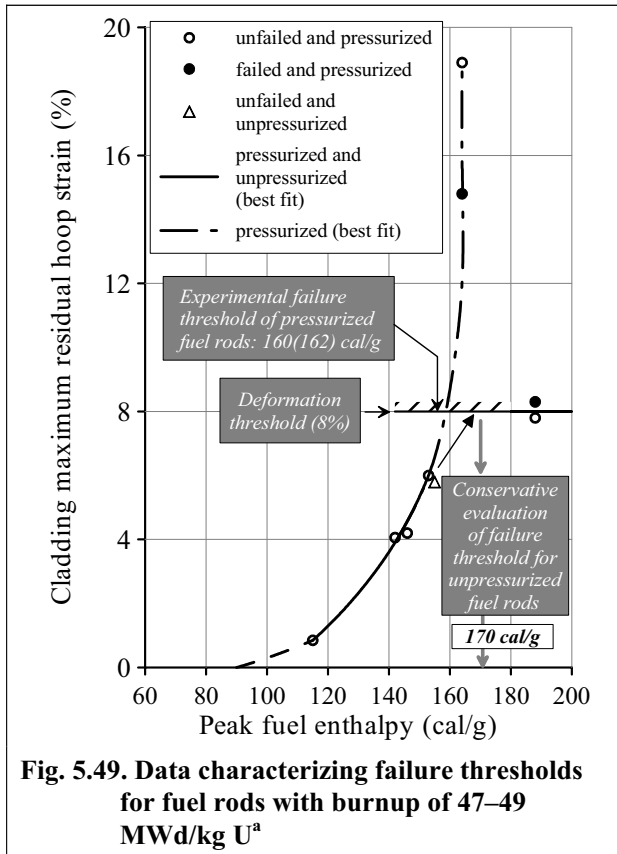


Fig. 5.48. The organized test data characterizing the Zr-1%Nb (E110) cladding mechanical behavior
a) the pressure at rupture in the temperature range of 423–1200 K and the β fraction in the cladding material vs. the temperature for two temperature increase rates (0, 40 K/s), b) results of biaxial tests at the high temperature and the temperature increase rate in the range of 0.5–40 K/s, c) the cladding maximum hoop strain as a function of fuel burnup, the temperature, the cladding initial pressurization in accordance with the BIGR test data

This intermediate conclusion provided the initiation of the consideration of the final important aspect of the BGR tests connected with the assessment of failure thresholds for the VVER high burnup fuel rods under the narrow pulse conditions. The organized test results collected separately for fuel rods with burnup of 47–49 and 60 MWd/kg U are presented in Fig. 5.49 and Fig. 5.50.



The analysis of the data devoted to high burnup fuel rods with burnup of 47–49 MWd/kg U led to the following set of observations and conclusions:

- the test data would be ample to assess the experimental failure threshold of high burnup fuel rods with the initial pressurization of 2.0–2.1 MPa. This failure threshold is correlated with the peak fuel enthalpy of 160 cal/g (162 cal/g in accordance with results of the formal graphical procedure);
- the consideration of the data presented in Fig. 5.49 and results of a special analysis performed in this section of the report (in the context of studies of failure mechanisms for tested types of fuel rods) allow the assumption (with a good accuracy) that the linear approximation (marked in Figure by an arrow) from the maximum residual hoop strain in the unfailed and unpressurized fuel rod #RT12 (5.8% at 155 cal/g) to the deformation threshold (8%), which was estimated with the use of data presented in Fig. 5.48b and with the use of the data characterizing the maximum hoop strain at rupture and the maximum hoop strain without rupture in the fuel rod #RT11 (8.2% and 7%, respectively, at 188 cal/g), which failed due to the hot PCMI loading, can be used as the conservative evaluation of the failure threshold for the unpressurized fuel rods (the conservatism was provided by the choice of such an angle of the arrow departure from the point

^a The data characterizing the cladding strain in failed fuel rods consist of:
 – strains at rupture;
 – maximum strains in unfailed regions of these fuel rods

(155 cal/g, 5.5%), which coincides with the tendency for pressurized fuel rod). In accordance with this procedure, the failure threshold of unpressurized fuel rods cannot be less than 170 cal/g.

The study of the data characterizing the behavior of fuel rods with burnup of 60 MWd/kg U revealed that:

- the number of tested fuel rods with this burnup was not sufficient to develop the best fits for the correlation between the cladding maximum residual hoop strain and the peak fuel enthalpy in pressurized and unpressurized fuel rods. Therefore, the appropriate approximation presented in Fig. 5.50 for the peak fuel enthalpy range of 70–125 cal/g has quite an illustrative character (the value of 70 cal/g was obtained on the basis of the FRAP-T6 calculations);
- nevertheless, the implementation of the approaches, which are similar to the approaches used in the analysis of fuel rods with burnup of 47–49 MWd/kg U, shown that:
 - ⇒ the conservative evaluation of the failure threshold for the pressurized fuel rods with burnup of 60 MWd/kg U is 130 cal/g;
 - ⇒ the conservative evaluation of the failure threshold for the unpressurized fuel rods with burnup of 60 MWd/kg U is 140 cal/g.

The additional analysis of the obtained data representativity will be continued in the next chapter of the report.

References

- 1 L. Yegorova, V. Asmolov, G. Abyshov, V. Malofeev, A. Avvakumov, E. Kaplar, K. Lioutov, A. Shestopalov, A. Bortash, L. Maiorov, K. Mikitiouk, V. Polvanov, V. Smirnov, A. Goryachev, V. Prokhorov, and A. Vurim “Data Base on the Behavior of High Burnup Fuel Rods with Zr-1%Nb Cladding and UO₂ Fuel (VVER Type) under Reactivity Accident Conditions”, *NUREG/IA-0156 (IPSN99/08-02, NSI/RRC KI 2179), Vol.2, 1999.*
- 2 E. Kaplar, L. Yegorova, K. Lioutov, A. Konobeyev, N. Jouravkova, A. Goryachev, V. Prokhorov, S. Yeregin, A. Svyatkin “Mechanical Properties of Unirradiated and Irradiated Zr-1%Nb Cladding”, RRC “Kurchatov Institute” report NSI RRC KI 2241, 2001 (also USNRC report NUREG/IA-0199 and IPSN report IPSN 01-16).
- 3 R. Manzel, M. Coquerell “Fission gas release at extended burn-up”, Enlarged Halden programme group meeting on high burnup fuel performance, safety and reliability, and degradation of in-core materials, and water chemistry effects, and man-machine research (HPR-347/21, Vol.2), Loen, Norway, May 19–24, 1996.
- 4 R. Yuda, Y. Ishii, M. Hirai, T. Hosokawa, K. Une, S. Kashibe, K. Nogita, S. Shimizu, T. Kubo “Effect of Pellet Microstructure on Irradiation Behavior”, Enlarged Halden programme group meeting on high burnup fuel performance, safety and reliability, and degradation of in-core materials, and water chemistry effects, and man-machine research (HPR-347/21, Vol.2), Loen, Norway, May 19–24, 1996.
- 5 L. Yegorova, V. Asmolov, G. Abyshov, V. Malofeev, A. Avvakumov, E. Kaplar, K. Lioutov, A. Shestopalov, A. Bortash, L. Maiorov, K. Mikitiouk, V. Polvanov, V. Smirnov, A. Goryachev, V. Prokhorov, and A. Vurim “Data Base on the Behavior of High Burnup Fuel Rods with Zr-1%Nb Cladding and UO₂ Fuel (VVER Type) under Reactivity Accident Conditions”, *NUREG/IA-0156 (IPSN99/08-02, NSI/RRC KI 2179), Vol.3, 1999.*
- 6 J. Papin, M. Balourdet, F. Lemoine, F. Lamare, J. Frizonett, and F. Schmitz “French Studies on High Burnup Fuel Transient Behavior under RIA Conditions”, *Nuclear Safety*, Vol.37, No.4, 1996.
- 7 H. Sasajima, J. Nakamura, T. Fuketa, H. Uetsuka “Fission Gas Release Behavior of High Burnup UO₂ Fuel under Reactivity Initiated Accident Conditions”, *Nuclear Technology*, Vol.36, No.11, 1999.
- 8 M. Cunningham, M. Freshley, D. Lanning: *J. Nucl. Mater.*, 188, 19–27 (1992).
- 9 C. Walker, *et al.*: *J. Nucl. Mater.*, 188, 73–79 (1992).
- 10 J. Spino, K. Vennix, M. Coquerelle: *J. Nucl. Mater.*, 231[3], 179–190 (1996).
- 11 I.L.F. Ray, Hj. Matzke, H.A. Thiele, M. Kinoshits “An Electron Microscopy Study of the RIM Structure of UO₂ Fuel with a High Burnup of 7.9% FIMA”, *J. Nucl. Mater.*, No.245, 1997.

- 12 R. Manzel, M. Coquerelle “Fission Gas Release and Pellet Structure at Extended Burnup”, *Proc. of Int. Topical Meeting on Light Water Reactor Fuel Performance*, Portland, Oregon, March 2–6, 1997.
- 13 M. Mogensen, J. Pearce, C. Walker “Behavior of fission gas in the rim region of high burnup UO₂ fuel pellets with particular reference to results from an XRF investigation”, *J. Nucl. Mater.*, No.264, 1999.
- 14 K. Une, K. Nogita, T. Shiratori, K Hayashi “Rim structure formation of isothermally irradiated UO₂ fuel disks”, *J. Nucl. Mater.*, No.228, 2001.
- 15 C. Walker, C. Bagger, M. Mogensen “Observations on the release of cesium from UO₂ fuel”, *J. Nucl. Mater.*, No.240, 1996.
- 16 J. Spino, K.Vennix, M. Coquerelle “Detailed characterization of the rim microstructure in PWR fuels in the burn-up range 40–67 GWd/t M”, *J. Nucl. Mater.*, V.231, No.3, 1996.
- 17 F. Lemoine “High burnup fuel behavior related to fission gas effects under reactivity initiated accidents (RIA) conditions”, *J. Nucl. Mater.*, No.248, 1997.
- 18 I. Kungurtsev, V. Zhitelev, V. Chesanov, V. Smirnov, I. Kuzmin, A. Leshchenko, Yu. Pimenov, L. Stupina, E. Zvir “The investigation of fission gas release and structure of VVER high burnup fuel at the heating up above the base irradiation temperature”, *Proc. of 6th Russian Conference on Reactor Physical Metallurgy*, V.2, Dimitrovgrad, September 11–15, 2000.
- 19 K. Une, K. Nogita, S. Kashibe, T. Toyonada, M. Amaya “Effect of Irradiation-Induced Microstructural Evolution of High Burnup Fuel Behavior”, *Proc. of International Topical Meeting on Light Water Reactor Fuel Performance*, Portland, Oregon, March 2–6, 1997.
- 20 J. Papin, H. Rigat, J.P. Breton “The Behavior of Irradiated Fuel under RIA Transients: Interpretation of the CABRI Experiments”, *Proceedings of the CSNI Specialist meeting on transient behavior of high burnup fuel*, Cadarache, France, 12–14 September 1995.
- 21 J. Papin, H. Rigat, J.P. Breton, F. Schmitz “The Behavior of Irradiated Fuel under RIA Transients: Interpretation of the CABRI Experiments”, *Proceedings of IAEA Technical Committee Meeting “Behavior of LWR core materials under accident conditions”*, Dimitrovgrad, Russian Federation, 9–13 October 1995 (IAEA-TECDOC-921).
- 22 L. Loshmanov, V. Rudnev, O. Nechaeva “The sensitivity of Zr-1%Nb alloy mechanical properties to the temperature and strain rate”, *Journal of Atomic Energy*, v2(81), 1996(rus).
- 23 L. Yegorova, F. Schmitz, J. Papin “Mechanical behavior of fuel element during RIA transient”, *Proc. of EUROSAFE meeting*, November 18–19, Paris, 1999.
- 24 K. Lioutov, L. Yegorova, E. Kaplar, A. Konobeyev, V. Smirnov, A. Goryachev, V. Prokhorov, and S. Yerebin “Mechanical properties of unirradiated and irradiated Zr-1%Nb cladding under accident conditions”, *Proc. of the 27th Water Reactor Safety Information Meeting*, NUREG/CP-0169, 1999.
- 25 R. Montgomery, Y. Rashid, O. Ozer, and R. Yang “Assessment of RIA-Simulation Experiments on Intermediate- and High-Burnup Test Rods”, *Nuclear Safety*, Vol.37, No.4, 1996.
- 26 M. Cunningham, C. Bayer, P. Megvedev, C. Berna “FRAPTRAN: A Computer Code for the Transient Analysis of Oxide Fuel Rods”, NUREG/CR-6739 Vol.1 PNNL-13576, September 2001.
- 27 R. Yang, R. Montgomery, N. Waackel, Y. Rashid “Industry Strategy and Assessment of Existing RIA Data”, *Proc. of the 2000 International Topical Meeting on LWR Fuel Performance*, Park City, Utah, April 10–13, 2000.
- 28 A. Romano and M. Zimmermann “Effect of the Power Pulse Shape on the Fuel Thermal-Mechanical Response to RIAs: a Study Using FALCON and SCANAIR”, *Proc. of 2005 Water Reactor Fuel Performance Meeting*, Kyoto, Japan, 2-6 October 2005.
- 29 Ye. Pirogov, M. Alimiv, L. Artiuchina “Creep of H-1 alloy in the range of phase transition”, *Journal of Soviet Atomic Energy*, v.65(3), p.293, 1988(rus).

30 O. Nechaeva, A. Salatov, P. Fedotov, A. Goncharov, A. Kumachev, A. Medvedev, V. Novikov, A. Onufriev, V. Molchanov, Yu. Pimenov, A. Alekseev, I. Kiseleva, V. Shulimov, I. Fedik, V. Nalivaev, N. Parshin, V. Konstantinov "Estimation of Water-Water Reactor Fuel Rod Failure in Design Basis Accidents", for publication in the *Proc. of 2005 Water Reactor Fuel Performance Meeting*, Kyoto, Japan, 2–6 October 2005.

6. THE COMPARATIVE ANALYSIS OF THE RIA TESTS WITH THE VVER AND PWR HIGH BURNUP FUEL RODS

The format and status of this work, devoted to the presentation of the BGR test data, did not allow a detailed comparative analysis of the BGR test results with the results of other RIA-type tests. Nevertheless, a brief consideration of the mechanical response of high burnup fuel to the test conditions and fuel rod types is presented in this chapter of the report. This consideration was mainly focused on the clarification of the sensitivity of high burnup fuel rod deformation and failure to such phenomena as the pulse width, the initial pressurization, fuel burnup, the pellet/cladding radial gap, the fuel rod materials and design.

The background of this sensitivity studies was connected with the choice of the test data for the comparative analysis. This choice was based on the following specialized RIA test programs conducted recently with high burnup fuel in different countries^a:

- the IGR test program (Russia) [1, 2];
- the CABRI test program (France) [3, 4, 5]
- the NSRR test program (Japan) [6–16].

Table 6.1 presents the general characteristics of these test programs and the BGR test program. Apart from the recent IGR, BGR, NSRR and CABRI programs, the RIA-type tests with burnup fuel were previously performed in the SPERT and PBF facilities [17]. But taking into account that burnup was low in these tests (6 MWd/kg U at the maximum), it was decided to remove this test program results from this consideration.

Table 6.1. The general characterization of the BGR, IGR, NSRR^b, CABRI^b test programs performed with the VVER and PWR (UO₂ fuel) high burnup fuel rods

Test program	Test fuel rods		Test conditions		Cladding oxidation before the RIA test (oxide thickness) (μm)
	Type	Burnup (MWd/kg U)	Coolant	Pulse width (ms)	
1. BGR [this report]	VVER	47–49, 60	Stagnant water at 20 C and atmospheric pressure	2.5–3.1 (narrow pulse)	3–15
2. IGR [1, 2]	VVER	46.8–49.3	Stagnant water at 20 C and atmospheric pressure	750–850 (wide pulse)	3–5
3. CABRI [3–5]	PWR	54–64	Liquid sodium loop: <ul style="list-style-type: none"> • 280 C • 0.5 MPa 	8.8–9.5, 31, 76 (narrow and medium pulses)	10–110
4. NSRR [6–16]	PWR	38–50	Stagnant water at 20 C and atmospheric pressure	4.4–9.3 (narrow pulse)	2–60

^a Initially, the authors did not plan to introduce a serious comparative analysis of non-Russian data into this report. Some comparison was conducted with the specific technical goal of assuring that the BGR test data were free from the systematic (procedure) errors.

Unexpectedly, validation effort showed that the BGR test data might provide an important missing link in current RIA analysis. It would allow a connection between previous separate results regarding the mechanical behavior of ductile cladding, and do so independently of the cladding source. Moreover, some BGR data could not be fully explained without comparison with other results – including non-Russian data – because the data were limited.

The combination of data from various sources clarified some urgent and important phenomena that previously remained in the shadow of discussions devoted to the effects of the cladding oxidation and pulse width. These behavior of ductile cladding during an RIA seemed so interesting that postponement of this information would be wrong.

Consequently, it was decided to consider the behavior of ductile cladding as part of a broader review of the sensitivity of high burnup fuel rods during a reactivity-initiated accident.

^b The analysis of the NSRR and CABRI data was made for the tests performed not later than at the beginning of 2002

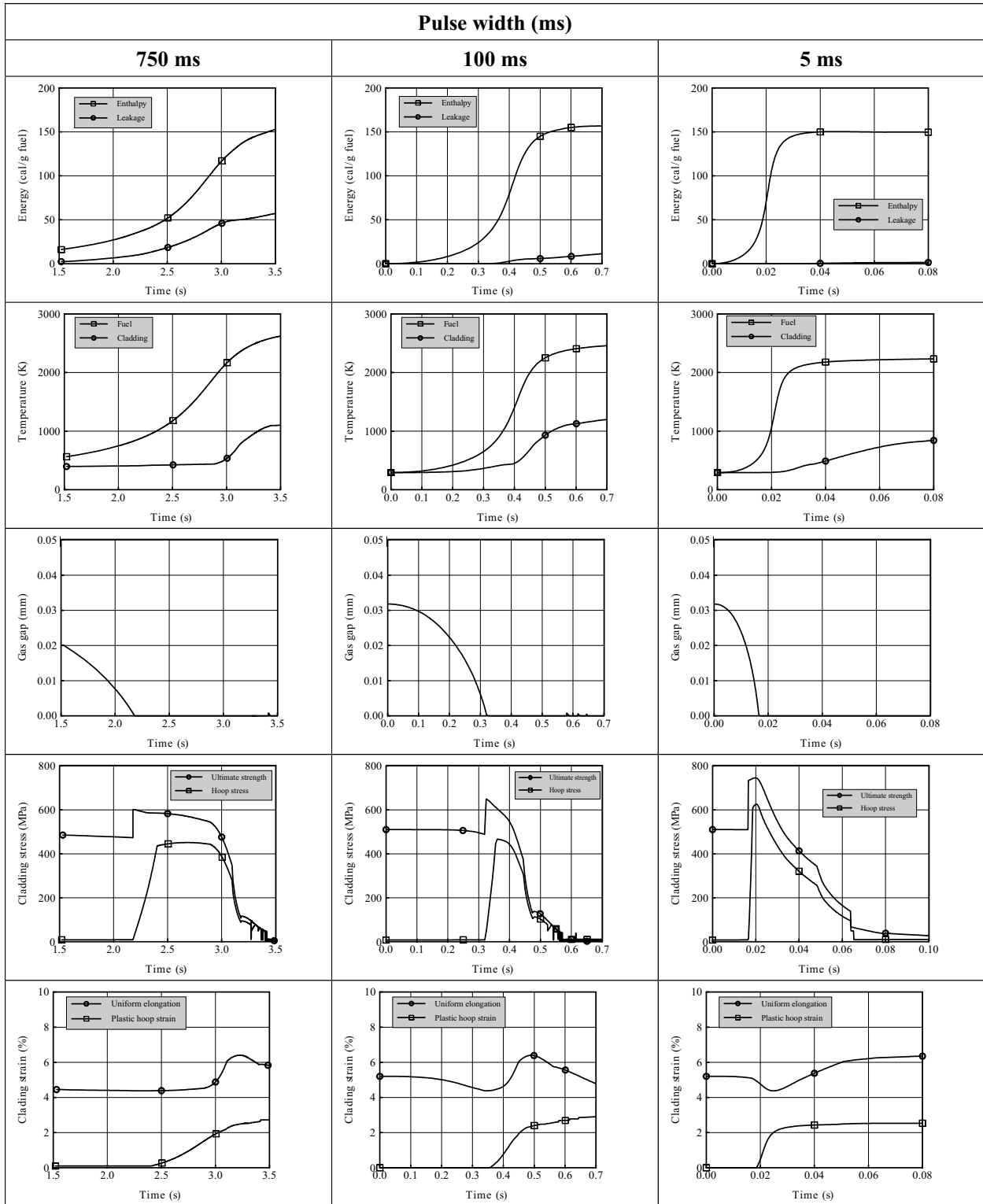
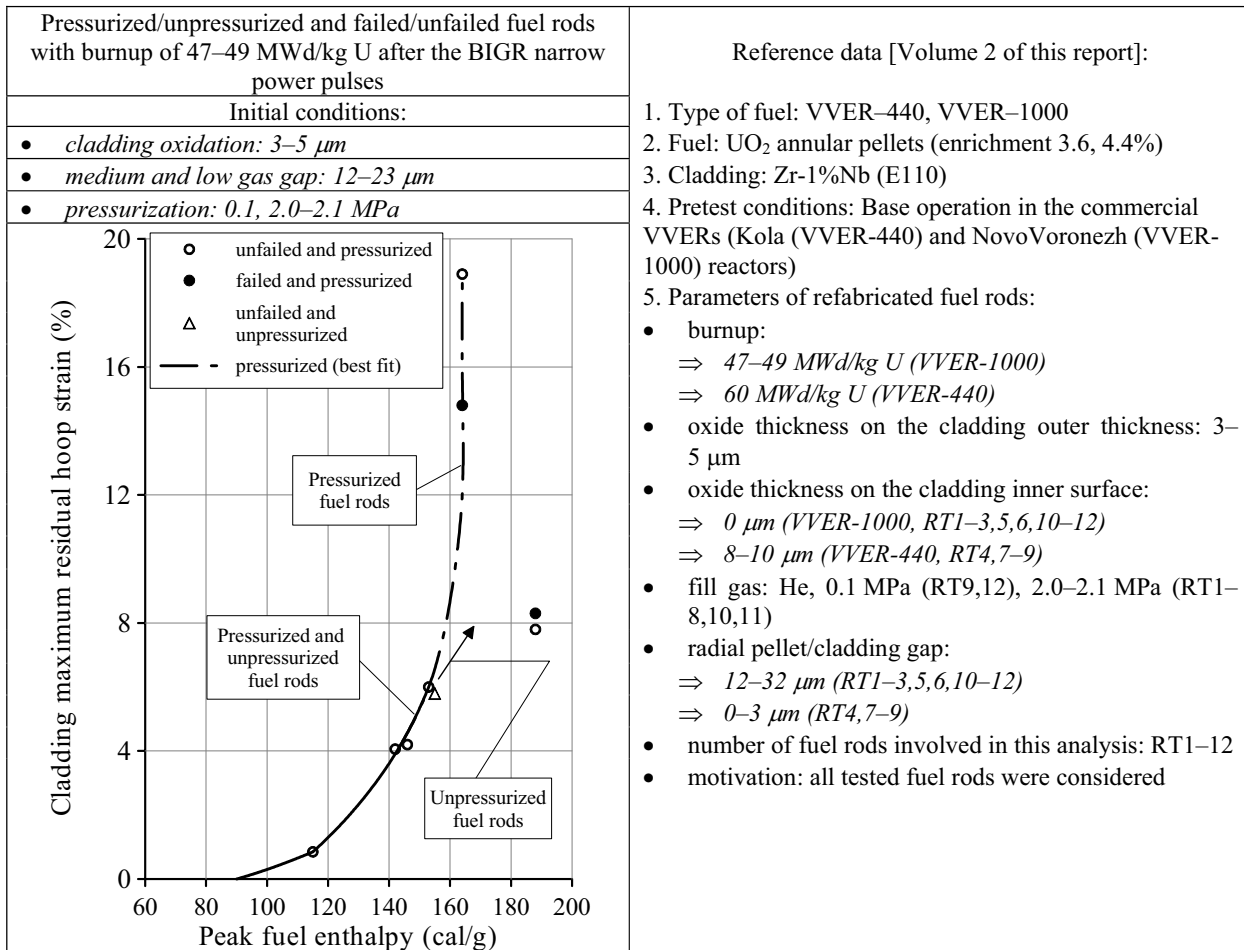
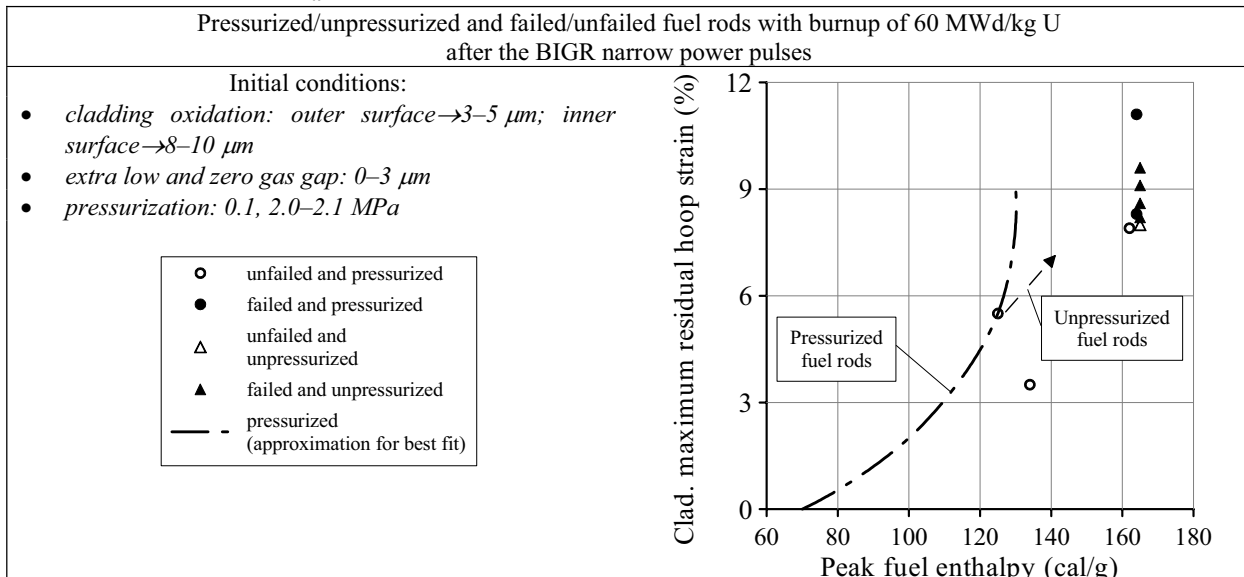


Fig. 6.1. The sensitivity of the thermal mechanical behavior of the VVER high burnup fuel rod (49.2 MWd/kg U) to the pulse width under the RIA test conditions^a

^a Results of the FRAP-T6/VVER calculations were used to develop this figure



a



b

Fig. 6.2. The reference data and interpretation of the BIGR tests performed with the low oxidized VVER high burnup fuel rods: (a) fuel rods with burnup of 47–49 MWd/kg U, (b) fuel rods with burnup of 60 MWd/kg U

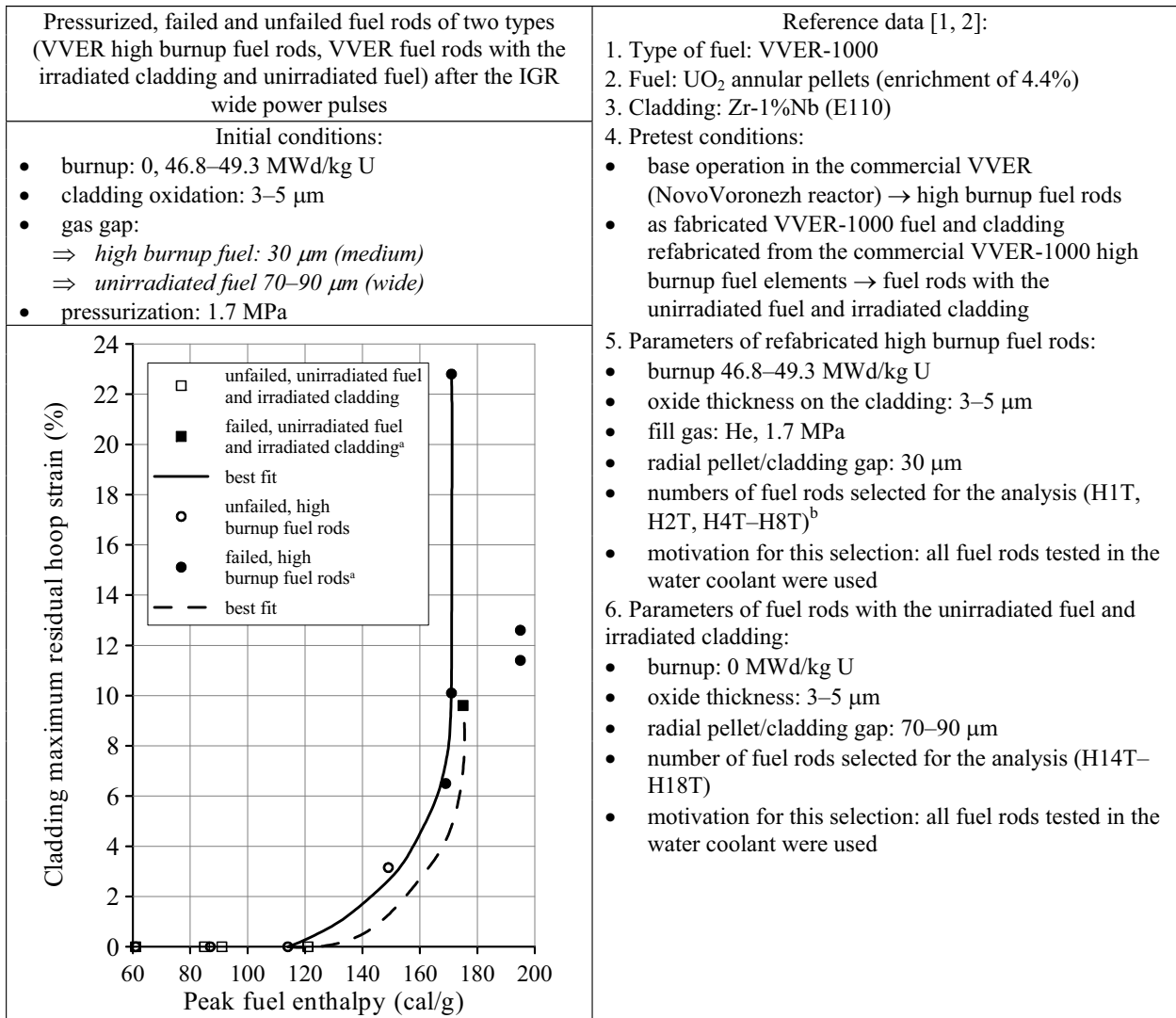


Fig. 6.3. Reference data and the RRC KI interpretation of the IGR tests performed with the low oxidized VVER high burnup fuel rods

Thus, the differences in the results obtained in the BGR and IGR pulse tests may be caused by two factors:

1. The pulse width (2.5–3.1 ms and 750–850 ms);
2. The initial pressurization (0.1 MPa and 1.7–2.1 MPa).

In spite of the practical importance of the factor connected with the initial pressurization, the BGR test data (see Fig. 6.2a) indicate that the cold PCMI stage and hot PCMI stage of pulse tests are insensitive to the initial pressurization of fuel rods. This conclusion is based on the comparison of the mechanical behavior of unpressurized and pressurized fuel rods at the cladding maximum residual hoop strains of less than 6%. Because the analysis performed in Section 5.5 of this volume of the report has shown that after the achievement of this value of the cladding strain, the reasonable difference in the mechanical response of unpressurized and pressurized fuel rods with burnup of 47–49 MWd/kg U is observed. Taking into account these considerations, the BGR and IGR test results may be compared directly using the data presented in Fig. 6.4.

^a The fuel enthalpy at failure was used for the presentation of failed fuel rods

^b The fuel rod #H3T was eliminated from the presentation because the fuel and cladding melting occurred in this fuel rod at the peak fuel enthalpy of 252 cal/g (see Fig. 6.4)

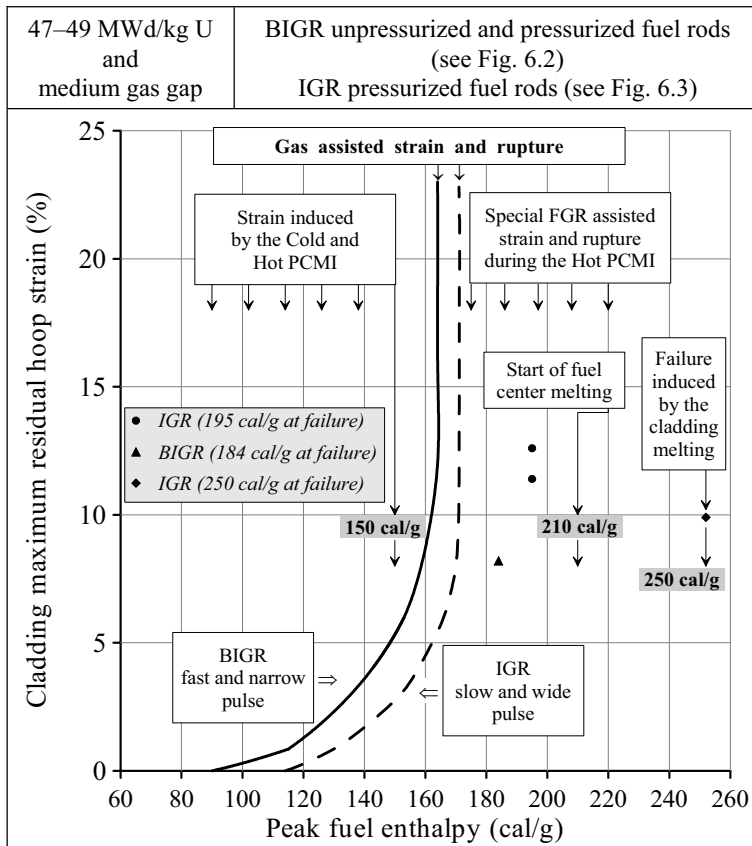


Fig. 6.4. The sensitivity of the VVER high burnup fuel behavior to the RIA pulse width

These comparative data indicated that:

- the initiation of the cladding residual hoop strain (the initiation of the cladding plastic flow) occurred at the peak fuel enthalpy of about 90 cal/g under the narrow pulse conditions as opposed to the wide pulse conditions, which are associated with 115 cal/g at the beginning of this process;
- the similar mechanical response of irradiated claddings was observed;
- the earlier initiation of all processes accompanying the cladding strain was noted at the narrow pulse. But the cost of this sensitivity is 10–15 cal/g of the peak fuel enthalpy.

So, in the aspect of the PCMI induced effects of the pulse width, the IGR and BGR comparative data allow the conclusion that the low oxidized (ductile) irradiated cladding provides for the prevention of the low enthalpy failure of the cold PCMI type independently of the pulse width in the range of 2.5–850 ms.

These test results showed that the mechanical behavior of high burnup fuel rods as a function of the peak fuel enthalpy was accompanied by the following

phenomena:

- at the peak fuel enthalpy less than 160 cal/g, the gradual transition from the cladding strain caused by the cold PCMI to the cladding strain caused by the hot PCMI was observed without the cladding failure up to the cladding maximum residual hoop strain of about 6%;
- at the increase of the peak fuel enthalpy somewhat higher than 160 cal/g, two possible variants for the progression of events were observed as a function of the fuel rod initial pressurization:
 - ⇒ a sharp increase of the cladding maximum hoop strain up to 23% and the cladding rupture were noted for pressurized fuel rods. It seems that this cladding specific high strain of pressurized fuel rods (caused by the gas loading) was the evidence of the so-called super plasticity effect introduced in the Russian scientific knowledge base many years ago to characterize the sharp increase of the Zr-1%Nb cladding total elongation on the initiation of the α to β phase/temperature transition in the E110 alloy^a.
 - ⇒ the lesser increase of the cladding strain without the rupture is expected in case when the VVER unpressurized fuel rods are to be tested under the same conditions. This prediction is based on the fact that there is no factor that could cause the super plasticity effect in this type of fuel rods.

It is very interesting and important that the cladding overstrains have been observed in a very narrow range of the peak fuel enthalpies. Observations have shown that the super plasticity effect may be produced only at the definite combination of several factors (the type of alloy, the temperature, the temperature strain rate, the temperature mode duration, etc.). If these conditions are not met, for example, at the increase of the peak fuel

^a This effect was also observed in different types of mechanical tests performed earlier for the support of the RIA test programs (see, for example, Appendix J of Volume 3 of the NUREG/IA-0156 report [2])

enthalpy higher than 180 cal/g, the hot PCMI continues to be the dominant mechanism for the cladding mechanical loading. But this test range is accompanied by the high fuel temperature, high fission product release and high cladding temperature. All these factors provided for the generation of the cladding local ballooning distributed along the fuel stack and the production of the cladding ruptures in the regions of the cladding maximum ballooning. The range of the cladding strains corresponding to these effects is approximately 8–13%.

It must be emphasized that these considerations are of more theoretical than practical application on the analysis of fuel rods with burnup of 47–49 MWd/kg U because the values of the peak fuel enthalpies associated with the above described effects are very high. These values are outside of the enthalpy range considered in the RIA safety analysis of Russian NPPs. However, the revealed effects can be used as the basis on considering superhigh burnup (higher than 60 MWd/kg U) because the test data base for this burnup is very limited and the effects corresponding to the high peak fuel enthalpies (higher than 160 cal/g) at burnup of 47–49 MWd/kg U can be observed at lower enthalpies for fuel rods with overburnup.

At the end of the analysis devoted to the BGR and IGR comparative test data, the test results concerning the behavior of high burnup fuel rods on melting will be briefly characterized. This problem continues to be urgent because the major task in the current safety analysis is to validate the prevention of the fuel element fragmentation caused by fuel melting. The BGR and IGR test data presented in Fig. 6.4 revealed that:

- the initiation of the fuel pellet central zone melting corresponds to the peak fuel enthalpy of approximately 210 cal/g; this process does not lead to the cladding melting or to the fuel rod fragmentation;
- moreover, the cladding local melting (in hot spots) and the relocation of molten fuel to the coolant is observed at 250 cal/g of the peak fuel enthalpy. But this process does not cause the fragmentation of the high burnup fuel rod tested in the IGR reactor;
- the fast BGR pulse accompanied by the peak fuel enthalpy of 188 cal/g in the VVER high burnup fuel rod confirms the test observations noted in the IGR wide pulse tests. No melting of the fuel central part and no indications of the fuel rod fragmentation are observed in this fuel rod.

All above formulated considerations concerning the behavior of high burnup fuel rods as a function of the pulse width were based on the comparison of the VVER fuel rods with burnup of 47–49 MWd/kg U tested in the BGR and IGR reactors. But in accordance with the list of the appropriate RIA-type tests presented in Table 6.1, the next comparative data base was obtained due to the numerous tests performed with the PWR high burnup fuel rods under the narrow pulse conditions (4.4–9.3 ms) in compliance with the NSRR research program [6–16]. The earliest stage of the program was devoted to the pulse tests of the JMTR fuel rods (see Fig. 6.5) [6–11].

The pretest irradiation of these fuel rods was performed in the Japan Material Testing Reactor (JMTR) up to burnup of 15–38 MWd/kg U. Other basic characteristics of these fuel rods before the NSRR tests are listed in Fig. 6.5. The studies of Japanese original publications devoted to the development of this test program and to the analysis of obtained results revealed that the JMTR fuel rods (after the preirradiation) had a low level of the Zircaloy-4 cladding oxidation (<2 μm), relatively low burnup (15–38 MWd/kg U), and relatively wide radial pellet/cladding gap (85 μm). Thus, the NSRR narrow pulse tests of these fuel rods provided the background for the interpretation of more complicated tests performed later with the PWR high burnup fuel rods. The analysis of data laid into this background due to the NSRR tests of JMTR fuel rods showed that there was a reason to remove the data characterizing the failure of the JMTR fuel rods under the NSRR conditions from the consideration. This reason was connected with the fact that the cladding local significant hydriding was detected in several failed fuel rods in the course of the post-test examinations [11]^a. This decision was provided with the general line of the studies presented in this report: to concentrate the efforts on the phenomena accompanying the mechanical behavior of the irradiated claddings with a significant margin of residual ductility. After the elimination of failed fuel rods from the consideration, the cladding maximum residual hoop strain measured in each JMTR unfailed fuel rod was pointed in Fig. 6.5 as a function of the peak fuel enthalpy generated at the NSRR pulses. After that, the best fit for the interpretation of obtained data was developed in the RRC KI.

^a The Japanese specialists assumed that this effect was caused by the presence of chemically active components of a minor concentration in the atmosphere of capsules containing the JMTR fuel rods on the long irradiation in the test reactor

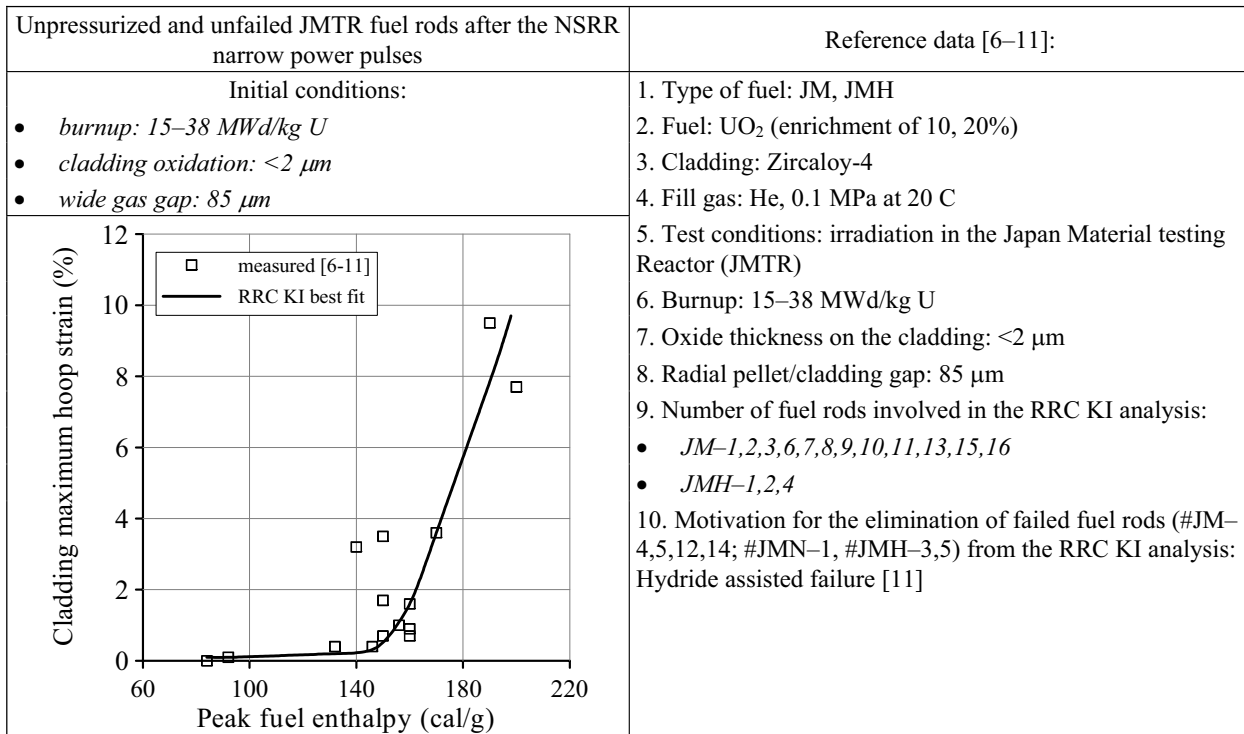


Fig. 6.5. Reference data and the RRC KI interpretation of the NSRR tests performed with the JMTR irradiated fuel rods

In this case, the obtained best fit characterizing the mechanical response of the Zry-4 low oxidized irradiated cladding to the NSRR narrow pulses was used for the comparison with the mechanical response of the Zr-1%Nb low oxidized irradiated cladding to the IGR wide pulses.

This comparison presented in Fig. 6.6 was focused on the identification of the PCMI effects under the following initial and boundary conditions:

- quite a ductile irradiated cladding of the Zr-1%Nb and Zry-4 types;
- quite a wide pellet/cladding gap (70–90 μm);
- minimum FGR effects due to the zero or not so high fuel burnup (0, 15–38 MWd/kg U).

The results of the NSRR tests with the JMTR fuel rods and of the IGR tests with the VVER fuel rods manufactured from the as fabricated VVER fuel (0 MWd/kg U) and with the irradiated Zr-1%Nb cladding refabricated from the VVER-1000 commercial fuel elements with burnup of 47–49 MWd/kg U (see also Fig. 6.3) corresponded quite well to the formulated initial and boundary conditions. This comparison could be useful for the demonstration of such phenomena as:

- the effect of the pulse width;
- the effect of the cladding pressurization;
- the effect of the cladding material and fuel

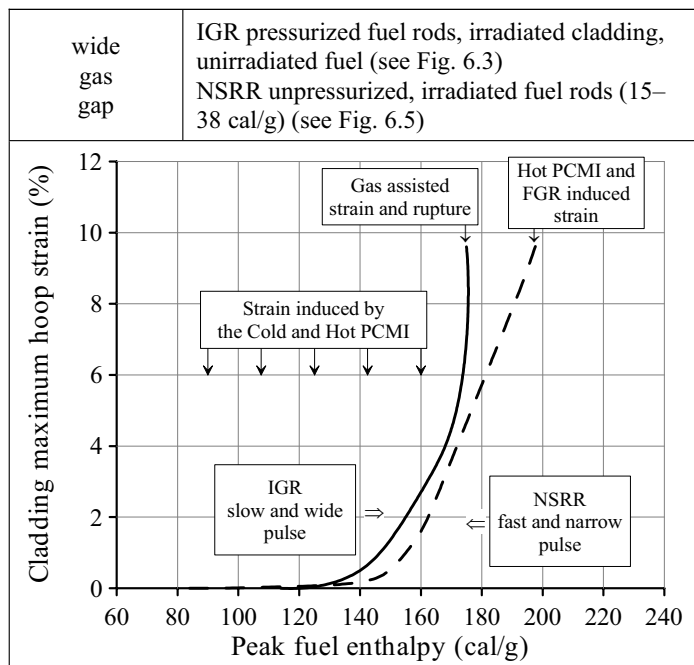


Fig. 6.6. The sensitivity of the mechanical behavior of the VVER and PWR low oxidized irradiated cladding to the RIA pulse width and cladding pressurization at the wide gas gap condition

rod design.

The consideration of the obtained IGR and NSRR comparative data led to the following observations:

- the cladding strain was relatively insensitive to the type of the cladding alloy (E110, Zry-4), the pulse width (narrow, wide), the cladding pressurization (0.1 MPa for the JMTR fuel rods, 1.7 MPa for the IGR fuel rods) up to the peak fuel enthalpy of approximately 170 cal/g;
- the beginning of the cladding ductile flow caused by the PCMI loading was a function of the pulse width from the formal point of view as the appearance of the cladding residual hoop strain corresponded to 90 cal/g of the peak fuel enthalpy at the narrow pulse (the same result was obtained in the BGR test (see Fig. 6.4). But as for the wide and slow pulse, this process was initiated at approximately 115 cal/g;
- the irradiated cladding was slightly sensitive to the cladding initial pressurization up to the cladding maximum hoop strain of 6.0% (the reference value). This strain was associated with the peak fuel enthalpies of 175 cal/g and 180 cal/g for the VVER pressurized fuel rods tested at the slow wide pulses and for the PWR unpressurized fuel rods tested at the fast narrow pulses, respectively;
- the sharp increase of the cladding strain caused by the effect of pressurization (the cladding gas loading) started at the peak fuel enthalpy of slightly higher than 175 cal/g, and the cladding rupture was observed in this case at the cladding strain of 9.5%;
- the gradual evolution of the cladding maximum residual strain without a rupture (from 6% up to 9.5%) characterized the behavior of unpressurized fuel rods tested in the range 180–195 cal/g of the peak fuel enthalpy.

The whole set of obtained data may be used for the analysis of the most interesting and difficult cases connected with the comparative interpretation of the high burnup fuel behavior basing on the test results obtained under the BGR and NSRR pulse conditions. The NSRR data were developed for this comparison using the following general principles:

- the test data characterizing the behavior of the PWR high burnup fuel rods with the low oxidized cladding were selected only from the total list of the appropriate NSRR tests [8–16];
- the upper boundary of the cladding oxidation in the selected PWR fuel rods was the same as that in the VVER fuel rods (15 μm , see Table 6.1).

Thus, in spite of the fact that the general range of the cladding oxidation in the PWR fuel rod was 2–60 μm (see Table 6.1), the set of rods used for the preparation of the data presented in Fig. 6.7 was limited by the range of 4–15 μm . The appropriate analysis performed at the next step of the NSRR data interpretation showed that before the RIA tests, the selected PWR fuel rods had variations in the following parameters:

- pressurization: 0.1 and 3.4–4.6 MPa;
- fuel burnup: 38.0–42.2 MWd/kg U and 46.0–50.0 MWd/kg U.

Taking into account these variations and the comments made earlier concerning the problem of regression correlations with the limited test data, several best fits and approximations were proposed to demonstrate the general physical tendencies revealed due to these tests. In accordance with this interpretation of the experimental results, the following comments can be suggested:

- the PWR high burnup fuel rods with the low oxidized Zry-4 cladding provide for the opportunity for the cladding strain without rupture up to very high values (15%, 25%)^a;
- it may be assumed that the PCMI type of the cladding loading provides for the main contribution in the cladding strain in the range of 0–5.5(6)% for all types of tested fuel rods;
- it seems that the pressurization effect has definite implications for the explanation of the cladding low strains also (in the range of 0–2%). But the appropriate experimental data may be the consequence of uncertainties caused by not so good accuracy in the low strain measurements;

^a All PWR fuel rods considered in Fig. 6.7 were unfailed in the NSRR tests

- it seems also that some effect connected with the increase of the cladding strain at the increase of fuel burnup from 40 MWd/kg U up to 50 MWd/kg U is observed.

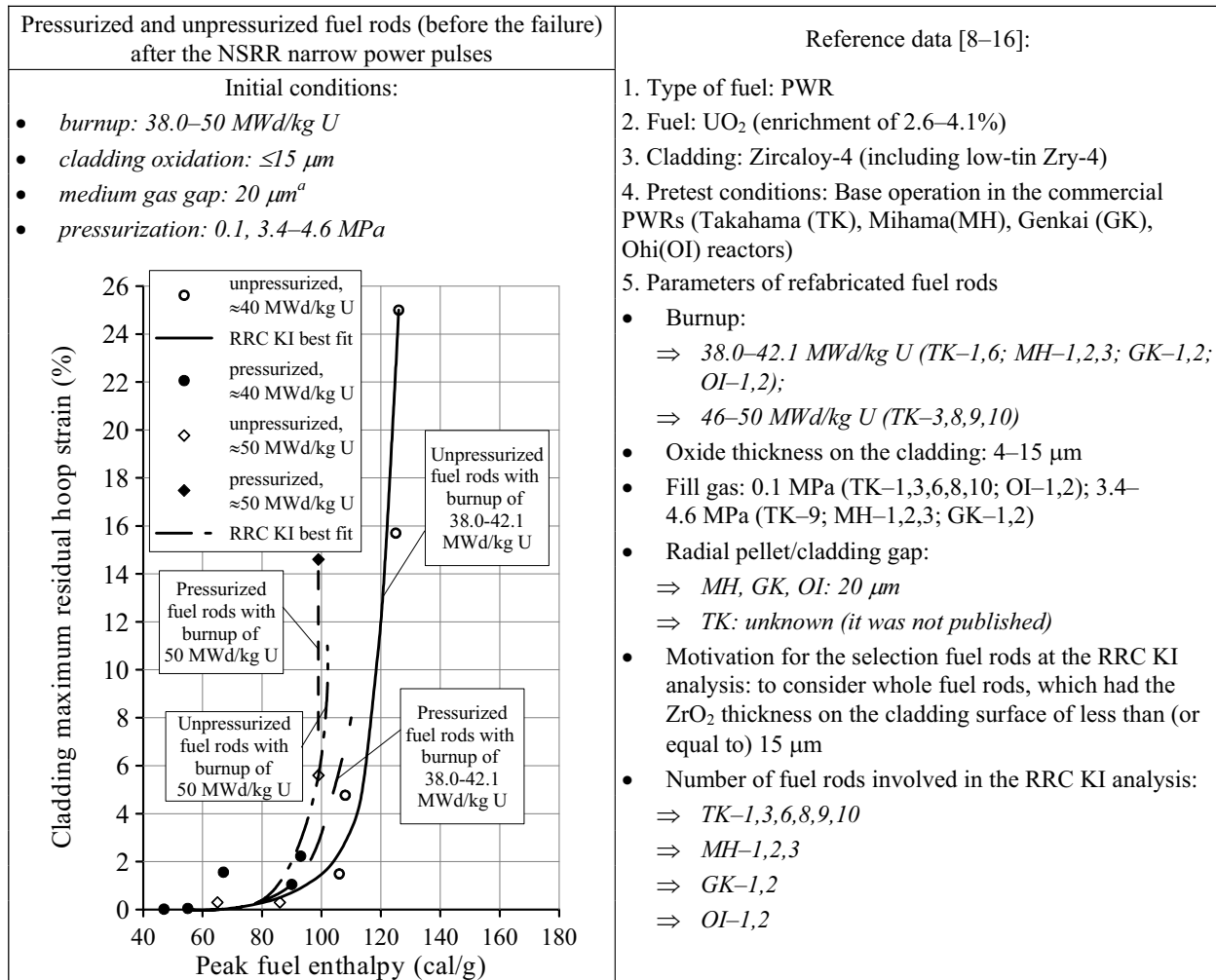


Fig. 6.7. Reference data and the RRC KI interpretation of the NSRR tests performed with the low oxidized PWR high burnup fuel rods

The comparison of these test results with the data characterizing the behavior of the JMTR fuel rods under the NSRR test conditions revealed two general effects:

1. Quite a different relationship between the cladding strain and the peak fuel enthalpy; for example: the cladding strain of 2% in the JMTR fuel rods was achieved at the peak fuel enthalpy of 160 cal/g but the same cladding strain in the refabricated PWR high burnup fuel rods correlates with the enthalpy range of 90–105 cal/g.
2. The pressurized and unpressurized PWR fuel rods demonstrate the tendency towards the sharp increase of the cladding strain in the enthalpy range of 100–120 cal/g. Moreover, careful post-test examinations performed by Japanese researchers show that the overstrain of the unpressurized fuel rod (25%) with burnup of 38 MWd/kg U (only) produces all indications of the PCMI type loading. But from the formal point of view, the only factor is varied if we compare this test result with the results of the JMTR fuel rod tests. This factor is the radial pellet/cladding gap: 85 μm and 20 μm in the tests of the JMTR and PWR fuel rods, respectively.

^a The gas gap in the TK type of fuel rods is unknown

Making an attempt to clarify the obtained results, the NSRR and BIGR test data were compared (see Fig. 6.8).

The first consideration of the presented comparative data aroused some bewilderment, which can be formulated in the form of the following question: why did high burnup fuel rods with the same fuel burnup ($\approx 50(40)$ MWd/kg U), with ductile claddings, and with the same radial pellet/cladding gap ($12\text{--}30\ \mu\text{m}$) tested at the same narrow pulse width ($2.5\text{--}9.3\ \text{ms}$) demonstrate the similar qualitative character of the cladding strain as a function of the peak fuel enthalpy at the significant difference between the critical fuel enthalpies corresponding to the sharp increase of the cladding strain ($>8\%$), that is, $100\text{--}115\ \text{cal/g}$ and $160\ \text{cal/g}$ for the NSRR and BIGR tests respectively?

Taking into account the experimental experience gained on solving the problems connected with the attempts to compare the test results obtained in different laboratories, the first answer to this question was as follows: it is necessary to compare the enthalpy effects on the basis of some other comparative test data. From the formal point of view, this comparison was performed on considering the IGR and NSRR test data presented in Fig. 6.6. But it is obvious that the effects of high burnup fuel were not so pronounced in these tests. Therefore, it was decided to compare the IGR, BIGR, and NSRR test data using the most representative indicator of the correlation between the fuel enthalpy and fuel response to the appropriate heating: the measured FGR was used as the indicator for this potential correlation dependence. The results of the appropriate investigations are demonstrated in Fig. 6.9.

In spite of the known problems connected with a relatively low accuracy of the FGR measurements, the obtained results showed that a good agreement was observed between the FGR (measured at the BIGR and NSRR narrow pulses) and the peak fuel enthalpy. After withdrawal of the problem connected with the representativity of the peak fuel enthalpy data, the next question may be formulated in the context of results presented in Fig. 6.8: What mechanism was responsible for the cladding strain in the NSRR tests of the PWR fuel rods? This question is especially urgent for the NSRR unpressurized fuel rods, which demonstrated the atypically large deformation. The analysis of the experimental results devoted to this issue resulted in the development of the comparative pictures illustrated in Fig. 6.10.

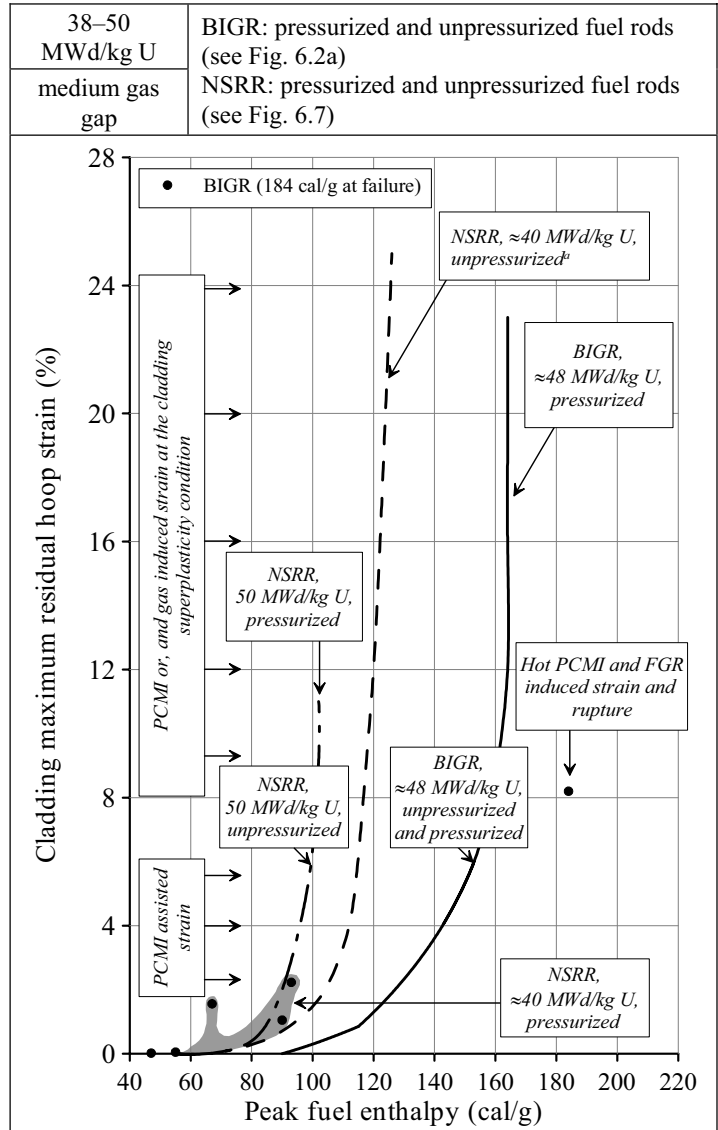


Fig. 6.8. The comparison of the VVER and PWR high burnup fuel rods behavior (fuel rods with the low oxidized cladding) under BIGR and NSRR narrow pulse conditions

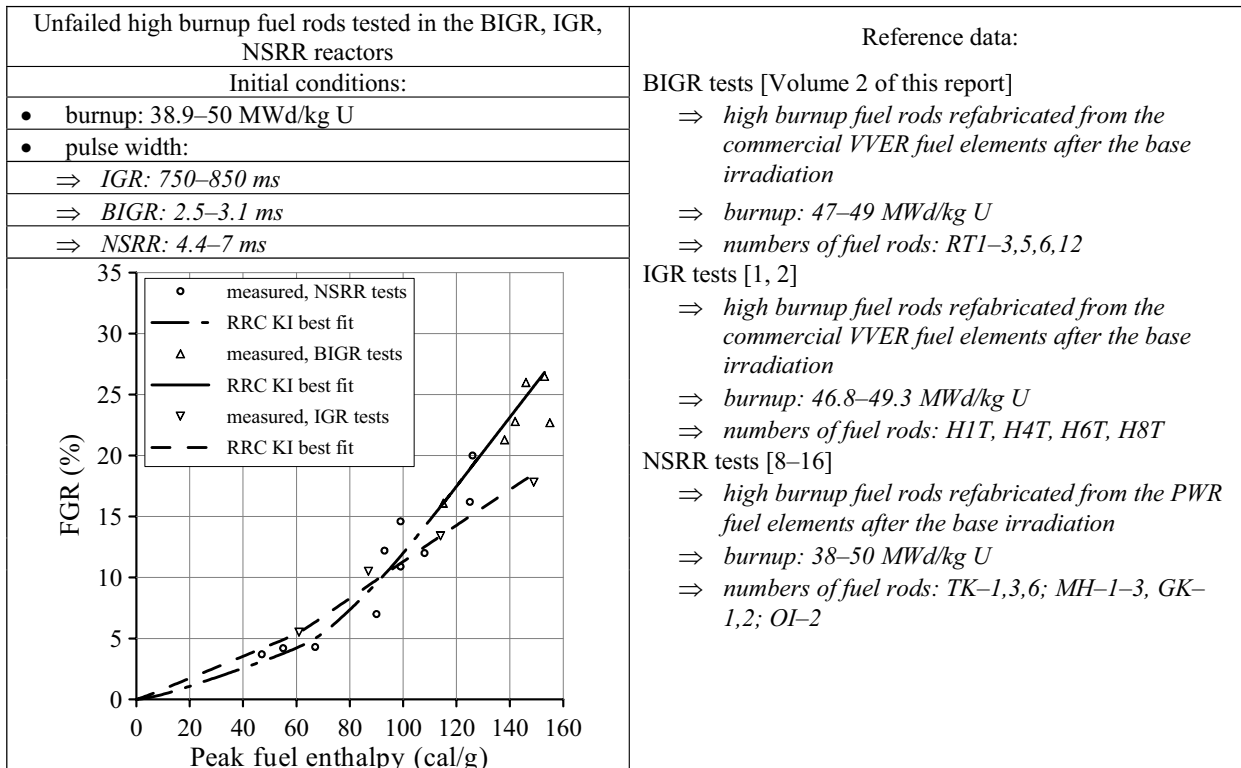


Fig. 6.9. Reference data and the RRC KI interpretation of the FGR in the VVER and PWR high burnup fuel rods tested under the IGR, BIGR, NSRR pulse conditions

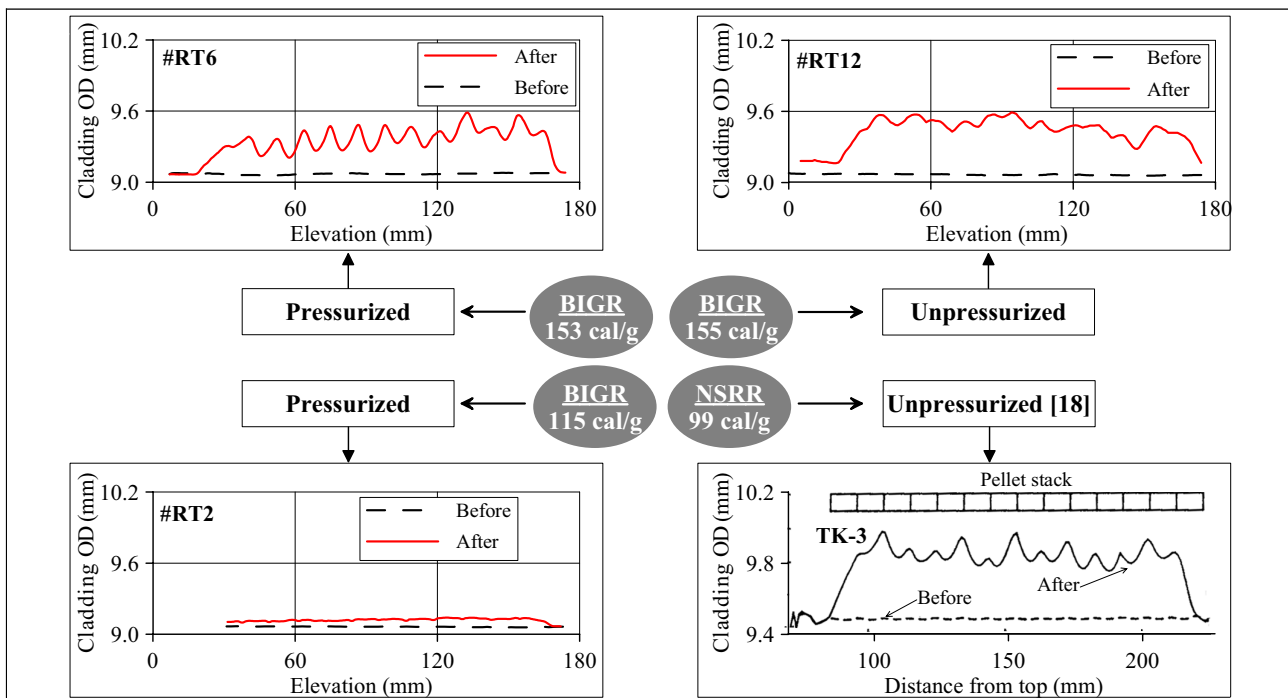


Fig. 6.10. Comparative data characterizing the cladding mechanical response at the BIGR and NSRR tests of the VVER and PWR high burnup fuel rods (≈50 MWd/kg U)

So, the most important fact observed systematically by Japanese researchers at the NSRR tests is the following: the axial distribution of the cladding outer diameter consists of the local maximums and minimums, which

alternated periodically along the fuel stack. In this case, maximums of the cladding outer diameter correspond to the middle parts of the fuel pellet (see Fig. 6.10) [19]. It seems that this fact correlates completely with the similar specific behavior of fuel rods tested in the BGR reactor (see Sections 5.4 and 5.5 of this volume of the report and Fig. 6.10). These comparative data show that the process of the local pseudo-ballooning formation at the RIA events^a is of quite the universal character for the ductile claddings. But in accordance with the data presented in Fig. 6.10, the following differences may be listed in the aspect of the BGR and NSRR comparison:

- the cladding residual hoop strain of the pressurized fuel rod tested in the BGR reactor at 115 cal/g was very small;
- the cladding residual hoop strain of the unpressurized fuel rod tested in the NSRR reactor at somewhat lower peak fuel enthalpy (99 cal/g) was significant (5.6%). This enthalpy caused the formation of the system of the local ballooning;
- the similar values of the cladding hoop strain (5.8–6%) were achieved in the BGR tests at the peak fuel enthalpy of 153–155 cal/g for both types of high burnup fuel rods: pressurized and unpressurized;
- moreover, the character of the cladding deformation of the unpressurized fuel rod tested in the NSRR reactor is more similar to the character of the cladding deformation of the pressurized fuel rod than to that of the unpressurized fuel rod tested in the BGR reactor.

Thus, the presented data allow the assumption that the same effects are responsible for the generation of pseudo-ballooning in these different fuel rods (of the VVER and PWR types) but these results do not answer both formulated earlier questions. Therefore, the next attempt was made to explain the revealed phenomena:

- it is known that if the response of some parameter is a function of the limited number of the key factors, the clear correlation will be observed between this parameter and each key factor with the reasonable variation of other key factors;
- in the given case, the parameter under consideration is the cladding residual hoop strain. The list of the key factors (at the same coolant conditions, approximately the same cladding ductility, fuel burnup, and pellet/cladding gap) contains the FGR (as the factor accumulating also such factors as the fuel temperature/fuel enthalpy), the pulse width, the cladding initial pressurization, and the fuel rod geometry;
- taking into account that the number of these factors is really limited and that the sensitivity of the cladding hoop strain to each of the above listed factors can be identified specially, it was decided to determine the cladding mechanical response to such key factor as the FGR at the following combination of other key factors: the VVER fuel rod design and the narrow pulse, the VVER fuel rod design and the wide pulse, the PWR fuel rod design and the narrow pulse. It was decided also to ignore the pressurization factor in this analytical investigation because it was assumed that this factor would be included in the obtained results automatically.

The results of this investigation are presented in Fig. 6.11. The developed approach provided quite interesting data, which demonstrated the clear relationship between the cladding strain and the FGR for all cases under consideration (the PWR/NSRR narrow pulse, the VVER/BGR narrow pulse, the VVER/IGR wide pulse). This fact confirmed that the FGR data was a good integral indicator of such parameters as the fuel temperature and fuel enthalpy. The analysis of three obtained regression correlations led to the following observations:

- in the studied range of test parameters, the cladding strain as a function of the FGR had a relatively low sensitivity to the pulse width at the same fuel burnup and fuel rod design;
- at the same fuel burnup and pulse width (the BGR/NSRR case), the significant increase of the PWR cladding strain was initiated at the FGR values far less than those occurring in the VVER cladding.

It is the next strange result because the FGR higher values correlate with the higher fuel temperature. Moreover, the fuel higher temperature must provide for the cladding higher temperature and the cladding high strain due to the increase of the cladding ductility. All these strange results generated a need to return to the analysis of the list

^a The same tendencies were observed in the IGR tests also. Moreover, this effect was observed in the BGR tests of the VVER unirradiated fuel rods

of the key factors being of importance for the consideration of the cladding mechanical response to the test conditions. The last unstudied factor presented in this list was the fuel rod design. As a rule, this factor was neglected on interpreting the appropriate data or at best, the pellet/cladding gap was used to characterize the design parameters of fuel rods. The same approach was applied to the presentation of the test results in the previous parts of this report. But the obtained strange disagreement between the BIGR and NSRR test data became the impulse for the consideration of the issues connected with the fuel rod design more carefully. The results of this consideration are organized in Table 6.2.

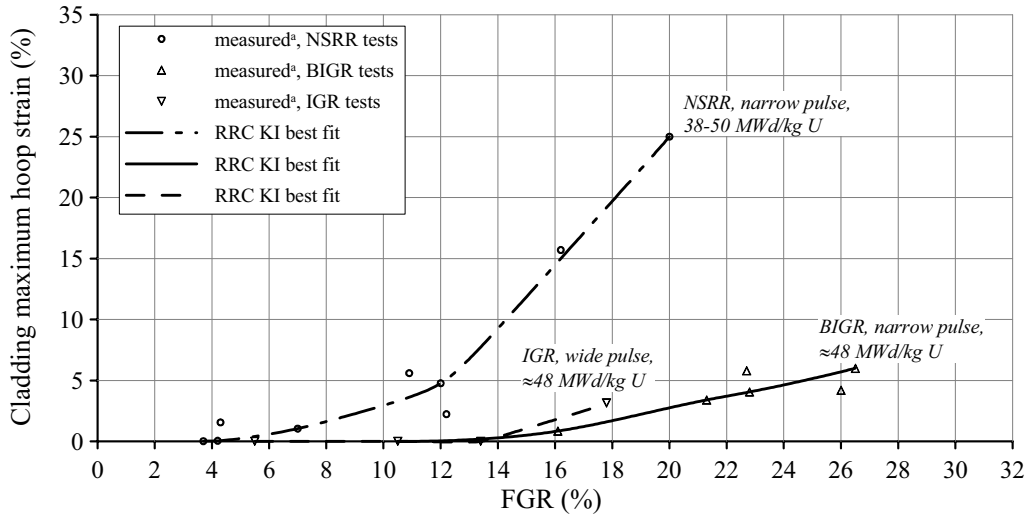


Fig. 6.11. The sensitivity of the cladding hoop strain to the fission gas release in accordance with the data of different pulse tests

Table 6.2. Some comparative data characterizing the design of the VVER and PWR high burnup fuel rods tested under the BIGR, IGR and NSRR pulse conditions

Fuel type	Fuel dimensions ^b			Cladding wall thickness (mm) ^b	Free gas volume (cm ³)
	OD (mm)	Diameter of central hole (d, mm)	Effective radius: (OD-d)/2 (mm)		
PWR (MH, GK, OI, TK) types of fuel rods (see Ref. data in Fig. 6.7 and additional data in [15])	9.29 (MH, GK types)	–	4.65	0.62	1.5 (plenum volume in MH and GK fuel rods)
	8.1 (OI type)	–	4.05		
	unknown (TK type)	–	unknown		
VVER–1000 (47–49 MWd/kg U) (see Volume 2 of the report)	7.57	2.4	2.59	0.69–0.70	6.0 (Total: plenum, gap, central hole)
VVER–440 (60 MWd/kg U) (see Volume 2 of the report)	7.56	1.65	2.96	0.69–0.70	6.0 (Total: plenum, gap, central hole)

^a NSRR data (○), IGR data (▽) and BIGR data (△) are corresponded with the test results described in Fig. 6.2, Fig. 6.3, Fig. 6.7, Fig. 6.9

^b as fabricated dimensions (before the base operation)

The preliminary analysis of the comparative data characterizing the design of the VVER and PWR test fuel rods shown that:

- the PWR fuel pellet OD was wider than that of the VVER fuel rod and taking into account that the VVER fuel pellets had a central hole (pellets of the annular type), the fuel real thickness along the fuel radius (the fuel effective radius) of the VVER fuel rods was less significant than that of the PWR fuel rods (2.59–2.96 mm and 4.05–4.65 mm, respectively);
- the cladding thickness in the PWR fuel rods was less than that in the VVER fuel rods;
- the free gas volume in the PWR fuel rods was also less significantly than that in the VVER fuel rods tested in the BGR and IGR reactors.

The revealed facts may be used as the basis for several logical assumptions.

So, at the same peak fuel enthalpy characterizing the specific energy generated in one gram of fuel during the RIA pulse, the absolute value of deposited energy in the PWR fuel will be higher than in the VVER fuel due to the above stated differences in the effective radii. In any case, this effect must lead to the cladding higher temperature in the PWR test fuel rod or, at the minimum, to the extension of the duration of film boiling^a. This explanation added with the contribution of the difference in the PWR and VVER cladding thicknesses is the first answer to the earlier formulated questions. The second assumption is connected with the effect of the central hole in the fuel pellet. The detailed comparative analysis of all NSRR and BGR data presented in this report and of the original data, which remained outside of the report (see, first of all, Fig. 6.8, Fig. 6.10, Fig. 6.11) leads to the understanding that a part of fission gases and of fill gas (contained in the empty volume of fuel rods) is removed from the fuel stack consisting of the annular pellets. The more significant gas plenum accompanying the VVER case of the narrow pulse tests was the additional factor for preventing the significant increase in the fuel rod pressurization at the end of the hot PCMI stage and at the beginning of the gas loading stage after the gas gap reopening. In this connection, it would be useful to report that in accordance with the obtained data, the maximum gas pressure in the PWR unpressurized fuel rod #TK-1 was about 2.5 MPa at the 2nd second of the NSRR test [14].

These observations have led to the necessity to perform the reconsideration of the comparative data presented in Fig. 6.8. This stage of the NSRR and BGR test data analysis suggested the following interpretation of disagreement effects revealed during the preliminary studies:

- in accordance with the data obtained in this research and in other previous investigations, the cold PCMI stage of the RIA tests is accompanied by the cladding hoop strain range of approximately 0–(1.5–2)%;
- due to the differences in the fuel effective radii, the PWR fuel with the larger radius produced (during the fuel swelling and thermal expansion) the higher fuel total pressure to the cold cladding in comparison with the VVER fuel, which has a relatively small fuel effective radius. These differences have led to the fact that the same PCMI assisted cladding strain is associated with the range of 50–100 cal/g of the peak fuel enthalpy for the PWR fuel and of 90–120 cal/g of the peak fuel enthalpy for the VVER fuel;
- moreover, it seems to be possible that the higher linear energy^b deposited by each PWR fuel pellet at the same peak fuel enthalpy provided the higher heat flux from fuel to the cladding and provided, respectively, the earlier initiation of the DNB conditions in comparison with the VVER fuel. This explanation allows an understanding of the reason of the earlier start of the hot PCMI stage in the NSRR test histories in comparison with the BGR test histories (the start of the hot PCMI stage corresponds to the inflection points of the NSRR regression correlations (1.5–2.0% of the cladding strain);

^a In accordance with the temperature measurements, the cladding temperature in the NSRR tests with the cladding high residual hoop strain was not so high: 600 C at the maximum for the fuel rod with the cladding strain of 25% (TK-1) and 700 C at the maximum for the fuel rod with the cladding strain of 5.6% (TK-3) [15]. But taking into account the general problems of the temperature measurements under these conditions, it seems that too much should not be made of the results of performed measurements

^b Linear energy is the fuel energy in 1 cm(m) of the fuel stack length

- it can be assumed with some degree of certainty that the standard hot PCMI stage of the cladding loading is connected with (1.5–2)–6% of the cladding hoop strains for both types of tests (BIGR and NSRR). The sharper increase of the cladding strain in a very narrow range of the peak fuel enthalpy observed for the PWR fuel rods in comparison with the VVER fuel rods is probably connected with the central hole effect. Because the whole volume of fission gases deposited before and generated during the RIA test and the whole volume of fill gas localized in the fuel microplenum (cracks, defects, pellet interfaces etc.) are involved into the process of the fuel swelling during the hot PCMI stage in the case with the PWR fuel rods consisted of the solid pellets without the central hole. As for the VVER annular pellets, a part of these gases concentrated in the microplenum directly connected with the central hole is not involved in the fuel swelling due to the relatively low hot gas pressure in the central hole (not higher than 3.0 MPa). Due to this effect, the cladding strain is not so sensitive to the peak fuel enthalpy for the VVER fuel rods;
- it should be especially emphasized that the cladding mechanical behavior both for the VVER fuel rods and for the PWR fuel rods at the cladding strain higher than 6% could be accompanied by two different processes:

1. At the relatively slow and minor increase of the peak fuel enthalpy, the effect of super sensitivity of the cladding strain as a function of the peak fuel enthalpy is observed. (A small bit of the additional enthalpy has led to the burst increase of the cladding strain from 6% up to 15–25%.) This case was called as the PCMI induced or and the gas induced strain at the cladding superplasticity condition illustrated in Fig. 6.8. This special case introduced in the analysis of the RIA specific effects is based on the establishment of the correlation relationship between the following phenomena:

- ⇒ numerous RIA type tests performed with different fuel rods under different test conditions demonstrated on occasion the appearance of untypical very high cladding hoop strains;
- ⇒ the numerous uniaxial and biaxial tests performed with the VVER and PWR unirradiated or irradiated (low oxidized) claddings showed that the super high cladding strain can be observed at the definite combination of the cladding temperature and strain rate. Moreover, there are grounds to believe that this effect in the Zircaloy cladding corresponds to the end of the α -phase temperature range. The Zr-1%Nb (E110) cladding demonstrated the same effect at the beginning of the α - β phase temperature range^a.

Thus, the previous investigations showed that the sharp decrease of the cladding strength accompanied by the sharp increase of the cladding strain is observed at the definite (for each cladding) combination of the test conditions. This explanation fully agreed with the obtained BIGR and NSRR data for the case with the super high cladding strains.

2. As for the second process, this case is presented in Fig. 6.8 as one point characterizing the VVER cladding hoop strain (8.2%) at the fuel enthalpy at failure of 184 cal/g (#RT11). But the regularity of the appearance of this case can be illustrated by the similar data presented in Fig. 6.2–Fig. 6.4. This second process is characterized by the peak fuel enthalpies, which exceed significantly the failure threshold. It is clear that the cladding rupture in this case occurs under the conditions when the fuel temperature increase rate is observed. Both of these factors provide for two effects:

- a. The gas gap reopening does not occur as the hot PCMI stage continues to define the cladding strain.
- b. The cladding deformation is accompanied by the more or less significant strain rate.

These factors led to the following remarkable results: all these fuel rods failed at the lower cladding hoop strain than the fuel rods considered in the Item 1 of this analysis.

The confirmation of general tendencies revealed in the comparative analysis of the BIGR and NSRR results can be found in the comparative analysis of the BIGR test data obtained for the VVER fuel rods with the burnup of 47–49 and 60 MWd/kgU (see Fig. 6.12).

^a The appropriate phenomena concerning the VVER cladding can be inspected using the results of mechanical tests presented in [2, 20]. The considerations presented in the analysis of the data in Fig. 5.48 of this volume of the report can be used also taking into account the following adjustment: the sharp decrease of the cladding strength properties in the narrow temperature range corresponds to the sharp increase of the cladding ductility (the cladding strain)

These BGR data showed that the cladding mechanical behavior of the VVER fuel rods with burnup of 60 MWd/kg U and, consequently, with the higher fission gas effect became closer to the NSRR behavior of the PWR fuel rods with burnup of 40–50 MWd/kg U in the part concerning the cold PCMI. The appropriate tendency was pronounced in the decrease of the peak fuel enthalpies associated with the generation of the cladding hoop strain in the range of 1–2% at the cold PCMI stage of the BGR test, while the disappearance of the gas gap in these fuel rods was the next factor, which provided for the higher stress in the cladding of fuel rods with burnup of 60 MWd/kg U in comparison with the cladding stresses induced by the cold PCMI in fuel rods with burnup of 47–49 MWd/kg U. But if we revert to the consideration of the BGR and NSRR comparative results, it should be noted that the difference in the behavior of the PWR fuel rods with burnup of 40–50 MWd/kg U and of the VVER fuel rods with burnup of 60 MWd/kg U continued to be observed at the enthalpies higher than approximately 100 cal/g because the cladding strain corresponding to the end of the standard PCMI stage of the cladding loading (5–6%) was achieved at the following comparative parameters:

- the VVER fuel rod with burnup of 60 MWd/kg U: 5.5% of the cladding strain at 125 cal/g (#RT4);
- the PWR fuel rod with burnup of 50 MWd/kg U: 5.6% of the cladding strain at 99 cal/g (TK-3);
- the PWR fuel rod with burnup of 39.2 MWd/kg U: 4.77% of the cladding strain at 108 cal/g (OI-2).

These results are in the agreement with the above-formulated hypothesis concerning the role of the fuel design and, especially, concerning the importance of the central hole as a factor to minimize the fission gas contribution to the cladding stress under the RIA conditions. In addition to effects corresponding to the standard PCMI stage of pulse tests, the data presented in Fig. 6.12 continue the discussion of issues, which reflect the behavior of the VVER high burnup rods at the peak fuel enthalpies higher than the failure threshold. This stage of the analysis is of the fundamental importance as well as of the practical importance because these tests data outline the problems connected with the fuel rod fragmentation. The organized file of experimental points characterizing the cladding strain of fuel rods with burnup of 47–49 and 60 MWd/kg U, which failed at the peak fuel enthalpy higher than 164 cal/g indicates that:

- there are no general differences in the mechanical behavior of these fuel rods as a function of burnup and pressurization;
- all fuel rods with burnup of 60 MWd/kg U have demonstrated the tendency towards the multirupture behavior of the failed cladding as well as the fuel rods with burnup of 50 MWd/kg U tested at the peak fuel enthalpy in the range of 187–252 cal/g under the IGR wide pulse conditions;

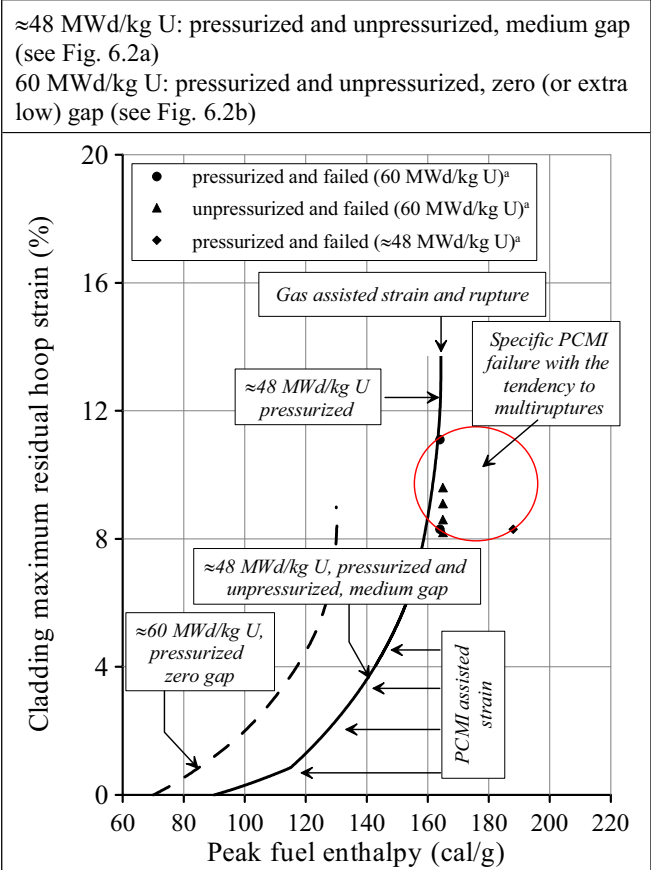


Fig. 6.12. The sensitivity of the mechanical behavior of the VVER low oxidized irradiated cladding to the fuel burnup under the BGR narrow pulse conditions

^a All these data are presented for the peak fuel enthalpy because the enthalpy at failure was not calculated for the fuel rods with burnup of 60 MWd/kg U

- the BIGR and IGR test data have revealed that the fragmentation of fuel rods was not observed up to the following enthalpies:
 - ⇒ the narrow pulse and 47–49 MWd/kg U: 188 cal/g;
 - ⇒ the wide pulse and 47–49 MWd/kg U: 252 cal/g;
 - ⇒ the narrow pulse and 60 MWd/kg U: 165 cal/g.

Unfortunately, this topic is the last analytical position considered in this report. Such important phenomena as listed below remained beyond the range of discussed issues:

- the representativity of obtained test data in the context of the real RIA cases;
- the sensitivity of test results to the cladding oxidation;
- the development of recommendations concerning the improvement of the code modeling for the RIA type tests.

But it can be assumed that these and other unconsidered aspects of the BIGR tests will be reflected in the future publications.

References

- 1 V. Asmolov, L. Yegorova “The Russian RIA Research Program: Motivation, Definition, Execution, and Results”, *Nuclear Safety*, Vol.37, No.4, 1996.
- 2 L. Yegorova, V. Asmolov, G. Abyshov, V. Malofeev, A. Avvakumov, E. Kaplar, K. Lioutov, A. Shestopalov, A. Bortash, L. Maiorov, K. Mikitiouk, V. Polvanov, V. Smirnov, A. Goryachev, V. Prokhorov, and A. Vurim “Data Base on the Behavior of High Burnup Fuel Rods with Zr-1%Nb Cladding and UO₂ Fuel (VVER Type) under Reactivity Accident Conditions”, *NUREG/IA-0156 (IPSN99/08-02, NSI/RRC KI 2179)*, Vol.1, 2, 1999.
- 3 J. Papin, M. Balourdet, F. Lemoine, F. Lamare, J. Frizonnet, and F. Schmitz “French Studies on High Burnup Fuel Transient Behavior under RIA Conditions”, *Nuclear Safety*, Vol.37, No.4, 1996.
- 4 F. Schmitz, J. Papin “High Burnup Effects on Fuel Behavior under Accident Conditions: the Test CABRI REP-Na”, *J. Nucl. Mater.*, No.270, 1999.
- 5 F. Lemoine “High burnup fuel behavior related to fission gas effects under reactivity initiated accidents (RIA) conditions”, *J. Nucl. Mater.*, No.248, 1997.
- 6 T. Fujishiro, K. Yanagisawa, K. Ishijima, and K. Shiba “Transient Fuel Behavior of Preirradiated PWR Fuels Under Reactivity Initiated Accident Conditions”, *J. Nucl. Mater.*, Vol.188, 1992.
- 7 T. Fuketa, Yu. Mori, H. Sasajima, K. Ishijima, and T. Fujishiro “Behavior of High Burnup PWR Fuel under a Simulated RIA Condition in the NSRR”, OECD Specialist Meeting on Transient Behavior of High Burnup Fuel, September 12–14, 1995, Cadarache, NEA/CSNI/R(95)22, 1996.
- 8 T. Fujishiro, K. Ishijima “NSRR Experiments to Study the Effects of Burnup on the Fuel Behavior under Reactivity Initiated Accident Conditions”, *Proc. of 22nd WRSN, NUREG/CP-0140*, Vol.2, 1994
- 9 T. Fuketa, H. Sasajima, Yo. Tsuchiuchi, Yu. Mori, T. Nakamura, K. Ishijima “NSRR/RIA Experiments with High Burnup PWR Fuels”, *Proc. of International Topical Meeting on Light Water Reactor Fuel Performance*, March 2–6, Portland, Oregon, 1997.
- 10 T. Sugiyama, T. Fuketa “Mechanical Energy Generation during High Burnup Fuel Failure under Reactivity Initiated Accident Conditions”, *J. Nuclear Science and Technology*, Vol.37, No.10, 2000.
- 11 T. Fuketa, H. Sasajima, Yu. Mori, K. Ishijima “Fuel Failure and Fission Gas Release in High Burnup PWR Fuels under RIA Conditions”, *J. Nucl. Mater.*, Vol.248, 1997.
- 12 T. Fuketa, F. Nagase, K. Ishijima, and T. Fujishiro “NSRR/RIA Experiments with High Burnup PWR Fuels”, *Nuclear Safety*, Vol.37, No.4, 1996, pp.328–342.

- 13 T. Nakamura, H. Sasajima, T. Fuketa, K. Ishijima “Fission Gas Induced Cladding Deformation of LWR Fuel Rods under Reactivity Initiated Accident Conditions”, *J. Nuclear Science and Technology*, Vol.33, No.12, 1996.
- 14 H. Sasajima, T. Nakamura, T. Fuketa, H. Uetsuka “Fission Gas Release Behavior of High Burnup UO₂ Fuel under Reactivity Initiated Accident Conditions”, *J. Nuclear Science and Technology*, Vol.36, No.11, 1999.
- 15 T. Fuketa, H. Sasajima, and T. Sugiama “Behavior of High-Burnup PWR Fuels with Low-Tin Zircaloy-4 Cladding under Reactivity-Initiated-Accident Conditions”, *Nuclear Technology*, Vol.133, No.1, 2001.
- 16 T. Nakamura et al. “NSRR RIA Tests Results and Experimental Programmes”, *Proc. of the Topical Meeting on RIA Fuel Safety Criteria*, Aix-en-Provence, France, 13–15 May 2002 (NEA/CSNI/R(2003)8/ Vol.2).
- 17 R. Meyer, R. McCardell, H. Chung, D. Diamond, and H. Scott “A Regulatory Assessment of Test Data for Reactivity-Initiated Accidents”, *Nuclear Safety*, Vol.37, No.4, 1996.
- 18 H. Uetsuka “Recent of Fuel Safety Research at JAERI”, *Proc. of the 23rd NSRR Review Meeting*, Tokyo, November 11–12, 1999.
- 19 K. Ishijima “Current Status of the NSRR Experiments with High Burnup LWR Fuels”, *Proc. of the First CABRI Technical Review Meeting*, Cadarache, France, 7–9 July, 1998.
- 20 E. Kaplar, L. Yegorova, K. Lioutov, A. Konobeyev, N. Jouravkova, A. Goryachev, V. Prokhorov, S. Yeremin, A. Svyatkin “Mechanical Properties of Unirradiated and Irradiated Zr-1%Nb Cladding”, RRC “Kurchatov Institute” report NSI RRC 2241, 2001 (also USNRC report NUREG/IA-0199 and IPSN report IPSN 01-16).

7. SUMMARY

A special test program was developed and implemented with the use of the BGR reactor to study the behavior of the VVER high burnup fuel rods under the narrow pulse conditions simulating the reactivity initiated accident. This chapter of the report contains the brief characterization of tested fuel rods, test conditions, test results and findings obtained due to the comparison of the BGR data with the data of other similar test programs.

1. Twelve test fuel rods refabricated from the commercial VVER-440 and VVER-1000 fuel elements irradiated under the base operation conditions up to burnup of 47–49 MWd/kg U and 60 MWd/kg U were tested in the BGR test reactor at power pulses with the width of 2.5–3.1 ms. The test fuel rods were placed in the capsule devices containing the stagnant water at the room temperature and atmospheric pressure. The range of the peak fuel enthalpy variations was 115–188 cal/g for fuel rods with burnup of 47–49 MWd/kg U and 125–165 cal/g for fuel rods with burnup of 60 MWd/kg U.
2. To provide the given range of the peak fuel enthalpy, the BGR reactor was modified. After that, special scoping tests and analytical investigations were performed to develop and to validate the procedures for the determination of such important parameters as: spatial and time dependent distributions of the fuel rod power, the correlation between the fission numbers in the VVER high burnup fuel and the energy deposition in the BGR reactor. The pre-test examinations and special radiochemical investigations were performed to develop the input data characterizing the geometry, fuel isotopic composition and microstructure of the VVER fuel rods before the BGR tests. In particular, it was revealed that the irradiated Zr-1%Nb (E110) cladding of high burnup fuel rods had the low outer oxidation (3–5 μm) and low hydrogen content (60–80 ppm by weight). It was also revealed that the cladding of fuel rods with burnup of 60 MWd/kg U had the inner oxidation (8–10 μm), and the bonding layer provided the direct pellet/cladding contact.
3. To develop the procedures for the energy deposition and fuel enthalpy determination in the high burnup fuel rods tested in the BGR reactor, a special cycle of experimental and analytical investigations was performed. Finally, two independent neutronic codes were used (in addition to the test data) for the determination of spatial and time dependent distributions of energy deposition in each tested fuel rods. Two independent thermal mechanical codes (verified especially for these test conditions) were also used for the determination of spatial and time dependent distributions of fuel enthalpy in twelve high burnup fuel rods. To provide the opportunity for the future independent calculations (including the verification of other computer codes on the basis of the BGR test data), the whole set of required test parameters characterizing fuel cycles of the VVER commercial fuel elements and the test data characterizing the parameters of test high burnup fuel rods before and after the BGR pulses were developed.
4. To provide the basis for the analysis of the high burnup fuel behavior as a function of fuel burnup, initial cladding pressurization and the peak fuel enthalpy, the post-test examinations of each tested fuel rod were performed. The typical list of these examinations included the following: the measurement of the cladding outer diameter in 16 azimuthal positions, the measurement of the fission gas release (FGR) in unfailed fuel rods, the γ -scanning and eddy-current examinations, the preparation of several metallographic samples characterizing the geometry and microstructure of tested fuel rods, the measurements of the cladding oxidation and azimuthal distribution of the cladding thickness.
5. The analysis of the test data characterizing the high burnup fuel behavior under the narrow pulse conditions revealed the following general effects:
 - The fuel structure along the radius consisted of three zones (inner, intermediate, peripheral):
 - ⇒ the inner (dark) zone demonstrated (at the enthalpy increase) the significant grain separation of the tangential type and the grain boundary opening caused by the temperature overpressurization of intergranular fission gas bubbles and by the fuel microcracking (due to the thermal expansion effect);
 - ⇒ the intermediate zone was formed between the inner zone with high compression stresses and the peripheral zone with high tensile stresses. Due to this fact, this zone had the uniform grains and uniform grain boundary separation as a function of the fuel enthalpy;
 - ⇒ high tensile stresses provided for the radially-pronounced grain separation and radial gas tunnels formation in the fuel peripheral zone at the fuel enthalpy increase. The numerous macroscopic cracks appeared in this zone. The gradual decrease in the grain size from the as-fabricated down to fine subgrains

in the rim layer was a specific feature of this zone. The tendency of the grain size decrease was accompanied by the tendency towards the gas porosity increase and towards the increase of plutonium concentration. In accordance with this systematization, the rim layer was considered as the outer part of the peripheral fuel zone;

⇒ the fuel structure with burnup of 60 MWd/kg U had one more zone, which was associated with the bonding layer between fuel and the cladding.

- The fuel mechanical behavior was accompanied by the following specific effects:

⇒ the radial cracking of the fuel peripheral layer, the separation and fragmentation of the rim layer were observed in all tested fuel rods. The scale of these effects was a direct function of the peak fuel enthalpy and fuel burnup;

⇒ the pronounced grain separation, which was enhanced at the increase of the fuel enthalpy, characterized the fuel matrix (the inner and intermediate zones);

⇒ the bonding layer provided for some features in the behavior of fuel rods with burnup of 60 MWd/kg U. At the stage of the gas gap reopening (this stage was observed in these fuel rods as the result of the cladding plastic hoop strain in spite of the gas gap absence before the test) the cladding was separated from fuel together with the bonding layer and fragments of the rim layer;

⇒ no melting was observed in the tested fuel up to 188 cal/g^a.

- The analysis of the FGR assisted phenomena suggests that:

⇒ an increase of the FGR from 16.1 up to 26.5% was measured at peak fuel enthalpy in the range of 115–155 cal/g in the unfailed fuel rods with burnup of 47–49 MWd/kg U;

⇒ the grain boundary separation, the formation of the tangential interconnected cracks in the inner fuel zone, the radial cracking of the peripheral zone accompanied by the fragmentation of the rim layer (which provides for the significant contribution in the total FGR) were responsible for the fission gas yield in the gas plenum at these superfast processes.

6. After the detailed studies of the cladding mechanical behavior under the BIGR test conditions, it was concluded that:

- the formation of local interconnected ballooning along the cladding length was the most important phenomenon observed in these tests;

- the careful experimental investigations showed that the axial distribution of local maximum strains (ballooning centers) corresponded to the mid-region of fuel pellets. Strain minimums were located near the fuel pellet-to-pellet interfaces;

- the combination of two causes may be responsible for the observed phenomena:

⇒ the barrel shape of fuel pellets formed at the early PCMI stage and resulted in the similar cladding plastic strain;

⇒ the nonuniformity of axial distribution of fission numbers (due to the decrease of fuel mass at the pellet interfaces) led to a nonuniform axial cladding temperature distribution during the narrow pulse. This nonuniformity may also occur when the radial heat flux defines the local cladding temperature and when local departure from nucleate boiling affects cladding temperatures. The regular alternating local maximums and minimums of the cladding temperature led to the formation of a specific sinusoidal form in the cladding strain along the length;

- the consideration of appropriate issues demonstrated that the fission gases generated during the hot PCMI stage of the BIGR tests provided for the cladding specific gas loading and formation of the local balloonings. Nevertheless, the higher fuel swelling in the middle of each fuel pellet made a certain contribution into this process;

^a Melting was observed at 252 cal/g in accordance with the IGR data

- the processing of the multidimensional profilometry data shown that the cladding plastic strain in the fuel rods with burnup of 47–49 MWd/kg U was insignificant to the peak fuel enthalpy of 115 cal/g (0.85% at the maximum). At the increase of the fuel enthalpy from 138 cal/g up to 153 cal/g, the cladding maximum residual hoop strain increased from 3.4% up to 6% (without the cladding rupture). In this range of the peak fuel enthalpy, there were no general differences in the mechanical behavior of pressurized and unpressurized fuel rods with burnup of 47–49 MWd/kg U. The cladding strain was sensitive to the increase of fuel burnup up to 60 MWd/kg U. The cladding maximum residual hoop strain of 5.5% was fixed at 125 cal/g of the peak fuel enthalpy;
- the cladding rupture effects in failed fuel rods can be characterized by the following features:
 - ⇒ the ductile type of the cladding rupture was noted for all cases of the fuel rod failure. This conclusion was made taking into account the fact that the necking process accompanied the cladding strain before the rupture;
 - ⇒ the maximum cladding strain revealed in the tested fuel rods was 18.9%;
 - ⇒ the cladding strain of 8% was estimated as the critical value before the rupture.

7. The following key phenomena, mechanisms and thresholds were determined for the failed fuel rods:

- Failure of tested fuel rods occurred only at high enthalpy. This finding was validated by the method of the progressive increase of the test enthalpy from rod to rod. Thus, the cold PCMI stresses were not critical for the low oxidized ductile cladding.
- The mechanical behavior of pressurized and unpressurized fuel rods with burnup of 47–49 MWd/kg U was approximately the same up to the peak fuel enthalpy of 153–155 cal/g, the maximum cladding strain in the local ballooning achieved 5.5–6%. The cladding loading was caused by the hot PCMI stage assisted with the fission gas loading and with the formation of the local ballooning system in the cladding hot areas. At seven percent increase of the peak fuel enthalpy (up to 164 cal/g), the cladding strain in the pressurized fuel rod increased sharply and the failure threshold was transcended (the cladding rupture occurred). The analysis of experimental data showed that the gas loading after the gas gap reopening was responsible for the failure mechanism of this pressurized fuel rod with burnup of 47.0 MWd/kg U. Thus, the peak fuel enthalpy of 160 cal/g can be considered as the failure threshold for this type of the fuel rod. There is certainty that the failure threshold of unpressurized fuel rods with burnup of 47–49 MWd/kg U will be significantly higher. But taking into account that this threshold was not determined experimentally, the peak fuel enthalpy of 160 cal/g can be used as a very conservative evaluation of the appropriate threshold. The important data for the characterization of the failure mechanisms of fuel rods with burnup of 47–49 MWd/kg U were obtained due to the test at 188 cal/g of the peak fuel enthalpy. Results of this test revealed that:
 - ⇒ the fragmentation of these fuel rods did not occur up to 188 cal/g;
 - ⇒ the mechanism of the fuel rod failure was somewhat changed at the test with the peak fuel enthalpy, which exceeded significantly the failure threshold (160 cal/g).

As for this case, the failure of the pressurized fuel rod occurred at the hot PCMI stage of the test, and the cladding loading was accompanied by the high strain rate. The combination of these effects led to the typical sinusoid type retention of the cladding hoop strain up to this high enthalpy. The critical strain at failure (8.2%) was lower significantly than that at the slower loading before the failure (18.9% as maximum at 164 cal/g).

- Quite unique results were developed for the characterization of the failure features in the fuel rods with burnup of 60 MWd/kg U. The unpressurized and pressurized fuel rods with this burnup were found failed after the tests with the same peak fuel enthalpy of 164–165 cal/g. Moreover, both of these fuel rods demonstrated the formation of the similar systems of connected ballooning distributed along the claddings. Several cladding ruptures at the strains of 8.2–11.1% were observed in each fuel rod. These results showed that the failure of fuel rods occurred at the hot PCMI stage of the tests. The fission gas generation was the key factor causing the cladding rupture. Taking into account that a large interval took place between the maximum peak fuel enthalpy in the unfailed fuel rod (125 cal/g) and the peak fuel enthalpy in the failed fuel rods (164–165 cal/g), a special analysis was performed to assess the failure thresholds of fuel rods with burnup of 60 MWd/kg U. In accordance with the analysis results, the following values of the peak fuel enthalpies were determined as the conservative evaluations of the appropriate thresholds:

- ⇒ 130 cal/g for the pressurized fuel rods;
- ⇒ 140 cal/g for the unpressurized fuel rods.

8. To compare the BIGR results with the results of other RIA-type tests, the test data were reassessed on the basis of the following research programs:

- the IGR program (Russia) performed with the VVER high burnup fuel rods, which were tested at the wide pulse conditions (750–850 ms) [1];
- the NSRR program (Japan) performed with the PWR high burnup fuel rods, which were tested at the narrow pulse conditions (4.4–9.3 ms) [2].

One important program, the CABRI program [3] was not considered in the current analysis because of two important facts:

- most CABRI tests were performed with the fuel rods, that had high oxidation and hydriding of the irradiated cladding;
- sodium coolant at 280 C was used in the CABRI tests in contrast to the BIGR, IGR and NSRR tests. This difference did not allow the direct comparison of the CABRI test results with the results of other tests.

In the context of the coolant problem, it should be noted that the same approach accompanying the BIGR, IGR and NSRR test programs (the capsule device with the stagnant water at the room temperature and the atmospheric pressure) was used for the location of the high burnup fuel rods before the pulse test.

8.1. The comparative analysis of these test program results clarified the following effects:

- the pulse width decrease from 750–850 ms (the IGR pulses) down to 2.5–3.1 ms (the BIGR pulses) led to the equidistant shift to the left by 10–15 cal/g in the regression correlation characterizing the cladding maximum hoop strain as a function of the peak fuel enthalpy. In other words, the regression correlations developed for the BIGR narrow and fast pulses and for the IGR wide and slow pulses had the similar shape. But the same cladding hoop strain was achieved for the BIGR tests at the peak fuel enthalpy, which was lower by 10–15 cal/g than that for the IGR tests. Moreover, as it was reported earlier, the failure threshold was insensitive to this difference with the accuracy of the test data;
- both types of the test programs (the IGR and BIGR ones) showed that the tests with high burnup fuel rods at the peak fuel enthalpies higher significantly than the failure threshold led to the fact that the hot PCMI stage became responsible for the cladding rupture independently of the cladding initial pressurization. In this case, the cladding hoop strain at rupture was always lower than that in the case, which corresponded to the failure threshold;
- the continuation of studies devoted to the sensitivity of the mechanical behavior of the irradiated cladding to the pulse width was performed for the case, which can be considered as the background for the understanding of the multidimensional and multiconnected space outlining the high burnup fuel phenomena. This case was presented by the JMTR type (approximately the PWR type) of fuel rods (with the low oxidized Zircaloy-4 cladding and fuel with burnup of 15–38 MWd/kg U), which were tested under NSRR narrow pulse conditions and the VVER fuel rods with the irradiated Zr-1%Nb cladding and unirradiated fuel, which were tested under IGR wide pulse conditions. Thus, this case allowed the additional assessment of the pulse width effect. The appropriate comparison showed that the mechanical behavior (the cladding hoop strain) of low oxidized Zircaloy-4 and low oxidized Zr-1%Nb claddings was insensitive to the pulse width (in the range of the peak fuel enthalpy of 80–170 cal/g) at the minimization of high burnup fuel effects provided by the wide gas gap (70–90 μm) and by low or zero burnup.

8.2. The direct comparison of the VVER and PWR high burnup fuel rod behavior tested under the BIGR and NSRR narrow pulse conditions was performed under the following boundary conditions:

- the comparison was carried out for the fuel rods with the same (approximately) burnup: 40–50 MWd/kg U in the PWR fuel rods and 47–49 MWd/kg U in the VVER fuel rods;
- the fuel rods with the low oxidized cladding (4–15 μm) were selected from the NSRR test data for these comparative studies.

8.3. The analysis of obtained comparative data revealed the following:

- the same general tendencies accompanied the cladding mechanical behavior of the VVER and PWR fuel rods tested under the BIGR and NSRR narrow pulse conditions: the formation of local connected ballooning distributed along the cladding length at the cladding hoop strain in the range of 0–6%, the supersensitivity of the cladding strain to the peak fuel enthalpy, when the failure threshold was approached (the maximum cladding residual strain before the rupture was 18.9% for the Zr-1%Nb cladding and 25% for the Zry-4 cladding), the absence of general difference in the behavior of pressurized and unpressurized fuel rods in the range of the cladding hoop strain up to 6%;
- but as for the absolute dependence between the cladding hoop strain and peak fuel enthalpy, the following differences were revealed:
 - ⇒ the initiation of the cladding plastic flow in the PWR fuel rods occurred at the lower fuel enthalpy than at that in the VVER fuel rod (65 cal/g and 90 cal/g, respectively);
 - ⇒ the achievement of high residual strain of 6% approximately (this event preceded to the process of the sharp increase of the cladding strain associated with the failure threshold) was observed at 90–110 cal/g and 150 cal/g of the peak fuel enthalpy in the PWR and VVER fuel rods, respectively;
 - ⇒ the analysis of reasons, which could cause the disagreement between the PWR and VVER high burnup fuel rod behavior under the narrow pulse conditions showed that most probably this was the result of differences in the fuel rod design. Due to the lower effective fuel radius and the central hole, the hot PCMI effects connected with the significant cladding plastic strain occurred in the VVER fuel rods at the higher peak fuel enthalpy than at that in the PWR fuel rods.

9. The comparative considerations of the VVER fuel behavior sensitivity to the increase of fuel burnup from 47–49 MWd/kg U up to 60 MWd/kg U resulted in the following findings:

- the increase of fission gases content in fuel at the burnup increase led to the displacement of the regression correlation connecting the cladding residual hoop strain in the range of 0–6% and the peak fuel enthalpy shifting to the left (to the lower enthalpies area);
- but the mechanical behavior of fuel rods tested at the enthalpy, which exceeded the failure threshold, was insensitive both to fuel burnup and to the fuel rod pressurization.

10. In accordance with the obtained data, the following general conclusions were made:

- if the reasonable margin of the residual ductility is provided for in the irradiated cladding at the end of the base operation, the pulse width can be left out of the set of key factors, which determine the risk of the low enthalpy failure (less than 100 cal/g) under the RIA conditions at the fuel burnup up to 60 MWd/kg U;
- the fuel design (the fuel outer diameter, central hole, cladding thickness, gas plenum) was underestimated at the previous RIA analysis. It can be assumed with the reasonable certainty that the RIA behavior of the LWR fuel elements (the VVER and PWR) will demonstrate the significant sensitivity to the fuel design at burnup higher than 50 MWd/kg U;
- taking into account that all types of studied high burnup fuel demonstrated the tendency towards the ballooning formation and to the appropriate fission gas induced rupture and that the previous RIA tests performed with fuel rods under more representative coolant conditions (the high coolant pressure) demonstrated the increase of the failure threshold (in comparison with the tests performed at the atmospheric coolant pressure) due to the prevention of ballooning effects [1], it would be expected that the obtained BIGR test data had some conservative margin in relation to the reactor case. But it is obvious that the final view of these issues will be obtained in accordance with the CABRI water loop program [4].

References

- 1 V. Asmolov, L. Yegorova “The Russian RIA Research Program: Motivation, Definition, Execution, and Results”, *Nuclear Safety*, Vol.37, No.4, 1996.
- 2 T. Fuketa, F. Nagase, K. Ishijima, and T. Fujishiro “NSRR/RIA Experiments with High Burnup PWR Fuels”, *Nuclear Safety*, Vol.37, No.4, 1996.
- 3 J. Papin, M. Balourdet, F. Lemoine, F. Lamare, J. Frizonett, and F. Schmitz “French Studies on High Burnup Fuel Transient Behavior under RIA Conditions”, *Nuclear Safety*, Vol.37, No.4, 1996.
- 4 J. Papin, J. Melis, C. Lecomte “Definition and Status of the CABRI International Program for high Burn-up Fuel Studies”, *Proc. of the Twenty-Eighth Water Reactor Safety Information Meeting*, NUREG/CP-0172, Bethesda, Maryland, 2000.

APPENDIX A

*The Characterization of Test Procedures Used
to Determine Parameters of High Burnup Fuel Rods*

A-1. Parameters of the commercial fuel elements after the base irradiation

The post-irradiation investigations of commercial fuel elements used for the refabrication of high burnup fuel rods to be tested under the BGR test program included nondestructive and destructive examinations. The brief characterization of appropriate studies is presented in Table A-1.

Table A-1. Major provisions for the procedures used to determine commercial fuel elements parameters

Parameter	Procedure
1. The gas composition volume under normal conditions	The laser puncture and attachment of the fuel element to the evacuated vessel, the pressure measurement, the calculation of the gas composition volume taking into account results obtained in accordance with the Item 2
2. Free gas volume	The gas evacuation to a special vessel containing gas at the given pressure, temperature, and volume
3. Gas pressure	Calculations with the use of test results obtained in accordance with the Items 1, 2
4. Gas composition	Mass spectrometric measurements of gas samples
5. FGR	Calculations with the use of results obtained in accordance with the Items 1-4
6. Pellet-cladding gap	The computer processing of cross-section photographs ^a
7. Burnup axial distribution	Gamma scanning and the data processing in accordance with the standard procedure
8. Fuel density	Hydrostatic weighing of fuel samples
9. Fuel outer diameter and central hole diameter	The computer processing of cross-section photographs ^a
10. Fuel grain size	The computer processing of fuel microstructure ^a
11. Rim layer thickness	The computer processing of fuel cross-section
12. Cladding outer diameter	Profilometry in two azimuthal positions and determination of the average measured value
13. Cladding thickness	The computer processing of cross-sectional samples ^a
14. Oxide thickness	The computer processing of cross-sectional samples ^a
15. Hydrogen content	The measurement by the method of the isotopic dilution

In addition to the parameters presented in Table A-1, a special set of parameters characterizing the base irradiation history of each commercial fuel element was determined also. A standard Russian procedure package was used for this goal.

^a The procedure of the computer processing consisted of the following major stages:

- outlining of the test sample or the test fragment;
- determination of the outlined surface area;
- determination of the sample diameter such that the sample area with the desired diameter equals the measured sample area

A-2. Parameters of refabricated high burnup fuel rods before the BGR tests

The whole set of these parameters can be divided into two groups:

1. Individual parameters of each fuel rod.
2. Reference parameters of fuel rods.

As for the individual parameters, these characteristics were personally measured in each fuel rod. The measurements performed in one of several selected samples on developing the commercial element data (see Table A-1) were used as the reference parameters for the refabricated fuel rods. The scope of appropriate characteristics is presented in Table A-2.

Table A-2. Major provisions for the procedures used to determine pre-test parameters of refabricated high burnup fuel rods

Parameter	Procedure
1. Gas pressure inside fuel rod	Direct measurement at the manufacture
2. Pellet-cladding gap	The special certificated procedure based on the cladding deflection (up to the contact with fuel) caused by the pressure of punch in the cross-sectional direction [1]
3. Burnup axial distribution	Gamma-scanning of the refabricated fuel rod and the obtained data processing in accordance with the standard procedure
4. Pellet stack axial coordinates	The measurement of the actual distance between the cladding and fuel stack ends performed after fuel removal from the top and bottom ends of refabricated fragment (with the measured axial coordinates) of the commercial fuel element
5. Undamaged section length	The processing of γ -scanning measurements
6. Total fuel mass	The direct weighing of the fuel element section (the section used for the refabrication after fuel removing from the end parts). The determination of fuel mass taking into account the cladding mass calculated using the cladding real dimensions
7. Axial distribution of fuel mass	See Appendix A-3
8. Fuel outer and inner diameter, fuel density, fuel grain size	In accordance with the data of Table A-1
9. Cladding outer diameter	Profilometry in two azimuthal directions and determination of the average value
10. Cladding thickness, oxide thickness, hydrogen content	In accordance with the results of post-irradiation examinations of commercial fuel elements
11. Total gas volume and axial distribution of the gas (empty) area	See Appendix A-4

A-3. Determination of the fuel mass axial distribution in refabricated fuel rods

The previous experience gained on preparing the IGR test program has shown that there is the risk that the axial distribution of fuel mass inside the refabricated fuel rods will not be uniform [2]. The appropriate analysis showed that the incompleteness of the refabrication procedure was mainly responsible for this fact at that time. In spite of the improvement of this procedure performed during the BGR test program development, it was impossible to exclude this risk in full. Therefore, a special procedure developed earlier was used for the determination of the linear fuel mass axial distribution on preparing the pre-test data of refabricated fuel rods. The major provisions for this procedure are the following [2]:

- the axial distributions of γ -activity of ^{134}Cs , ^{137}Cs , ^{154}Eu isotopes were used as the input data for this procedure. The appropriate activities were measured by the γ -scanning of each refabricated fuel rod;
- it was shown that the relationship between the spectrometer count rate and fuel mass in the given axial position is reflected by the formula:

$$S = C k_s n m ,$$

where S= the count rate in the photopeak while recording gamma-quanta of a certain energy (1/s);

C= the coefficient, which is not a function of fuel mass and irradiation conditions (1/s);

k_s = the coefficient of self absorption of gamma-quanta of a certain energy in the fuel pellet (per-unit);

n= the average concentration of a given isotope in fuel (1/g);

m= the fuel mass in this axial section (g).

- due to the additional procedures, the coefficients C, k_s and isotopic average concentrations (n) were determined for all considered cases and the axial distribution of the fuel mass was calculated for each high burnup fuel rod^a.

A-4. Determination of the axial distribution of the free gas volume in the refabricated high burnup fuel rods

Taking into account the consideration concerning the specific features of the refabrication procedure, it was impossible to provide for absolutely the same axial distribution of free gas volume in each fuel rod. To take into account the individual character of this distribution, the analytical procedure was developed. The major provisions for this procedure were as follows:

- the fuel cross-section area was determined as a function of the fuel stack length (on the basis of the fuel density and fuel mass axial distribution);
- taking into account the axial distribution of the fuel cross-section area, the cladding inner diameter, and the central hole diameter, the axial distribution of free gas volume along the fuel stack was calculated;
- the axial distribution of the free gas volume along the upper and low plenums were determined using the design documentation of refabricated fuel rods.

A-5. Parameters of refabricated high burnup fuel rods after the BGR tests

After the BGR tests, the following nondestructive post-test examinations were performed for each fuel rod:

- visual observations and photograph preparation;
- profilometry in the 16 azimuthal positions;
- γ -scanning;

^a A. Bortash (RRC KI) performed all these calculations

- the preparation of X-ray photograph.

Besides, the following destructive investigations were performed also:

- the FGR determination;
- the measurement of ¹⁴⁰Ba activity, fuel isotopic composition and fuel burnup in fuel samples;
- the preparation of metallographic samples and the performance of the appropriate studies.

This scope of test manipulations allowed the characterization of high burnup fuel rods in accordance with the list presented in Table A-3.

Table A-3. The major provisions for the procedures used to determine parameters of high burnup fuel rods after the BGR tests

Parameter	Procedure
1. The gas composition volume in unfailed fuel rods under normal conditions	The laser puncture and the attachment of the fuel rod to the evacuated vessel, the pressure measurement and the calculation of gas composition volume taking into account results of measurements performed in accordance with the Item 2
2. Free gas volume	The gas evacuation to a special vessel containing gas at the given pressure, temperature, and volume The calculation of the free gas volume taking into account the measured pressure decrease in the combined system (the rod and vessel)
3. Gas pressure	The calculation with the use of results obtained in accordance with the Items 1, 2
4. Gas composition in the unfailed fuel rods	The mass spectrometric measurements of taken gas samples
5. Fuel outer diameter, central hole diameter	The computer processing of cross-section photographs ^a
6. Fuel isotopic composition	See Appendix B of this volume of the report
7. Cladding outer diameter	Profilometry in the sixteen azimuthal positions
8. Cladding residual hoop strain	The calculation in accordance with the following formula: $\varepsilon = \frac{OD_{av.after} - OD_{av.before}}{OD_{av.before}} 100\% ,$ <p>where ε= the cladding residual hoop strain (%); $OD_{av.after}$= the average cladding outer diameter after the BGR test (mm); $OD_{av.before}$= the average cladding outer diameter before the BGR test (mm)</p>
9. Cladding outer diameter	Profilometry in two azimuthal directions and determination of the average value
10. Cladding thickness, oxide thickness	The computer processing of the cladding cross-section photographs

^a The procedure of the computer processing consisted of the following major stages:

- outlining of the test sample or the test fragment;
- determination of the outlined surface area;
- determination of the sample diameter such that the sample area with the desired diameter equals the measured sample area

References

- 1 S. Amosov, S. Pavlov “Specific features of the determination of the pellet-cladding gap of the fuel rods by non-destructive method”, *Proc. of a Technical Committee meeting "Advanced post-irradiation examination techniques for water reactor fuel"*, 14-18 may 2001 Dimitrovgrad pp.73-79 IAEA-TECDOC-1277.
- 2 L. Yegorova, V. Asmolov, G. Abyshov, V. Malofeev, A. Avvakumov, E. Kaplar, K. Lioutov, A. Shestopalov, A. Bortash, L. Maiorov, K. Mikitiouk, V. Polvanov, V. Smirnov, A. Goryachev, V. Prokhorov, and A. Vurim “Data Base on the Behavior of High Burnup Fuel Rods with Zr-1%Nb Cladding and UO₂ Fuel (VVER Type) under Reactivity Accident Conditions”, *NUREG/IA-0156 (IPSN99/08-02, NSI/RRC KI 2179)*, Vol.2, 1999.

APPENDIX B

*The Major Provisions for the Procedure Developed to Determine
the Ratio between Fission Numbers in the VVER High Burnup Fuel
and the BGR Energy Deposition*

B-1. The use of the test ratio between the number of fissions in the VVER unirradiated fuel and the energy deposition in the BGR reactor for the determination of the number of fissions in high burnup fuel

The major task at this stage of investigations was to develop a method relating the number of fissions in the VVER high burnup fuel with the measured energy deposition in the BGR core. The measurement of the BGR energy deposition was a standard procedure for this reactor and the appropriate measurements were performed with a high accuracy. The procedure is based on the measurement of a special nickel sample activity after the BGR test. To determine the number of fissions in the VVER high burnup fuel using the measured activity of the nickel sample (the activation detector located in the standard position before each BGR test), the method characterized in Fig. B-1 was developed.

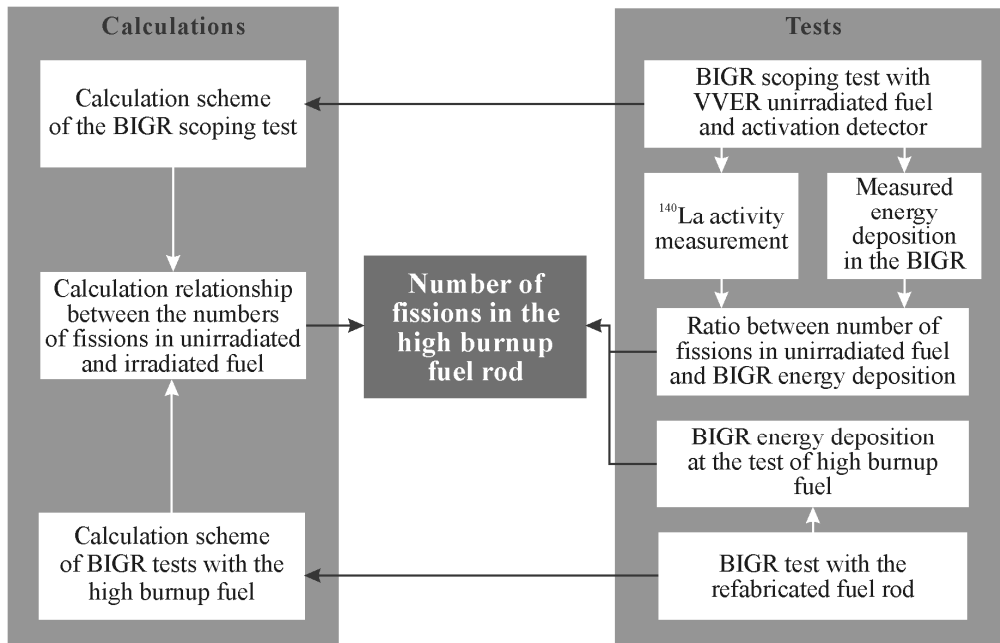


Fig. B-1. The major provisions for the procedure developed to determine the number of fissions in the VVER high burnup fuel rods on the basis of the test ratio between the number of fissions in unirradiated fuel and the BGR energy deposition

In accordance with this method, the following formula was used to determine the number of fissions in high burnup fuel:

$$n_{irr} = \frac{k_{unirr} E}{k_{irr}},$$

where n_{irr} = the number of fissions in the VVER high burnup fuel (fiss/g);

k_{unirr} = the correlation coefficient characterizing the ratio between the number of fissions in the VVER unirradiated fuel and the BGR energy deposition (fiss/g MJ);

E = the BGR energy deposition (MJ);

k_{irr} = the ratio between the numbers of fissions in the unirradiated and irradiated fuel (per-unit).

This method was implemented in accordance with the following approach:

- Several scoping BGR tests were carried out with the VVER unirradiated fuel rods. The test arrangement of this program stage was identical to the BGR tests with high burnup fuel rods.
- The correlation coefficient (k_{unirr}) was determined in each test using the formula:

$$k_{unirr} = \frac{n_{unirr}}{E},$$

where n_{unirr} = the number of fissions in the VVER unirradiated fuel (fiss/g).

After that, the regression analysis was used to perform the best estimation of this coefficient on the basis of the test data presented in Table B-1.

- The coefficient k_{irr} was calculated individually for each VVER refabricated fuel rod with the use of two independent packages of neutronic codes (the RRC KI and VNIIEF calculations). After that, the average value of this coefficient was determined for each high burnup fuel rod.

The numbers of fissions in the VVER refabricated fuel rods were calculated with the use of coefficients k_{unirr} , k_{irr} and the BGR energy deposition (E) measured in each BGR test. The set of these data obtained for six high burnup fuel rods is presented in Table B-2.

Table B-1. The major results of the BGR scoping tests

Test number	BGR energy deposition (MJ)	Measured number of fissions in unirradiated fuel (n_{unirr} , fiss/g)	The correlation coefficient (k_{unirr} , fiss/g MJ)
1.	10.1	2.47	2.44
2.	5.1	1.26	2.47
3.	9.0	2.25	2.50
4.	88	21.67	2.45

Table B-2. The data characterizing the procedure for the determination of the number of fissions in refabricated fuel rods #RT7–RT12

Fuel rod number	BGR energy deposition (E, MJ)	Calculated number of fissions in the unirradiated fuel (n_{unirr} , 10^{13} fiss/g)	Coefficient k_{irr} (per-unit)		Number of fissions in irradiated fuel (n_{irr} , fiss/g)	
			RRC KI	VNIIEF	RRC KI	VNIIEF
RT7	261	6.39	2.69	2.64	2.38	2.42
RT8	288	7.06	2.49	2.37	2.84	3.02
RT9	288	7.06	2.49	2.40	2.84	2.94
RT10	254	6.22	2.00	2.08	3.11	2.91
RT11	291	7.13	2.09	2.07	3.41	3.35
RT12	240	5.88	2.01	2.01	2.93	2.88

B-2. The determination of the number of fissions in the VVER irradiated fuel on the basis of radiochemical measurements

The schematic description of this procedure is presented in Fig. B-2. The major goal of these very specialized investigations was to develop the multifactor data to verify:

- the computer calculations connected with the determination of the correlation coefficient characterizing the ratio between the numbers of fissions in the VVER unirradiated and irradiated fuel (k_{irr});
- the computer calculations of the isotopic composition in the VVER high burnup fuel;
- the procedure for the fuel burnup determination based on the γ -scanning results.

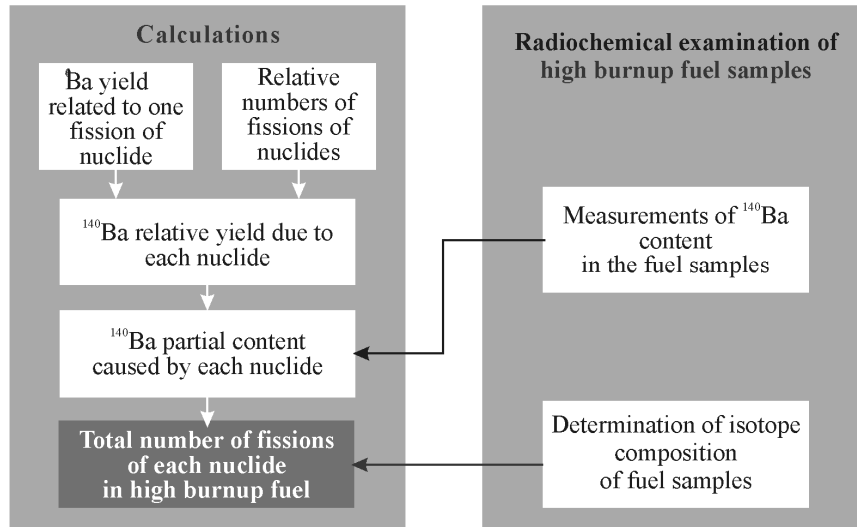


Fig. B-2. The major provisions for the procedure used to determine the number of fissions in the VVER high burnup fuel on the basis of radiochemical investigations

In accordance with the presented scheme, the appropriate procedure consisted of the following stages^a:

- the reference data were organized characterizing ¹⁴⁰Ba yield at one fission of each isotope, which was selected to determine energy deposition in the VVER high burnup fuel;
- ¹⁴⁰Ba relative yield was calculated for each considered isotope;
- taking into account ¹⁴⁰Ba measured content, ¹⁴⁰Ba relative yield, the fuel measured isotopic composition: ¹⁴⁰Ba partial content was calculated for each fissile nuclide;
- the obtained data were introduced into the decay disintegration chain and the numbers of fissions caused by each fissile isotope were determined.

As for the radiochemical procedure for the determination of ¹⁴⁰Ba content, of the isotopic composition and burnup in selected fuel samples, the general set of experimental studies is presented in Fig. B-3^b.

^a The procedure was developed by A. Bortash (RRC KI). He also performed all appropriate analytical works and calculations connected with this procedure

^b The whole set of these works was performed by the RIAR researchers under the direction of T. Timofeyev and A. Chetverikov

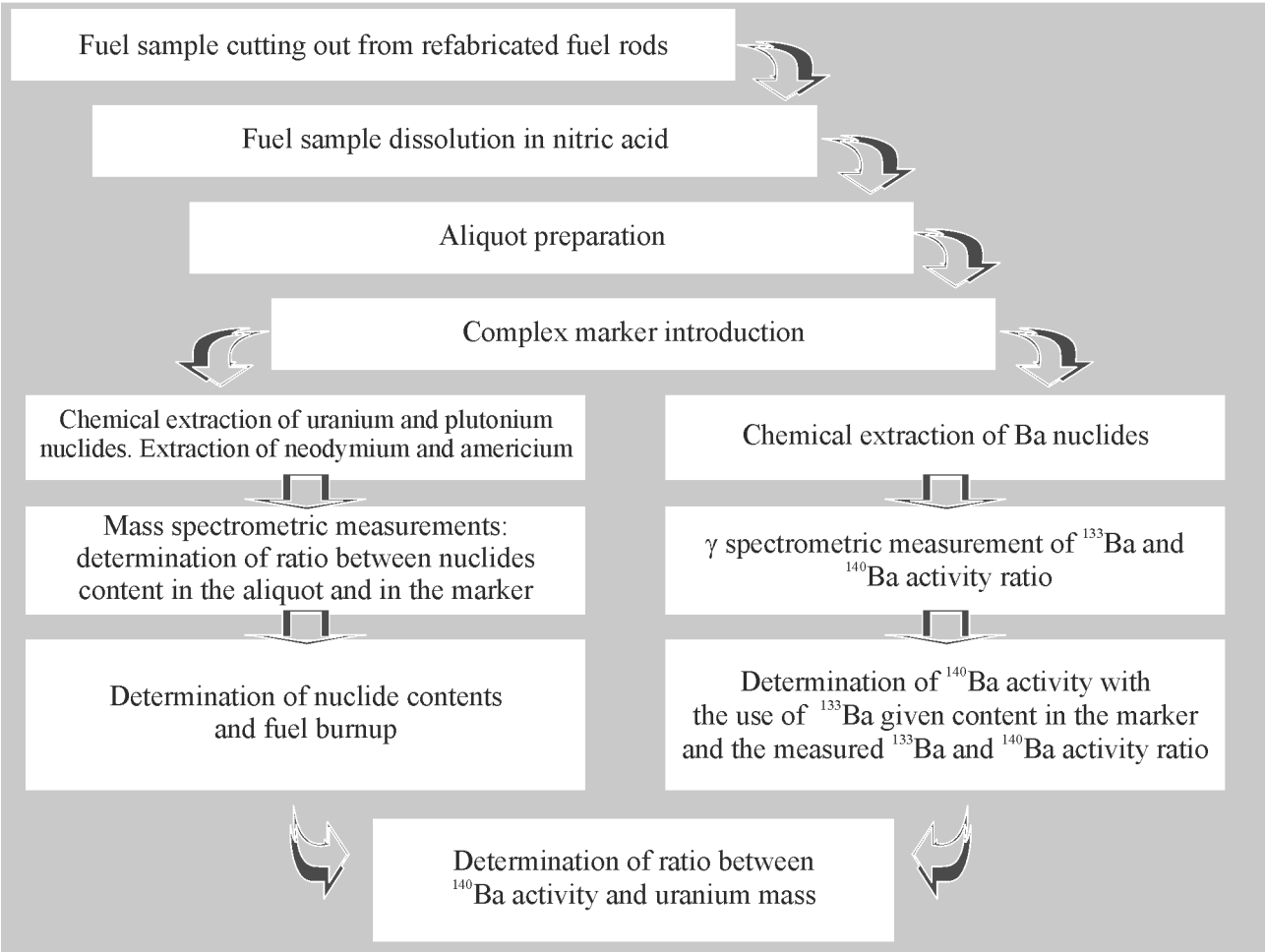


Fig. B-3. The major provisions for radiochemical measurements

APPENDIX C

Description of Some Models in the RAPTA-5 Computer Code

Taking into account that the RAPTA-5 code^a is used for the commercial design calculations, this code has not been published officially with a full description of the code models. To provide for the opportunity to assess the approaches implemented in this code for the modeling of the fuel rod transient behavior, the description of some models is presented in this appendix.

Heat conduction in the fuel rod

The following equation is used to calculate the transient heat conduction in the radial direction:

$$C_p \rho \frac{\partial T}{\partial t} = \frac{1}{r} \frac{\partial}{\partial r} \left(k r \frac{dT}{dr} \right) + q(r, t),$$

- where C_p = specific heat (J/kg K);
 ρ = density (kg/m³);
 T = temperature (K);
 t = time (s);
 r = calculation radius (m);
 k = thermal conductivity (W/m K s);
 q = volumetric heat generation rate (W/m³).

To take into account axial variations in the thermal conductivity, multiple axial zones can be used at the appropriate opportunity.

The fuel rod – to – coolant heat transfer

The heat transfer models used in the BGR calculations (before the special modification made as a result of the verification procedures) are listed in Table C-1.

Table C-1. The RAPTA-5 heat transfer models developed for the impulse capsule tests^b

Model	Description ^c
Convection to liquid	$\alpha = \frac{\lambda \text{Nu}}{z}$, $\text{Nu} = \text{C Ra}^n$, $\text{Ra} = \text{Gr Pr}$, $\text{Gr} = \frac{g \beta (t_w - t_f) z^3}{\nu \cdot a}$,
Nucleate boiling	$\alpha = 4.34 \cdot Q^{0.7} \cdot (P^{0.14} + 1.35 \cdot 10^{-2} \cdot P^2)$
Transition boiling	$\log \alpha = \frac{A \cdot \log(T_w - T_f) + B}{(T_w - T_f)}, \quad A = 1 + \frac{\log\left(\frac{\alpha_{\text{crit}}}{\alpha_{\text{sf}}}\right)}{\log\left(\frac{T_{\text{crit}} - T_f}{T_{\text{sf}} - T_f}\right)}$ $B = \frac{\log(T_{\text{crit}} - T_f) \cdot \log(\alpha_{\text{sf}}) - \log(T_{\text{sf}} - T_f) \cdot \log(\alpha_{\text{crit}})}{\log\left(\frac{T_{\text{crit}} - T_f}{T_{\text{sf}} - T_f}\right)}$
Film boiling	$\alpha = 0.25 \left(\lambda_g^2 \cdot C_{\text{pg}} \cdot g \cdot (\rho_f - \rho_g) \frac{\rho_g}{\mu_g} \right)^{\frac{1}{3}}$

^a The RAPTA-5 code was developed in the VNIINM [1, 2]

^b The original symbols used in the RAPTA-5 code are listed in this Table

Model	Description ^c
Critical heat flux	$Q_{crit}^o = Ckr\sqrt{\rho_g} \sqrt[4]{\sigma g(\rho_f - \rho_g)}, C = \frac{\pi}{24}, k = \sqrt{\frac{\rho_f}{(\rho_f - \rho_g)}}$ $Q_{crit} = Q_{crit}^o \left[1 + 0.1 \left(\frac{\rho_f}{\rho_g} \right)^{0.75} (h_{fsat} - h_f) / r \right]$

^c The following symbols are used in the model descriptions:

Nu = Nusselt number;	Pr = Prandtl number;
Re = Reynolds number;	Ra = Rayleigh number;
Gr = Grashof number;	λ = thermal conductivity coefficient (W/m K);
D_g = hydraulic diameter (m);	z = fuel stack length (m);
Q = heat flux (W/m ²);	P = pressure (Pa);
ΔP = pressure drop on the saturation line corresponding to the cladding temperature and saturation temperature (Pa);	T_{crit} = cladding temperature at critical heat flux (K);
F, S = empirical coefficients (per-unit);	$T_{sf} = 1.34(T_{sat} - T_f) + 400$;
T_{sf} = temperature condition of the film boiling initiation (K);	ΔT_{sat} = water under heating to saturation temperature (K);
T_{sat} = saturation temperature (K);	α_{sf} = heat transfer coefficient at T_{sf} (W/m ² K);
α_{crit} = heat transfer coefficient at the critical heat flux (W/m ² K);	β = coefficient of volumetric expansion (per-unit);
λ_g = thermal conductivity coefficient of water steam (W/m K);	ν = kinematic viscosity (Pa s);
μ_g = coefficient of water steam dynamic viscosity (kg/m s);	C_{pg} = steam water specific heat (J/kg K);
a = thermal diffusivity coefficient (m ² /s);	ρ_g = steam water density (kg/m ³);
C_{pf} = liquid specific heat (J/kg K);	σ = surface tension coefficient (N/m);
ρ_f = water density (kg/m ³);	g_c = gravitation constant (m ³ /kg s ³);
g = free fall acceleration (m/s ²);	h_{fsat} = coolant enthalpy at saturation condition (J/kg);
$T_g = \frac{T_w + T_f}{2}$;	h_f = coolant enthalpy (J/kg);
	r = vaporization heat (J/kg).

The gas thermal conductivity in the pellet–cladding gap

The modified model of Ross and Stoute is used in the RAPTA-5 code. But the special empirical coefficients were developed for this code. The model content is presented in Table C-2.

Table C-2. The model used in the RAPTA-5 code for the description of thermal conductivity of pellet–cladding gap^a

Model	Description ^b
Thermal conductivity of pellet–cladding gap	$\alpha_g = \frac{\lambda_g}{\Delta_g + g_T + g_o} + a_1 \tilde{\lambda} R \left(\frac{P_k}{R H} \right)^m + \alpha_{rad},$ $\Delta_g \geq C(R_T + R_o)$

^a The original symbols used in the RAPTA-5 code are listed in this Table

^b The following symbols are used in the model descriptions:

λ_g = thermal conductivity of gas composition (W/m K);	P_k = contact pressure (Pa);
Δ_g = thickness of pellet-cladding hot gap (m);	a_1, m = empirical coefficients (per-unit);
R_T = fuel surface roughness (m);	$R = \frac{\sqrt{(R_T^2 + R_0^2)}}{2}$ = effective roughness (m);
R_0 = cladding surface roughness (m);	H = cladding Meyer hardness (Pa);
C = empirical coefficient (per-unit);	α_{rad} = radiation heat conductivity (W/m ² K);
g_T, g_0 = fuel and cladding jump distances, respectively (m);	$\tilde{\lambda} = \frac{2\lambda_T\lambda_0}{\lambda_T + \lambda_0}$ = fuel-cladding effective contact thermal conductivity (W/m K).

Cladding mechanical response model

The content of the cladding mechanical response model used in the RAPTA-5 code is presented in Table C-3. This model is based on the following assumptions:

- the cladding is represented as a thin wall cladding;
- the cladding material is anisotropic with the isotropic work hardening;
- deviators of stresses and increments in the creep induced strain are proportional.

The cladding stress-strain condition is determined using the creep flow theory taking into account the additivity of elastic and creep strains. The elastic strain is calculated in accordance with Hooke's law. The creep strains are determined with the use of Prandtl-Reuss flow rule, which was modified for the creep and combined with the Hill's yield function for the orthotropic material. The calculation of the cladding stress-strain state at the deformation of the ballooning type is accompanied by the rupture deformation criterion. This criterion was developed on the basis of the biaxial mechanical tests of the Zr-1%Nb (E110) cladding. The parameters of the cladding failure (the time before failure and the plastic strain at failure) are calculated basing on the principle of elementary damages summation at the isothermal steady state loading. The failure criterion corresponds to the damages sum equal to 1.

Table C-3. The RAPTA-5 cladding mechanical model^a

Model	Description ^b
Stress strain equations	$\varepsilon_\theta = (\sigma_\theta - \nu\sigma_r - \nu\sigma_z) / E + \alpha T,$ $\varepsilon_r = (\sigma_r - \nu\sigma_\theta - \nu\sigma_z) / E + \alpha T,$ $\varepsilon_z = (\sigma_z - \nu\sigma_\theta - \nu\sigma_r) / E + \alpha T.$
The Prandtl-Reuss flow rule	$\dot{\varepsilon}_j = \dot{\varepsilon} \partial \sigma / \partial \sigma_j, \quad j = \theta, z, r$ $\sigma = [H(\sigma_\theta - \sigma_z)^2 + G(\sigma_z - \sigma_r)^2 + F(\sigma_r - \sigma_\theta)^2]^{1/2}$ $\dot{\varepsilon} = f(T, \sigma)$
The PCMI model	Fuel strain induced by the temperature: $\varepsilon_{fuel} = \alpha_{fuel} \Delta T_{fuel}$ The cladding plastic strain ($d\varepsilon_\theta^p$) induced by the fuel thermal expansion is determined taking into account the following contact pressure: $P_k \leq \frac{\sigma_{0.2} \cdot h_{cl}}{R_{cl}} + P_{cool} - P_{gas},$ where $\sigma_{0.2}$ = the yield stress as a function of the temperature and strain rate factor
Cladding material properties	The VNIINM data base for the Zr-1%Nb (E110) cladding

^a The original symbols used in the RAPTA-5 code are listed in this Table

Model	Description ^b
Cladding rupture criteria	<p>The criterion of the elementary damage linear summation:</p> $\int_0^{\varepsilon_{\theta f}} \frac{d\varepsilon_{\theta}}{\varepsilon_{\theta f}} = 1,$ <p>where $\varepsilon_{\theta f}$ = the cladding hoop logarithmic strain at failure under isothermal conditions</p> <p>The Garofalo's criterion (connecting the creep rate and the time before failure under isothermal conditions) [3]:</p> $\int_0^{\tau} \frac{d\tau}{\tau_r} = 1,$ $\tau_r \dot{\varepsilon}_{\theta \min}^n = c,$ <p>where τ_r = the time to failure</p>

^b The following symbols are used in the model descriptions:

α = coefficient of the cladding thermal expansion (K^{-1});	P_{cool} = coolant pressure (Pa);
E = modulus of elasticity (Pa);	$\sigma_{0.2}$ = cladding yield stress (Pa);
ν = Poisson's coefficient (per-unit);	P_{gas} = gas pressure in the fuel rod (Pa);
$\varepsilon_{\theta}, \varepsilon_z, \varepsilon_r$ = cladding total strain in tangential, axial, radial directions (respectively) (per-unit);	h_{cl} = cladding thickness (m);
$\sigma_r, \sigma_{\theta}, \sigma_z$ = stress components (Pa);	R_{cl} = cladding average radius (m);
α_{fuel} = coefficient of fuel thermal expansion (K^{-1});	$\dot{\varepsilon}_j, \dot{\varepsilon}$ = creep rate in the j direction and its intensity, respectively (s^{-1});
ΔT_{fuel} = fuel temperature increment (K);	F, G, H = anisotropy coefficients (per-unit);
P_{cont} = solid-solid pressure (Pa);	$\varepsilon_{\theta f}$ = cladding strain at failure (per-unit).

References

- 1 Yu. Bibilashvili, N. Sokolov, A. Salatov, L. Andreeva-Andrievskaya, O. Nechaeva, F. Vlasov "RAPTA-5 Code: Modelling of Behavior of Fuel Elements of VVER Type in Design Accidents. Verification Calculations", *Proc. of IAEA Technical Committee Meeting on "Behavior of LWR Core Materials under Accident Conditions"*, Dimitrograd, Russia, on 9-13 October 1995, IAEA-TECDOC-921, Vienna, 1996.
- 2 Yu. Bibilashvili, N. Sokolov, A. Salatov, L. Andreeva-Andrievskaya, O. Nechaeva, V. Nalivaev, V. Semishkin, V. Smirnov at al. "Experimental Researches and Modeling of WWER Fuel Rods Behavior in LOCA Conditions using RAPTA-5 Code", Third International Seminar on WWER Fuel Performance, Modeling and Experimental Support, Pamporovo, Bulgaria, 4-8 October 1999.
- 3 F. Garofalo "Fundamentals of Creep and Creep-Rupture in Metals", The MacMillan Company, New-York (1965).

BIBLIOGRAPHIC DATA SHEET

(See instructions on the reverse)

NUREG/IA-0213, Vol. 1
IRSN/DPAM 2005-275
NSI RRC KI3230

2. TITLE AND SUBTITLE

Experimental Study of Narrow Pulse Effects on the Behavior of High Burnup Fuel Rods with Zr-1%Nb Cladding and UO₂ Fuel (VVER Type) under Reactivity-Initiated Accident Conditions: Program Approach and Analysis of Results

3. DATE REPORT PUBLISHED

MONTH

YEAR

May

2006

4. FIN OR GRANT NUMBER

Y6723

5. AUTHOR(S)

L. Yegorova, K. Lioutov, N. Jouravkova
O. Nechaeva, A. Salatov
V. Smirnov, A. Goryachev
V. Ustinenko, I. Smirnov

6. TYPE OF REPORT

International Agreement

7. PERIOD COVERED (Inclusive Dates)

8. PERFORMING ORGANIZATION - NAME AND ADDRESS (If NRC, provide Division, Office or Region, U.S. Nuclear Regulatory Commission, and mailing address; if contractor, provide name and mailing address.)

Nuclear Safety Institute of Russian Research Centre "Kurchatov Institute" Moscow, Russian Federation
A.A. Bochvar All-Russian Research Institute of Inorganic Materials Moscow, Russian Federation
State Research Centre "Research Institute of Atomic Reactors" Dimitrovgrad, Russian Federation
Russian Federal Nuclear Centre "All-Russian Research Institute of Experimental Physics" Sarov, Russian Federation

9. SPONSORING ORGANIZATION - NAME AND ADDRESS (If NRC, type "Same as above"; if contractor, provide NRC Division, Office or Region, U.S. Nuclear Regulatory Commission, and mailing address.)

Division of Systems Analysis and Regulatory Effectiveness
Office of Nuclear Regulatory Research
U.S. Nuclear Regulatory Commission
Washington, DC 20555-0001

10. SUPPLEMENTARY NOTES

11. ABSTRACT (200 words or less)

This report contains a detailed description of calculation and test results obtained in the fast-pulse graphite-reactor (BGR) tests of twelve fuel rods refabricated from the VVER-440 and VVER-1000 high burnup fuel elements (50 - 60 MWd/kgU).

12. KEY WORDS/DESCRIPTORS (List words or phrases that will assist researchers in locating the report.)

BGR
Cladding
E110
Kurchatov Institute
Nuclear Fuel
Reactivity-Initiated Accident
Russian
Zirconium

13. AVAILABILITY STATEMENT

unlimited

14. SECURITY CLASSIFICATION

(This Page)

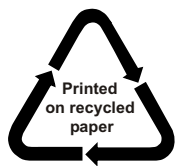
unclassified

(This Report)

unclassified

15. NUMBER OF PAGES

16. PRICE



Federal Recycling Program